A mineralogical approach to use the non-qualified fine aggregates in asphalt concrete pavement

Chi-Wei Chen

UNIVERSITÉ PARIS-EST

ÉCOLE DOCTORALE

Sciences, Ingénierie et Environnement

Thèse de doctorat

Spécialité : géotechnique

Chi-Wei CHEN

A MINERALOGICAL APPROACH TO USE THE NON-QUALIFIED FINE AGGREGATES IN ASPHALT CONCRETE PAVEMENT

Thèse dirigée par Jean-Pierre MAGNAN

Soutenue le 29 Mars 2016

Jury :

Rapporteurs :	George E. CHRISTIDIS	Technical University of Crete
	Véronique SCHMITT	Université de Bordeaux
Examinateurs :	Anne PANTET	Université du Havre
	Jean-Eric POIRIER	Colas Groupe
Directeur de thèse :	Jean-Pierre MAGNAN	IFSTTAR
Co-Directeur de thèse :	Yannick DESCANTES	IFSTTAR
Co-encadrant de thèse :	Myriam DUC	IFSTTAR
	Vincent GAUDEFROY	IFSTTAR

To my grandmother, every word was crafted while missing you.

I know you are sitting on a rainbow and being pround of me.

Preface and acknowledgments

My curiosity started growing by encountering the construction problem in pile foundation while I was working as a geotechnical Engineer 8 years ago. My engineering background was unable to explain the occurrence of construction damage, but I knew there was a better solution than pouring more and more concrete into the foundation: it is finding the solution by seeing problem through scientific and engineering aspects. Therefore, I left my engineer position and started the journey of completing my Geo-scientific knowledge. Time was too fast to rewind the life after it – warming up for living abroad through working holiday at Australia, learning Geomaterials and Geosciences through International Master of Advanced Clay Science (IMACS), seeing the world through traveling and living in foreign countries, and being tough through finding my own strength. There was nothing easy, but these experiences fertilized me to have hands-on competence for completing the PhD in Geotechnical engineering.

The work of my master thesis collaborated between IMACS and IFSTTAR enlightened me to solve Engineering problem by applying Geo-scientific and Geotechnical engineering skills. My beloved supervisor, M. Duc, recruited me for PhD and showed me the beauty of seeing through the problems and the excitement of bottoming up the solutions. I have not only learnt to be a passionate scientist from her, but also saw the most grateful heart during these years, which fills with trust, sympathy and supporting. By seeing the valuable personalities of my dear co-director, Y. Descantes, I have also learnt to be helpful, to be self-required and to be realistic for my work. I have also seen the patience, compassion and kindness whenever I asked advices to my adorable director, J.-P. Magnan, Moreover, I have learnt to be efficient, to be rational and to be cheerful from my delightful co-supervisor, V. Gaudefroy. I appreciate all of them that brought me on their shoulders to see further during these 3.5 years. Certainly, working with them was the best gift in my PhD life. Moreover, this PhD work was credited to E. Hamard, A. L'alloret, O. Burban, J. Demoncheaux, D. Demare, O. Garcin, F. Hammoum, T. Gabet, B. Bechet, A. Cothenet, J.-P. Terrier, F. Buisson, S. Buisson and N. Buisson from IFSTTAR as well. Their generosity and help made the success of this study and my fantastic stay at Nantes.

Luckily, I have met my international family, M. Harikiopoulo, J-P.Harikiopoulo, A. Guimond-Barrett, L. Radtke, S. Miñarro, J. Yousaf, S. kleinz, A. Maloula, A., Potysz, A. Ganzenko, F. Dudouyt, K. Pluta, L. Lefort, A. Themeli, E. Gennesseaux, F. Maillet and my softball teammates, BK Paris, supported me and listened to me all over these years. I appreciate their protection and warming me up when I lost the faith and missed the direction in life. Last, to my original Family in Taiwan, thank you for these unconditional loves even with my 8 years absence, the honor of this PhD title belongs to you.

To who is interested in my work, wish you a pleasant reading journey in my PhD dissertation.

Chi-Wei CHEN

Marne-la-Vallée, March 29, 2016.

Abstract

The need to save natural aggregate resources in a sustainable development approach led to consider quarry sands of bad quality. The presence of clays in the fine fraction of these sands has been known for long to increase the water sensitivity of hot-mixed asphalt (HMA), with the risk of mitigating the lifetime of asphalt concrete pavements. In order to detect the presence of clay fines and quantify their harmfulness, methylene blue (MB) tests are routinely performed on sands used for HMA mix design. As the relation between the MB value of a fine aggregate and the Duriez value assessing the water sensitivity of a HMA mixture is questionable, MB tests may by mistake disqualify some sands. The present research investigates the clay mineralogy of various sands to better predict the water sensitivity of a HMA mixture. Water sensitivity seems to be caused by cohesive failure in kaolinite-HMA mixtures, whereas swelling properties of clays are responsible for the stripping of HMA incorporating illite or montmorillonite. As a consequence, HMA mixtures comprising kaolinite have a higher water resistance than HMA mixtures comprising illite or montmorillonite. Furthermore, the high valence of compensating cations onto clay surface coupled to small cation radius (eg. Ca^{2+} and La^{3+}) may improve the water resistance of illite- and montmorillonite- HMA mixtures. Upon observing the correlations between Duriez test, MB value or CEC value and clay mineralogy, a new methodology for sand qualification was suggested and validated successfully on several natural fine aggregates. This methodology is comprised of four steps: when the conventional MB_{drop} test (step 1) used to qualify fine aggregates in France is in excess of MB2 threshold, cation exchange capacity (CEC or MB_{CEC}) (step 2) measurements are performed which generally extend the range for fine aggregates qualification. Would the fine aggregate remain non-qualified, clay mineralogy is identified and quantified using XRD powder pattern and Reitveld method, as far as possible validated by a complementary method using chemical analysis. The clay mineralogy is then used to calculate the Duriez value that has to be compared to the 0.8 threshold (step 3) whereas the experimental Duriez test (step 4) is performed when the conclusions from step 3 are unclear.

Key words: clay, mineralogy, asphalt concrete pavement, hot mix asphalt, stripping, methylene blue value, qualification, Duriez test, surface energy.

Résumé

La nécessité d'économiser les ressources naturelles en granulats dans une logique de développement durable conduit à s'intéresser à certains sables stériles de carrière. La présence d'argiles dans la fraction fine de ces sables est connue pour accroître la sensibilité à l'eau des enrobés hydrocarbonés à chaud (EHC), avec le risque de raccourcir la durée de vie des chaussées. Afin de détecter la présence de telles fines et de quantifier leur nocivité, des essais de bleu de méthylène (MB) sont usuellement réalisés sur les sables entrant dans la confection des EHC. Cependant, la relation entre la valeur MB d'un sable et la valeur de Duriez caractérisant la sensibilité à l'eau d'un EHC n'étant pas explicite, cette pratique est susceptible de disqualifier à tort certains sables. La présente recherche examine la minéralogie des argiles de différents sables afin de mieux prédire la sensibilité à l'eau d'un EHC. Celle-ci semble se traduire par une rupture cohésive de la phase liant à l'interface eau-bitume-argile dans un EHC contenant de la kaolinite, alors que les propriétés de gonflement des argiles de type illite et montmorillonite sont responsables du désenrobage dans les EHC correspondants. Par conséquent, un EHC contenant de la kaolinite est moins sensible à l'eau qu'un EHC contenant de la montmorillonite ou de l'illite. De surcroît, la valence élevée des cations compensateurs à la surface de l'argile ainsi que leurs petits rayons (par exemple Ca^{2+} et La^{3+}) peuvent améliorer la résistance à l'eau d'un EHC contenant de l'illite ou de la montmorillonite. A partir de l'observation des corrélations entre l'essai Duriez, la valeur de bleu ou la capacité d'échange cationique et la minéralogie de leurs argiles, une nouvelle méthodologie de qualification des sables pour EHC est proposée et a été validée avec succès sur quelques sables naturels. Quatre étapes composent cette méthodologie: lorsque la valeur de bleu MB_{drop} classique (étape 1) utilisée pour qualifier des sables en France est supérieure au seuil MB2 habituel, la mesure de la capacité d'échange cationique (CEC ou MB_{CEC}) (étape 2) permet d'élargir la gamme des sables qualifiables. Faute de qualification, les argiles sont ensuite identifiées et quantifiées en soumettant le sable à une analyse par diffraction de rayons X sur poudre avec exploitation du diffractogramme par la méthode Reitveld, si possible suivie d'une validation par une méthode 'complémentaire' utilisant l'analyse chimique. La minéralogie de l'argile est alors utilisée pour estimer la valeur de Duriez qui doit être comparée au seuil de 0,8 (étape 3), tandis que la mesure de la valeur de Duriez (étape 4) est réalisée lorsque les conclusions de l'étape 3 ne sont pas claires.

Mots-clés: argile, minéralogie, mélanges bitumineux pour couche de chaussées, bitume à chaud, désenrobage, bleu de méthylène, qualification, test Duriez, énergie de surface.

TABLE OF CONTENT

LIST OF FIGURES

LIST OF TABLES

Terminology and glossary

Natural aggregate	Aggregate from mineral sources subjected to nothing else than mechanical processing
All-in aggregate	A mixture of coarse and fine aggregates. It can be produced without the separation into coarse and fine fractions or it can be produced by combining coarse and fine aggregates
Aggregate size	Designation of aggregate which particles size ranges between d (the lower size) and D (the upper size)
Coarse aggregate	Aggregates with the highest size D (D less than or equal to 45 mm) and the lowest size d (d greater than or equal to 2 mm)
Filler aggregate	Aggregate with the most particles size lower than 0.063 mm (added to other aggregates in order to provide particular properties)
Added filler	Filler aggregate with a mineral origin, added to a aggregate
Mixed filler	Filler aggregate of mineral origin but mixed with lime (CaO)
Fine aggregate	Aggregates with the smallest size D (less than or equal to 2 mm) and containing particles mostly retained on the 0.063 mm sieve. Fine aggregate can be produced by natural alteration of rock or gravel, and/or by the crushing of rock or gravel, or by a process to manufacture aggregate.
Fine fraction (fines)	Particle size fraction of an aggregate passing the 0.063 mm sieve
Sand fraction	Particle size fraction of an aggregate between 0.063 mm and 2 mm
Clay	A material in which major phases are one or several clay minerals. Clay is used with a mineralogical sense and doesn't represent the fraction with a size lower than 2 µm. In this case, the term of 'clay fraction' is used (clay minerals are generally the main component of the clay fraction)
Clay mineral	A pure mineralogical phase that belongs to the clay groups
Commercial clay	Clay produced by industrial process with a drying at 230 °C and potentially treated with chemical products
Raw clay (or extracted clay)	Extracted clay from clay rock (and never dried over 40 °C in this study)
Unknown fine aggregate (or 'blinded' fine aggregate)	Tested natural fine aggregates supplied by quarrymen, the geological origin of which remains unknown (sample used for blind test in quantitative analysis)
Diorite	An intrusive igneous rock composed principally by silicate minerals such as plagioclase feldspar (typically andesine), biotite, hornblende, and/or pyroxene. The chemical composition of diorite is intermediate, between that of mafic gabbro and felsic granite.
Sericite	Fine fragments of mica (muscovite or paragonite) and common alteration mineral of orthoclase or plagioclase from feldspars
MB covering percentage	It represents the percentage of MB molecules adsorbed on clay surface compared to the adsorbed quantity of cobaltihexamine ions (represented by CEC). $MB_{\text{covering percentage}}$ (%) = MB (g/kg)/319.5*100/CEC (meq/100g)
d(*hkl*)	It corresponds to inter-reticular distances between crystalline plans *(hkl)* in a crystalline structure and hkl correspond to the Miller indexes. The distance between clay basal plane is d (*001*) whereas d (*060*) is non-basal reflection.
Quasicrystals	An ordered but not periodic structure

Abbreviations

AD	Air dry
AC	Asphalt concrete
Abs.	Absorbance
Calci.	Calcimeter
Calc.	Calculated
CEC	Cation exchange capacity
CEMs or CEECs	Cation exchanged materials
Chem.	Chemical
Chl.	Chlorite
Comm.	Commercial product
Compl.	Complementary (for complementary tests or method for mineralogical quantification)
C_i	Initial concentration of a compound in solution
C_f	Concentration of a chemical compound in solution after adsorption by sample
D_x	Grain diameter of the particles in a granular material for which the cumulated percentage of particles is 10%. It is read on the particle size distribution curve.
$D_{0/0.063\ mm}$	It corresponds to fine fraction. Fraction of aggregates with particle size between 0 and 0.063 mm
$D_{0/2\ mm}$	It corresponds to sand fraction $D_{0.063/2\ mm}$ added to the fine fraction $D_{0/0.063}$. Fraction of aggregates with particle size between 0 and 2 mm
$D_{2/4\ mm}$	It corresponds to coarse fraction. Fraction of aggregates with particle size between 2 and 4 mm
Dio.-	Dioctahedral structure (for clay mineralogy)
EG	Ethylene Glycol
Ext.	Extracted
Est.	Estimated
Fin.	Final
I. or Ill.	Illite
HMA	Hot Mix Asphalt
I/S	Interstratified illite-smectite mix layer
ICP-OES	Coupled Plasma-Optical Emission Spectroscopy
ICDD-PDF2	Mineral database provided by International Centre for Diffraction Data
Init.	Initial
K. or Kao.	Kaolinite
LCPC	Laboratoire Central des Ponts et Chaussées (name of IFSTTAR laboratory before the merge with INRETS)
M. or Montm.	Montmorillonite
MB	Methylene Blue
MB_{drop}	MB value from drop method (*NF EN 933-9)*
$MB_{UV\text{-}pho.}$	MB value from UV-photometer method
MB_{CEC}	MB value associated to the CEC measure : MB_{CEC} (g/kg) = CEC (meq/100g) x 319,85 / 100
Meas.	Measured
MIF	Mineral intensity factor
PO	Preferred orientation

R^2	Coefficient of determination fitting)
R_a	Arithmetic mean deviation
RCMs	Reduced-charge montmorillonite
RIR	Reference intensity ratio
γ_{ad}	Interfacial tension
γ_L	Surface energy of liquid
γ_S	Surface energy of solid
γ_L^P	Polar forces of liquid
γ_L^D	Dispersive forces of liquid
γ_S^P	Polar forces of solid
γ_S^D	Dispersive forces of solid
ref.	Reference
rpm	Round per minute
S.D.	Standard deviation
STD.	Standardized (for MB value from drop method)
Std.	Standard
Therm. analysis	Thermal analysis
Tri.-	Trioctahedral structure (for clay mineralogy)
V.	Vermiculite
Vol or V (ml)	Volume
V/S	Interstratified vermiculite-smectite mixed layer
W_{ad}	Work of adhesion
wt%	Weight percentage
XRD	X- Ray diffraction
θ	Contact angle

Introduction

Asphalt concrete (AC) pavement is the surface course of road covered by bitumen and aggregates mixture, and it has been applied worldwide since the 20th century due to its construction efficiency, structural flexibility and durability. However, even a good AC pavement will not last forever. The presence of clay in aggregates raises the water sensitivity of AC mixture and shortens the durability of AC pavement (*Tarrer 1986;Transportation Research Board 2003*). Regarding the increase of water sensitivity of AC mixture, water may easily intrude into bitumen-aggregates matrix, reduce the adhesive strength into AC mixture (*Mo et al. 2009*) and then combined to loading, water may devastate the structure of AC pavement. Damage in AC mixture that occurs from adhesion failure induced by water, is also called "stripping". In general, the degradation of AC pavement from stripping is slow at first, and then it accelerates when time goes by.

Clays (or clay material) contain clay minerals as main components with particle size around 0.002 mm, commonly present in natural fine aggregate ($D_{0/2\ mm}$) from quarries. The evaluation of fines content ($D_{0/0.063\ mm}$) in fine aggregates ($D_{0/2\ mm}$) is required by European standard (*NF EN 13043 2003*) to qualify the material to be used in AC pavement and additional tests are imposed if the fine content is higher than 3%. In France, additional tests such as methylene blue test are applied whatever the fine content. When the fine aggregates ($D_{0/2\ mm}$) contain high amount of fines and prior to incorporate them into AC mixture, the practice is either to remove fines particles by washing with water or to improve clay properties by lime treatment (*Huet 1989;Lesueur et al. 2013;Mehrara and Khodaii 2013;Tarrer and Wagh 1991*). Otherwise, the non-qualified fine aggregates have to be stocked as waste to fill cavities on site at the closure of the quarry or to be used for another application (application to find). For example, according to French quarry Le Boulonnais, up to 50% of extracted fine aggregates may be stocked in the quarry without any potential application because of the too high amount of fine particles in material.

In practice, suppliers in France systematically wash aggregates without caring the initial clay content in material, and then filler or qualified fine particles are added into washed aggregates in order to fulfill its grading curve in accordance with application. As fine particles in aggregates are replaced by chosen mineral, the natural resource is seriously wasted because of the unclear understanding of the role of clay on the stripping in AC mixture. Note that fourteen million tons of fine aggregates are consumed per year in France (*Duc et al. 2011*) while forty million tons of bitumen are produced for AC pavement incorporating fine aggregates. In practice, the improvement of the water resistance for AC pavement is associated with (1) the drying temperature increase of fine aggregates (before the incorporation into bitumen), (2) the improvement of physical properties of AC mixture and (3) the replacement of clay particles by limestone filler. These applications enhance the water resistance of AC pavement mostly through the modification of clay in fine aggregates. The high temperature applied on fine aggregates reduces the swelling property of clay. Thus, the fine aggregates may become qualified by the additional test (such as methylene blue test), and the water resistance of AC mixture will be improved as well. But such method is strongly energy consuming (because of the increase of the temperature in the dryer drum). The increase of bitumen content, using harder grade of

bitumen and the decrease of $D_{2/6mm}$ fraction of aggregate are suggested to improve also the water resistance of AC mixture through physical properties (*Delorme and Wendling 2007*). In French regulation, the bitumen (binder) film has to keep a constant thickness around aggregates. The increase of bitumen content will be applied if the specific surface area of fine aggregates is increased in presence of clay particles. However, the cost (to supply petroleum product) and the environmental impact is a significant drawback. Moreover, it is well known in asphalt science that siliceous fine particles have the worst adhesive strength towards bitumen compared with limestone aggregate (*Bagampadde et al. 2004;Curtis et al. 1993;Grönniger et al. 2011;Hicks 1991*). Therefore, several countries such as Germany, United Kingdom etc. make the choice to wash the sand fraction generated by igneous rocks. The modified particle size distribution curve of washed fine aggregates is fulfilled by the addition of limestone filler ($CaCO_3$) required to decrease the water sensitivity of AC pavement. Such washing needs high amount of water that has to be treated and recycled, and huge quantity of energy is needed in order to dry the aggregates.

In France, the standard *NF XP P18-545 (2011)* indicates the required tests and the parameter limits for fine aggregate qualification for road application. The harmfulness of fine in fine aggregate can be qualified either by using the methylene blue test (*NF EN 933-9 2009a*), or by using the sand equivalent test (*NF EN 933-8 2015*). The practice demonstrated that the sand equivalent test is not adequate and it's less and less used. Methylene blue test is largely applied by the producers for fine aggregate qualification when aggregates are for AC mixture (whatever the fine content). Fine aggregates are qualified if MB adsorption is lower than 2 g per kg of $D_{0/2\ mm}$ sample (Table 1).

Table 1 Evolution of the protocol and limits for methylene blue adsorption standardized test

Standards for aggregate in AC pavement	**P18101 (*1990*)**	**XP P 18540 (*1997*)**	**NF P 18-545 (*2011*)**		
Standardized tests of MB measurement	P18592 (*1990*)	Pr EN 933-9	NF EN 933-9 (*1999*)	NF EN 933-9 (*2009*)	NF EN 933-9 (*2013*)
Material preparation	undried samples	sample dried at 110°C	sample dried at 110°C	undried sample	sample dried at T°max < 45 °C
Particle size of tested material	0/80 µm fraction by wet sieving	0/2 mm fraction of the 0/D aggregate by dry sieving			
The threshold of MB value for fine aggregate used in AC mixture	Vbta < 1 g/100g Vbta x f [a] ≤ 20	VB ≤ 2	MB ≤ 2	MB ≤ 2	MB ≤ 2

[a] f is the < 80 µm fraction measured on the 0/2 mm fraction of the 0/D aggregate

The MB^+ molecule adsorption onto the aggregate surface is related to the specific surface area and the negative surface charge of clay particles. Indeed, the decrease of the particle size induces high surface area. Therefore, the clays with their small size are particularly sensitive to MB test. If MB value is over 2 g/kg, degradation of AC mixture due to the presence of clays is expected considering empirical observations. However, the MB2 threshold for the evaluation of the clay harmfulness in fine aggregate has no real scientific evidence. MB value is capable to indicate only the difference of specific surface

area of fine aggregate but not to tell the clay mineralogy, the bitumen-aggregate interaction at micro scale, the nature of the cation onto clay and the stripping of AC mixture at macro scale.

Without the understanding of the interactions at water-bitumen-clay interface and clay mineralogy, the qualitative method using MB test will be still questionable. Moreover, the impacts of MB-clay interaction on MB adsorption have to be clarified as well. Without a better understanding of the MB-clay interaction, the modification of the protocol since 1990 (Table 1) can't be understood while the MB2 threshold for fine aggregate qualification is remained unchanged.

Finally, in a context of natural resource scarcity, the fine aggregates keeps on coming from far regions. So the purchasing of aggregates far from the construction sites implies transport that produces huge quantity of CO_2 while fine aggregates potentially available in close quarry are wasted. Solutions exist but the lime treatment (with pH and CO_2 effect on the environment) and the washing of crushed rocks (that consumes water and energy) are short term solutions. With high economic expenses and a noticeable environmental footprint, actual practice can be improved if the relation between clay mineralogy in fine aggregates and the stripping of AC pavement is better understood. In this case, most of natural aggregates will be properly used without wasting resources. So, the impact of clay mineralogy in fine aggregates on MB adsorption, bitumen-aggregate interaction and stripping of AC mixture constitute the heart of scientific work in this thesis. The PhD work consisted in:

- the comparison of different methods to identify and quantify the mineralogical composition of clay minerals in fine aggregates;
- the study of the different parameters that impact on MB adsorption onto clays and the relation between clay mineralogy and MB value;
- the study of the relation between clay mineralogy and water-bitumen-clay interaction from microscale approach (using surface energy) and from engineering approach (using standardized Duriez test).

The manuscript is divided into 5 sections that follows previous plan. The first chapter of this dissertation deals with the literature review. The current state-of-the-art reviews are grouped around the stripping of AC pavement, the mineralogical analysis including clay properties and MB adsorption, and the water-bitumen-clay interaction from micro- and macro-aspects. The chapter 2 provides the samples preparation, the applied methods and experimental plan followed in this work. The results are presented in chapter 3 divided in four parts: mineralogical analysis, MB adsorption, water-bitumen-clay interaction from micro-aspect and engineering approach. The chapter 4 (called discussion) correlates clay mineralogy with MB value or stripping of AC mixtures. Based on experimental evidences provided by this study, a new strategy to evaluate AC stripping based on mineralogy is proposed. Conclusions and perspectives complete the manuscript before appendixes and references.

Chapter 1 Literature review

The surface course of roads is often made of hot-mixed asphalt (HMA), which is basically composed of aggregates bound in hot temperature conditions by a thin bitumen film. This technique has been applied worldwide since the 20th century due to its construction efficiency, structural flexibility and durability. In order to maximize both the mechanical strength and durability of HMA, a number of requirements have been set. These requirements not only cover the performances of HMA, but they also apply to the characteristics of HMA constituents. Among these, a major set of requirements addresses the water sensitivity of HMA, since water is always present in road surface course and may affect its durability *(Delorme and Wendling 2007)*. This water sensitivity is known to significantly increase when aggregates, especially the sand fraction, incorporate clay fines. The following sections first highlight the water sensitivity of HMA incorporating clay fines and then successively investigate the role played by clay, bitumen and clay/bitumen/water interface to better understand the origins of the clay-induced water sensitivity of HMA.

1.1 Water sensitivity of hot-mixed asphalt (HMA) incorporating clayey aggregates

1.1.1 Composition of hot-mixed asphalt materials

According to *Delorme and Wendling (2007)*, HMA materials consist of coarse and fine aggregates mostly of natural origin. Coarse aggregates refer to particles retained on a square mesh sieve whose nominal dimension of aperture is 2 mm, whereas particles passing this sieve are known as fine aggregates. Among the latter, particles passing a sieve with an aperture size of 0.063 mm are called fines and they often incorporate clay, especially among particles smaller than 0.002 mm. The fines content of fine aggregates usually varies between a few percent up to roughly 35% by mass, whereas the share of fine aggregates in the overall aggregate mix may reach 40% depending on the HMA material.

Further to aggregates which often represent over 90% of their volume and shall meet a number of requirements defined in European Standard EN 13043, HMA materials generally contain a few percent by volume of two other constituents:

- an added filler, which consists of particles passing a sieve with an aperture size of 0.125 mm, with at least 70% by mass of particles smaller than 0.063 mm. Limestone fillers with a high calcium carbonate content are often used;
- at least 3% by mass of bitumen refined from the vacuum distillation of petrol, which is used as a binder.

HMA materials are prepared upon mixing the various constituents at a temperature in the order of 170°C *(Le Guen et al. 2013)*. However, prior to being laid on roads, HMA materials shall first meet mix design performance requirements (*Delorme and Wendling 2007*). These requirements address:

- the residual void achieved by the mix once compacted under a prescribed loading using a dedicated gyratory compactor, which shall be low to avoid additional permanent deformation under traffic loading, but not too low to avoid fatigue cracking;

- the residual permanent strain depth caused by a standard-weight-wheel rolling back and forth on the bituminous mix, which shall not be in excess of a tabled threshold value for a prescribed number of cycles to avoid inacceptable rutting;
- the stiffness of the mix to ensure that, once compacted, the mix will deform within its elastic domain while loaded by the traffic;
- the fatigue resistance of the mix to ensure that it may withstand a prescribed number of cycle loads within its elastic domain without undergoing inacceptable cracks;
- eventually, the water sensitivity of the mix;

1.1.2 Water sensitivity assessment

Water sensitivity of HMA may be defined as its ability to preserve its design performances over time despite the adverse action of water. For this reason, water sensitivity is generally assessed through its consequences in terms of macroscopic mechanical strength drop. Two European test methods have been designed to assess it (*Delorme and Wendling 2007*):

- the Duriez axial compression test (*Duriez and Grelot 1950; EN 12697-12, method B*), according to which two series of bituminous mix specimens compacted under prescribed loading conditions are stored for 7 days, one in the air at 18°C and 50% relative humidity, and the other immersed in water at 18°C, before being axially loaded to rupture. The Duriez or I/C ratio, calculated as the ratio of mean compressive strength of air stored to immersed specimens, decreases from 1 to 0 with increasing water sensitivity;
- the indirect tensile test (*NF EN 12697-12 2008;* method A), which substitutes indirect tension for Duriez axial compression to determine an indirect tensile strength ratio (ITSR) and slightly alters the storage duration and thermodynamic conditions (three-day-immersion at 40°C to make bitumen more fluid).

Other countries assess the water sensitivity from other tension tests such as Original/modified Lottman Indirect Tension Test (*AASHTO T 283 2014;Lottman 1978*), or Immersion–Compression Test (*AASHTO T165 1997;ASTM D1075-11 2011*), some from rutting tests such as Hamburg Wheel-Tracking Device (*NF EN 12697-22 2010*), and some from freeze-thaw resistance tests such as Texas Freeze–Thaw Pedestal Test (*Kennedy et al. 1982*). In France, Duriez test is the preferred water sensitivity test method because test results are 50% less scattered than those obtained with indirect tension tests.

Alternative assessments of the water sensitivity of HMA may be performed upon considering the detrimental action of water regardless of the mix macroscopic strength:

- Water may induce stripping to the bituminous mix, which may be defined as the loss of adhesive bonding between mineral surface and bitumen under the adverse action of water or moisture, causing the removal of bitumen cementing film from mineral surface (*Transportation Research Board 2003*). Several tests may be performed to assess stripping, among which the boiling test (*ASTM D3625 2005;Kiggundu and Robberts 1988*) consisting in visually assessing the detachment of bitumen from mineral surface after boiling in water, or the pneumatic adhesion tensile testing

instrument (PATTI, *(ASTM D4541 2009)* designed to measure the bond strength between a coating and a substrate;

- Water may also cause the swelling of hydrophilic minerals such as clay minerals when they are present in the aggregate skeleton. The most common tests for swelling clay detection are sand equivalent (SE, *NF EN 933-8 2015*) and methylene blue (MB, *NF EN 933-9 2009*) tests, both performed on the fine aggregate fraction of the mix free of bitumen. The SE test consists in immersing the sample in a solution and forcing hydrophilic fines into suspension, then letting the solution at rest for a prescribed duration and finally assessing the height of sediment as a percentage of total height of sediment and suspension; The MB test consists in adding increments of methylene blue dye to the sample immersed in pure water until no more dye may adsorb on the mineral surface, the MB value being expressed as the mass of adsorbed dye per unit sample mass. Thus, in the absence of clay, sands have SE values close to 100% and MB values close to zero.

The major advantage of macroscopic strength drop tests over the others is that the mix physical and mechanical properties, water/traffic action, and pore pressure effects are account for by the former, whereas the latter are performed on loose test samples. Furthermore, results of macroscopic strength drop tests may always be quantified, which minimizes subjective evaluation as is the case with the boiling test. Their drawbacks are that more elaborate testing equipment, longer testing times, and more laborious test procedures are needed, all the more that their correlation with field performance is sometimes disputable due to specific in-situ conditions (UV aging, freeze-thaw,…).

1.1.3 Clay effect on the water sensitivity of HMA

1.1.3.1 Mineralogical contributions

High moisture sensitivity in AC mixture was observed if aggregates consisted of quartz and alkali feldspars *(Bagampadde et al. 2006;Bagampadde and Isacsson 2005;Caro et al. 2008)*. Yet, the very high resistance of moisture damage was found with 100% quartz content. The reason is that clay minerals are formed by replacing alkali and plagioclases feldspars during weathering (*Velde and Meunier 2008*), and generally appear with feldspars in aggregates.

Table 2 Degree of AC stripping related to mineral of aggregates (*Hicks 1991 cited by Anastasio 2015*)

Slightness	Moderateness	Severeness
Biotite	Biotite	Biotite
Hornblende	Hornblende	Hornblende
Feldspars: Labradorite, Bytownite, Anorthite	Feldspars: Oligoclase, Albite, Anorthite	Feldspars: Oligoclase, Albite Anorhoclase, Microcline, Perthite, Andesine
Chlorite	Garnet	Chalcedony
Sericite, muscovite	Quartz	Quartz
Diopside	Muscovite	
Olivine		
Olivine		
Pyroxenes		
Augite		
Calcite		

1.1.3.2 Experimental contributions

The water sensitivity of HMA has received wide attention in the past decades, but very seldom in the presence of clay in the aggregate mix. Yet, clay in the aggregate mix has been known for long to significantly affect the water sensitivity of HMA.

Duriez tests performed on bituminous mixtures comprising various quantities of clays have evidenced a i/C ratio decrease with increasing clay quantities (*Campanac 1981;Huet 1989*). Tests were performed on AC-BBSG and AC-GB mixtures[1] as well as bituminous fine aggregate samples (mastics). Left chart of Figure 1 shows that i/C ratio decrease is linked to the mineral composition of clay, the presence of swelling clay (bentonite in this study) yielding the most remarkable decrease whereas kaolinite appears less harmful. The right chart of Figure 1 evidences a relation between i/C decrease and MB adsorption value increase. Note that a fixed MB value on the right chart corresponds to very different clay quantities on the left chart, depending on clay type. A consequence is that fixing a requirement on MB value is likely to disadvantage kaolinite-containing HMAs though their i/C ratio may still be acceptable.

Hamburg Wheel-Tracking Device (HWTD) and modified Lottman Indirect Tension Tests performed on HMA samples incorporating clay-rich aggregates show similar trend. Indeed, regardless of clay type, *Kandhal et al. (1998)* statistically analyzed the results of these water sensitivity tests in light of SE and MB tests performed on the fine aggregate fraction of each tested mix. As shown on Figure 2, the author reports a correlation between methylene blue test results and modified Lottman Indirect Tension Test (R^2=0.63).

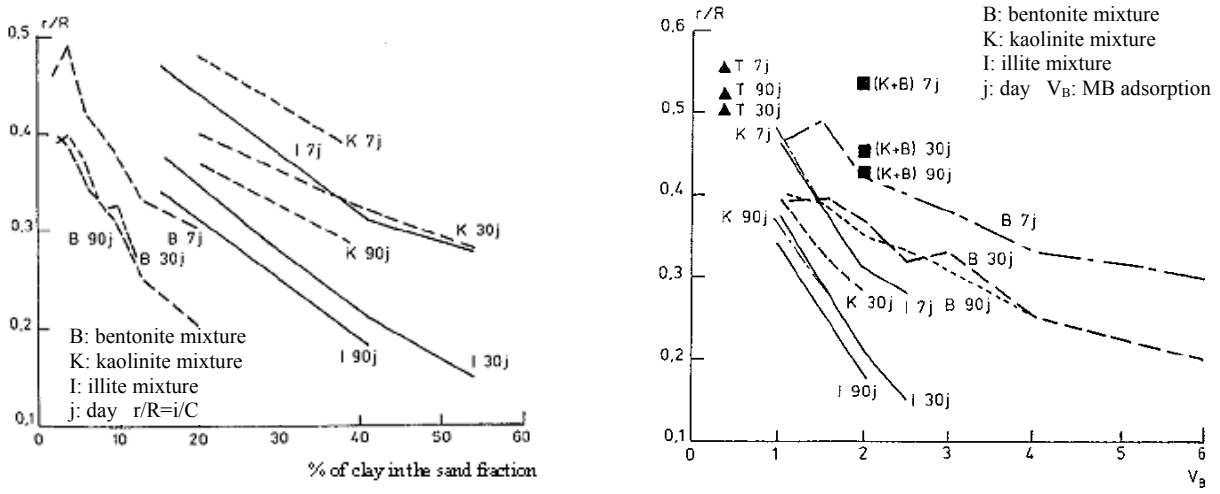

(a) (b)

Figure 1 i/C value (r/R) of asphalt mastic from Duriez test with (a) the quantity of clay and (b) the MB value of clay (g/kg). K, I and B are for kaolinite, illite and bentonite respectively. 7j, 30j and 90j are samples conditioned during 7 days, 30 days and 90 days respectively (*Huet, 1989*)

[1] See NF EN 13108-1 (*2006*) / NF P98-150-1 (*2008*)
AC-BBSG : Béton Bitumineux Semi-Grenu in French. It's highly used in France for bituminous pavement. The thickness of the layer is around 6 cm.
AC-BBTM : Béton BitumineuxTrès Mince (thickness = 2,5 cm).
AC-GB : Grave bitume in French (asphalt mixture with lower content in asphalt destined to sub-base or base layer).
AC-BBMA (0/10 or 0/14) : Béton Bitumineux Mince in French and A corresponds to the granular discontinuity (2/6). Their thickness varies between 3 and 5 cm

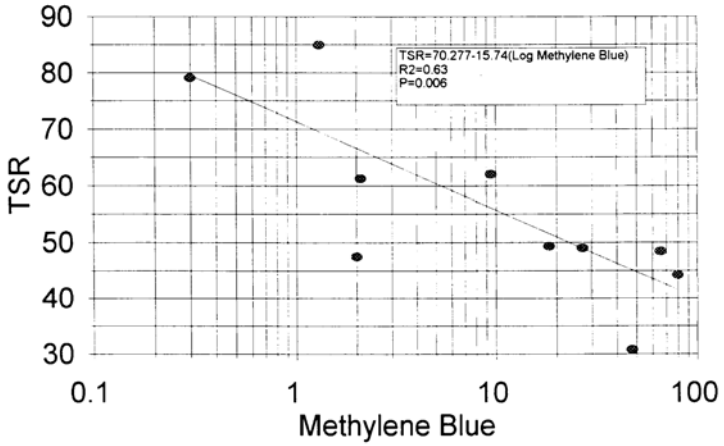

Figure 2 Methylene blue value versus TSR from modified Lottman Indirect Tension Test (*Kandhal et al. 1998*)

Examination of MB and SE results in light of Duriez i/C ratio from a database allowed to identify threshold values for the formers (MB_2 and $SE10_{55}$) that indicate water sensitivity in Figure 3 (*Dupriet 2010*). Aggregates loose samples failing these criteria are potentially water sensitive, but the definition of a pass/fail criterion with loose aggregate samples remains no easy task.

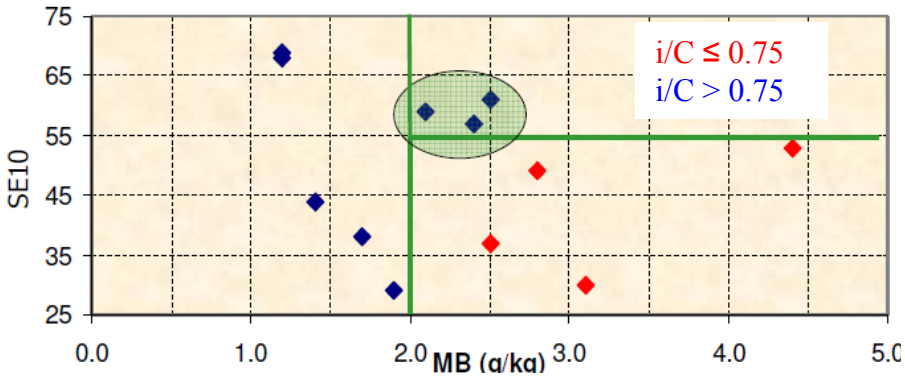

Figure 3 The i/C value of BBMA from Duriez test after 28 days of curing with the properties of aggregate Methylene blue value (MB) and sand equivalent (SE10) (*Dupriet, 2010*)

Clay was also found to stiffen HMA materials, thus mitigating compaction efficiency and causing excessive void in the total mix (VTM) compared to target value (*Aschenbrener 1995;Huet 1989;Kandhal et al. 1998*). In fact, appropriate VTM is important as it controls water penetration into HMA which causes moisture damage**.** Delorme and Wendling *(2007)*, citing the study from *Huet (1989)*, states that clay in fine aggregate induces the following effects on the characteristics of a AC-BBSG and AC-GB:

- rise of the percentage of gyratory compactor voids (+ 2% for MB = 2 g/100g),
- decrease in rutting depth (2,3 mm for MB = 4 g/100g)

Significantly higher bitumen content compared to clay-free aggregates was added to ease compaction and achieve target VTM, however *Kandhal et al. (1998)* noted that this was not sufficient to prevent water damage in HMA incorporating clay, according to results of tensile strength retaining tests (TSR). *Terrel and*

Shute (1989) reported that the critical range of VTM which seriously triggers water damage is between 6% and 14% (*Bahia and Seemab 1999;Kandhal and Rickarda 2001*). *Birgisson et al (2003)* claimed that dense fine graded mixtures and coarse gap-graded mixtures are more prone to moisture damage (*Graf 1986*). Many researches established that a proportional relationship exists between the permeability and moisture damage of HMA materials. *Masad et al. (2006)* reported that permeability lower than 10^{-3} cm/s prevents moisture damage.

1.1.3.3 Numerical contributions

Very few studies reporting on the numerical modeling of moisture damage caused to HMA by the presence of clay have been identified. The latest studies introduce the fact that fine-aggregate matrix (FAM which contains clay) triggers the stripping of AC mixture (Figure 4) (*Arambula et al. 2010*). The rate of moisture arrival changed along the aggregate-FAM interface, and the interfacial zones received large amounts of moisture to initiate adhesive fracture. The finite element method is used to simulate the water sensitivity of HMA due to moisture diffusion under prescribed loading conditions. Input parameters are moisture diffusion coefficients of FAM and coarse aggregates respectively. Results suggest that the water diffusion coefficient in the FAM and coarse aggregates, as well as the bond strength at coarse aggregate-FAM interface have a major influence on HMA water sensitivity (*Caro et al. 2012*).

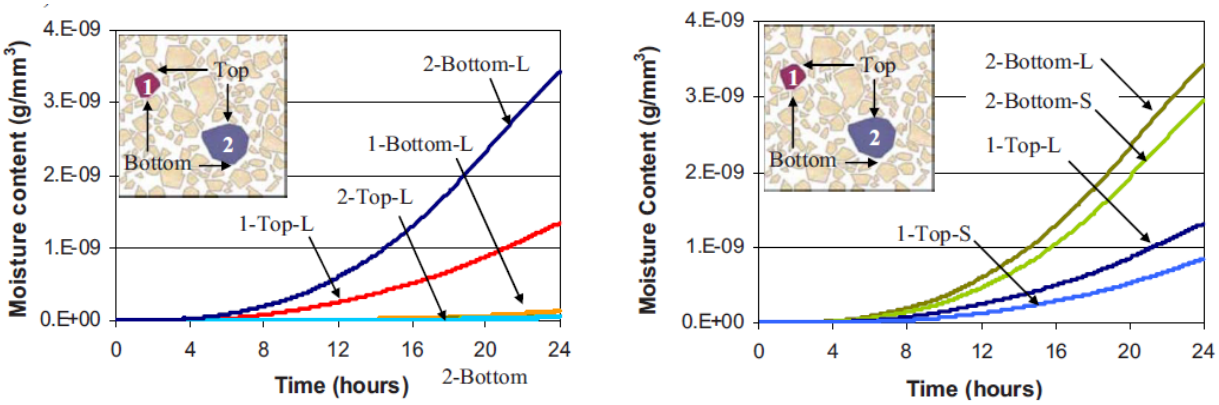

(a) (b)

Figure 4 Increase of moisture content within the FAM phase: (a) for the mixture with limestone aggregate; (b) for the two mixtures (numbers refer to individual aggregates, L: limestone mixture, S: sandstone mixture) (*Arambula et al. 2010*)

However, no numerical model accounting for the chemical composition of clay, the quantity of clay and bitumen-clay interaction to simulate the stripping of AC mixture has been identified.

From this brief overview of experimental and numerical contributions, it may be concluded that the effect of clay on the water sensitivity of HMA materials is closely monitored by water intrusion and its adverse action at the bitumen/clay interface. Hence, the mineralogy of clay, the composition of bitumen as well as mechanisms taking place at the bitumen/clay interface when water intrudes shall be investigated.

1.2 Clay in aggregates

1.2.1 Geological origin and definition of clay in natural aggregates

Most aggregates used to produce HMA come from natural rocks. Depending on their mineral composition and genesis conditions, these rocks are more or less subject to weathering caused by climate conditions (*Bowen 1922*). Weathering may be of physical origin, such as freezing and salt crystallization, or chemical origin such as hydrolysis by surface water which produces residual minerals and leached ions. As highlighted in Table 3, clays are residual minerals mainly resulting from the weathering of minerals composing common rocks. Figure 5 illustrates the weathering sequence of various primary minerals under different weathering conditions (see also *Fieldes and Swindale 1954*), yielding common clay types such as chlorites, vermiculites, kaolinites or montmorillonites depending on released ions. Weathering being an on-going process, aggregates are always partially composed of clay.

Table 3 Weathering of common rocks (*Nelson 2014*)

Rock	Primary minerals	Average mineralogical composition (%) [a]	Residual minerals [b]	Leached ions
Granite	Feldspars	52.4	Clay minerals	Na^+, K^+
	Mica	14.3	Clay minerals	K^+
	Quartz	31.3	Quartz	N/A [c]
	Fe-Mg Minerals	2.0	Clay minerals +Hematite +Goethite	Mg^{2+}
Basalt	Feldspars	46.2	Clay Minerals	Na^+, Ca^{2+}
	Fe-Mg Minerals	9.3	Clay minerals	Mg^{2+}
	Magnetite	44.5	Hematite, Goethite	N/A [c]
Limestone	Calcite	76.0	None	Ca^{2+}, CO_3^{2-}
	other minerals	24.0	Clay minerals	Na^+, K^+, Ca^{2+} Mg^{2+}
Sand stone	Feldspars	11.5	Clay minerals	Na^+, K^+
	Quartz	66.8	Quartz	N/A [c]
	Fe-Mg Minerals	2.0	Clay minerals +Hematite +Goethite	Mg^{2+}
	Clay minerals	6.6	quartz	Na^+, K^+, Ca^{2+}
	Calcite	11.1	None	Ca^{2+}, CO_3^{2-}

[a] (*AgriInfo.in 2011*)
[b] Residual minerals are the minerals that are stable at the earth's surface and left in the rock after weathering
[c] N/A : Physical weathering or oxidiation

Although various definitions coexist, a simple way of defining clay takes advantage of its particularities:

- a grain size generally smaller than 0.002 mm,
- usually a high aluminum content compared to other rock materials,
- a layer structure incorporating hydrous silicates (phyllosilicates).

Hence, the general definition for clay adopted in this manuscript is "clays are phyllosilicates which normally dominate the fine fraction of rocks". This definition does not attempt to separate clay minerals from their coarser equivalents in the realm of classical mineralogy, and it excludes accessory minerals such as quartz and feldspar (Figure 6).

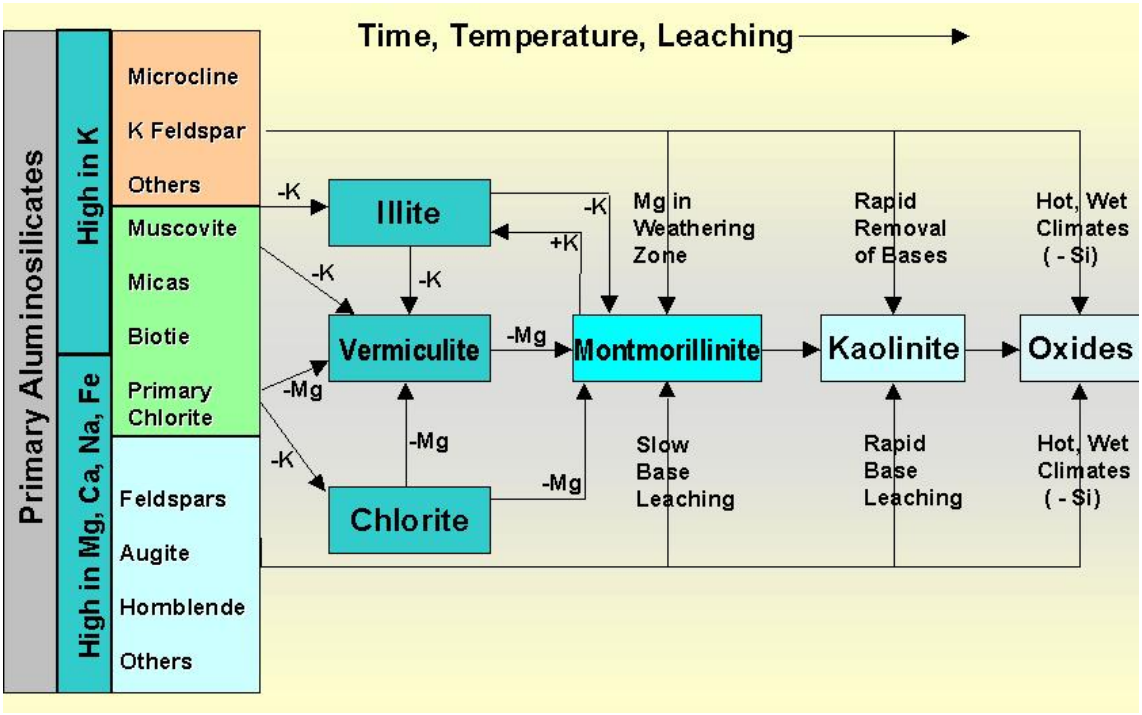

Figure 5 General conditions for the formation of various clays, iron and aluminum oxides (*Buckman and Brady 1969 cited by http://faculty.plattsburgh.edu/robert.fuller/370%20files/week6mineralogy/clayformation.htm*)

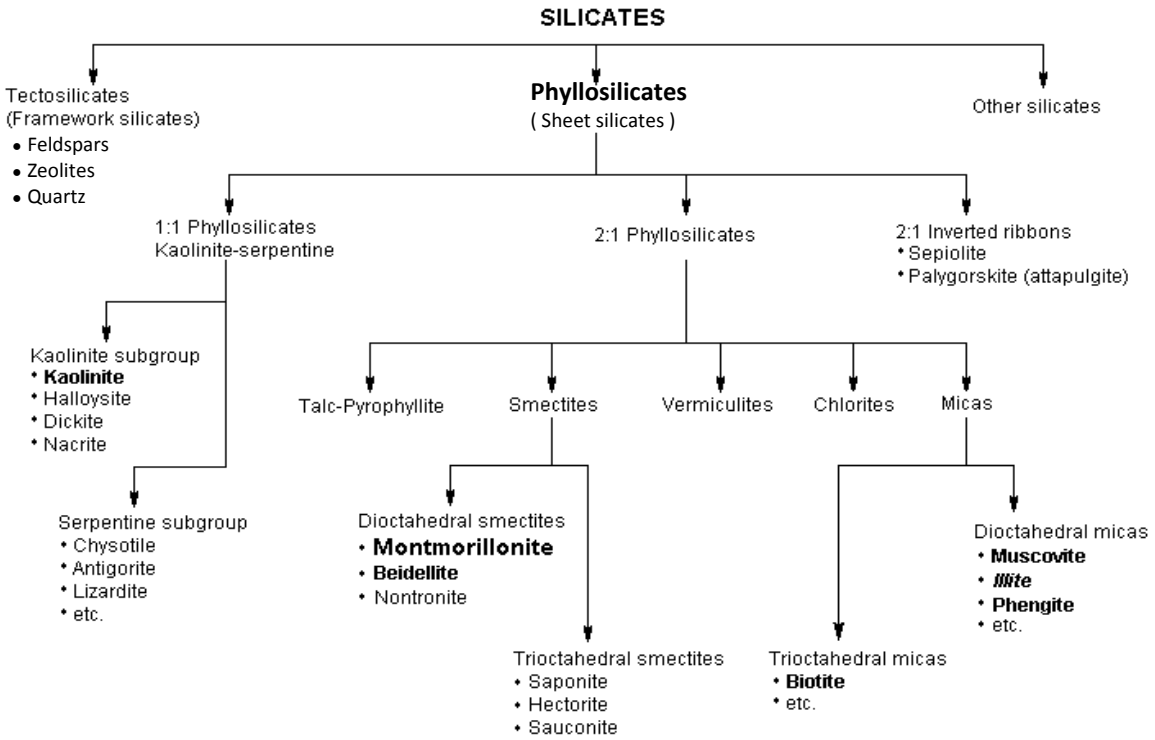

Figure 6 Classification of silicates (*Bailey 1980;Rieder et al. 1998*). Clay minerals that can be frequently found in fine aggregate are in bold. Illite is classified as a dioctahedral mica.

1.2.2 Clay properties

Clay minerals are characterized by several properties (*Bergaya and Lagaly 2006*) including:

- a multiscale structure consisting of individual 0.001 mm-wide sheets whose thickness may vary from 0.7 nm to about 1 nm (*Dyal and Hendricks 1950*), which superimpose to form particles,
- a strong anisotropy of the sheets or particles,
- a layer charge which influences sheets attraction and particles flocculation
- the ease with which the external, and often also the between-sheets interlayer surfaces may be modified,
- plasticity,
- hardening after drying or firing.

1.2.2.1 Clay structure

A clay layer contains two distinct sheet types, tetrahedral and octahedral (Figure 7), that superimpose in different arrangements on which the classification of clay minerals lies.

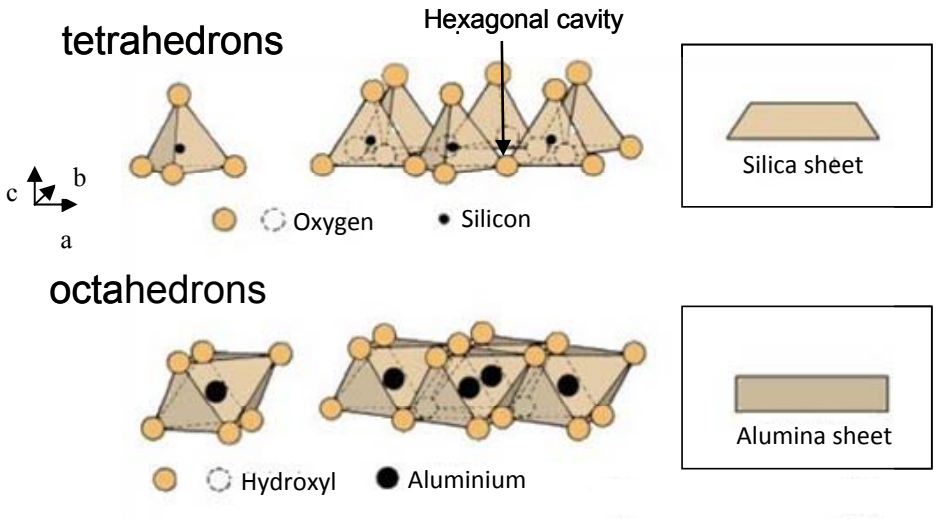

Figure 7 Basic units of clay minerals forming silica and alumina sheets (from *Mitchell, 1993*)

Each tetrahedron subunit consists of a central silicon cation Si^{4+} coordinated to four oxygen atoms, and linked to adjacent tetrahedra by sharing three corners (the basal oxygen atoms) to form an infinite two-dimensional 'hexagonal' mesh pattern along the a and b crystallographic directions. The basic formula of a tetrahedral layer is $Si_2O_5^{2-}$.

Each octahedron comprises two planes of OH^- groups, with its central site possibly occupied by cationic metals which are usually Al^{3+}, Fe^{3+}, Mg^{2+}, or Fe^{2+}, though other cations such as Li^+, Mn^{2+}, Co^{2+}, Ni^{2+}, Cu^{2+}, Zn^{2+}, V^{3+}, Cr^{3+} and Ti^{4+} were identified. Connections between adjacent octahedra are made by sharing edges following a hexagonal or pseudo-hexagonal symmetry along the a and b crystallographic directions. The valence of the octahedral cations differentiates octahedral layers into two basic types:

- **trioctahedral layers**, in which a divalent cation (e.g. Fe^{2+} or Mg^{2+}) occupies each octahedral site with the ideal formula $Mg_3(OH)_6$;
- **dioctahedral layers**, in which trivalent cations (e.g. Al^{3+} or Fe^{3+}) occupy two out of three octahedral sites with the ideal formula $Al_2(OH)_6$ (*Nesse 2000*) .

The bonding observed between tetrahedral and octahedral sheets occurs by sharing OH^- groups of octahedra with apical oxygen atoms of tetrahedra. Then phyllosilicates, clays, are grouped on the basis of their sheet composition, with two predominant layer structures (although mixed layer types do occur):

- **1:1 clay layer**, whose structure consists of tetrahedral-octahedral (TO) sheets. 1:1 clay layer typically exhibit an interlayer spacing of ~7Å, are electrically neutral, are bonded via van der Waals interactions and hydrogren bonds (H-bonding), and are relatively soft compared to 2:1 clay minerals due to the weak nature of their electrostatic bonding *(Nesse 2000)*.
- **2:1 clay layer**, whose structure consists of tetrahedral-octahedral-tetrahedral (TOT) sheets (Figure 8) (*Dyal & Hendricks 1950*). 2:1 clay layer exhibit a range in interlayer spacing between 10 to 14Å. The TOT sheets of 2:1 phyllosilicates may be neutrally-charged such as talc ($Mg_3Si_4O_{10}(OH)_2$) or pyrophyllite ($Al_2Si_4O_{10}(OH)_2$), but they often show a net layer charge negativity.

1.2.2.2 Clay charge

Two types of charges coexist in clay (*Bentahar 2010*): an external surface charge caused by the OH^- groups of the octahedral sheet which is pH-dependant and a structural charge. The latter is caused by isomorphic substitutions of central cations which may occur in tetrahedral and octahedral sheets of 2:1 clay minerals, with Si^{4+} being replaced by trivalent metal cations such as Al^{3+} and Fe^{3+} in tetrahedral sheet, or Al^{3+} by Mg^{2+} and the other cations in octahedral ones (*Nesse 2000)*, thus inducing or increasing their interlayer surface charge negativity.

To balance this net negative charge, the interlayer of 2:1 clay minerals typically incorporates either:

- cationic metals (e.g. Ca^{2+}, Na^+, K^+), which promote the formation of both Van der Waals interactions and ionic bonds between adjacent sheets, or
- an additional octahedral sheet, forming a TOTO sheet, in which the net negativity of the TOT subunit is compensated by the net positive charge of the additional octahedral sheet (Figure 8) (*Bhattacharyya and Gupta 2008;Nesse 2000;Sposito 1984*).

In the nature, three basic types of clay minerals exist : kaolinite, smectites, and illites (also referred to as mica-like clay minerals, attributed to compositional and structural similarities of illites to muscovite) (*Nesse 2000*).

The TOT + cation clay minerals can be further characterized based on the magnitude of their TOT sheets charge negativity (Table 4 and Figure 8):

- medium permanent charge clay minerals (e.g. smectites) are those that feature a net negative charge between 0.2-0.6 per formula subunit, and this charge is most often compensated by the addition of

Ca^{2+} and Na^{+} cations in the interlayer. The smectite clay mineral, montmorillonite, is an example of a medium charge 2:1 clay mineral (TOT + cation);

- high permanent charge clay minerals (e.g. illites) are those with a net negative charge between 0.8-1.0 per formula subunit, and this permanent charge is typically compensated by the addition of K^{+} cations into the interlayer.

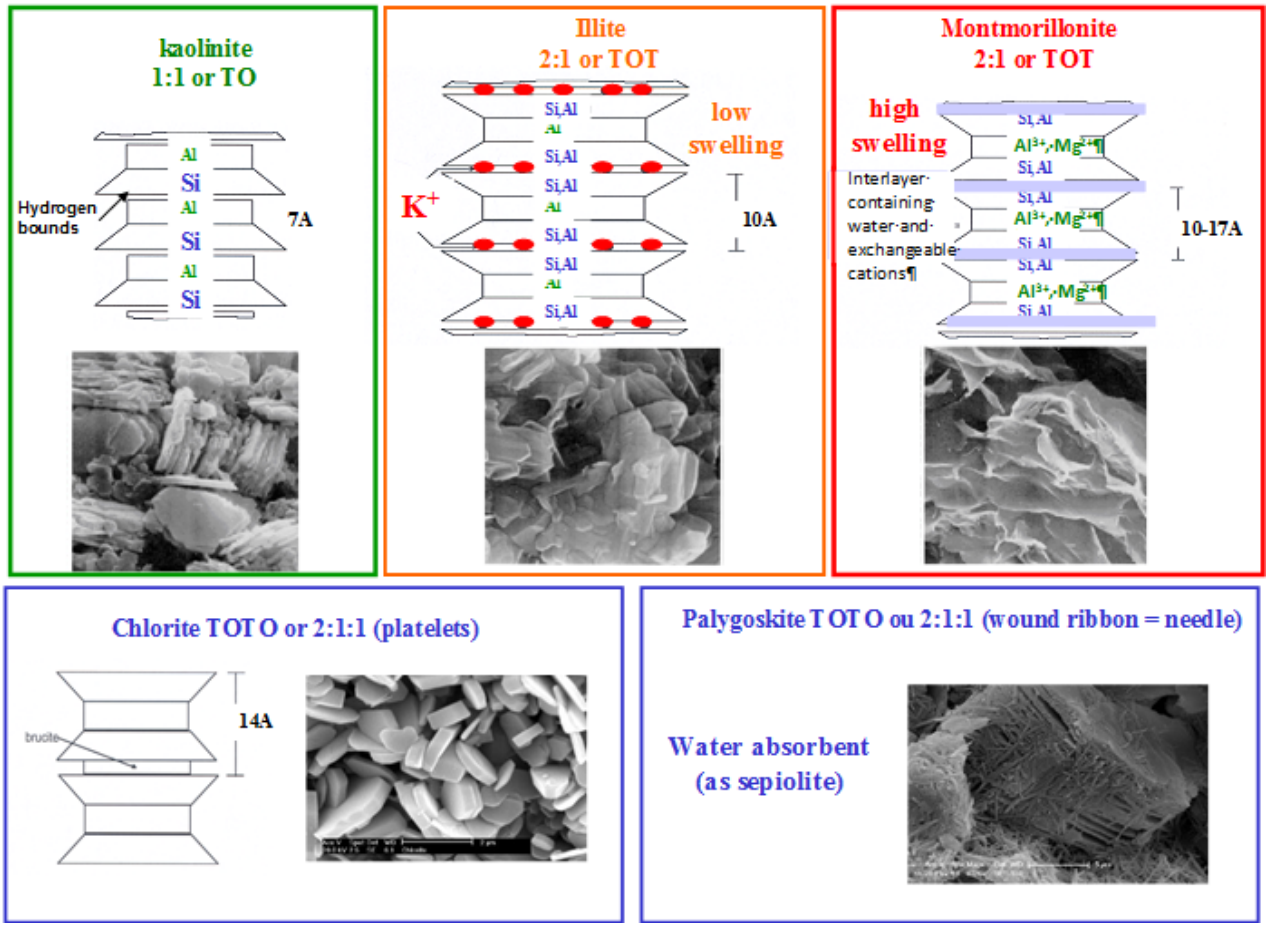

Figure 8 Schematic view of clay minerals layer structures, including 1:1 clay types with tetrahedral -octahedral sheets (TO), and 2:1 clay types with tetrahedral-octahedral-tetrahedral sheets (TOT). Mechanisms of permanent layer charge balance in 2:1 clays include incorporation of cationic metals (TOT + cation) or an additional octahedral layer into the interlayer (*Dyal & Hendricks 1950*)

1.2.2.3 Clay swelling and cation exchange capacity (CEC)

The swelling of clay minerals reflects the ease with which water molecules may enter the interlayer. Importantly, medium permanent charge clay minerals swell upon exposure to water, while high permanent charge clay minerals do not. In fact, water is unable to enter the interlayer of high charge clay minerals, due to the abundant interlayer compensating cations and resultantly stronger electrostatic layer bonding (*Nesse 2000*). However, medium permanent charge clay minerals contain relatively few interlayer cations and inherently weaker electrostatic bonding, thus allowing polar water molecules to cause swelling upon

hydrating the charge compensating cations. As a consequence, further to its layer charge, the swelling of clay is controlled by its cation exchange capacity (CEC), layer charge and the type of exchangeable cation.

Table 4 indicates the correlation between clay structure, structural permanent charge, CEC and swelling properties. The highly swelling smectite group which is marked with orange color has the highest CEC but intermediate layer charge, while the low-swelling illite group has a medium CEC but high layer charge (yellow color).

Table 4 Correlation between clays and its structure, its layer charge, its cation exchange capacity (CEC) and its swelling capacity (S) (*Bouchet et al. 2000*)

Charge (x) of ½ unit cell [a]	CEC	Di-octahedral	Tri-octahedral	S [b]
		Phyllosilicate 1:1		
0	0	kaolinite $Al_2 Si_2 (O_5) (OH)_4$	Serpentine $Mg_3 Si_2 (O_5) (OH)_4$	nS [c]
		Phyllosilicate 2:1		
0	0	pyrophyllite $Al_2 Si_4 (O_{10}) (OH)_2$	Talc $Mg_3 Si_4 (O_{10}) (OH)_2$	nS [c]
		SMECTITES		
0.2 to 0.6	High	Octahedral substitutions montmorillonite $(Al_{2-x}Mg_x) Si_4(O_{10})(OH)_2(CE)_x$ Tetrahedral substitutions beidellite $Al_2 (Si_{4-x} Al_x) (O)_{10} (OH)_2(CE)_x$	Hectorite $(Mg_{3-x}Li_x)Si_4(O_{10})(OH)_2(CE)_x$ Saponite $Mg_3(Si_{4-x}Al_x) (O_{10})(OH)_2(CE)_x$	High S
		MICAS		
0.6 to 0.9	Middle	illite $(Al_{1,75}R_x) Si_{3,5} Al_{0,5} (O_{10})(OH)_2K_{0,75}$	Vermiculite $(MgFe_3)(Si_{4-x}Al_x)$ $(O_{10})(OH)_2Mg_x$	Low S
1	Low	glauconite $(Al_{2-x}Fe^{3+}{}_*Fe^{2+}{}_*Mg_*)(Si_{3,75}Al_{0,25})(O_{10})(OH)_2K$ muscovite $Al_2(Si_3Al)(O_{10})(OH)_2K$	Phlogopite $Mg_3(Si_3Al)(O_{10})(OH)_2(K)$ lépidolite biotite	nS [c]
2		paragonite : CEC Na margarite : CEC Ca	$(Mg,Fe^{2+})_3(Si_3Al)(O_{10})(OH)_2(K)$ clintonite : CEC Ca	
		Phyllosilicate 2:1 + Phyllosilicate hydroxide		
other		donbassite, cookeite, sudoite	chlorite, chamoisite, nimite	nS [c]

[a] Permanent layer charge from clay structure [b] Abbreviation for swelling [c] No swelling

1.2.2.4 Clay specific surface

The specific surface of clay may be defined as the sum of external and interlayer surfaces area per unit mass. Table 5 gathers specific surface area values of the main clay groups together with properties such as cation exchange capacity (*Pentrák et al. 2012*) or the number of layers per particle (*Bentahar 2010*). Observe that water content and cation exchange capacity appear closely related to the specific surface of clay minerals, whereas the number of layers per particle doesn't. In fact, specific surface is often assimilated to the exchange surface. In nonexpanding phyllosilicates such as kaolinite and illite, exchange surface is limited to external surfaces, with the interlayer space between individual subunits remaining void (kaolinite), or

containing interlayer cations (illite) which increase the attraction between the net negatively-charged sheets (*Nesse 2000*). In contrast, expanding phyllosilicates such as montmorillonite are characterized by high specific surface, mainly extensive interlayer surface area available for cation exchange further to external surfaces (*Carter et al. 1986;Maurice 2009)*.

Table 5 Comparison of clay properties

Type of clay	CEC [a] (meq/100g)	Interlayer cations	Number of sheet per particle	Specific surface area SSA[b] (m^2/g)	Water content (5Å layer) (%) [d]
Kaolinite	3-15	n/a	10-150	5-20	0.5
Illite	10-40	K	5-20	50-200	5
Montmorillonite	70-120	Ca ; Na	1-10 (Na) 10-40 (Ca)	700-800	50
Vermiculite [c]	100-150	-	-	760	-
Chlorite	10-40	n/a	-	n/a	-
Sépiolite Palygorskite	20-30	n/a	-	n/a	-

[a] (*Pentrák, Czímerová, Madejová, & Komadel 2012*) [b] (*Bentahar 2010*) [c] *(Morel 1996)* [d] (*Taylor 1969*)

1.2.3 Identification and characterization of clay properties in aggregates

1.2.3.1 X-ray diffraction

According to the statistic report of the Reynolds Cup, which is the international quantitative competition on sedimentary rocks initiated in 2002, more than 97% of the participants apply X Ray Diffraction (XRD) to identify and quantify clay (see appendix 1.2). Usual minerals may be identified by their crystal structure reconstructed from powder XRD pattern upon determining peaks positions and intensity ratio between peaks. Classically, experimental pattern is compared to that of standards from mineralogical database and a good match allows identifying the mineral phases present in the sample (*Brindley and Brown 1980a*).

With clays, identification is more complex. The official classification of phyllosilicates established by the International Mineralogical Association deals only with pure end-number minerals, and divides them into groups, subgroups, and species. Hence, a two-steps procedure is usually implemented (*Laruaz et al. 2013*):

- First, XRD pattern of powder sample hkl planes, where hkl determine the planes orientations using the Miller indexes, allows detecting the presence of various minerals among which clay. In particular, this step allows distinguishing di-octahedral clay minerals, tri-octahedral clay minerals (subgroups) and other complexity (stacking sequences, polytypes et etc.). The preparation of powder sample is, without doubt, one of the most critical step in qualitative and quantitative phase analysis by XRD (*Bish and Howard 1988;Moore and Reynolds 1997*). The success of a preparation technique is strongly dependent on the properties of the multi-phase samples and that no universal procedure is applicable to a wide spectrum of minerals. However, the caring of the two basic steps of sample preparation may probably improve the result from X-Ray powder analysis, namely the fine grinding of the samples and the preparation of the random powder mounts (*Kleeberg et al. 2008*).

- Second, XRD patterns of several oriented glass slides made with sample extracted and treated clay fractions are determined. Clay minerals and their groups can be identified based on the *00l* basal reflections position and evolution before and after treatments.

The references for determination of clay minerals by X-Ray powder and oriented sample are shown in appendix 1.1 for the further details.

There are several methods for quantitative phase analysis used by X-Ray powder diffraction technique, all of them having their advantages and drawbacks (*Brindley 1980;Snyder and Bish 1989;Srodon et al. 2001*). Generally, methods can be divided into two groups: single peak and full pattern fitting methods. Both may easily be applied for quantitative analysis of both oriented samples and random powders.

- Single peak methods (*Chung 1974a;Chung 1974b*) assume that the X-ray energy diffracted by a given clay mineral, calculated as the area of the corresponding major peak, is related to its weight fraction in the mixture by means of a predetermined constant of proportionality. Several such constant values, termed Reference Intensity Ratios (RIR) or mineral intensity factors (MIF) for the two most outstanding methods, are tabulated (*Biscaye 1964;Schultz 1964*) (see appendix 1.2). In the RIR method, RIR coefficients are determined with reference to an easy-to-quantify phase which is often corundum; hence corundum shall be artificially incorporated into the randomly oriented powder samples prior to XRD tests. Note that RIR quantification is absolute, whereas MIF quantification is relative since it refers to an extracted and treated sample of particles generally smaller than 2 μm, hence the share of extracted and treated sample in the original one shall be measured for example using sedimentation. Unfortunately, those predetermined constants as well as details of the evaluation method used are not always available in the literature, yet sometimes kept secret by the laboratories who determined them experimentally (namely within the Reynolds cup).
- The full pattern fitting method (*Bish & Howard 1988*) assumes precise identification of each mineral phase present in the powder sample tested as well as knowledge of a preferred orientation if any. This method consists in simulating the XRD pattern over a wide range of 2 μm values using a pondered sum of simple functions, the ponderation coefficients being the unknown proportions of the various phases. Simple functions may be Gaussians parameterized by their FHWM, each of them describing a peak of the XRD pattern. The simulation quality is maximized upon minimizing the differences between actual and simulated XRD patterns using the pondered least squares method.

The state of clay particles disaggregation, their alteration from chemical pre-treatment, the particle size separation (sedimentation, centrifugation…), the preferred orientation of crystallites in prepared powder samples and the method of assessing clay mineral proportions from the diffraction pattern may all contribute to error in both quantitative methods (*McManus 1991*). Apart from above, the problem with full pattern fitting method is obtaining pure enough standard to maintain a database for use of routine analysis. Besides, the database standard can be useless if the observed, analyzed pattern has not been collected under the same experimental condition, the same diffractomter geometry and even on the same diffractometer type (*Eberl 2003*).Furthermore, wrong instrument setting and inappropriate or incorrect use of software

(*The clay mineral society 2013*), as well as inexact qualitative identification of the minerals are additional sources of bias.

Single peak techniques are simple since direct calculation of mineral phase quantities may be performed, and some authors stated that single peak method is more precise than the full pattern fitting method (*Hillier 2000;Srodon et al. 2001*). However, this quantitative analysis through orientated samples suffered from two facts: there is no reason to expect that all phases have the same degree of preferred orientation and that the analyzed size fraction is representative of the clay in the bulk sample. Moreover, sample preparation for single peak techniques is time consuming, coiefficients, RIR and MIF, for clay minerals are uncertain, and certitude for manual peak decomposition is ongoing.

In the light of the general remark addressed above, the mineralogical analysis of clay-rich aggregates represents specific problem owing to their clay particle size, their flaky shape, the variety of their chemical compositions and structures (presence of polytypes), and their stacking defaults (*Bish and Post 1993*). Thus, published methods of quantitative analysis for clay bearing samples commonly result in a standard deviation up to 20% (*Moore and Reynolds 1989*). The solution to this problem is structure modeling with the Rietveld method (*Rietveld 1969*). The Rietveld method was primarily used as a method for resolving crystal structures because it allows to refine structure parameters. This is the reason that Rietveld method is advocated by 57% of the Reynolds cup participants since it is less time consuming and yields accurate quantification of minerals if the clay composition is known, especially in the absence of a preferential orientation.

1.2.3.2 Methylene blue (MB) tests

Methylene blue has had for a long time many uses in different fields, such as biology and chemistry. In civil engineering, the ability of methylene blue dye to adsorb on soil and rock is used to discriminate the clay mineralogy, essentially according to its particularly high specific surface area and cation exchange capacity compared to other rocks.

Methylene blue (MB) is a heterocyclic aromatic chemical compound with the molecular formula $C_{16}H_{18}N_3SCl$ and a parallelepiped shape of dimensions 17Å x 7.6 Å x 3.25 Å (Figure 9). At room temperature, it appears as a solid, odorless, dark green powder. MB yields a blue solution when dissolved in water. It's a cationic dye. The hydrated form of MB contains 3 water molecules per MB molecule. This molecule may interact with mineral and organic matter by electrostatic forces as it is positively charged.

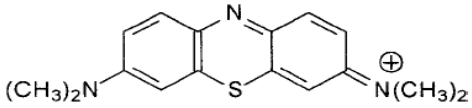

Figure 9 The structure of MB molecule

As shown in Table 6, MB absorption capacity of non-swelling and swelling minerals follows more or less the same tendency as the cation exchange capacity (CEC) *(Pentrák et al. 2012*) and the specific surface area (SSA) (*Bentahar 2010*). The mineral particle size and polar forces (clay surface property that plays a role in MB adsorption) sensitively vary with clay chemical composition and nature of exchangeable cations. Other

parameters may impact also on MB absorption onto clay (in particular the parameters used for testing the adsorptive capacity of aggregates as shown below).

Table 6 Comparison of clay properties (in addition toTable 5)
*** Clay mineral characteristic (*Goldman and Greenfield 1990*)**

Type of clay	MB (meq/100g)	CEC (meq/100 g)	SSA (m^2/g)
Kaolinite	0.5-2	3-15	5-20
Illite	3-5	10-40	50-200
Montmonrillonite	6-30	70-120	700-800
Vermiculite	--	80-150 [a]	600-800 [b]
Chlorite	3-5	10-40	70-100 [b]
Sepiolite palygoskite	--	20-30	n/a

[a] (*Miller and Donahue 1977*) [b] (*www.d.umn.edu/~pfarrell/Soils/powerpoints/Clay%20Mineralogy.ppt*)

MB test procedures

Although several test procedures are in use for assessing the MB adsorption of aggregates, two of them are worth being described:

- The reference MB test method (drop method) described in European standard *NF EN 933-9 (2009)* basically consists in successively adding 5 ml increments of a 10g/l concentrated MB solution to a suspension composed of a 200 g dry mass fine aggregate sample immersed into 500 ml distilled water, then in checking the dye adsorption after each addition by carrying out a stain test on filter paper until the presence of free dye is detected;
- An alternative test method (UV-method) relies on the ability of MB dye to absorb visible UV rays in the [570 nm-760 nm] wavelength range. Indeed, upon calibration using various solutions of known MB concentrations, height measurement of the absorption peak for a fixed wavelength may be used to calculate the residual MB concentration in a solution which has been in contact with an aggregate sample. Practically, the test protocol consists in immersing 0.1- 10 g of fine aggregates into 35 ml of a 1g/l concentrated MB solution, then agitating for 2 hours. Solid and liquid phases are then separated using centrifugation at 19 000 rpm for 20 minutes, and the MB adsorption value is deduced from measuring the difference between initial and final MB concentration in a supernatant sample of the solution using a UV-visible photometer.

MB molecular aggregation on clay surface and clay layer charge effect

In dilute aqueous solutions, methylene blue is a cationic dye that absorbs visible light around wavelength 664 nm, with a weak shoulder at 605 nm. As shown in Table 7, each absorbance wavelengths in the UV-visible domain relates to a more or less aggregated configuration of MB molecules, which is depicted in Figure 10. This molecular aggregation is due to hydrophobic interactions, which is a general tendency of non-polar molecules to associate physically in aqueous solutions (*Bujdák 2006*).

When clay is added to the MB suspension, MB is rapidly and strongly adsorbed on clay surfaces (*Margulies et al. 1988*). Two phenomena may explain this adsorption: first, MB molecules are positively charged and may interact with clay surface through electrostatic forces; second, hydrogens attached to alpha-carbon

atoms of methylene blue molecules may also become active by forming hydrogen bonds with oxygen atoms of the clay mineral layer *(Brindley and Brown 1980b)*. The dye adsorption is always accompanied by color changes which are attributed to the formation of densely packed 2-dimensional cationic dye agglomerates at the clay surface, called H-aggregates, and to clay surface acidification (protonation). *Bergman and O'Konski (1963)* were the first who observed the MB molecular aggregation in montmorillonite suspension by visible spectroscopy.

Table 7 MB molecule configuration related to its absorbance wave lengths in UV-visible domain (*Cione et al. 2000; https://en.wikipedia.org/wiki/Methylene_blue*)

Aggregate	Type	Absorbance of MB solution	Absorbance of MB-clay suspension
MB^+	Monomer	664 *(Margulieset al. 1988)*.	650 (on the external surface of clay) 673 (on the internal surface of clay)
MB_2^+ (or MBH^{2+})	J-aggregate(or MB bivalent protonated compound)	741	763 (on the internal surface of clay) *(del Monte and Levy 1999)*
$(MB^+)_2$	H-dimer	605 *(Margulies et al. 1988)*	596
$(MB^+)_3$	H-aggregate	580 *(Grim et al. 1947;Vansant and Uytterhoeven 1972)*	570 (on the external surface of clay)
peak non associated	--		632

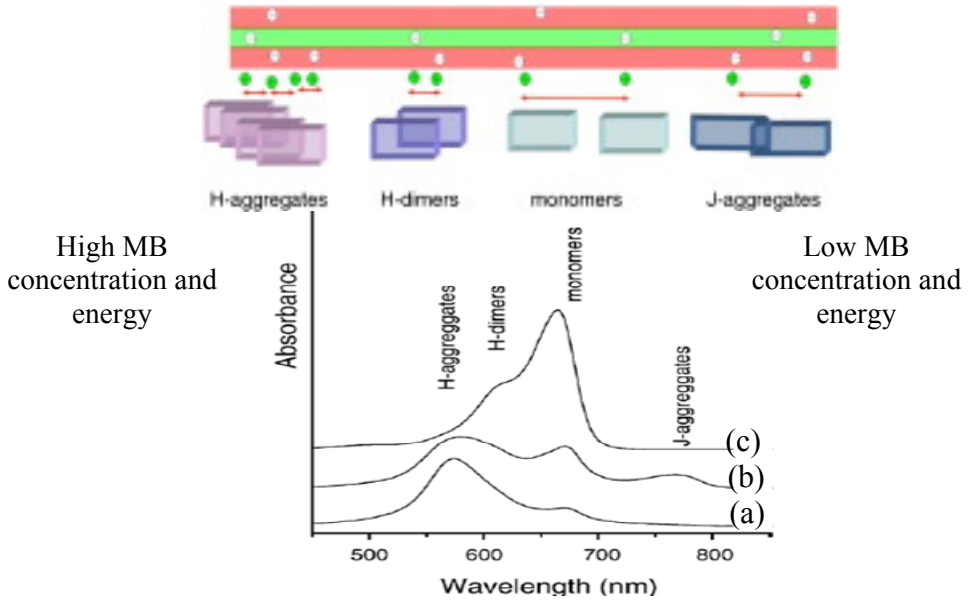

Figure 10 The configuration of MB molecules in clay suspension related to its absorbance wavelength, its concentration and its energy. The spectra of the dispersion measured 1 min (a) and 24 h (b) after mixing the dye solution with the clay dispersion are compared with the MB solution (c) *(Bujdak 2006;Pentrák et al. 2012*)

The properties of H-aggregates can be compared to the behavior of the long chain of adsorbed alkylammonium cations. The high affinity of the clay surface to long-chain alkylammonium cations was ascribed to strong Van der Waals forces between alkyl chains. These forces increase with the size of the alkyl chains *(Grim et al. 1947;Vansant & Uytterhoeven 1972)*. In a similar approach, a face-to-face

interaction between the cationic dye molecules increases the adsorption energy of the adsorbed dye onto the clay surface.

Now, H-aggregates may dis-agglomerate with ageing that's to say by increasing the contact time between clay and MB molecule. For montmorillonites, the persistence of the cationic dye agglomerates against a re-distribution (dis-agglomeration) over time depends on clay layer charge. This dependence was first investigated by *Bujdak (2001)* using a series of reduced-charge smectites (RCMs) resulting from Li-saturation following heating at 200°C (*Bujdak et al 2001;Glaeser and Mering 1967;Greene-Kelly 1955;Hofmann and Klemen 1950*), though similar investigations were also performed on smectites of variable structure, composition and layer charge (*Bujdak et al. 1998;Bujdak and Komadel 1997;Laribi et al. 2008*). Upon performing MB adsorption tests, Bujdak observed that larger agglomerates of MB molecules (H-aggregates) formed predominantly at the surface of high-charge smectites, whereas lower layer charges led to a decrease with time in the length of dye cation agglomerates adsorbed on clay surface in favor of monomers, protonated MB molecule and/or J-aggregates. This was later confirmed by other authors (*Bujdak et al. 2002;Czímerová et al. 2004;Li et al. 2011;Neumann et al. 2002;Pentrák et al. 2012;Yenera et al. 2012*).

Consequently for a fixed quantity of adsorbed MB molecules, the surface of high layer charged clay is covered by islands of dye aggregates instead of being covered homogeneously with dye cations such as monomers (*Ono et al. 1999*). Furthermore, high layer charge holds more tightly the clay layers, which inhibits the migration of the dye into the interlayer space and decreases available clay surface area. Hence, H-aggregates adsorb predominantly at the external surface of high-charge smectites, all the more that strong Van der Waals forces between adsorbed MB molecules prevent their re-arrangement or desorption from clay surface and subsequent adsorption on still uncovered clay sites, resulting in H-aggregates remaining stable with time as confirmed by the persistent peak around 570 nm.

With low layer charged clay, MB molecules may disaggregate into monomer and H-dimer, and then migrate in the interlayer space. *Jacobs and Schoonheydt (2001)* explained that MB interaction at clay surface is a competitive adsorption of water molecules and cationic dye. It leads to the presence of MB molecules either on basal surface or in the electric double layer (generated by surface charge), where MB molecules are surrounded by water molecules and not directly in contact with clay surfaces. These interpretations support the following adsorption processes: first, MB aggregation instantaneously occurs in the vicinity of clay colloid particles within the electric double layer; Second, decomposition of the dye molecular aggregates starts in order to achieve a balance between MB and clay charges (*e.g., Bujdák et al., 1998, 2002a*). Dye aggregate decomposition proceeds slowly for hours or days (see Figure 11) after or during the adsorption of initially formed aggregates that reached the clay basal surfaces (*Bujdak J., 2002*). Consequently, monomers, protonated dye cations and/or J-aggregates are favored (*Bujdak, 2001*), though J-aggregates which are formed by head-to-tail intermolecular interaction *(Kobayashi, 1996)* only occur at solid-liquid interface in low concentrated dye solutions *(del Monte, 1999).*

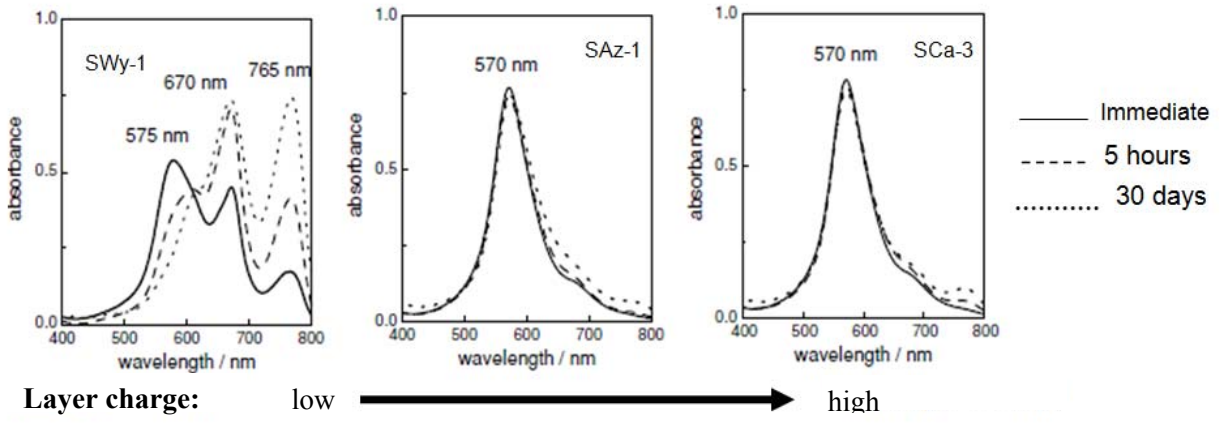

Figure 11 Evolution with contact time of UV-visible absorbance peak measured on MB suspension of various charged bentonites (*Neumann et al. 2002*)

Table 8 Characteristics of the three bentonites in Figure 11 (*Neumann et al. 2002; http://www.clays.org/SOURCE%20CLAYS/SCdata.html*)

Properties	SWy-1	SAz-1	SCa-3
Charge:			
Octahedral	-0.53	-1.08	-1.29
Tetrahedral	-0.02	0	-0.19
Interlayer	-0.55	-1.08	-1.48
CEC (meq/100g)	79	120	153
Specific surface area (m^2/g)	800	736	825
Substitution	Predominantly octahedral		
Origin from U.S.A.	Wyoming.	Arizona.	California.
Composition			
SiO2	62.9	60.4	64.4
Al2O3	19.6	17.6	14.4
Fe2O3	3.35	1.42	1.77
MgO	3.05	6.46	9.87
Na2O	1.53	0.063	3.28
CaO	1.68	2.82	0.053

MB molecular orientation on clay surface

The conventional assumption of MB adsorption with a molecular orientation parallel to the surface (Figure 12 (a), right particle), which had long been assumed for clay surfaces, was disputed after a study on mica surface behavior. It was reported that the MB molecules were tilted (Figure 12 (a) left particles and b,), with their largest face inclined at 65–70° with respect to the mica surface (*Hähner et al. 1996*) and up to almost 90° *(Kobayashi 1996*). High charge density on mica surfaces could explain such a tilted arrangement, as it allows a higher density of dye cations to be adsorbed thanks to a reduction in the covered area from 130 $Å^2$ for the conventional assumption to 66 $Å^2$ per molecule. Furthermore, this tilted arrangement allows the formation of large-size molecular aggregates on flat surfaces.

A similar model for MB molecular orientation was stated in later studies on MB-clay suspension (*Bujdak et al. 2003*) and on clay Langmuir–Blodgett films (*Umemura 2003*). *Bujdak (1997, 1998)* reported that the surface area occupied by a MB cation on a smectite where it is adsorbed is about the same as the average

area per negative layer charge (*Bujdak et al. 1997*). The distribution of the negative layer charge controls the distances between the adsorbed neighboring MB cations at the smectite surface. Orientation of MB cations nearly perpendicular to the clay mineral basal surface, as was proved for micas, enables the existence of large, multi-cation dye agglomerates that keep basal spacing d_{001} of MB-clay complexes ≤ 17,5 Å *(Bodenheimer and Heller 1968;Hang and Brindley 1970*). Although the dye molecular plane is perpendicular with respect to the clay surface plane, the longest axis of a MB cation may remain rather parallel or tilted at low angles with respect to the clay surface plane (Figure 12 (c)) (*Bujdak et al. 2003*). The angle of tilted MB plane is modified by the layer charge of mineral, and probably, electrostatic interaction between negatively charged surface and positively charged groups of dye cations that plays a major role (*Bujdak et al. 2008*).

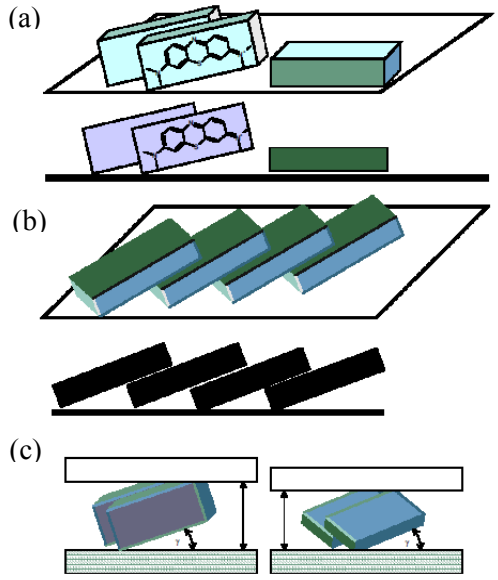

Figure 12 The model of the orientation of MB molecules on various surface. (a) The model of tilted orientation with cations facing the surface with their edges as it mostly appears in the literature (left), and parallel orientation (right). (b) The model of interdigitated arrangement of dye cations adsorbed on the clay surface. (c) Tilted orientation as shown in (a) without (left) and with a tilt to other side by rotation around the longest molecular axes (right). The effect of the tilting to the other side on the basal spacing is shown.(*Bujdak, Iyi, Kaneko, & Sasai 2003)*

Parameters affecting MB adsorption measurement

As previously mentioned, MB molecules may have different configurations (aggregation and orientation) when in contact with clay, which will affect the quantity of MB adsorbed on clay surfaces. In the presence of MB aggregation, MB adsorption onto a clayey material will increase compared to the case without aggregation, thus operator obtains a large MB value interpreted as high clay content. Not only the clay mineralogy impacts on the MB adsorption value but also other parameters such as the clay layer charge, contact time, temperature, MB measuring conditions (such as the MB concentration or the solid concentration used during the test), solution pH and salt concentration, nature of the cations, particle size,… The parameters which modify the MB aggregation are listed in Table 9 (additional details are given in Appendix 2). These effects may differently affect the MB value depending on the protocol of measurement: although commonly applied, the drop method disregards MB adsorption kinetic or clay particle size and is

biased by the operator subjectivity; MB test based on UV-method may produce MB values of higher quality if the protocol of measurement is totally mastered, but then difficulties remain to decouple all effects evidenced on UV-visible spectra. Hence, considering the large number of parameters impacting on MB adsorption, the MB test for engineering purpose as done actually may be questioned. In practice for engineers, it means that MB measurement doesn't represent in all cases the specific surface area of the material. Thus, understanding the impact of those parameters on MB test is a key step to improve the representativeness of MB value in terms of clay harmfulness in engineering field.

Table 9 Factors which impact MB or clay aggregation and MB adsorption on clay

Parameters	criterion	Impact on MB adsorption		
		Increase	Decrease	Ref.
pH (for kaolinite)	pH value compared to that of clay PZC	when pH away from PZC	when pH is close to PZC	*(Al-Ghouti et al. 2003;Ghosh and Bhattacharyya 2002;Gurses et al. 2006;Schroth and Sposito 1997;Zhang et al. 2013)*
Temperature	Sign of free enthalpy of adsorption	Low temperature (since ΔH>0)	High temperature (since ΔH>0)	(*Gurses et al. 2004, 2006; Zhang et al. 2013)*
Testing time (contact time)	MB diffusion into interlayer	Complete dispersion	Incomplete dispersion	(*Cione et al. 1998)*
MB concentration in solution	Higher than CEC or not	High MB concentration	Low MB concentration	(*Jacobs and Schoonheydt 1999;Schoonheydt and Heughebaert 1992*)
Ionic force	Ion concentration in solution	Lower salinity	Higher salinity	(*Cione et al. 2000;Neumann et al. 2002)*
Nature of exchangeable cations	Hydrated radius of ion	Large hydrated radius	Small hydrated radius	(*Conway and Ayranci 1998;Cotton and Wilkinson 1980;Czímerová et al. 2004;Dzene et al. 2015;Li et al. 2011;Michot and Villieras 2006;Myers 1999;Neumann et al. 2002;Smith 1977;Tansel et al. 2006;Xu et al. 2008;Zhang et al. 2013)*
Clay particle size	Specific surface	Small particle size	Large particle size	*(Bujdak et al. 2001;Cenens and Schoonheydt 1988;Gessner et al. 1994;Kobayashi 1996;Neumann et al. 2002)*
Clay mineralogy/layer charge	Swelling / non-swelling	Swelling (low layer charge)	Non-swelling (high layer charge)	*(Goldman & Greenfield 1990)*

1.2.3.3 Cation exchange capacity (CEC) test

The determination of soluble cations, bound cations and cation exchange capacity are used to evaluate the exchange complex and the cation exchange capacity from clay-rich fine aggregates (*ASTM D7503-10 2010*). The cation exchange capacity test measured by UV-photometer is commonly applied in the laboratory because of its less time consuming. As the same principle and protocol as MB UV-method, CEC test relies on the ability of dye to absorb visible rays. Hexaamminecobalt chloride is a one of cation exchange dyes used to measure CEC value by detecting absorb visible UV rays in the [350 nm; 600 nm] wavelength range.

For clay minerals, the CEC is dependent upon the pH of the sample. As sample acidity increases (pH decreases), more H^+ ions are attached to the colloids. They have pushed the other cations from the colloids and into the soil water solution. Inversely, when soils become more basic (pH increases), the available cations in solution decrease because there are fewer H^+ ions to push cations into the soil solution from the colloids (CEC increases) (*Havlin et al. 2010*).

1.2.4 Correlations between clay properties

1.2.4.1 Correlation between clay structure and electric charge

Christidis and Eberl (2003) reported that there is a relation between the total charge calculated using the LayerCharge program and d_{001} (or interlayer spacing) value analyzed from the K-saturated, ethylene glycol-solvated, oriented samples. The method utilizes the different degrees of swelling of smectite layers depending on layer charge and charge distribution. As the low - and high - charge smectites are separated by amount of scattering from XRD, he suggested the layer-charge boundary between low - and high - charge smectites is -0.47 per half unit-cell, with the 001 reflection boundary at 15.5 Å (Figure 13).

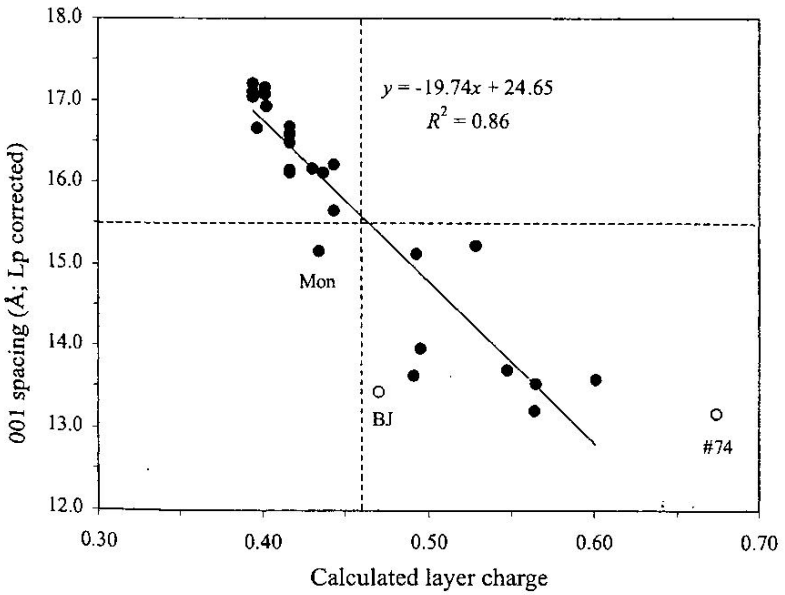

Figure 13 Relationship between calculated layer charge and d_{001} spacing of K-saturated smectites. LCS = low-charge smectites, HCS = high-charge smectites, Mon, BJ and #74 is the name of sample which is not following this classification. The dashed lines separate low-from high-charge smectites according to their layer charge and d_{001} spacing (*Christidis and Eberl 2003*).

1.2.4.2 Correlations between MB value, SSA and CEC

The relations are based on the conventional assumption that MB molecules form a monolayer of monomer (non-aggregated molecules) whose largest surface lies parallel to the clay surface (the unit surface coved by a molecule is 130 $Å^2$ in this case) (*Hang & Brindley 1970*). Correlation between MB adsorption (MB in g/100g) and specific surface area (SSA in m^2/g) measured by ethylene glycol adsorption (Eq. 1) was exposed in 1950 by *Dyal (1950)*, whereas the correlation between MB adsorption (MB in g/100g) and cation exchange capacity (CEC in g/100g, see Eq. 2) was exposed in 1988 (*Clement 1988*). Between 1950

and 1988, Hang and Brindley *(1970)* published also the measurement of specific surface area of clay and CEC using the methylene blue as adsorbate.

$$\text{SSA } (m^2/g) = \frac{\text{MB (g/g of material)}}{\text{Mwt of MB (g/mol)}} \times 130 \ \frac{10^{-20}\,m^2}{\text{molecule}} \times 6.02 \times 10^{23} \ \frac{\text{molecule}}{\text{mol}} \qquad \text{Eq. 1}$$

$$CEC \ \ (meq/100g) = \frac{10 \times MB \ \ (g/g)}{\text{Mwt of MB (g/mol)}} \qquad \text{Eq. 2}$$

with Mwt, the molar mass of methylene blue : Mwt (MB) = 319.9 g/mol

However, equations Eq. 1 and Eq. 2 may be questioned because experimental results demonstrated that the above-mentioned conventional assumption was wrong. Indeed, MB molecules may aggregate and have an orientation on clay surface that is not parallel to their larger face. As a consequence, the quantity of adsorbed methylene blue molecules is no longer proportional to the surface area of clay but depends also on several parameters such as the clay layer charge or the protocol of measurement. A change in the protocol of measurement may impact the resulting MB value. In practice, the drying of clay-rich sand before MB test may induce a change in MB value. Such an observation illustrates the misunderstanding of the relation between clay behavior and MB adsorption.

1.3 Bitumen

1.3.1 Definition and functional groups

Bitumen[2], so called asphalt, may be seen as a colloidal system consisting of high molecular weight micelles dispersed or dissolved in a lower molecular weight oily medium (*Read and Whiteoak 2003*). It is elaborated in refineries where crude oil is separated, purified, blended, and sometimes chemically or physically changed into organic compounds suitable for asphalt concrete pavement uses. Approximately 85 % of all industrial bitumen is used nowadays in airfield and road construction or maintenance, the remaining 15% being mainly made of oxidized bitumen for applications such as roofing, paints, carpet tiles etc. (*Allsop et al. 1995b*).

As bitumen contains too many organic compounds to be studied one by one, these have been gathered into four "**functional groups"** concisely named SARA after their different functions conferred by their composition, chemical reactivity and rheological properties (Figure 14): asphaltenes, resinous components (polar aromatics), non-polar aromatics (naphtene aromatics) and saturates (*shell bitumen 1995*). Asphaltenes are black or brown amorphous solids corresponding to the insoluble part of bitumen in n-heptane, but soluble in toluene (*ASTM D3279 2007*). Note that solubility must be understood here as "not generating a precipitate" and not as molecular solubility, since asphaltenes are known to form micelles in toluene. Further to hydrogen and carbon, asphaltenes contain some heteroatoms such as nitrogen, sulphur, oxygen, which are responsible for their polarity, and traces of transition metals such as Ni, Va, Fe, etc... The remaining three functional groups are n-heptane soluble and they form the oily medium called the maltenes,

[2] The terms **bitumen** and **asphalt** are mostly interchangeable, except where asphalt is used as an abbreviation for asphalt concrete

because of their resemblance to maltha, a soft kind of native bitumen (*Richardson 1910*). At room temperature, saturates are colorless to lightly colored hydrocarbon compounds, whereas naphtene aromatics are yellow to red liquids and resins are black solid hydrocarbons containing small amounts of oxygen, sulfur and nitrogen heteroatoms (*Corbett 1969*). Figure 15 illustrates the organization of bitumen compounds. Additional description of functional groups may be found in Appendix 3..

Further to these functional groups, most bitumens contain a small percentage of paraffin constituents, the amount, chemical constitution and consistency of which vary with the origin of the crude oil and the processing route used. The wax content is specified in a number of countries, as it may change the rheology of bitumen.

1.3.2 Properties of functional groups

For a given HMA, bitumen is generally selected based on macroscopic thermomechanical properties such as **penetration grade**[3], rheology, viscosity, stability, etc., on which requirements are set to meet climate, traffic load and materials (aggregates) constraints. These properties are mainly controlled by the microscopic properties of bitumen functional groups pondered by their relative proportions, which shall be examined as they affect the bitumen-clay adhesion.

Table 10 summarizes the main properties of bitumen functional groups. Saturates and aromatics may be seen as carriers for the polar aromatics, i.e. resins and asphaltenes. The polar aromatics are responsible for the visco-elastic properties of bitumen at ambient temperature due to association of the polar molecules which leads to large structures and in some cases even three-dimensional network, i.e. the so-called "gel" type bitumen. The degree to which this association takes place depends on the temperature, molecular weight distribution, concentration of polar aromatics and solvating power of saturates and aromatics in the maltenes phase. If the concentration and molecular weight of asphaltenes is relatively low, they will appear fully peptized resulting in "sol" type bitumen. The different constituents of bitumen follow a colloidal law, expressed by the colloid index *(Gaestel et al. 1971;Pfeiffer and Saal 1940;Pfeiffer and van Doormaal 1936*):

$$\text{Colloid index } (CI) = \frac{dispersed constituents}{flocculated constituents} = \frac{aromatics + resins}{saturates + asphaltenes} \qquad \text{Eq. 3}$$

A high colloidal index means that the asphaltenes are more peptized by resins in the oil based medium. The molecular weight of nonpolar molecules, which are saturates and aromatics, is related to low temperature performance (*Jones, 1992*). A preponderance of high-molecular weight molecules such as aromatics will lead to asphalts that stiffen and perform poorly at low service temperatures, whereas an excess of saturates will make bitumen crystallize at low temperatures and become crack susceptible. The association process

[3] *The penetration grading system was developed in the early 1900s to characterize the consistency of semi-solid asphalts. Penetration grading quantifies the following asphalt concrete characteristics: penetration depth of a 100 g needle 25° C (77° F), flash point temperature, ductility at 25°C (77°F), solubility in trichloroethylene, thin film oven test(accounts for the effects of short-term aging that occurs during mixing with hot aggregate), retained penetration, ductility at 25° C (77° F). Penetration grading's basic assumption is that the less viscous the asphalt, the deeper the needle will penetrate. This penetration depth is empirically correlated with asphalt binder performance. Therefore, asphalt binders with high penetration numbers* ***(called "soft")*** *are used for cold climates while asphalt binders with low penetration numbers* ***(called "hard")*** *are used for warm climates. (from : http://www.pavementinteractive.org/article/penetration-grading/)*

persists within the bitumen on cooling and forms the basis of the colloidal structure of bitumen. The gel structure is destroyed on heating and reforms on cooling. On stronger and more prolonged heating the asphaltenes micelles may dissociate. Hence, the asphaltenes content has a large effect on the rheological characteristics of bitumen. Increasing the asphaltenes content produces harder bitumen with lower penetration grade, higher softening point and consequently higher viscosity (*Bukka et al. 1994;shell bitumen 1995*).

Polar molecules network assembles thanks to hydrogen and rigid covalent chemical bonds, the latter consisting of strong σ-bonds and weak aromatic-specific π-bonds[4] responsible of their graphite-like stacks (*Transportation Research Board, 2003*). Nonpolar functional groups form the matrix in which the network is embedded (*Jones 1992*). The degree of polarity is the most important property of polar molecules, while the degree of aromaticity refers to the chemically stable nature of rings of atoms which is the second most important property. Highly polar and highly aromatic molecules form the most interactive and strongest molecular networks. Nonpolar molecules do not interact strongly enough to form networks, but they do substantially influence asphalt performance. Furthermore, asphaltenes carry permanent electrical charges which are caused by their π–bonds, yielding an overall positive charge (*Becker 1997;Bukka et al. 1994;Fotland and Anfindsen 1998;Taylor 1998*).

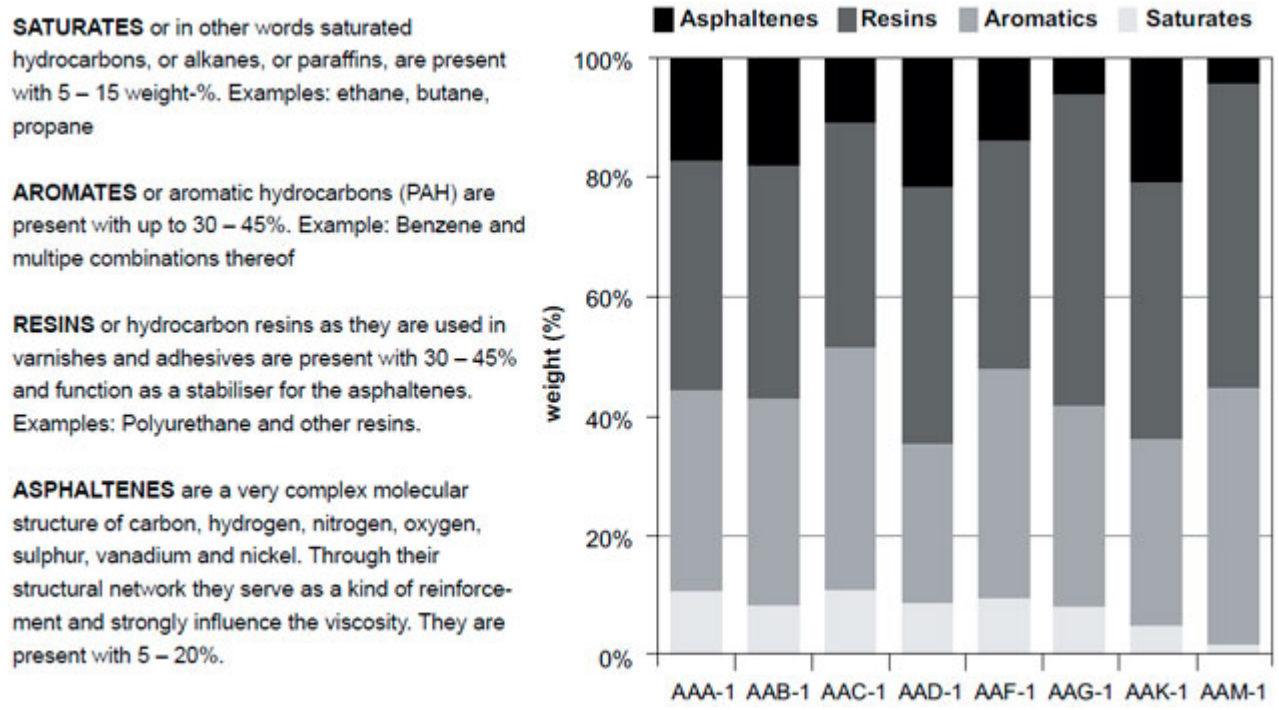

Figure 14 The bitumen chemistry: short description of SARA groups and examples of bitumen compositions (http://www.bitumina.co.uk/bitumen-crude.html)

[4] Sigma bonds (σ bonds) and pi bonds (π bonds) are the covalent bonding mainly generated by the structure of chemical compound. In the bitumen chemistry, sigma bonds are the strongest type of covalent chemical bond whereas π–π bonds are unique to aromatic molecules (*Transportation Research Board, 2003*).

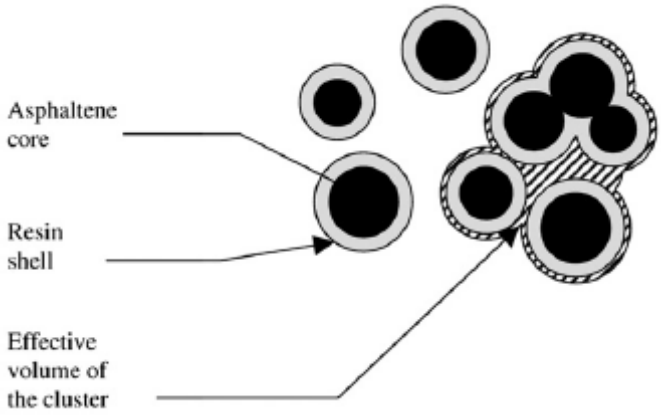

Figure 15 A simplified view of the colloidal structure of bitumen: the asphaltenes micelles are pictured as spherical to illustrate the concepts of salvation layer (resin shell) and effective volume. The oily dispersion medium is called the maltenes. (*Lesueur, 2009*)

Table 10 The properties of functional groups in bitumen

	Group by solubility	Solubility parameter [a] (MPa)	Color	Polarity	Molecular weight (g/mol)	Wt.%	Density at 20°C (g/cm^3)	Structure	H/C [b]	Viscosity	Particle size
Saturates	n-heptane soluble: Maltenes (*Richardson, 1910*)	15-17 *(Speight, 1999)*	lightly colored liquid	**Very few**	600 *(Lesueur, 2009)*	5-15 *(Corbett, 1969; Claudy, 1992)*	0.9 *(Corbett, 1969)*	Mainly Aliphatic *(Pieri, 1995)*	2 *(Lesueur, 2009)*	Low	-
Aromatics (naphthene aromatics)		17-18.5 *(Speight, 1999)*	yellow to red liquid	**non**	800 *(Lesueur, 2009)*	30-45 (*Corbett, 1969*)	1 (*Corbett, 1969)*	slightly aliphatic; lightly condensed aromatic rings	N/A	Higher than saturates *(Claudy, 1992 a&b)*	-
Resins (Polar aromatics)		18.5-20 *(Speight, 1999)*	black solid (*Corbett, 1969)*	**polar**	1100 *(Koots, 1975)*	30-45 *(Corbett, 1969)*	1.07 *(Corbett, 1969)*	fused aromatic rings *(Pieri, 1995)*	1.38-1.69 *(Koots, 1975)*	Close to asphaltenes	1-5 nm *(Transportation Research Board, 2003)*
Asphaltenes	n-heptane insoluble: asphaltenes *(ASTM D3279, 2007)*	17.6-21.7 in toluene *(Speight,1999; Lian et al. 1994; Laux et al. 1997)*	black solid *(Corbett, 1969)*	**highest**	1,000-10,000 *(Allsop, 1995; Lesueur, 2009; Speight, 1999)*	5-20 *(Corbett, 1969; Speight, 2004)*	1.15 (*Corbett, 1969*)	fused aromatic rings with pending aliphatic chains; more condensed aromatic rings	0.98-1.56	Highest	5-30 nm (2-5 nm/unit) *(Yen, 1961)*

[a] positive square root of cohesive-energy density (potential energy per unit volume) (*Lian et al. 1994*)
[b] hydrogen to carbon molar ratio

1.4 The interaction between water, bitumen and clay

Clay takes the form of dust coated more or less uniformly on aggregate surface, or clusters embedded into bitumen coated fine aggregates (mastic) (Figure 16). Given its hydrophilic behavior which is known to impact on the mechanical resistance of HMA, clay shall be protected against water. As this may be achieved by bitumen, a state-of-the-art review of bitumen/clay bonding will first be performed, then this review will be extended to the adverse effect of water at the bitumen/clay interface. In both cases, parameters influencing the bitumen/clay or bitumen/clay/water interaction will be identified.

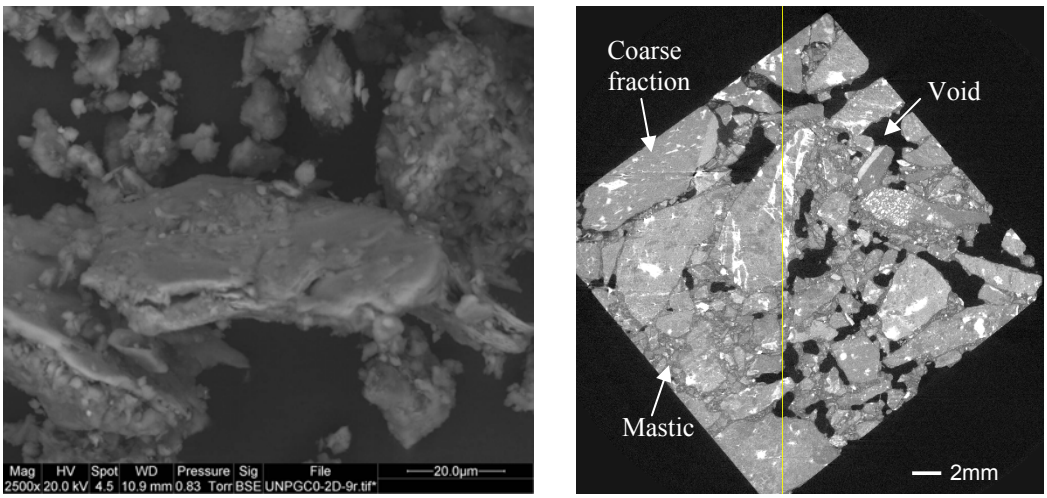

(a) (b)

Figure 16 The images of (a) clay-rich fine aggregates from SEM and (b) clay-rich AC mixture reconstructed by tomography (illustration from this study)

1.4.1 Bitumen-clay bonding

1.4.1.1 Bonding theories

Terrel and Shute (1989) describe four theories often used to explain the adhesion between bitumen and aggregate: **chemical reaction, molecular orientation, mechanical adhesion and surface energy** The chemical reaction theory is based on work performed by *Hubbard (1938)*, who postulated that bitumen acidic constituents such as carboxylic acid (asphaltenes functional group) react with aggregate to form ionic-bound water-insoluble compounds. Though Taylor (*1998*) and Fotland (*1996*) concluded that asphaltenes could hence behave like ions in solution. Hefer and little (*2005*) showed that the weak nature of carboxylic acid was unlikely to yield such strong bounds, making a stronger case for weaker hydrogen bonds between carboxylic acid and silanol groups. Furthermore, *Yoon and Tarrer (1988)* reported that functional groups involved in the bitumen/aggregates chemical bonding depends on aggregate mineralogy, with non-polar bitumen molecules (saturates and naphthene aromatics functional groups) bonding aggregates with low silica content through dispersive Van der Waals interactions. The molecular orientation theory assumes that polar bitumen molecules (resins and asphaltenes functional groups) orient themselves in the direction of polarization of aggregate ions so that the former migrate towards the latter under electrostatic forces. Mechanical adhesion is caused by the interlocking of bitumen into the surface

microtexture or accessible porosity of aggregates. Eventually, surface energy refers to the predominant theory invoked to explain both the bitumen/aggregate adhesion and bitumen internal cohesion caused by intermolecular forces, which is detailed in the next section.

1.4.1.2 The surface energy theory

By definition, the surface energy γ (J/m²) of a solid or liquid is the energy dW (J) needed to disrupt intermolecular bonds in order to create a new element area of surface dS (m²) under vacuum:

$$\gamma = \frac{dW}{dS} \qquad \text{Eq. 4}$$

As a consequence, causing a rupture inside a liquid, which creates two element areas, will require the following cohesion energy W_L:

$$W_L = 2\gamma_L \qquad \text{Eq. 5}$$

Note that γ is homogenous to a force by unit length (N/m), called surface tension. Hence, γ may equally well be called surface energy or surface tension.

Upon assuming that intermolecular bonds consist of polar metal or hydrogen bonds or originate from dispersive Van der Waals forces, Fowkes (*1964*) gave the following empirical expression of the surface energy:

$$\gamma = \gamma^p + \gamma^d \qquad \text{Eq. 6}$$

where p and d indexes refer to polar metal/hydrogen and dispersive bond energies respectively.

When two non-miscible liquids are in contact, say liquids 1 and 2, dissymmetrical intermolecular forces inside each liquid yield the creation of an interface. The interfacial energy γ_{12} needed to create an element area of the interface corresponds to the surface energy of each liquid less the energy corresponding to attraction forces between liquids. Upon limiting the latter to dispersive forces, Fowkes (*1964*) gave the following expression of the interfacial energy:

$$\gamma_{12} = \gamma_1 + \gamma_2 - 2\left(\gamma_1^d \gamma_2^d\right)^{1/2} \qquad \text{Eq. 7}$$

$$\text{where } W_{12} = 2\left(\gamma_1^d \gamma_2^d\right)^{1/2} = \gamma_1 + \gamma_2 - \gamma_{12} \qquad \text{Eq. 8}$$

corresponds to the reversible adhesion energy.

Interaction between bitumen and aggregates involves a liquid and a solid. When such a liquid droplet is deposited on a perfectly flat and horizontal solid surface, equilibrium as shown on Figure 17 is eventually reached. Upon writing the equilibrium of surface tension forces at the triple point, where solid, liquid and air phases intersect, Young (*1805*) established the following relation between the liquid contact angle θ_{SL}, the solid and liquid surface tensions γ_S and γ_L, and the interfacial tension γ_{SL} (the spreading pressure resulting from adsorption of the liquid vapor on the solid surface is assumed to be equal to zero) (*Young 1805*):

$$\gamma_L \cos\theta_{SL} = \gamma_S - \gamma_{SL} \qquad \text{Eq. 9}$$

Dupre (1869) expressed the work of adhesion W_{ad} between solid and liquid as (*Dupre and Dupre 1869*):

$$W_{ad} = \gamma_S + \gamma_L - \gamma_{SL}$$ Eq. 10

Upon injecting Eq. 9 into Eq. 10, the work of adhesion may be expressed as:

$$W_{ad} = \gamma_L (1 + \cos\theta_{SL})$$ Eq. 11

Then, Owens and Wendt (1969) have adapted the Fowkes (*1964*) model to liquid/solid interaction, upon considering both polar and dispersive adhesion forces (*Ottner et al. 2000*):

$$\gamma_{SL} = \gamma_S + \gamma_L - 2(\sqrt{\gamma_S^P \gamma_L^P} + \sqrt{\gamma_S^d \gamma_L^d})$$ Eq. 12

Hence, Eq. 9 and Eq. 12 yield the following relation:

$$\frac{\gamma_L (\cos\theta_{SL} + 1)}{2(\gamma_L^d)^{1/2}} = (\gamma_S^P)^{1/2} \frac{(\gamma_L^P)^{1/2}}{(\gamma_L^D)^{1/2}} + (\gamma_S^d)^{1/2}$$ Eq. 13

Whereas Eq. 10 and Eq. 12 yield the following expression of the work of adhesion:

$$W_{ad} = 2(\sqrt{\gamma_S^P \gamma_L^P} + \sqrt{\gamma_S^d \gamma_L^d})$$ Eq. 14

Based on Fowkes' work, *Van Oss et al (1987)* have refined the polar terms appearing in Eq. 6 and Eq. 12 by suggesting that these terms refer to Lewis[5] acid-base interactions which are furthermore asymmetrical (*van Oss et al. 1987*), insofar as Lewis acid or Lewis base properties of each interacting material involve different surface energy polar components. As a consequence, they have rewritten these polar terms as:

$$\gamma^p = \gamma^- + \gamma^+$$ Eq. 15

$$\sqrt{\gamma_S^P \gamma_L^P} = \sqrt{\gamma_S^- \gamma_L^+} + \sqrt{\gamma_S^+ \gamma_L^-}$$ Eq. 16

where "-" and "+" refer to Lewis base and Lewis acid components of each interacting material respectively.

Finally, Eq. 11 and Eq. 14 yield the following relation:

$$\gamma_L (\cos\theta_{SL} + 1) = 2(\sqrt{\gamma_S^- \gamma_L^+} + \sqrt{\gamma_S^+ \gamma_L^-} + \sqrt{\gamma_S^d \gamma_L^d})$$ Eq. 17

In practice, although the solid surface is neither perfectly flat nor horizontal, using several liquids of known (γ_L^P; γ_L^D) or (γ_L^-; γ_L^+; γ_L^D) values and measuring corresponding θ_{SL} contact angles allows calculating the solid surface energy values (γ_S^P; γ_S^D) through Eq. 13 or (γ_S^-; γ_S^+; γ_S^D) through Eq. 17.

Once these values are known, the quality of adhesion of liquids of known polar and dispersive components on the solid may be assessed, which strongly depends on solid surface wettability. According to Lavielle (1989), a liquid wets a solid if the work of adhesion W_{ad} of this liquid on the solid is higher than the cohesion energy W_L of the liquid, otherwise stated if the spreading coefficient S_E of the liquid on the solid is positive or equal to zero, with $S_E = W_{ad} - W_L$. Using Eq. 5, Eq. 10 and Eq. 11, S_E may be expressed as:

$$S_E = \gamma_S - \gamma_L - \gamma_{SL} = -\gamma_L (1 - \cos\theta_{SL})$$ Eq. 18

Eq. 17 shows that positive values of S_E correspond to high surface energy of the solid, low surface energy of the liquid and low contact angle (Figure 17).

[5] Lewis acid is a chemical specie that reacts with a Lewis base to form a Lewis adduct. A Lewis base, then, is any species that donates a pair of electrons to a Lewis acid to form a Lewis adduct. For example, OH^- and NH_3 are Lewis bases, because they can donate a lone pair of electrons (*Wikipedia*).

According to this theory, interaction between bitumen and aggregates may be described using contact angle and polar or dispersive components associated to the functional groups that act at the interface. The goal is to increase the wettability to have a good covering of the aggregate surface by bitumen. A low contact angle (Figure 17) corresponds to a good adhesion and is obtained when bitumen and aggregates have the same type of surface forces on both sides (dispersive–dispersive or polar-polar).

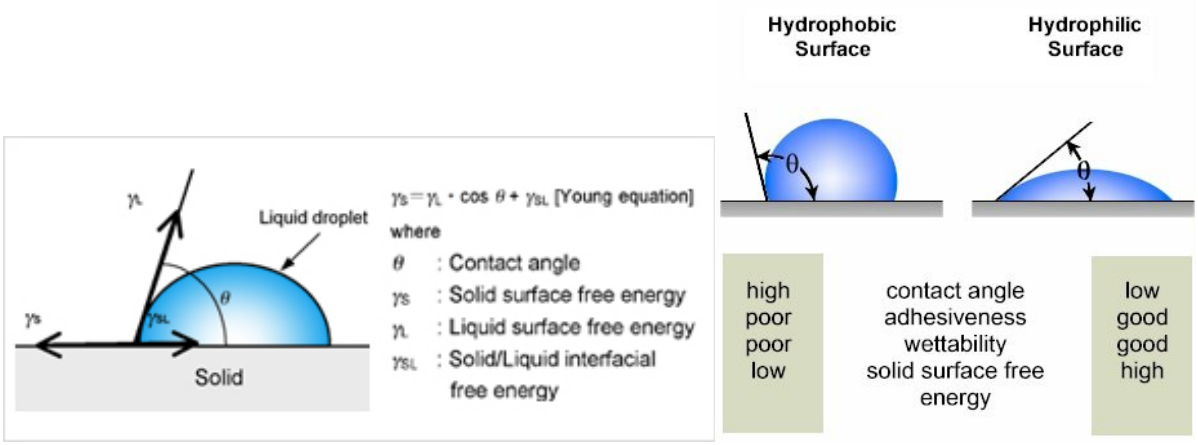

Figure 17 Contact angle between a droplet (L) and a flat horizontal solid surface (S) on which it is deposited, (left) Illustration of Young's equation at equilibrium (*Jouany 1991*), (right) illustration of surface wettability by the liquid as a function of contact angle (*http://www.ramehart.com/contactangle.htm*).

1.4.1.3 Clay surface energy measurements from contact angle methods

Contact angle measurements are often used to indicate clay wettability and interfacial tension (*Rogers et al. 2005*). *Shang et al. (2008)* recommends in Table 11 specific methods for contact angle measurements for typical soil colloids.

Table 11 Recommended contact angle measurement methods for subsurface colloids with water (*Shang et al. 2008)*

Subsurface colloid	Contact angle measurement method				
	Static sessile drop	Dynamic sessile drop	Wilhelmy plate	Thin-layer wicking	Column wicking
Ca-smectite	×	○	×	○	○
Ca-kaolinite	×	×	×	×	○
Ca-illite	○	×	×	○	○
Goethite	×	×	○	○	○
Hematite	×	×	○	○	○

× denotes recommended method.
○ denotes not recommended method.

Among these methods, the static sessile drop method (*Neumann and Good 1979*) is of particular interest as it has been widely used to assess the surface energy of solid surfaces. The method consists in depositing a few microliters of a liquid onto a plane horizontal solid surface, then in measuring the contact angle previously defined (Figure 17) using a microscope-goniometer system. For powders, a preliminary step aiming to obtain a horizontal plane surface is required. This may be achieved upon conditioning the test

sample made of particles smaller than 2 microns, either by preparing a suspension and evaporating the solvent once deposited on a thin slide, or by lyophilizing the powder and pressing discs at 100 MPa..

1.4.1.4 Parameters affecting the bitumen-clay bonding

Terrel and Shute (1989) explain that adhesion between bitumen and aggregate is affected by several factors, among which some are applicable to the bitumen/clay bonding:

surface tension of bitumen and clay,

- clay moisture content and temperature at the time of mixing with asphalt.
- chemical composition of bitumen and clay,
- aggregate clay coating porosity (air void),
- bitumen viscosity,

Surface tension

According to Eq. 14, bitumen/clay adhesion reaches a maximum when polar constituents of bitumen are in contact with those of clay while dispersive components of bitumen are in contact with those of clay, whereas polar-dispersive forces interaction across the interface decreases the work of adhesion W_{ad} and favors the possibility of binding interruption.

An order of magnitude of **clay surface free energy** broken down into **dispersive and polar forces** is given in Table 12. These values were obtained from contact angle measurements using the static sessile drop test performed respectively on kaolinite, illite (No.36) and montmorillonite (SAz1). Although *Shang et al. (2008, 2010)* suggested that the value of illite measured by static sessile drop method should not be taken into account as no other test method yields a similar result, Table 12 shows that the 3 main clays met in clayey sands have a higher polar component compared to the dispersive component.

Table 12 Comparison between clay surface energy properties

Type of clay	Surface free energy (mN/m)	
	Dispersive component	Polar component
Mont. (SAz1)[a]	16.3	51.3
Illite (No.36)[a]	23.7 [b]	37.7 [b]
Kaolinite	20.4 [a]	48.9 [a]
	36.8 [c]	69.4 [c]

[a] Surface energy of KGa1b1 kaolinite, No.36 illite and SAz1 are calculated by the contact angles from static sessile drops measured by Shang et al. (*2010*) respectively. The surface energy of dioodomethan was referred to Yu et Dekker (*1982*). [b] The value of illite obtained from static sessile drop method is not recommended to use (*Shang et al. 2008*). [c] The kaolinite came from Valencia, Spain (*Janczuk et al. 1989*)

On the other hand, **asphalt, composed chiefly by high molecular weight hydrocarbons, exhibits little polar activity** in the order of 2 to 3 mJ/m², whereas its dispersive component reaches 45 to 50 mJ/m² (*Hefer and Little 2005*).

Therefore, bonds that develop between asphalt and clay are expectedly primarily due to relatively weak dispersion forces. Experimentations performed by *Liu et al. (1992)* confirm the prominence of such dispersion bonds on silica-based aggregates when they are initially coated with non-polar compounds, evidencing the substantive importance of first coated compound on the type and amount of interactions between bitumen and aggregate surface up to the point where bitumen polar compounds do not bind aggregates whose polar compounds are masked (*Curtis 1992*). Yet, several studies (*Frouin 1989;Reed 1968*) focused on identifying bitumen functional groups adsorbed on various clays surfaces have reported the large prominence of polar compounds from asphaltenes and resins, which is consistent with observations made by other authors (*Curtis et al. 1993;Petersen et al. 1982;Plancher et al. 1977*) who examined the interface between bitumen and various natural aggregates from adsorption/desorption experimentations.

Clay moisture content and mixing temperature

The prominence of polar bitumen compounds at clay surface may be explained by clay hydration state. Indeed, **clay surfaces are usually extremely hygroscopic**, in other words highly polar water molecules are strongly attracted to clay than bitumen in order to satisfy unbalanced charge present on clay surface (*Bagampadde et al. 2004;Department of Scientific and Industrial Reaserch 1962;Tarrer & Wagh 1991*). As a consequence, adsorption of liquid or vapor on clays severely decreases the dispersive component of their surface energy as shown on Figure 18 for a Montmorillonite (*Chassin et al. 1986*). Note that the influence of clay surface energy becomes insignificant when the water content exceeds 50%, in other words the surface energy of adsorbed water molecules takes over from that of clay.

Although subject to drying in asphalt mixing plant, experiments conducted by Thelen (*1958, cited by Hefer and Little 2005*) with fresh quartz aggregates show that silica-based mineral surfaces adsorb a water layer several molecules thick, which would require a temperature over 1000°C to be completely driven off within the plant process. Aggregate temperature in mixing plant processes reaches generally no higher temperature than 270°C given the short time of exposure to flame, and *Le Guen (2013)* reports that fine aggregates reach a stable temperature around 160°C after drying and heating process. Furthermore, clay structure shall be dried above 500 °C to be irreversibly collapsed (*Bradley and Grim 1951;Serratosa 1960*) and above 600 ° to achieve calcination that prevents water adsorption in the interlayer space (*Alexander 2004*). Hence, water molecules are absorbed reversibly on clay surface at mixing plant drying temperature (*Bradley, 1951*), and clay in HMA may still contain remaining water molecules in its interlayer space.

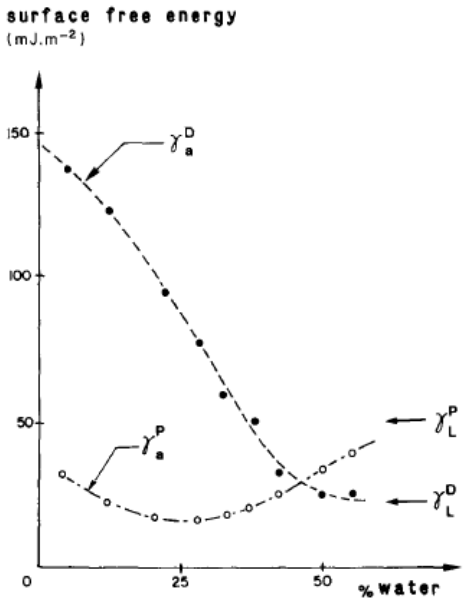

Figure 18 Variation of polar force, γ_a^P , and dispersive force, ,γ_a^D of montmorillonite with water content (*Chassin, 1986*)

Chemical composition of bitumen and clay

The chemical composition of clay and bitumen can explain the prominence of one of their surface energy component over the other, which controls their binding (*Birgisson et al. 2005*).

From clay point of view, chemical sites associated with high affinity for bitumen include in general elements such as aluminum, iron, magnesium and calcium *(Jamieson et al. 1995*). The first three elements are present on clay edge surface or basal surface as metal oxides while the last one belongs to exchangeable cations on clay. Chemical elements associated with low bonding affinity include sodium and potassium, which are exchangeable cations too. In the presence of water, **metal oxides as functional groups on clay surfaces form hydroxyl groups (SiOH, AlOH, MgOH, FeOH…)** which increase the polar component of its surface free energy. This increase depends on metal oxide hydration energy, which is proportional to valency and radius of cations (exchangeable or not) present onto clay surface (*Maes and Cremers 1979*). Experimental results from *Janczuk et al.(1989)* confirm partial increase of kaolinite polar surface energy component with cation valency and show that polar surface energy increases almost linearly with the entropy of hydrated ions (Figure 19).

From bitumen point of view, asphaltenes and resin polar compounds control to a large extent its affinity to mineral surfaces as already mentioned. Acidic compounds from asphaltenes - carboxylic acids, 2-quinolones and dicarboxylic anhydrides – have the highest affinity to mineral surface, though basic compounds incorporating nitrogen, oxygen or sulfur heteroatoms such as ketones and pyridine demonstrate good bonding properties (*Plancher et al, 1977; Petersen et al, 1982; Curtis, 1993)*. *Petersen and Plancher (1998)* observe that poly-functional compounds such as ketones, anhydrides and pyridine are the most strongly adsorbed on mineral surface.

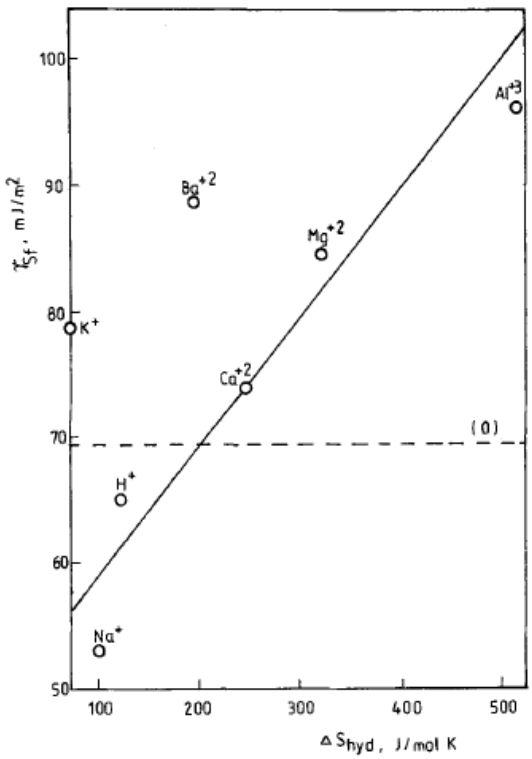

Figure 19 Correlation between non-dispersive component of surface energy of kaolinite samples modified with various ions (marked inside) and entropy of ion hydration (*Janczuk et al. 1989*).

Several chemical adhesion mechanisms may occur. The strongest is acid-base adhesion between acidic or basic compounds of asphaltenes and metal hydroxyl groups on clay surface, with amphoteric hydroxyl groups acting either as electron donor or acceptor depending on acidic or basic nature of first asphaltenes component binding with clay surface (*Hefer and Little 2005*). With increasing moisture content of clay, acid-base bonds may be replaced by weaker hydrogen bonds. In the absence of hydroxyl groups on clay surface, which is the case of 'surface-dry' clay or Ca-montmorillonite for example, bitumen/clay bonding may be explained by dispersive Van Der Waals bonds in the former case or by ionic bonds between bitumen heteroatoms and clay cations such as cation/π bonds or saline bridges.

Clay coating porosity and bitumen viscosity

Scanning electron microscopy (SEM) coupled with fractal analyses have revealed that clay coating on aggregate surface had a fractal porosity, the fractal dimension of which varies between 2.5 for kaolinite and 2.8 for montmorillonite (*Frouin, 1989*). Furthermore, this author established experimentally that bitumen, unlike methylene blue or water, adsorbed exclusively on the very external surface of clay coating, which he assigns to the high viscosity of bitumen making it unable to enter clay porosity.

Yet, exudation and insudation of bitumen dropped onto mineral porous surface had earlier been suspected as the presence of superficial hard and brittle bitumen compounds, similar to those resulting of short term aging[6], had been reported (*Plancher et al, 1977*), from which it had been postulated that aggregates surfaces exhibiting high porosity act as **molecular sieves**, separating highly associated polar molecules (resins and

[6] Evaporation of volatile compounds during the processing of hot mix asphalt

asphaltenes) from low molecular oily bitumen fractions (*Jeon and Curtis 1990*). Though later investigation reported by *Curtis et al. (1993)* concluded to the absence of selective absorption evidences, a test procedure initially designed to detect cracked petroleum residues caused by excessive heating of bitumen (*Oliensis 1961*) was adapted to assess bitumen/aggregate compatibility (*ASTM D1370 2012*). This test consists in placing a small drop of molten bitumen on a freshly talced[7] surface and judging the degree of development of an oily ring in the talc surrounding the drop (Figure 20), thus assessing bitumen segregation caused by superficial dust. The reason of using talced surface for Oliensis test was unexplained from literature.

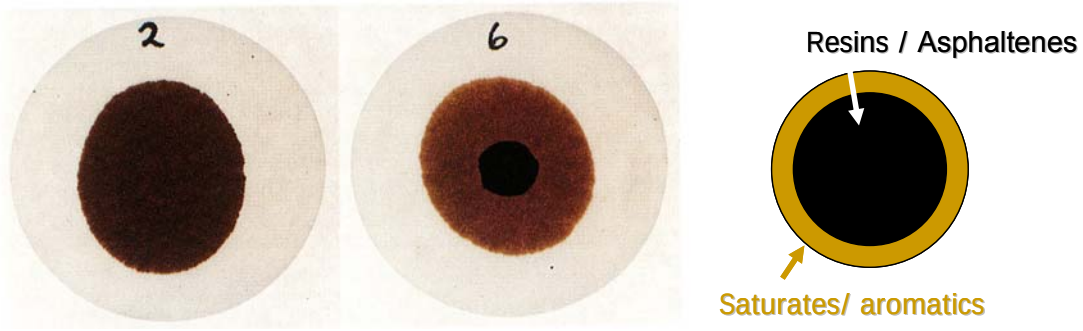

Figure 20 Oliensis spot test results (*shell bitumen 1995*) : low polar saturates and aromatics are outside and high polar resins and asphaltenes are at the center of the spot.

1.4.2 Bitumen-clay-water interaction - stripping phenomenon

1.4.2.1 Stripping phenomenon

Stripping may not occur in AC pavement if no moisture can move into the bitumen/aggregate interface *(Cheng et al. 2002)*, although *Bagampadde et al. (2004)* suspected osmosis to induce a water concentration gradient across the bitumen film. In fact, mixing in asphalt plants is often insufficient to ensure that bitumen coats the entire aggregate surface; hence water is able to penetrate into asphalt pavement and weaken the bonding at bitumen-aggregate interface (*Kanitpong and Bahia 2003*). Tarrerand Wagh *(1991)* reported that the presence of clay in aggregates weakens the bitumen-aggregates bonding and also promotes stripping by creating channels at the interface, through which water can penetrate (*Tarrer and Wagh 1991*). Numerical simulations of water vapor diffusion through AC mixtures were also performed, evidencing stripping at the coarse aggregate/fine aggregate mixture (FAM, incorporating bitumen) interface as a major contributor to AC mechanical strength undermining (*Arambula et al., 2010)*. The authors reported that AC mixture was highly influenced by the water diffusion coefficients of its constitutive phases classified as air, fine aggregates or coarse aggregates, and that the rate of moisture penetration changed along the aggregate/FAM interface or **interfacial zones**.

[7] Talc is a fine-grained white mineral ($Mg_3Si_4O_{10}(OH)_2$), having a soft soapy feel and used in talcum and face powder, as a paper coating, and as a filler for paint and plastics. It belongs to phyllosilicate group (magnesianTOT clay with no permanent charge).

Several stripping modes in bituminous pavements have been identified *(Curtis, 1993)*:

- Separation of the bond at the interface between bitumen and aggregate,
- Failure within the bitumen where soluble components are removed,
- Cohesive failure within the aggregate,
- Phase separation of components when the presence of water increases the solubility of polar compound impacting hydrogen bonding.

Tarrer (1996) stated that the **chemical reactivity** of aggregate surface controls the properties leading to stripping (*Tarrer 1996*). In the case of clay, strong evidences show that **surface energy at bitumen/clay** interface has to be taken into account to evaluate stripping. The parameters inducing stripping at clay/bitumen interface are summarized in Table 13 according to chemical reactivity and surface energy aspects.

Table 13 The stripping mechanisms that affect bitumen-clay bonding

Description of the stripping	Mechanisms	Parameters	
		Bitumen	Clay
Surface energy aspect	The **wetting** behaviour of bitumen at the bitumen-aggregate-water-air interface	Polarity The wetting depends also on: viscosity	packing density
Interfacial chemical properties	The **adsorption** of chemical component at bitumen-aggregates interface	Chemical factors Chemical mechanisms are : • Salt hydrolysis • pH evolution	

Once surface energy approaches in the presence of three distinct phases have been described, stripping of AC mixture incorporating clay will be reviewed in the following paragraphs, first from bitumen point of view and second from clay point of view, using both the chemical and surface energy descriptions

1.4.2.2 Three phases surface energy approaches

The removal of hydrocarbon film from solid surface S under the action of water (Figure 21) was studied by *Chassin (1986)* with Ca-Montmorillonite taken as the solid surface. According to the author, Eq. 13 and Eq. 17 shall be rewritten to account for two separate constituents, bitumen H (hydrocarbon) and water W. Young's Eq. 9 hence rewrites:

$$\gamma_{HW} \cos\theta_{SWH} = \gamma_{SH} - \gamma_{SW} \qquad \text{Eq. 19}$$

The work of adhesion for two phases writes, in accordance with Eq. 10:

$$W_{SW} = \gamma_S + \gamma_W - \gamma_{SW} \quad \text{at the clay/water interphase} \qquad \text{Eq. 20}$$

$$W_{SH} = \gamma_S + \gamma_H - \gamma_{SH} \quad \text{at the clay/bitumen interphase} \qquad \text{Eq. 21}$$

Furthermore, upon observing that the polar component of bitumen is negligible compared to the dispersive one, the work of adhesion at clay/bitumen interphase writes (Eq. 8):

$$W_{SH} = 2\left(\gamma_s^d \gamma_H^d\right)^{1/2} \qquad \text{Eq. 22}$$

whereas the work of adhesion at clay/water interface shall account for both polar and dispersive components and thus rewrites, upon taking the harmonic mean of polar components as suggested by *Wu (1973)* (Eq. 14):

$$W_{SW} = 2\sqrt{\gamma_S^{\,d}\,\gamma_W^{\,d}} + 4\frac{\gamma_S^{\,P}\,\gamma_W^{\,P}}{\gamma_S^{\,P} + \gamma_W^{\,P}} \qquad \text{Eq. 23}$$

Stripping occurs when $W_{SW} > W_{SH}$, which may be checked upon calculating unknowns γ_S^P and γ_S^D. This may be done upon combining Eq. 19 to Eq. 23, which yields the following expression:

$$\gamma_{HW}\cos\theta_{SWH} + \gamma_W - \gamma_H = 2\sqrt{\gamma_S^{\,d}}\left[\left(\gamma_W^{\,d}\right)^{1/2} - \left(\gamma_H^{\,d}\right)^{1/2}\right] + 4\frac{\gamma_S^{\,P}\,\gamma_W^{\,P}}{\gamma_S^{\,P} + \gamma_W^{\,P}} \qquad \text{Eq. 24}$$

whose unknowns γ_S^P and γ_S^d may be determined using successively at least 2 bitumen (non-polar) compounds with water.

Similarly, Van Oss equations written in section 1.4.1.2 shall be updated to account for the presence of water as a third phase. *Van Oss et al (1987; 1994)* proposed the following expression of the work of adhesion between two solid surfaces – for example clay and hardened bitumen – immersed into water acting as a stripping agent:

$$W_{SWH} = \left[\begin{array}{c} 2\sqrt{\gamma_S^{\,d}\,\gamma_W^{\,d}} + \sqrt{\gamma_H^{\,d}\,\gamma_W^{\,d}} - \sqrt{\gamma_S^{\,d}\,\gamma_H^{\,d}} - \gamma_W^{\,d} + \\ \sqrt{\gamma_W^{\,+}}\left(\gamma_S^{\,-} + \gamma_H^{\,-} - \gamma_W^{\,-}\right) + \sqrt{\gamma_W^{\,-}}\left(\gamma_S^{\,+} + \gamma_H^{\,+} - \gamma_W^{\,+}\right) - \sqrt{\gamma_S^{\,+}\,\gamma_H^{\,-}} - \sqrt{\gamma_S^{\,-}\,\gamma_H^{\,+}} \end{array}\right] \qquad \text{Eq. 25}$$

whose unknowns γ_S^d, γ_S^- and γ_S^+ may be determined using successively at least three different hardened bitumen compounds of known surface energy components with water. According to the authors, no stripping may occur when $W_{SWH} > 0$.

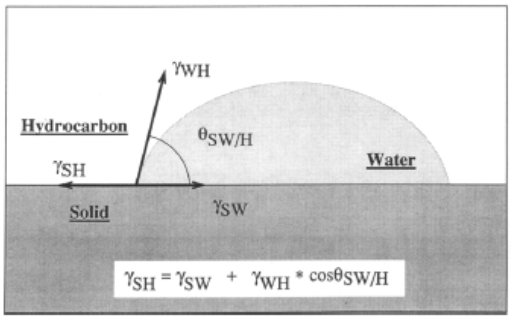

Figure 21 Illustration of Young's equation and contact angle at the equilibrium in the solid (S)- liquid 1(Water) - liquid 2(Hydrocarbon) system when stripping occurs (*Jouany 1991*)

1.4.2.3 The role of bitumen properties into stripping of AC mixture

The contribution of bitumen to stripping of AC is a function of bitumen chemistry, surface energy and viscosity (*Bahia & Seemab 1999;Cheng et al. 2002;Cheng et al. 2003*).

Chemical composition of bitumen

The chemical composition of bitumen which is partly responsible of stripping in AC mixture was at the heart of the pioneering work by *Plancher et al (1977)*. They stated that **carboxylic acids, dicarboxylic**

anhydrides and 2-quinolones, which are the most highly concentrated compounds at bitumen/siliceous aggregate interface (*Allsop, 1995*), are also the principal actors of stripping *(Hefer and Little 2005;Robertson 2000;Transportation Research Board 2003*). Furthermore, carboxylic acids are known to form salts of carboxylic acids with clay monovalent cations such as sodium and potassium, which have the highest moisture sensitivity (*Plancher et al. 1977*).

Besides, bitumen molecules may irreversibly evolve through chemical aging which is generally thought to be a sum of oxidation reaction and polymerization, and to a lesser extent, lighter components evaporation (*Bell 1989;Delorme & Wendling 2007a;Read and Whiteoak 2003;Traxler 1961*). This chemical shift, which produces compounds such as sulfoxides, ketones or anhydrides, leads generally to a global hardening of material (*Read and Whiteoak 2003;Wright 1965*), which in turn increases the cracking probability of bitumen (*Isacsson and Zeng 1998*), thus increasing the probability of stripping occurrence. Furthermore, *Cheng (2002)* reports that oxidative aging of bitumen involves an increase of its polarity, making it even more moisture-sensitive.

Surface energy

Basu et al (1996, 1998, 2000, 2004) have examined the displacement of a bitumen droplet coated on a hydrophilic glass slide when exposed to various aqueous environmental conditions. They reported an increase in the bitumen dynamic and static contact angle measurements with the pH of water, which is consistent with results reported by *Scott (1978)* for pH > 9, meaning that the bitumen/glass bonding is severely weakened when pH increases, and slightly more when temperature increases. This weakening in basic conditions may cause the detachment of the bitumen droplet from the glass surface. It may be explained by progressive rupture of glass/bitumen hydrogen bonds as bitumen acidic compounds deprotonate due to solvent basicity (*Hefer and Little 2005)*. Basu et al also observed a decrease in bitumen/glass contact angle when sodium chloride salt was added to water, though addition of kerosene counteracted this trend (Figure 22).

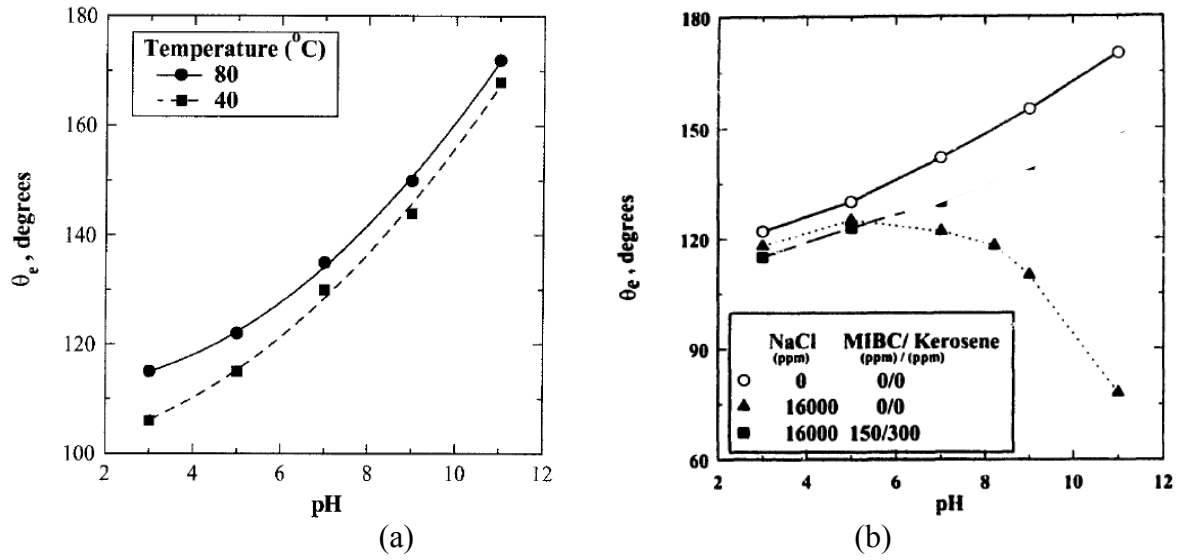

Figure 22 Effect of (a) pH on the equilibrium contact angle of bitumen, and (b) different NaCl concentration on equilibrium contact angle of bitumen at 40°C (*Basu 1998, 1996*)

A more pronounced decrease of bitumen/glass contact angle, in other words an increased water resistance of bitumen/glass bonding, was observed when adding calcium divalent ions. This was partly explained by calcium ions adsorption on bitumen and glass surfaces, and partly by the compression of the repulsive electric double layers of bitumen and glass caused by less negative zeta potentials in the presence of calcium as suggested by *Liu et al. (2005)*.

Viscosity

Bitumen viscosity plays two contradictory roles: In asphalt plants, the viscosity of hot bitumen - which decreases when temperature increases, but increases with the volume fraction of mineral filler in the mix (cited by Lesueur et al. 2013) - opposes coating on full mineral surface, thus leaving coating defects (*Gzemski, 1968*) through which water intrudes into the HMA and causes stripping (*Frouin, 1989*); Contrariwise, once bitumen coating has cooled down, its high viscosity slows down its desorption from mineral surface, especially when high molar mass bitumen compounds are adsorbed *(Brown and Kuntze 1972*).

1.4.2.4 The role of clay properties into stripping of AC mixture

As already mentioned in 1.4.1.4, clay surface in HMA is always more or less hydrated, either by air moisture or residual clay water content. Water being a highly polar molecule, this hydration may significantly increase the polar component of clay surface energy. As a consequence, when HMA is immersed into water, clay surface attracts more other highly polar molecules such as other water molecules than bitumen, thus increasing the probability of stripping occurrence through hydrolysis. The stripping potential increase may also result from the segregation of high and low molar mass bitumen compounds by clay coated on fine aggregates surface or in mastic, as it increases the cracking probability of bitumen (*Isacsson and Zeng 1998*). Eventually, as mentioned in 1.4.1.4, the high porosity of clay coated on aggregate surface is inaccessible to bitumen, but forms channels at bitumen/clay interface through which water can penetrate and cause clay swelling, which strongly impacts the stripping potential of clay-rich AC mixture.

Yet, due to the presence of water as a third phase, stripping from clay point of view is a time-dependent phenomenon governed by additional parameters, namely the nature and valence of cations on clay surface, the pH value and the zeta potential at bitumen/clay interface.

Impact of the nature and valence of clay surface cations on stripping

In hydrolyses reaction occurring at bitumen-clay-water interface, water acting as either a base or an acid, forms a stronger hydrogen bond with clay compared to the bond formed with bitumen. Hence, *Hefer and Little (2005)* suggest for example that the hydrogen bond between a silanol group and carboxylic acid are susceptible to be displaced or interrupted by water according to the following reaction:

$$-SiO\cdots HO-\overset{\overset{O}{\|}}{C}R + 2H_2O \rightleftharpoons -SiO\cdots HOH + H_2O + RC-OH$$

where first "…" denotes silanol/carboxylic acid hydrogen bond and second "…" silanol/water hydrogen bond.

The ease with which bitumen/mineral surface hydrogen bound may be interrupted by water depends on clay nature and valence. Plancher et al. (*1977*) explain that monovalent cation salts, such as sodium and potassium salts of carboxylic acids in asphalt, can be easily removed from the aggregate surface because they are essentially surfactants or soaps, which debond under the scrubbing action of traffic in the presence of water. This phenomenon is known as salt hydrolysis (*Ardebrant and Pugh 1991;Bagampadde et al. 2004;Simmons and Beard 1987;Yoon & Tarrer 1988*). Contrariwise, divalent cations such as calcium form strong insoluble bonds with bitumen carboxylic acids (*Hefer and Little 2005;Plancher et al. 1977;Transportation Research Board 2003;WRI 2003)*.

WRI researchers (*2003*) focused also on the identification of specific chemical reactions by which acidic bitumen compounds (mostly carboxylic acids such as stearic acid) and basic components on aggregates produce water-soluble salts. By methodically changing the stoechiometric amounts of bitumen and aggregate reactants, results from freeze-thaw experiments on manufactured briquettes show that laboratory performance of these specimens increase with the share of divalent (insoluble) cations and stearic acid (Figure 23), confirming that acid-base reactions control the performance.

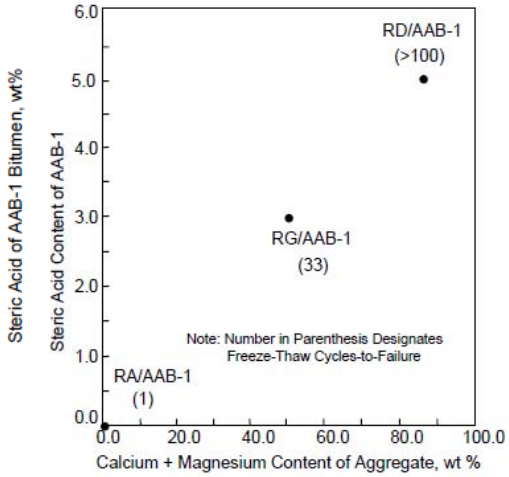

Figure 23 Effect of stearic acid content in AAB-1 bitumen and carbonate content in aggregate on failure measured by freeze-thaw-cycles (*WRI, 2003*)

Impact of pH value and zeta potential at bitumen/clay interface on stripping

In oil sand ore recovery, where the objective is to separate oil from clayey sand on which it is bound, researchers have observed that high pH and low divalent cation content facilitate oil droplets coagulation and coalescence, thus yielding high oil flotation recovery (*Liu et al. 2005*). High content of divalent cations, namely calcium, increases the interstitial solution ionic force, which reduces the thickness of the repulsive electric double layer that surrounds clayey sand particles *(Liu et al. 2005;Masliyah 2003*), thus promoting their adhesion. The thickness reduction of the repulsive electric double layer surrounding montmorillonite and kaolinite clay particles was confirmed by *Liu et al.(2004*) who reported zeta potential measured values becoming less negative when calcium content increases (see Figure 24).

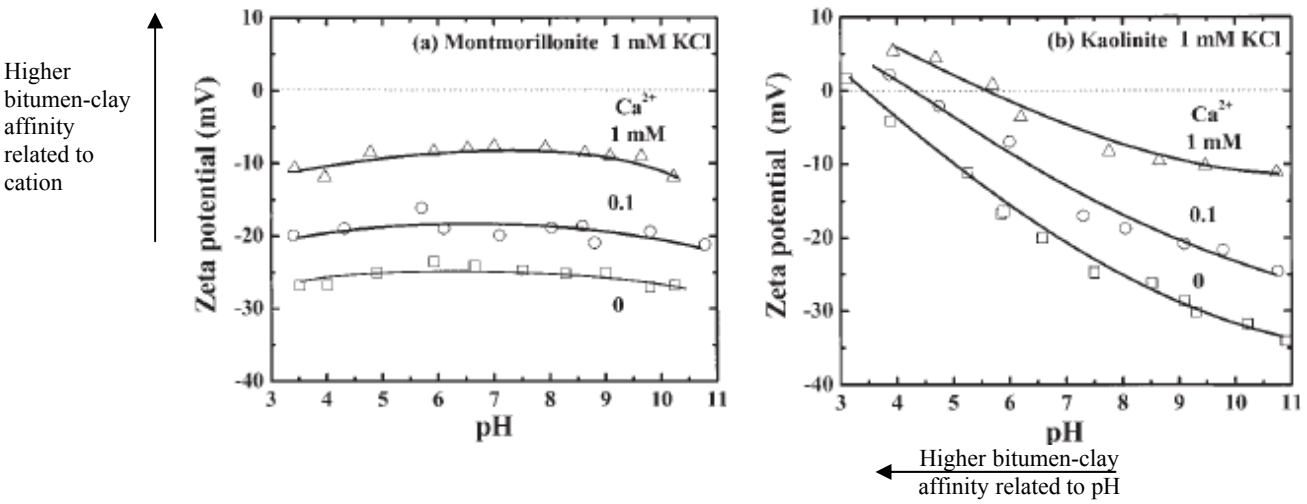

Figure 24 Average zeta potentials of (a) montmorillonite and (b) kaolinite as a function of pH (*Liu et al. 2004*)

Decreasing zeta potential with increasing pH values of kaolinite were also observed, whereas pH had no effect on the zeta potential of montmorillonite (*Liu et al. 2004,* see Figure 24). The fact that the amphoteric edge of montmorillonite represents only 1% of its total surface area justifies its permanent charge and its pH-independent zeta potential (*Sondi et al., 1996, 1997*). Yet, other authors have reported more or less different variations of zeta potential of montmorillonite or kaolinite with pH and cation concentration (Figure 25 and Figure 26), suggesting that pH effect on zeta potential measurements should be considered with caution.

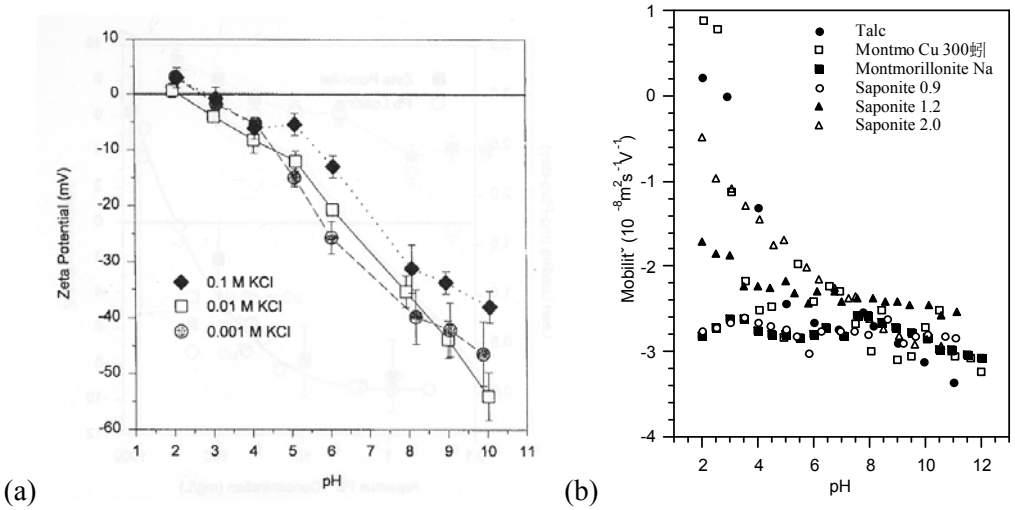

Figure 25 (a) Zeta potential of kaolinite suspension versus pH in 0.1, 0.001 et 0.001M KCl after 20-24h contact (*Vane and Zang 1997*). (b) Zeta potential versus pH for different clay with variable permanent charge (saponite with increasing permanent charge, talc with no charge, sodic montmorillonite with high permanent charge or zero charge after Cu exchange and thermal treatment) (*Thomas et al. 1999*).

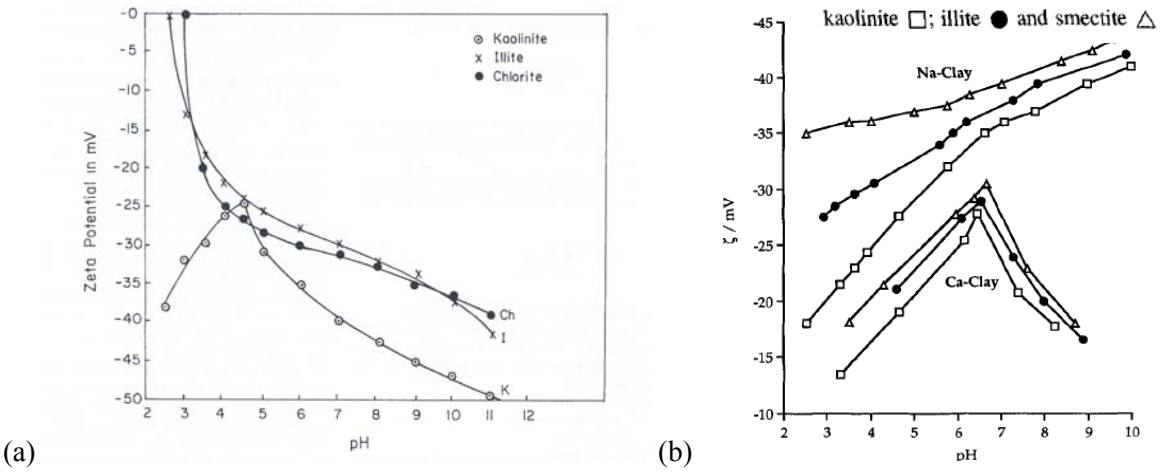

(a) (b)

Figure 26 (a) Zeta potential of kaolinite, illite and chlorite suspension in distilled water with HNO_3 or NaOH addition after 10 min of contact (*Hussain et al. 1996*). (b) Zeta potential of Na-clays and Ca-clays versus the pH of the clay suspension (*Chorom and Rengasamy 1995*)

Similarly, the stripping sensitivity of HMA will increase as the pH of water in the pavement increases (*Basu et al. 1996 1998 2000 2004;Chefetz et al. 2011;Hughes et al. 1960;Kennedy et al. 1984;Kiggundu and Robberts 1988;Scott 1978;Tarrer 1996;Transportation Research Board 2003;Yoon & Tarrer 1988;Yoon 1987*). As shown on Figure 27 , basic pH values arise from most aggregates in contact with water, especially with high carbonates content, whereas high silica content yields slightly acid contacting water. Furthermore, the basic pH of water micro droplets intruding the bitumen film to the mineral surface may be sufficient to dissociate hydrogen bonds and salt links between adsorbed bitumen compounds and mineral surface (*Scott, 1978; Yoon and Tarrer, 1988*).

In general in HMA, pHs as high as 9 or 10 will not dislodge amines of carboxylic acids from the acidic surfaces of aggregates, hence no stripping should occur. pH values higher than 10 do normally not develop in asphalt mixtures unless a caustic product such as lime is added, whereas pH values lower than 4 are not observed in HMA (*Jada et al. 2004*).

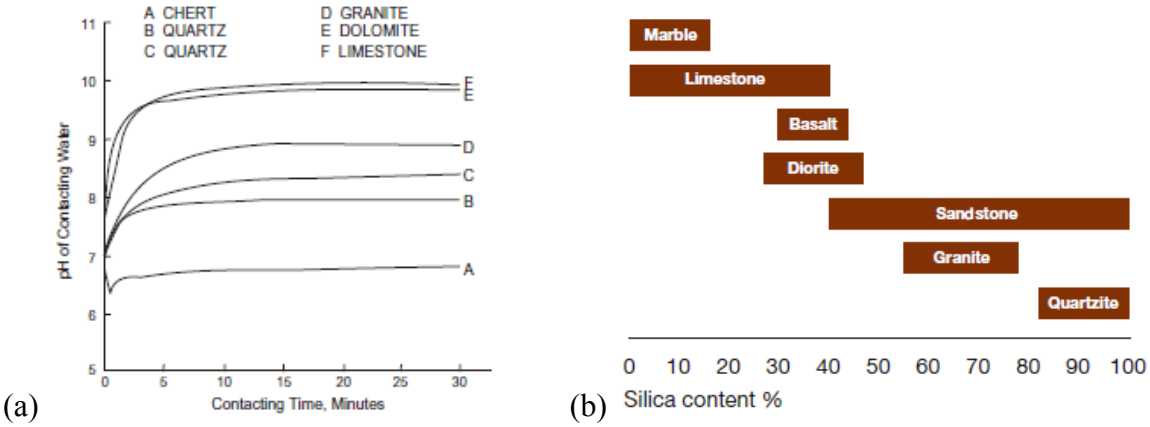

(a) (b)

Figure 27 (a) Influence of aggregate type on pH after a contact with water (*Yoon and Tarrer 1988*), (b) Silica content in typical material in quarry (*AkzoNobel 2015*)

1.4.3 Improvement of bitumen-clay bonding

Bitumen-clay bonding may be improved using additives, which are organic or mineral compounds intended to modify the physical or mechanical characteristics of HMA (*Delorme and Wendling, 2007*). Additives may be introduced either directly into the bitumen tank or into the formula at the time of mixing. In the former case, the additive is called an **adhesion enhancer** or **antistripping agent** and contains essentially nitrogen-based surfactants derived from fatty acids (e.g. amines, polyamines…), though lime or limestone filler may also be used. In the latter case, limestone filler is often used.

1.4.3.1 Use of antistripping agents

The effectiveness of antistripping agents varies with the type of agent, as well as with the asphalt and aggregates types. The composition of antistripping agents includes fatty amines, amine based antistripping agent, solid and liquid antistripping agents, heat stable antistripping agents, iron naphthenate and hydrated lime (*Tarrer and Wagh 1991*). Their surfactant action consists in decreasing the non-polar γ^D component of bitumen surface free energy in favor of the polar component, thus yielding a better match of surface energy components with those of siliceous aggregates for an improved interfacial adhesion hence an improved fracture resistance of the mix (*Howson et al. 2010*).

From a chemical point of view, antistripping agents contribute to a 0.5 Å to 1.0 Å apparent contraction of the thickness of the Van der Waals potential associated with the adsorbed cations at the bitumen-clay interface. Similar results have been obtained for numerous complexes with aromatic and cyclo-aliphatic compounds (*Brindley and Hoffman 1962;Greene-Kelly 1955*), amino acids and peptides (*Greenland et al. 1962;Talibudeen 1954*), straight chain aliphatics (*Hoffman and Brindley 1960*) and alkylammonium ions (*Diamond and Kinter 1961;Fripiat et al. 1962;Sieskind and Wey 1958*). Different mechanisms have been postulated to account for this contraction:

The formation of C--H... O hydrogen bonding between the methylene groups of the molecules and the silicate surface (*Bradley 1945*),

- The compression of the molecules at the clay surface,

The 'keying' of the adsorbed molecules or cations into the hexagonal depressions of the silicate surface such as hexagonal cavities on clay (*Greene-Kelly, 1955; Greenland et al. 1962*).

The addition of hydrated lime to bitumen triggers a mechanism which ties up carboxylic acids and 2-quinolones by an insoluble salt of carboxylic acid, so that these compounds are no more available to form moisture-sensitive bonds with hydrogen bonding functionalities on aggregate surface (Eq. 26):

$$Ca(OH)_2 + 2RCOOH \rightarrow (RCOO^-)_2 Ca + H_2O \qquad \text{Eq. 26}$$

The interaction of lime with bitumen constituents not only prevents the formation of moisture-sensitive bonds but also subsequently allows the proliferation of **more resistant bonds** involving nitrogen compounds of bitumen (*Thomas, 2002*). Author points out that an additional benefit of the use of lime is to react with (or adsorb) compounds that would otherwise be oxidized and increase bitumen viscosity as a result of oxidation. It is common in literature that hydrated lime-modified bitumen show a decreased ageing susceptibility, as materialized by a slower increase in viscosity (or any other mechanical property) versus

time. In all cases, asphaltenes content increase at a slower rate in hydrated lime-modified bitumen compared with non-modified bitumen. In parallel, the rate of carbonyl formation, which correlates well with the viscosity increase, slows down in hydrated lime-modified bitumen (*Lesueur et al. 2013*).

1.4.3.2 Other additives

Anionic/cationic/nonionic surfactants

Authors (*Cipriano et al. 2005;Dharaiya and Jana 2005;Janczuk et al. 1989;Jouany and Chassin 1987;López-Durán et al. 2003*) evidenced contact angle variations on surfactant-treated clays. Cipriano et al (*2005*) observed that the adsorption of imidazolium surfactant onto a mica surface makes it hydrophobic. Similarly, Jouany and Chassin (*1987*) reported on the adsorption of a cationic surfactant with its positively-charged head group onto the negatively-charged clay surface, thereby exposing the hydrophobic surfactant tail to the solution. **Thus, while native montmorillonite surface is hydrophilic, adsorption of a small amount of surfactant on the surface can render it hydrophobic.** Besides, many studies can be found dealing with surfactant modified clays (anionic, cationic and nonionic). These studies investigate the electro-kinetic properties of surfactant-modified clays, such as zeta potential, cation exchange capacity (CEC) and electrical conductivity (*Akbulut et al. 2012*). Akbulut (*2012*) studied the relation between contact angle and water affinity of clays. Clay pellets modified by nonionic and anionic surfactants gave lower contact angles with water than natural clays, whereas clay pellets modified by cationic surfactants gave the highest contact angles. Hence, anionic-surfactants-modified clays are the most hydrophilic and cationic-surfactants-modified clays the most hydrophobic.

Lime treatment

Hydrated lime $Ca(OH)_2$ or lime CaO, added as alkaline calcium hydroxide, gives good results at any pH including high pHs. Hydrated lime is known to improve the adhesion of limestone aggregates as well (*Huang et al. 2005;Mohammad et al. 2008*). Lime contributes to form a very strong chemical bond between the asphalt and aggregate although, for the same valence of ion, *Johansson et al. (1995)* observed that no anti-ageing effect was present with $Mg(OH)_2$, a weaker base than $Ca(OH)_2$ (*Johansson et al. 1995*).

National lime association from America (2003) reported 5 common methods for adding hydrated lime to HMA:

- Hydrated lime injected into drum mixer,
- Hydrated lime added to aggregate in pug mill,
- Dry hydrated lime added to moist aggregate with marination,
- Slurry lime added to aggregate with or without marination.

When hydrated lime is used, its role is similar to that observed in soil treatment (*Little 1995*): lime **flocculates** clay particles, preventing them from building a water-displaceable barrier between bitumen and aggregate. Such an effect is rapid after contact. A German study with controlled clay contamination in

aggregates confirmed that hydrated lime efficiently counteracts the effect of clay (*Eulitz et al. 1998;Schellenberg and Eulitz 1999*).

Furthermore, the effects of hydrated lime are to allow for the **precipitation of products rich in calcium** or to bring calcium ions onto the clay surface, making it more **favorable to bitumen bonding**. This effect has been recognized already in a study by *Ishai and Craus (1977)*. Once lime has been added to the mastic (Figure 28 a), calcium ions can accumulate at the aggregate surface and then bond with the acidic compounds of bitumen, forming water-insoluble salts (Figure 28 b). As a consequence, a surface treatment of the aggregate with almost no remaining hydrated lime particles already improves the bitumen–clay adhesion (*Blazek et al. 2000*).

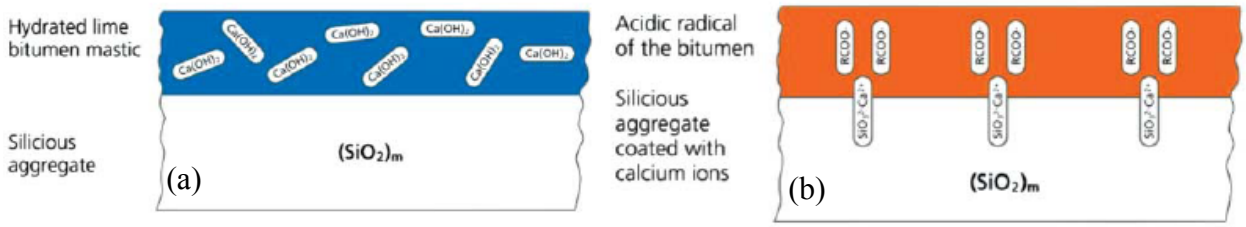

Figure 28 The effect of hydrated lime on the aggregate surface as proposed by Ishai and Craus (1977)

In the presence of CO_2 and then precipitated calcium carbonates, *Logaraj (2002)* states that when aggregates are exposed to a direct flame in the hot-mix plant, at least for a brief moment, temperatures up to 700°C can be encountered (*Logaraj 2002*). Under these conditions, the calcium carbonate surface may decompose into calcium oxide (CaO or quick lime) and carbon dioxide. Calcium oxide, which is a strong base, will react instantaneously with acids in bitumen. Hence, lime slurry treatment of aggregate results in the formation of calcium salts at the asphalt-aggregate interface, yielding a material that is more resistant to stripping (*Tarrer and Wagh 1991*).

Tarrer (1996) also found that bonds in hydrated lime mixes build up rapidly (15 to 30 minutes) compared to mixes incorporating liquid anti-stripping agents (over 3 hours). Author concluded that (a) bonds between asphalt and aggregates depend on surface chemical activity, (b) water on aggregate surface is generally at a high pH, (c) some liquids used as antistripping agents require a long curing period (in excess of about 3 hours) to achieve resistant bonds at high pH levels, and (d) it is possible to achieve a strong chemical bond between aggregate and bitumen that is resistant to pH shifts and high pH environment. This strong chemical bond can be achieved by the formation of insoluble organic salts (such as calcium-based salts), which are formed rapidly and are not affected by high pH levels or pH shifts.

Although pH shifts affect some chemical bonds, it is important to keep in mind the magnitude of pH shifts. Normally, pHs as high as 9 or 10 will not dislodge amines from the acidic surfaces of aggregates, and they won't affect hydrated lime. Values of pH higher than 10 are not normally observed in bituminous mixtures unless a caustic product such as lime is added. However, pHs below about 4 may dislodge amines from an aggregate surface and may dissolve lime, depending on the type of acid used. But these low pH conditions are not found in hot-mix asphalt (*Delorme and Wendling 2007*).

1.5 General conclusions and objectives of the study

The depletion of natural resources in many places around the world as well as environmental challenges yield more and more countries to assess the harmfulness of fines in sand fractions to see whether they may be discarded or not before producing HMA.

Based on literature review, MB test appears as the usual method in France to assess the harmfulness of clay in fine aggregates, but it is not always a good indicator for estimating the stripping potential of AC mixtures. It is due to the lack of consideration paid to clay mineralogy and water-bitumen-clay interaction. Furthermore, several parameters seriously bias the MB value, such as the layer charge of clay, clay-MB contact time, concentration of MB solution etc., which may mislead aggregate producers regarding the qualification of fine aggregates and yield the waste of natural resources.

Although a solution detailed in the literature review to reduce stripping is the use of lime, the present research work investigates an alternative yet more environmentally-friendly strategy to save natural resources through a performance-based approach of clay harmfulness. This strategy comprises five tasks:

- The qualitative and quantitative analysis of clay in fine aggregates,
- The assessment of water-bitumen-clay interaction in relation to clay mineralogy,
- The assessment of stripping in clay-rich AC mixtures correlated to clay mineralogy,
- The clarification of the variability of MB value considering different parameters.
- Propose a strategy to evaluate the stripping of AC mixture occurred by clay regarding the tasks mentioned above.

The aim of this (the qualification of fine aggregates for asphalt concrete pavement considering the mineralogical point of view) will be reached using test methods, protocols and experimental design as well as materials (artificial or natural fine aggregates) whose characteristics are detailed in the following chapter.

Chapter 2 Materials and methods

2.1 Materials

In order to evaluate the possibility of using certain fine aggregates in AC mixtures, the following materials were studied in this research from a mineralogical point of view:

- extracted (raw) natural clays,
- washed sand,
- artificial fine aggregates made from extracted clays and washed sand,
- fine aggregates of unknown sources with their natural clays to blind test. The practicability of a mineralogical sand qualification approach.
- asphalt concrete mixtures containing the fine aggregates mentioned above.

The source of these materials and their treatment/preparation methods are introduced in the following paragraphs.

2.1.1 Clays

2.1.1.1 Sources

Three types of clays were used in this study due to their availability, their purity and their properties:

- the kaolinite Sialite from "Société Kaolinière Armoricaine" (SOKA) in France,
- the green illite from "Argile du Velay" company (Arvel) in France,
- and the montmorillonite from Mediterranean Sea (supplied by Argile du Bassin Mediterranéen or ABM) from Sardaigne (Italy).

Clay rocks of illite and montmorillonite were transported from quarries and extracted in the laboratory, whereas the extracted kaolinite was supplied from SOKA without any drying of the material, and then ground in the laboratory. By controlling the processing of clay extractions from rocks (above all the step of drying), clay properties were preserved and the characteristics and behavior of the tested materials remained representative of natural clays.

2.1.1.2 Preparation

The intact clay rocks of illite and montmorillonite transported from quarries were disaggregated by immersion in water (Figure 29). Unlike the montmorillonitic rocks which were easily disaggregated into small particles in the presence of water, illitic rocks were also manually fractured in a mixer after immersion in water. Such expected differences are generated by the diagenetic smectite-to-illite conversion *(Bouchet et al. 2000)*. Then, the separation of clay particles was pursued by wet sieving (*Soukup et al. 2008*) through 0.063 mm sieve and passing particles were dried at 40 °C. After drying and reaching the constant mass, the clays were gently crushed by the machine used for Los Angeles tests. These extracted

kaolinite, illite and montmorillonite clay powders were collected after confirmation by dry sieving that their particle size was less than 0.063 mm. Such preparation took more than 6 months and allowed to produce a few kilograms of clay from each raw clay rock..

(a) (b)

Figure 29 Difference of softness after 2 weeks of
(a) illitic rock and (b) montmorillonitic rock immersed in water

2.1.2 Fine aggregates

2.1.2.1 Preparation of blends, so called artificial fine aggregates

St. Colomban Sand was chosen for the study and this siliceous sand was supplied from GSM Company (France). Several hundred kilograms were washed with tap water to clear away particles with grain size less than 0.063 mm. Finally, the artificial fine aggregates were prepared from the 0.063mm to 2 mm sand fraction dried in the oven at 105 °C over night and the extracted clays (with particle sizes smaller than 0.063 mm).

The procedure of blending clay with fine aggregates to simulate natural fine aggregates followed Leroux's method (*Le roux, 1980*) with the modification from this study. The procedure is described below.

- The designed masses of sand and clay portions were prepared with consideration paid to their water content.
- The sand portion was humidified in a mixer with tap water to reach a moisture content of 5%.
- Clay was gradually added and mixed with pre-soaked sand in the mixer until the whole clay portion was incorporated.

Macroscopic and optical microscopic observations have confirmed that the clay coating on sand particles is homogenous with this protocol (Figure 30). The fines coating of fine aggregates resulting of this protocol is similar to that of natural sands from quarries. The physical behavior of these artificial materials may hence be expected to be similar to that of natural clay fine aggregates.

(a) (b)

Figure 30 (a) The watered-washed sand before mixing with clay,
(b) Sand homogeneously coated with clay as the clay-rich fine aggregates from quarry

In this study, clay-rich fine aggregates were prepared and grouped into 3 series noted S1, S2 and S3, which correspond to artificial sand aggregates with one, two or three types of clay fines respectively. Moreover, each series consisted of various quantities of clay in the fine aggregates selected to approach target Duriez value0.8 (Table 14). The percentage of dry weight of material is given and mixtures were made by taking into account the residual water content in clay and sand. After mixing with an addition of water, blends were divided into the designed mass for each test and stored in sealed bag. Systematically, the water content was measured before starting any test.

Table 14 The design of clay fine aggregates blends

Series	name	Preparation of sand and raw clays (dry mass wt%)				Total clay fraction in sand (dry mass wt%)
		sand	kao	illite	montm	
Reference	Non clay	100.00	0.00	0.00	0.00	0.00
S1	S1-K2	78.56	21.44	0.00	0.00	21.44
	S1-K3	70.00	30.00	0.00	0.00	30.00
	Max. Kao.	65.42	34.58	0.00	0.00	34.58
	S1-I4	92.78	0.00	7.22	0.00	7.22
	S1-I9	80.00	0.00	20.00	0.00	20.00
	S1-I13	70.00	0.00	30.00	0.00	30.00
	Max. Illite	63.90	0.00	36.10	0.00	36.10
	S1-M2	99.48	0.00	0.00	0.52	0.52
	S1-M4	98.63	0.00	0.00	1.37	1.37
	S1-M12	95.23	0.00	0.00	4.77	4.77
	Max. Montm.	65.09	0.00	0.00	34.91	34.91
S2	S2-KI2	67.38	26.27	6.35	0.00	32.62
	S2-KI8	75.66	8.91	15.43	0.00	24.34
	S2-IM6	88.21	0.00	7.47	4.31	11.79
	S2-IM10	90.28	0.00	3.56	6.16	9.72
	S2-KM3	69.86	27.24	0.00	2.90	30.14
	S2-KM11	88.14	4.34	0.00	7.52	11.86
S3	S3-2	69.35	28.43	1.56	0.66	30.65
	S3-3	73.41	16.63	6.92	3.05	26.59
	S3-5	81.60	9.61	3.22	5.57	18.40

2.1.2.2 Unknown fine aggregates for blind tests

Five unknown fine aggregates, noted A to E (Figure 31), were supplied by quarries without any technical information except their size fractions (see Table 15). As the samples B and C were 0-4 mm fractions ($D_{0/4mm}$), the particle size $D_{2/4mm}$ was removed from the samples by dry sieving. Then, the $D_{2/4mm}$ fraction was brushed and washed on a 2 mm sieve to collect all the particles smaller than 0.063 mm. The collected fine fraction was air-dried, ground to pass through a 0.063 mm sieve and incorporated into its corresponding $D_{0/2mm}$ sand fraction. Besides, the particle sizes of unknown fine aggregates A, D and E which were noted by producer as 0/2mm sand were "strictly" cut at 2mm following the same procedure as applied on fine aggregates B and D. In fact, according to standard (*NF EN 13043*), the general grading requirement for fine aggregates is no more than 15 wt% of particles from fine aggregates remaining on 2mm the sieve (G_F85).

A, fraction 0-2 mm ($D_{0/2\ mm}$)

B, fraction 0-4 mm ($D_{0/4mm}$)

C, fraction 0-4 mm ($D_{0/4mm}$)

D, fraction 0-2 mm ($D_{0/2mm}$)

E, fraction 0-2 mm ($D_{0/2mm}$)

Figure 31 Unknown fine aggregates from quarries

Table 15 Particle size of unknown aggregates

Unknown fine aggregate	Particle size indicated in as-received material by producer	wt% remaining on 2 mm sieve in as-received material	Studied particle size (after preparation)
A	$D_{0\text{-}2\ mm}$	8.28%	$D_{0\text{-}2\ mm}$
B	$D_{0\text{-}4\ mm}$	31.68 %	$D_{0\text{-}2\ mm}$
C	$D_{0\text{-}4\ mm}$	27.84 %	$D_{0\text{-}2\ mm}$
D	$D_{0\text{-}2\ mm}$	2.25 %	$D_{0\text{-}2\ mm}$
E	$D_{0\text{-}2\ mm}$	4.46 %	$D_{0\text{-}2\ mm}$

2.1.3 *Coarse aggregates, filler and bitumen*

Diorite[8] coarse aggregate (a siliceous rock) was used to provide the $D_{4/6\ mm}$ fraction for all AC mixtures, whereas limestone filler with particle size less than 0.063 mm was used to acheive constant content fines content of the mixture. The bituminous binder is a paraffinic one and shows a pen-grade type of 35/50. The softening point is equal to 58.8 °C and the penetration at 25°C is between 35 and 50 dmm[9] (*Somé 2012*).

2.1.4 *Asphalt concrete mixtures for water intrusion tests and Duriez tests (NF EN 12697-12 2008)*

Seven specimens (noted No.1 to 7) were used to perform water intrusion tests with various blending protocol for incorporating of harmful clay (montmorillonite). These specimens were prepared following mix design requirements of 0/6 mm gap-graded AC mixture (BBTM6A, see *Delorme and Wendling 2007*), or so called EB6 from European standard (*NF EN 13108-1, 2007)*. The composition of each specimen is shown in Table 16, and the definition and calculation of binder content, richness modulus (3.6), can be found in appendix 4.1. Moreover, AC mixtures No.3 to 7 were prepared for Duriez tests as well.

Table 16 Design of AC mixtures for water intrusion tests (samples of AC mixtures No. 3 to No. 6 were composed of bitumen, montm., washed sand and diorite, by varying the location of montmorillonite. AC mixture No. 7 is a lime treated specimen)

Material	Particle size	Pure bitumen	Mastic	Design of AC mixture (wt%)				
		N°1	N°2	N°3	N°4	N°5	N°6	N°7
Bitumen	--	100	50	richness 3.6 [a]	richness 3.6 [a]	richness 3.6 [a]	richness 3.6 [a]	richness 3.6 [a]
Montm.	$D_{0/0.063mm}$	--	50	9	9	9	9	9
Washed sand	$D_{0.063/2mm}$	--	--	16	16	16	16	16
Diorite	$D_{4/6mm}$	--	--	75	75	75	75	75
Protocol of mixture	--	--	--	Sand was coated with montm. [b]	Diorite was coated by montm. [b]	No coating of sand or diorite by montm.	Clay balls [c] mixed with washed sand	Sand was coated with montm. [b] and treated with 3% lime CaO [d]

[a] Richness modulus (see appendix 4.1) [b] Protocol of clay/sand blending inspired from *Leroux and Unikowski (1980)* [c] The montm. aggregated balls are formed by spreading water on clay particles before their mixture with washed sand and diorite [d] The specimen is prepared by dry hydrated lime addition to moist aggregate with marination (*National lime association from America, 2003*)

Other specimens were prepared for Duriez tests. Blended fine aggregates (see chapter 2.1.2) and unknown fine aggregates were used to prepare BBTM6A AC mixtures. Mixtures contain sand, bitumen, filler and coarse aggregates with the fine fraction content taken as the maximum permitted value from BBTM6A regulation (Table 17). Percentages by mass (wt%) of AC mixture constituents were calculated with respect to standards (*NF EN 12697-35+A1 2007;NF EN 13108-1 2006;NF P 98-251-1 2002*). The constant thickness of bituminous film was fixed by the richness modulus to 3.6. The content of fine aggregates and clay presented in volume (vol%), and the density of the AC mixtures were calculated by considering the density of each aggregate fraction. The values are shown in Table 18.

[8] An intrusive igneous rock composed principally by silicate minerals such as plagioclase feldspar (typically andesine), biotite, hornblende, and/or pyroxene. The chemical composition of diorite is intermediate, between that of mafic gabbro and felsic granite

[9] dmm= 1/10 mm

Table 17 Design of gap-graded BBTM6A/EB6 AC mixtures with artificial fine aggregates

Design	Binder	Coarse aggregates	Artificial and unknown fine aggregates	
Aggregates fraction	-	Coarse fraction	Sand fraction	Fine fraction (including filler)
Material	Bitumen $_{35/50}$	Diorite	Sand retained on sieve 0.063 mm	Fine particles which is particle size less than 0.063 mm and added filler to reach targeted fine fraction content
Particle size (mm)	N/A	$D_{4/6}$	$D_{0.063/2}$	$D_{0/0.063}$
Content (wt%)	richness 3.6 [a]	75%	16%	9%

[a] see appendix 4.1

Table 18 Experimental design of gap-graded BBTM6A/EB6 AC mixtures with blended (artificial) and unknown fine aggregates

Series	Name	Material of in-all aggregates					Density of AC mixture [c] (g/cm^3)
		< 0.063 mm [a] (wt%)	Fine aggregates [b] (wt%)	< 0.063 mm [a] (vol% [c])	Fine aggregates [b] (vol% [c])	Bitumen (wt%)	
Reference	No clay	0.00	24.81	0.00	26.47	5.75	2.60
Blended fine aggregates -S1	S1-K2	4.37	25.00	4.77	26.79	5.81	2.59
	S1-K3	6.86	25.00	7.48	26.87	5.86	2.59
	Max. Kao.	8.57	24.79	9.35	26.70	5.80	2.60
	S1-I4	1.24	25.00	1.61	26.88	5.77	2.59
	S1-I9	4.00	25.00	5.12	27.36	5.85	2.57
	S1-I13	6.86	25.00	8.73	27.85	5.94	2.55
	Max. Illite	9.11	25.23	11.52	28.46	5.86	2.54
	S1-M2	0.08	25.00	0.11	26.68	5.73	2.60
	S1-M4	0.22	25.00	0.30	26.71	5.74	2.60
	S1-M12	0.80	25.00	1.08	26.84	5.76	2.59
	Max. Montm.	8.69	24.88	11.47	28.42	5.89	2.54
-S2	S2-KI2	7.75	25.00	8.72	27.11	5.90	2.58
	S2-KI8	5.15	25.00	6.23	27.29	5.87	2.57
	S2-IM6	2.14	25.00	2.80	27.07	5.80	2.58
	S2-IM10	1.72	25.00	2.28	27.01	5.79	2.58
	S2-KM3	6.90	25.00	7.69	27.00	5.87	2.58
	S2-KM11	2.15	25.00	2.70	26.99	5.79	2.59
-S3	S3-2	7.07	25.00	7.82	26.96	5.87	2.58
	S3-3	5.80	25.00	6.77	27.18	5.87	2.58
	S3-5	3.61	25.00	4.33	27.07	5.82	2.58
unknown fine aggregates	A	5.58	25.00	- [d]	26.75	5.81	2.59
	B	4.37	25.00	- [d]	26.73	5.78	2.59
	C	6.36	25.00	- [d]	26.76	5.82	2.59
	D	3.20	25.00	- [d]	26.71	5.76	2.59
	E	6.00	25.00	- [d]	26.75	5.82	2.59

[a] Fine fraction without filler
[b] Fine fraction + sand fraction + filler
[c] Value was calculated by the density of materials. The density of kaolinite, illite, montmorillonite, filler and sand used in this study are 2.6 g/cm^3, 2.2 g/cm^3, 2.1 g/cm^3, 2.7 g/cm^3 and 2.65 g/cm^3, respectively (*Ayadi et al. 2013; Pham 2008; http://www.mindat.org/min-2156.html; http://webmineral.com/; http://appliedgeophysics.berkeley.edu/gravity/grav23.pdf; https://en.wikipedia.org/wiki/Main_Page*)
[d] Unable to calculate because the density of particle size less than 0.063 mm is unknown.

2.2 *Experimental protocols*

In order to prepare homogenous samples, all the solid materials were divided into desired quantities by rotative sample divider PT100 from Retsch Germany, except coarse aggregates and filler. Indeed, these coarse aggregates and fillers were supplied by producers with a very low variability in their particle size, their mineralogical composition and their properties.

X-ray diffraction (XRD) is the principal method chosen in this study to identify and quantify mineral phases, as suggested in the report from Reynolds cup *(Raven and Self, 2013*). Furthermore, complementary methods, chemical analysis by ICP/OES, thermal analysis (TG/DTA), calcimeter *(NF P94-048 2003*), cation exchange capacity *(NF EN ISO 23470 2011;NF X31-130 1999)* and size distribution *(NF P94-057 1996;XP CEN ISO TS 17892-4 2005;XP P 94-041 2014*), were used as complimentary methods to judge the accuracy of quantitative results from XRD.

2.2.1 Mineralogical analysis by X-ray diffraction (XRD)

2.2.1.1 Sample preparation for X-ray diffraction

Powder samples: the main cores for mineralogical analysis in this study were prepared following the recommendations by *Jelavic (2012)* and *Vecchione (2014)*. Whole samples which were homogeneously divided via sample divider were gently ground and sieved through the 0.032 mm mesh. In order to minimize preferred orientation (PO) of minerals and segregation, samples were mounted on sample holders by top loading passing through a 125 µm mesh. Then, the surface of samples was leveled off using a thin razor-blade in perpendicular directions to avoid preferred orientation (PO) and minimizing sample surface roughness. The samples used for RIR method, were prepared using this powder, after homogeneously mixing the same dry mass <0.032 mm sample powder and corundum powder (Al_2O_3 Alfa Aesar with 99.98% purity).

Oriented glass slides: the oriented clay mineral fractions were prepared by following the combined method from *Thiry (2013) and Jermouni (2015).* Fines ($D_{0/0.063\ mm}$) from fine aggregate were collected from wet sieving with distilled water *(Soukup et al. 2008*), and then particles were separated from water by centrifugation using a Sorvall RC 6 Plus centrifuge with 19000 round per minute (rpm) in 20 minutes to discard the transparent supernatant. The process of fines decarbonation by HCl addition was also applied with acid added until the pH remained stable in acidic medium. Cationic saturation of clay was performed if necessary, upon agitating extracted clay 1 mol/L NaCl, KCl, $MgCl_2$ or $CaCl_2$ solution over night. Then, clay was separated from solution by centrifugation with the previously mentioned setting. After repeating this cation saturation procedure 3 times, the cation-saturated clay was washed 3 to 5 times with ultra pure water and separated again by centrifugation *(Duc, 2002)*. Ideally, the clay suspension obtained at the end of the preparation remained stable after 24h (particles stay in suspension and sediment slowly).The clay suspensions for orientated glass slides were maintained in continuously agitated 0.4 wt% suspension

The oriented glass slides were prepared by gently dropping 1.5 ml of a 0.4 wt% suspension on clean and dry glass slides (2.5 cm × 2.5 cm), and then drying at room temperature over a day to form a clay film less than 10 µm thick. For efficient identification and quantification of mineral phases (*Laruaz et al. 2013; Brindley and Brown 1980*), the experimental design used for cation-saturation of clay and treatment of glass slides is

shown in Table 19. Natural or air dried (AD) glass slides are analyzed and completed by three other treatments: one AD glass slide is heated at 550°C no less than 2 hours, an other one at 300°C during 2 hours minimum as well and the last one is put in contact with ethylene glycol vapor (EG) in an hermetic desiccator put in an oven overnight at 55°C.

Table 19 Treatment of clay suspension and orientated glass slide for each sample

Material	Cation-saturated suspension					Treatment			
	non exchanged	Mg-	Ca-	K-	Na-	AD	EG	550°C	300°C
All the extracted clays: Kaolinite, Illitic and Montmorillonite	x					x			
	x						x		
	x							x	
	x								x
		x					x		
			x				x		
				x			x		
Extracted montmorillonite					x	x			
Clay particles from unknown fine aggregates	x					x			
	x						x		
	x							x	
			x				x		

* x: The treatment of sample; Underline: Sample has not been saturated by cation

2.2.1.2 Setting of X-Ray diffractometer

The X-Ray diffractometer, D8 Advance from BRUKER (θ–θ mode), produced mineralogical analysis with the settings in Table 20. The corundum sample was regularly applied to standardize the diffractometer.

Table 20 The setting of X-Ray diffractometer

Item	Setting
Radiation	CoKα
Goniometer	217.5 mm
Temperature	25°C
Specimen	Flate-plate rotating by spinner in 30 rpm
Power Setting	35 kV, 40 mA
Soller Slit	2.5°
Divergence Slit	0.3° (fixed)
Receiving slit	0.15°
Monochromator	no
Detector	Lynx eye (rapid 1D detector with an opening 3°)
Collimator	Knife edge collimator
Filter	Iron filter for K_β ray ($K\alpha_2$ is corrected thanks to EVA)
2θ range for powder sample	2–80° 2θ
2θ range for orientated glass slide	2-45° 2θ
Step width	0.01° 2θ
Time of acquisition per step	1.5 s

2.2.1.3 Identification and quantification of mineral phases

The identification of mineral groups was done by using XRD pattern from <0.032 mm sized powder particles and orientated samples deposited on glass slide. The XRD pattern formed by detectable mineral phases in the sample was analyzed by referring to mineralogical data base ICDD-PDF2 using the EVA software. This data base collects the d-spacing of crystallographic atomic places characteristic of each mineral at the origin of X ray reflection (*Brindley and Brown 1980*). The information of XRD identification is shown in appendix 1.1.

The quantification of mineral phases was done by several methods, in order to turn the most reasonable value and identify the best compromise from methodology. The reference intensity ratio (RIR) and Rietveld method were applied to powder samples, whereas the mineral intensity factor (MIF) method was used for EG-orientated glass slides. According to the theory of each method, the calculation can be shortly introduced in the following paragraphs.

Reference intensity ratio (RIR) method

The quantity C_q of mineral phase q is calculated by the following equation 27:

$$C_q = C_{cor} * \frac{(RIR)_{cor}}{(RIR)_q} * \left(\frac{A_q}{A_{cor}}\right) \quad \text{Eq. 27}$$

Where:

- C_q and C_{cor} are the unknown weighted concentration of phase q and the weighted concentration of corundum Al_2O_3 added to the sample (a 50/50 mixture by weight);
- $(RIR)_{cor}$ and $(RIR)_q$ are the reference intensity ratio of corundum ($RIR_{corundum}$ is equal to 1.07 for our corundum) and the reference intensity ratio of phase q (from ICDD database), respectively. When the RIR doesn't exist in data base (it's the case for clay), arbitrary RIR were used. In practice, RIR were taken equal to MIF : $RIR_{kaolinite}$ = 0.5, RIR_{illite} = 1, $RIR_{montmorillonite}$ = 1,5 and $RIR_{chlorite}$= 1. The $RIR_{kaolinite}$ is close to RIR = 0.52 found by Hillier (*2000*) with the spray dryer method used to dry clay before analyses, which produces spherical clay particles and lower the preferential orientation of clay particle and its effect on X-ray pattern. For Illite, the RIR values from both references are very different. For montmorillonite, no RIR are available in the literature.
- A_q and A_{cor} are the net peak areas of the major diffraction peaks for q and corundum phases respectively. They are measured on raw XRD patterns and subsequently corrected using EVA software to account for background correction and overlapping by other peaks.

When all the C_q are calculated from Eq. 27, final concentrations Cq' are calculated using Eq. 28:

$$C'_q(\%) = \frac{C_q}{\sum_i C_i} \times 100 \quad \text{Eq. 28}$$

Mineral intensity factor (MIF) method

The quantification of clay into the clay fraction associated with the < 2µm fraction was calculated using Eq. 29 by multiplying the d(00x) EG treated peak area and the MIF coefficient given by *Holzapfell (1983).* The

applied factors are 0.5, 1, 1.5 and 1 for kaolinite, illite, montmorillonite and chlorite respectively. A correction is applied to peak areas to account for their overlapping by other peaks. Two strong hypotheses are made: clays are the only phases that compose the < 2 μ m fraction and all the clay in the each sample is gathered in the < 2 μ m flocculated fraction.

$$C_{clay,i}^{2\mu}(\%) = \frac{A_{d(00x),i}}{\sum_i A_{d(00x),i}} \times 100 \qquad \text{Eq. 29}$$

The clay content in the whole sample $C_{clay,i}(\%)$ is calculated by multiplying $C_{clay,i}^{2\mu m}(\%)$ by the percentage of < 2 μ m fraction measured by sedimentometry. This percentage depends on the ability to perfectly disperse the material and it was observed that dispersion is variable according to clay nature. Two standardized methods for capturing the particle size distribution (XP CEN ISO/TS 17892-4 and XP P 94041) were tested. They differ by the use or not of sodium hexametaphosphate to disperse particles before wet sieving at 0.063 mm and by the drying or non drying of the extracted fine particles before sedimentometric tests.

$$C_{clay,i}(\%) = C_{clay,i}^{2\mu m}(\%) \times (< 2\mu m\%) \qquad \text{Eq. 30}$$

Rietveld method

The quantities of mineral phases determined by Rietveld method were given by Topas software. The reason for applying this method is that high standard deviation (20%) from clay quantification of clay bearing samples (*Moore and Reynolds 1989*) can be solved by the structure modeling of clay mineral.

Essentially, these result from fitting the observed diffraction pattern with a calculated one which is a sum of patterns calculated for each phase in the sample (*Snyder and Bish 1989; Bish 1994*).The difference between calculated and observed patterns noted Rwp is minimized by an interactive refinement/optimization procedure. The amount of phases present in the sample is directly obtained from the final value of the scale factor refined for each phase when the pattern of the sample powder is considered. The same work can be done on the 50/50 mixture between the material and corundum. In this case, the final value of the refined scale factor for each mineral refers to the mixture, hense the phase concentration in the sample is given by Eq. 31:

$C_i(\%) = \frac{C_i^{50/50}(\%) \times 100}{\%cor}$ where % corundum is the percentage of corundum in the mixture (~ 50%).

The final concentration is calculated using : $C'_i(\%) = \frac{C_i(\%) \times 100}{\sum_i C_i}$ Eq. 31

Basically, most mineral structures have been studied and can be found in the mineral database. However, this database misses complex mineral structure as well as mineral varieties observed with clay, amorphous, interstratified minerals, etc.. In this study, each input clay mineral phase has been confirmed and agreed thanks to mineralogical results such as chemical composition, d (*001*) basal space, exchangeable cation, etc. The coordination of atoms, parameter of clay and clay structure has to be cross-checked after each refining sequence from Topas in order to come up with the reasonable clay mineral. Moreover, mineral phase fitting and calculation errors are better indicators for the quantitative results than Rwp.

2.2.2 'Complementary method' or 'Chemical method'

Several methods were used and combined to propose or validate each quantitative analysis. These complementary methods are chemical analysis, thermal analysis and cation exchange capacity measurement.

2.2.2.1 Chemical analysis

For chemical analysis tests, 500 mg of < 0.08 mm ground sample were calcined at 450 °C. Then, the solid was dissolved in Hydrogen fluoride (HF) with $HClO_4$ at 160°C. One millilitre of HNO_3 Suprapur (d=1.33) was added, then the final solution was filtered and ultra pure water was added to obtain a volume of 100 ml. For silica analysis, another protocol was applied. 300 mg ground samples were calcinated at 1100 ° C after mixing with 2g of lithium tetraborate ($Li_2B_4O_7$), and then, dissolved by 500 ml of Suprapur HNO_3 (d =1.33) diluted at 1.2% by volume. The solutions after dissolution were analyzed using the 720-ES Coupled Plasma- optical Emission Spectroscopy (ICP-OES) from Varian. A plasma was used to ionize the chemical elements present in the solution in high temperature conditions (5000 to 6000 ° C) to measuring the percentage of analyzed elements. Excited elements spontaneously de-excite while emitting photons whose wavelength (or energy) measurement by the optical device called holographic grating allows element identification by the computer program. The chemical composition is given in atomic percentage or oxide percentage and has to be completed supplemented by the loss on ignition (noted LOI) to reach 100%. LOI is measured by thermal analysis and corresponds to the mass loss of the sample at 1200°C, that's to say the loss of water (H_2O) and carbon dioxide CO_2 for our samples as these elements are not quantified by ICP-OES.

2.2.2.2 Thermal analysis

Further to assisting mineral identification, thermal analysis allows quantifying some mineral phases such as calcite or kaolinite. However, as several reactions may occur simultaneously, for example the loss of OH from illite occurs in the same range as the loss of CO_2 by calcite, only the global los of weight maybe used. Hence, the loss of water at low temperature H2OBT (≤ 230°C), the loss of water at high temperature H2OHT added to the loss of CO_2 between 230°C and 1200°C will be measured. The total mass loss corresponds to LOI.

A few milligrams of < 0.08 mm ground sample were placed in a tarred platinum crucible and calcined. The thermal analysis test was performed by a simultaneous thermal analyzer STA 409E from NETZSCH. It measures the amount sample mass change as a function of temperature in a controlled atmosphere. Measurements are used primarily to determine the composition of sample and to predict its thermal stability at temperatures rising from 25 °C to 1200 °C at a rate of 10°C/min through nitrogen sweep (80 ml/min). The material may be characterized from mass loss due to decomposition, oxidation, or dehydration. Any temperature for which a mass loss occurs is a specific reaction that occurs in the sample, this reaction being linked to the nature of the minerals which are present (i.e. calcite, kaolinite).

2.2.2.3 Cation exchange capacity (CEC)

CEC measures the maximum quantity of cations that a material is able to exchange with surrounding medium at a given pH value. Such measurements are useful to interpret methylene blue value variations and provide assistance for sample quantitative analyses.

The quantity of undried sample tested to measure the cation exchange capacity (CEC) varies from 50 mg to 10 grams depending on clay mineralogy (as the test is a colorimetric test using a spectrophotometer, the quantity of sample has to be sufficient to detect a drop in color intensity of the reactive solution and small enough not to discolor all the reactants). The water content of sample was measured in parallel on another subsample and introduced in the CEC calculation.

The protocol of CEC test using 0.05N cobaltihexamine chloride solution as applied in this study is based on *NF X31-130* standard. The suspension of sample mixed with 35 ml of 0.05N cobaltihexamine chloride solution was agitated during 2 hours in a 60 ml centrifuge tube, and then the supernatant was collected after centrifuging at 19000 rpm for 20 minutes (more if particles remain in suspension). The remaining concentration of cobaltihexamine ions in the supernatant, which gives an orange color to the reactant, was measured using a spectrophotometer V-630 from JASCO. The wavelengths of UV-visible peaks used for quantification range between 389 nm and 600 nm. The quantification is made thanks to a calibration curve drawn from measured absorbance of several diluted solutions of known 0.05N cobaltihexamine chloride concentration. Then, the calculation of CEC value is:

$$CEC(meq/100g) = \frac{(C_i - C_f) \times V_1 \times 100}{m}$$

Where:

- C_i *and* C_f are the initial concentration (0.05N) and final concentration of cobaltihexamine solution,
- V_1 (ml) is the volume of cobaltihexamine solution put in contact with the sample,
- m (g) is the dry mass of sample calculated from humid sample mass and its water content.

2.2.2.4 Principle of 'Complementary method'

This method has been applied in the geological field since 1915 (*Emerson 1915*). It consists to adjust the calculated chemical composition of the material by varying the quantity of each mineral phase in order to fit the measured chemical composition (given by ICP/OES). The adjustment needs the knowledge of the stoechiometry of each mineral phase (which represents a difficulty for both clays or feldspars). To go further and exclude most data sets of quantities, the software MINRERAUX developed and applied in LCPC fit not only the chemical composition but also the thermal analysis (H2OHT and CO2 content). In this study, the size distribution of sample (< 2 µm associated to clay content and the < 63µm associated to feldspar and clay fractions) is introduced to guide the calculation and the cation exchange capacity is also fitted. A homemade excel file (Appendix 1) was established to adjust the clay mineralogy by fitting the CEC value, the chemical composition and the thermal analysis, as well as the stoechiometry of clays (the initial set of data introduced comes from TOPAS, RIR and/or glass slides analysis, see appendix 1.2). The calculation of CEC value from clay stoechiometry uses the estimation of the number of isomorphic

substitutions in illite or montmorillonite (no substitution is assumed to be present in kaolinite). In the case of illite, the CEC is taken as 1/16 to 1/10 of the quantity of isomorphic substitution in crystal cell corresponding to the quantity of potassium (the quantity of K is equal to 1 mol / mole of crystal cell in the case of muscovite and 0.75 for illite). For other clay, an average value of the CEC value given by literature for pure mineral phase is used.

2.2.3 Protocols to study MB adsorption on material

MB adsorption on aggregates were measured by drop test (*NF EN 933-9*) commonly used in quarries (MB_{drop}), and UV-photometer is used by academic field ($MB_{UV\text{-}pho}$). MB $_{UV\text{-}pho}$ was measured using a protocol similar to the CEC protocol: the residual concentration of MB solution after contact between MB and fine aggregates is measured thanks to a colorimetric test using the spectrophotometer and a calibration curve. In parallel, MB adsorption onto clay was investigated using UV-visible spectrum measured on MB-clay suspension.

2.2.3.1 $MB_{UV\text{-}pho}$ measurement on MB-clay solution

As for CEC measurement, the quantity of tested sample (50 mg to 10 g) is adjusted to the clay nature and its proportion in the sample until the tested quantity yields a $MB_{UV\text{-}pho}$ value within the calibration range of the spectrophometer. The water content is measured in parallel on another subsample. After agitating in 35 ml of a 1 g/L MB solution during 2 hours, the supernatant is separated from solid particles by centrifugation at 19000 rpm for at least 20 minutes, depending on the presence of remaining particles in the supernatant. The residual MB concentration in the supernatant after adsorption is determined using the V-630 spectrophotometer, from JASCO. The wavelength of the UV-visible peak used for quantification is at 663 nm. It corresponds to the monomer form of MB molecules aggregates. To determine the residual MB quantity in solution, a calibration curve is drawn using several diluted MB solutions from 0 to 20 mg/L (Figure 32). Contrary to the CEC, the calibration curve is not strictly linear as expected from Beer Lambert law. This is due to MB molecule aggregation in solution: monomers content decrease while dimmers content increase when MB concentration increases in solution. To reduce the aggregation effect, the maximum absorbance of supernatant is fixed to 1, corresponding to a MB concentration in supernatant < 3 mg/L. A limited calibration curve is drawn on the range 0-5 ml/L instead of 0-20mg/L. The measurement is more accurate and closer to zero the absorbance (but Abs must be > 0.01). For each test, 3 measurements are performed to assess the standard deviation.

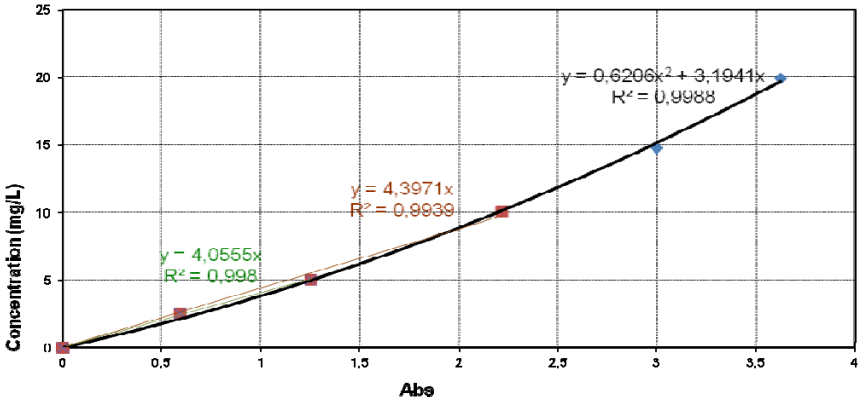

Figure 32 MB calibration curve

The calculation of $MB_{spectro}$ adsorption is:

$$MB_{UV-pho}(g/kg) = \frac{(C_i - C_f) \times V_1 \times 10^{-3}}{m}$$

Where:

- C_i *and* C_f (g/l) are the initial concentration and final (residual) concentration of MB solution, respectively;
- V_1 (ml) is the volume of MB solution put in contact with the sample;
- m (g) is the dry mass of sample calculated from the humid sample mass and water content.

2.2.3.2 $MB_{UV\text{-}pho}$ measurement on MB-clay suspension

Cation exchange treatment was applied to clay suspension and to the extracted fine fraction ($D_{0/0.063mm}$) of unknown fine aggregates. Clayey fractions were saturated with various cations by agitating the suspension with concentrated salt solutions (Table 21). The procedure of clay cation saturation is similar to the protocol mentioned from Duc *(2002)*.

Table 21 Salt solution for cation-saturation treatment

Cation	Li	Na	K	Mg	Ca	Cs	La
Chemical compound	LiCl	NaCl	KCl	$MgCl_2$	$CaCl_2$	$CsCl_2$	La (N_3O_9)*$6H_2O$
Concentration (mol/L)	1	1	1	1	1	0.05	0.01

Once a known quantity of fine particles has been submitted to cation exchange in cation saturated condition, 0.4 w% cation exchanged clayey material (CEMs) suspensions were carefully prepared with ultra pure water and kept agitated until spectrum analysis. Spectrum is obtained on the suspension after addition of 1g/L MB solution until the absorbance, Abs, reaches 1. Several suspensions had to be prepared and tested to reach this condition and spectrum was then recorded just after the addition or after different contact time. CEMs suspensions were also used in the sessile drop test detailed in chapter 2.2.4.1.

Samples of reduced-charge montmorillonite (RCMs) were prepared from Li-Saturated montmorillonite. By referring to the protocol of RCMs preparation from Greene-Kelly (*1953*) and Bujdak (*2001*), Li-saturated montmorillonite was dried at 40 °C to constant mass and ground until particles pass through a 0.063 mm mesh. Then, this powder was divided into seven equal portions. One of seven portions was used as the parent sample, whereas the others were heated at 105 °C, 120 °C, 140 °C, 180 °C or 200 °C for 24h. Then, 0.4w% RCMs suspensions were prepared by measuring dry samples and adding distilled water. Suspensions were kept agitated until the spectrum measurement after the addition of MB solution to reach abs=1 as previously explained.

Each designed MB-suspension using the initial 0.4w% suspension of clay or CEMs or RCMs contained approximately 7×10^{-2} g/L of fine particles and the residual concentration of MB molecules in solution after adsorption on particles was no higher than 5 mg/L (the closer to 0).

Even though *Bujdak (2001)* stated that the equilibrium of MB-suspension was achieved after 18 hrs of agitation, MB-suspensions were continuously agitated and the evolution of suspension spectrum was measured from 2 minutes up to one month after the addition of MB solution into clay suspension, in the

event that the equilibrium status would be modified by the material. The UV-visible adsorption spectrum of each MB-suspension was measured with V-630 spectrophotometer from JASCO. The wavelengths of the observed UV-visible peaks cover the range from 400 nm to 800 nm, all types of MB molecule aggregates may be observed.

2.2.4 Protocols to study water-bitumen-clay interactions

The study of water-bitumen-aggregate interactions consists of four types of tests:

- the sessile drop test is used to study interactions from surface energy point of view. It was applied to clay thin films deposited on glass slides with or without treatments,
- a home-designed water intrusion test was developed and applied to understand water penetrates AC materials in the presence of montmorillonite. We wanted to see whether the water resistance at the montmorillonite/aggregate interface in AC mixtures would vary with various location of montmorillonite dispersion in fine aggregates,
- a test applied to thin clay films was inspired from the standardized oliensis test to discuss. The compatibility between bitumen and clay.
- the standardized Duriez test was applied to study the water sensitivity of AC mixtures.

2.2.4.1 Sessile drop test

Samples for sessile drop tests were prepared using the 0.4w% CEMs suspensions mentioned in 2.2.3.2 and 0.4w% natural clay (NC) suspensions, extracted from clay rocks but without any cation exchange treatment. After preparation, 1.5 ml of each suspension was gently dropped on a clean and dry 2.5 cm × 2.5 cm thin glass slide *(Basu S. et al. 2000*; *Shang et al. 2008*). The deposit on each glass slide was air-dried at room temperature over a week to form a continuous clay film less than 10 µm thick.

The sessile drop test was performed using a Drop Shape Analyser coupled with a heating chamber for high temperatures (TC21 from Kruss GmbH) and four liquids (water, glycerol, ethylene glycol and diiodo-methane), whose surface energy characteristics are known (see Figure 33 and Table 22). One drop of each liquid was deposited through 0.5 mm diameter of needle on intact clay thin film so that contact angle is measured automatically using a 1024 x768 pixels camera and an adapted light.

The work of adhesion W_{ad} of bitumen on clay surface at bitumen-clay interface was calculated from corresponding contact angle measured in the heating chamber at a constant temperature of 140°C. The temperature reduction from 160°C (common AC temperature) to 140°C was applied to increase the viscosity of bitumen in order to stabilize the volume of the bitumen drop. The drop volume and surface energy of liquids and bitumen are shown in Table 22.

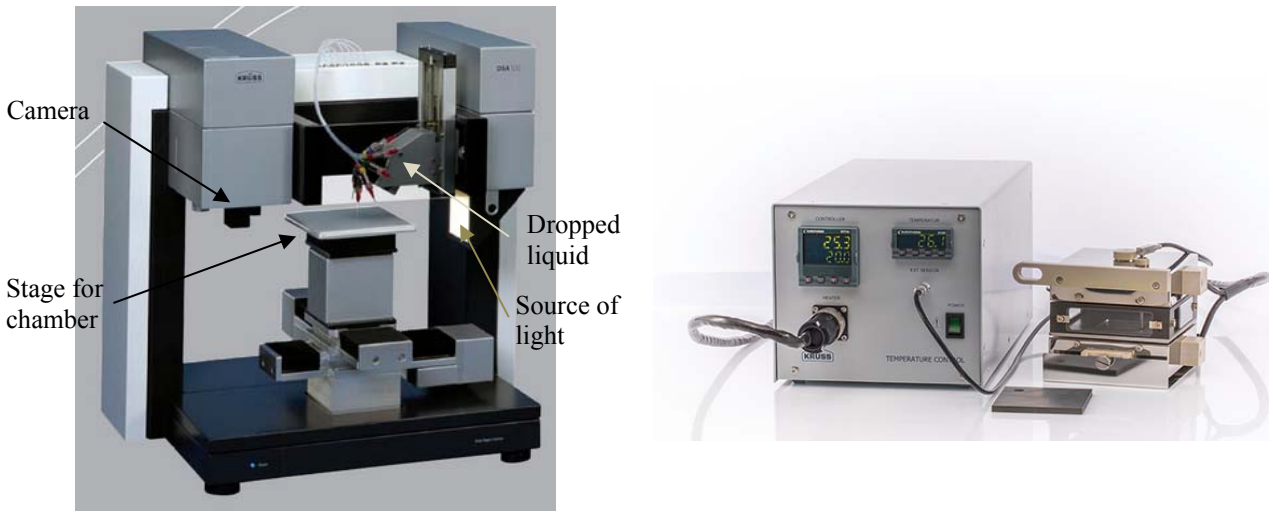

(a) (b)

Figure 33 (a) Drop Shape Analyser DSA100 coupled with the (b) Kruss tempering chamber for high temperatures (TC21)

Table 22 Drop volume and surface energy of test liquids and bitumen

Material	Type	Drop volume	Polar component of surface energy γ^P (mJ/m^2)	Dispersive component of surface energy γ^D (mJ/m^2)	Surface energy $\gamma = \gamma^P + \gamma^D$ (mJ/m^2)
Liquids	Water [a]	7 µl	51.0	21.8	72.8
	Ethylene glycol [a]	5 µl	16.8	30.9	47.7
	Glycerol [a]	10 µl	26.4	37	63.4
	Diiodo-Methane	1.5 µl	0.0[b] ; 6.7 [c]	50.8 [b] ; 44.1 [c]	50.8
Bitumen	35/50 at 140°C [d]	12 µl	5.0	23.0	28.0

[a] *Strom, 1987* [b] *Rosenholm, 2007* [c] *Yu et Dekker, 1982* [d] *Somé, 2012*

2.2.4.2 Modified oliensis spot test (inspired from *ASTM D1370 2012*)

Clay thin films obtained from the deposition of 0.4w% clay suspensions on glass slides were used for 'modified' oliensis spot test. The standardized test procedure (*ASTM D1370, 2012*) provides a mean to evaluate the contact compatibility between asphalt and clay, and also to assess the degree of interaction between asphalt and the different types of clay. A drop of molten bitumen (12 µl± 1.1) was placed on the thin clay film at a constant temperature of 140°C, and kept for 4 hours. Oliensis result was calculated as the ratio of the thickness of the oil ring surrounding the drop to the spot radius (oil ring + drop).

2.2.4.3 Water intrusion test

BBTM6A AC mixtures numbered No.1 to 7 (Table 16) were separately placed in 2 liter glass beakers and immersed in methylene blue (MB) solutions (see Figure 34a). The MB solutions played the role of chemical probe: the decrease of MB concentration in the solution indicated the dye adsorption by clay after water intrusion into the specimen. The residual MB concentration in the solution in contact with each specimen was measured by UV-photometry at different times during 23 days. The concentration allows the tracing of

MB route into the specimen until the clay particles (the hypothesis is that only clay may adsorb MB molecules). When the MB concentration reached a value too low to be measured, new MB molecules were introduced in the beaker. This test was performed in a light isolated environment due to the UV sensitivity of MB molecule.

(a) (b)

Figure 34 Water intrusion test measured by MB solution,
(a) sample before immersing in MB solution and (b) a box is used as a light isolated system during 1 month

2.3 Plan of experiments

This work focused on:

- quantitative methods to determine the mineral phases content in fine aggregates,
- methylene blue value to better understand how the testing protocol impacts the measured value and how the mineralogical characteristics of aggregates impact their methylene blue value,
- the effect of mineralogical characteristics of clay on the interaction between clay and bitumen in terms of mechanical properties and adhesive resistance in asphalt mixture.

In order to fulfill this task, this study is divided into 2 sub-objectives, a mineralogical approach of aggregates for engineering purposes and a qualification of the water resistance of AC mixtures. The schematic diagram of research objective and experimental design is shown in Figure 35.

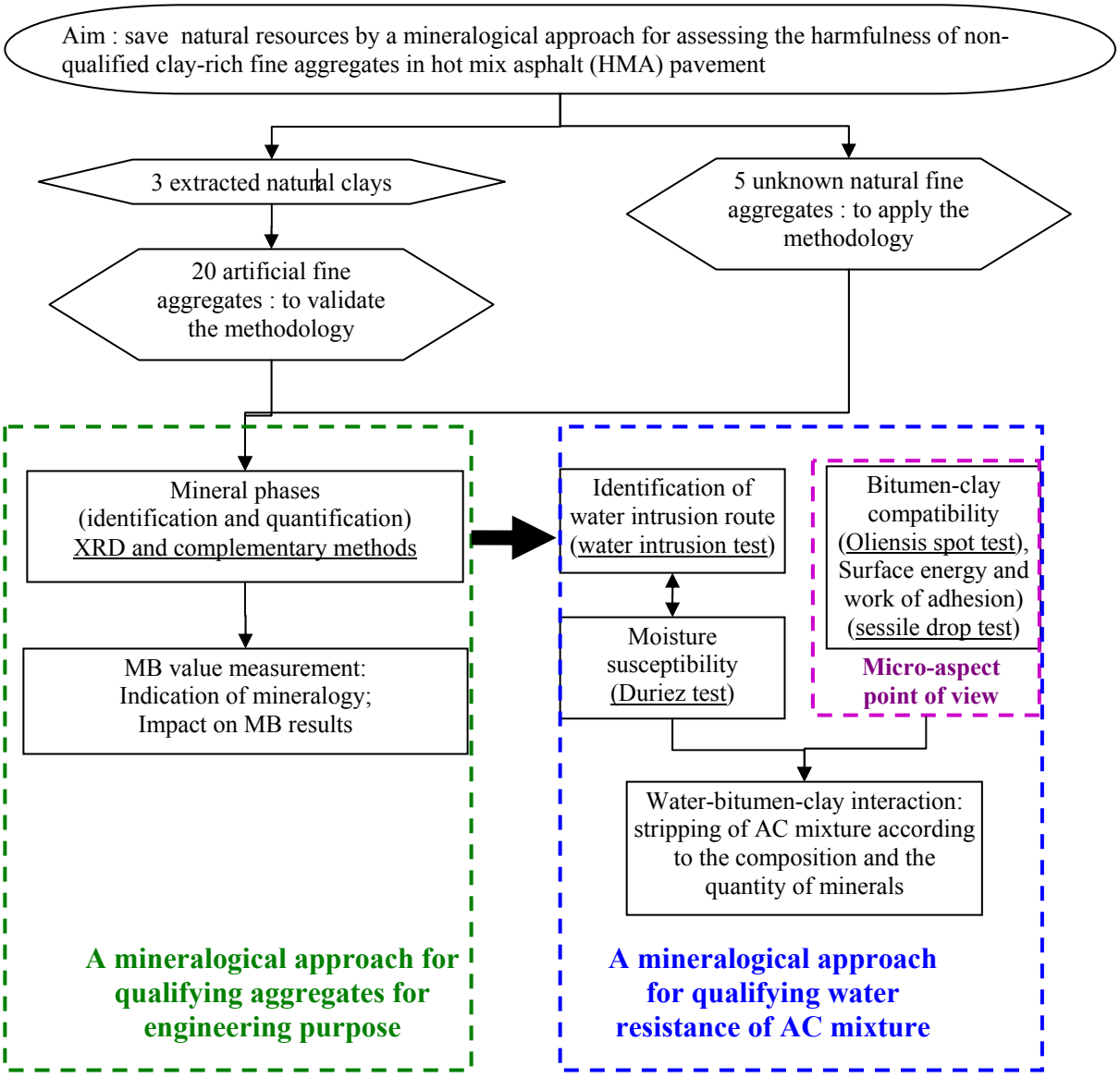

Figure 35 The schematic diagram of PhD work objectives and the experimental design

Chapter 3 Experiment results

3.1 Mineralogical analysis

The identification and quantification of materials were achieved by using the usual X-ray patterns from powder sample and orientated glass slides. Complementary methods which consisted of particle size distribution, cation exchange capacity, calcimeter test, thermal analysis and chemical analysis, were applied in this study in order to judge the quantitative results from X-ray diffraction. Different methods of quantification were applied on extracted clays (with a mineralogical composition close to pure clays) and on artificial fine aggregates to compare their accuracy. In particular, the analysis focused on the ability of methods to detect and quantify low amount of clays which may control the stripping phenomenon in asphalt concrete pavement. Taking into account the expertise acquired on artificial sands, methodologies of quantification were also applied on blinded fine aggregates the identification of which can be complex and needs generally the knowledge of the geological origin of sands and its history from the quarry to the lab (presence or not of a treatment, mixtures between different source of aggregates…).

3.1.1 Identification of mineral phases from X-ray diffraction

3.1.1.1 Extracted clays and washed sand

The XRD patterns on powder sample of extracted clays, kaolinite, illite and montmorillonite and the washed sand (Figure 36) allowed the identification of the mineral phases that composed samples.

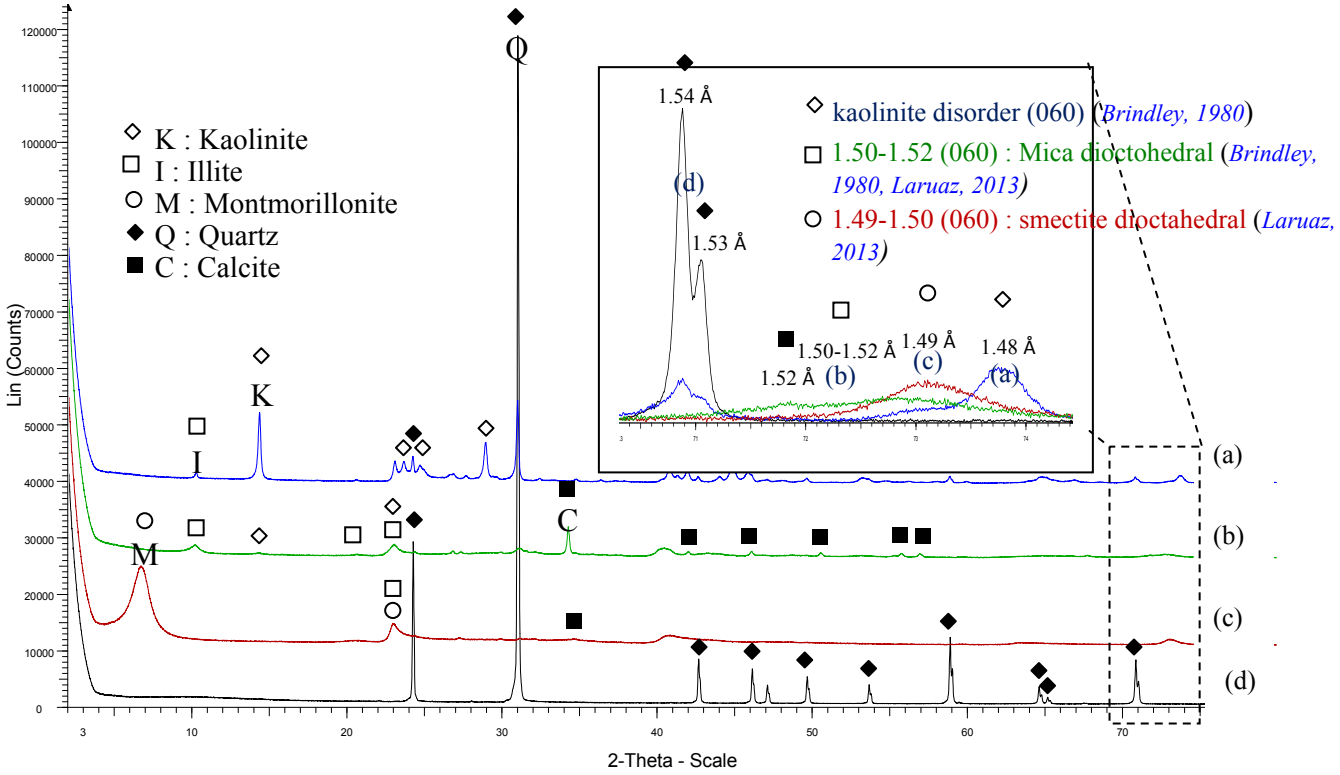

Figure 36 XRD patterns of extracted (a) kaolinite, (b) illite, (c) montmorillonite and (d) washed sand in powder.

The major mineral phases in extracted kaolinite, illite, montmorillonite and washed sand was evaluated and sum up in Table 23. The main phases were kaolinite for extracted kaolinite (with illite), illite for extracted illite (with kaolinite), montmorillonite for extracted montm. (with illite). Extracted clays consisted also of secondary mineral phases as well such as calcite in extracted illite or montmorillonite and quartz in extracted kaolinite or illite. The washed sand is composed exclusively by quartz.

Table 23 Mineral phases of extracted clays and washed sand (maj.: main phase)

Sample	Mineral phase					
	Kaol.	**Illite**	**Montm.**	**V/S**	**Calcite**	**Quartz**
Ext. Kao.	P, O (maj.)	P, O				P
Ext. illite	P, O	P, O (maj.)			P	P
Ext. Montm.		P, O	P, O (maj.)	O	P	
Wash sand						P (maj.)

P, O indicate if the phase is present on powder sample and/or on orientated sample.
Maj. indicates the major phase. V/S: interstratified vermiculite-smectite mix layer.

Major phases (with a content usually higher than 1%) were detected on powder sample whereas X-ray diffraction was less sensitive to amorphous phases that appeared as large peaks. No amorphous phases were clearly detected. Because peaks at low 2θ° angles on powder sample might be attributed to several types of clay, the identification of clay fractions were confirmed using X-ray patterns on orientated glass slides. From powder sample, the analysis of non-basal d (*060*) reflection on Figure 36 provided also a satisfactory way to confirm the nature of the major clay. The (060) reflection peak of disorder kaolinite, illite group and dioctahedral smectite (montmorillonite) were detected at the 1.48 Å, 1.50 Å and 1.49 Å positions, respectively (*Brindley, 1980, Laruaz et al. 2013)*. The information for clay mineral phases identified by XRD qualitative analysis can be also found in appendix1.1.

The reflection at 14,5 2θ° corresponding to kaolinite or chlorite d (*001*) basal space around 7 Å decreased after the heating at 550°C. It indicates the existence of **kaolinite phase** in the extracted kaolinite (Figure 37) or in the extracted illite (Figure 38). The **dioctahedral micas** were also confirmed by the presence of d (*001*) basal space around 10 Å at 10.3 ° 2θ on all the treated and cation exchanged glass slides of extracted kaolinite, illite and montmorillonite (Figure 37, Figure 38 and Figure 39). The presence of swelling clays was rigorously evaluated considering their strong impact on asphalt concrete behavior and the appearance of stripping in contact with water. No trace appeared in kaolinite or illite whereas the main clay extracted from extrac. Montm. behaved as expected for a swelling clay : the increase of the (*001*) peak intensity at 10 Å on heated montmorillonite glass slides at 300°C and 550°C indicates the existence of swelling mineral phase (Figure 39). This phenomenon came from the loss of water molecules from the montmorillonite interlayer space after heating which induced the collapse of the d (*001*) basal space from 15 Å to 10 Å (*Pham and Brindley 1973*). The (001) peak shift towards 17 Å after EG treatment also confirmed the presence of montmorillonite. Vermiculite or a interstratified vermiculite-smectite mix layer (V/S) was also identified by the treated and cation exchanged montmorillonite glass slides (see appendix1.1)(*Brown and Brindley 1984*). This Vermiculite or V/S mix layer was probably formed by the evolution of cations in the interlayer of structure during weathering (*Buckman and Brady 1969;Fieldes and Swindale 1954*). The Mg-

saturated glass slide shall be treated with glycerol to further confirm the mineral phases between vermiculite and V/S mix layer.

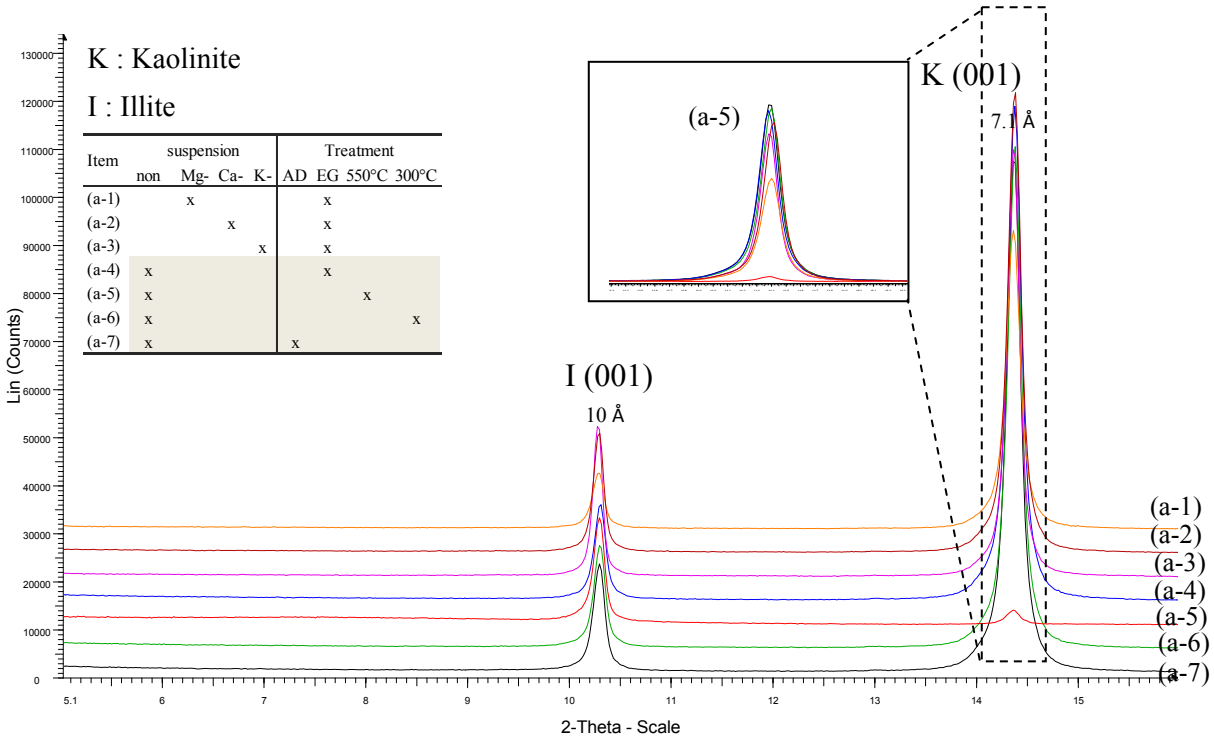

Figure 37 XRD patterns of extracted kaolinite in (a-1) Mg-, (a-2) Ca-, (a-3) K- and (a-4) non-cation exchanged-glass slides with EG treatment, and in the temperature heated up to at (a-5) 550 °C, (a-6) 300 °C and (a-7) non-heating glass slides with AD treatment

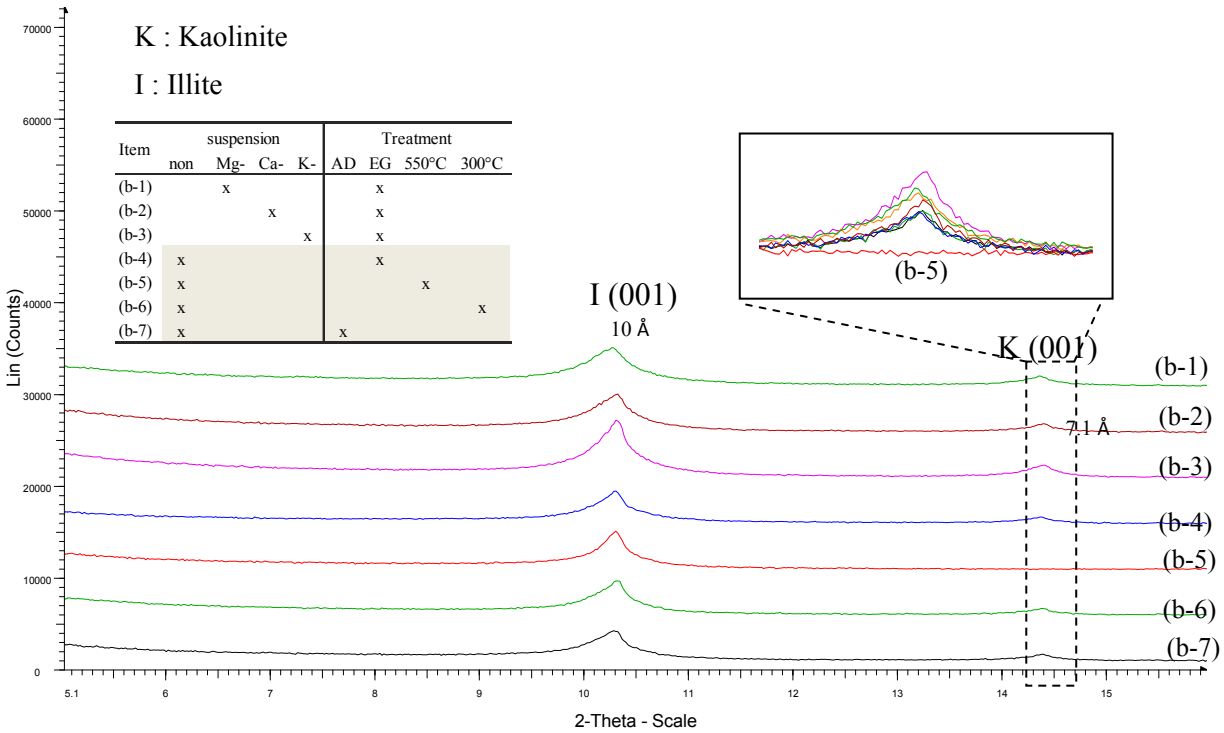

Figure 38 XRD patterns of extracted illite (b-1) Mg-, (b-2) Ca-, (b-3) K- and (b-4) non-cation exchanged- glass slides with EG treatment, and XRD patterns of extracted illite heated up to at (b-5) 550 °C, (b-6) 300 °C and (b-7) non-heated glass slides with AD treatment (AD for air dried).

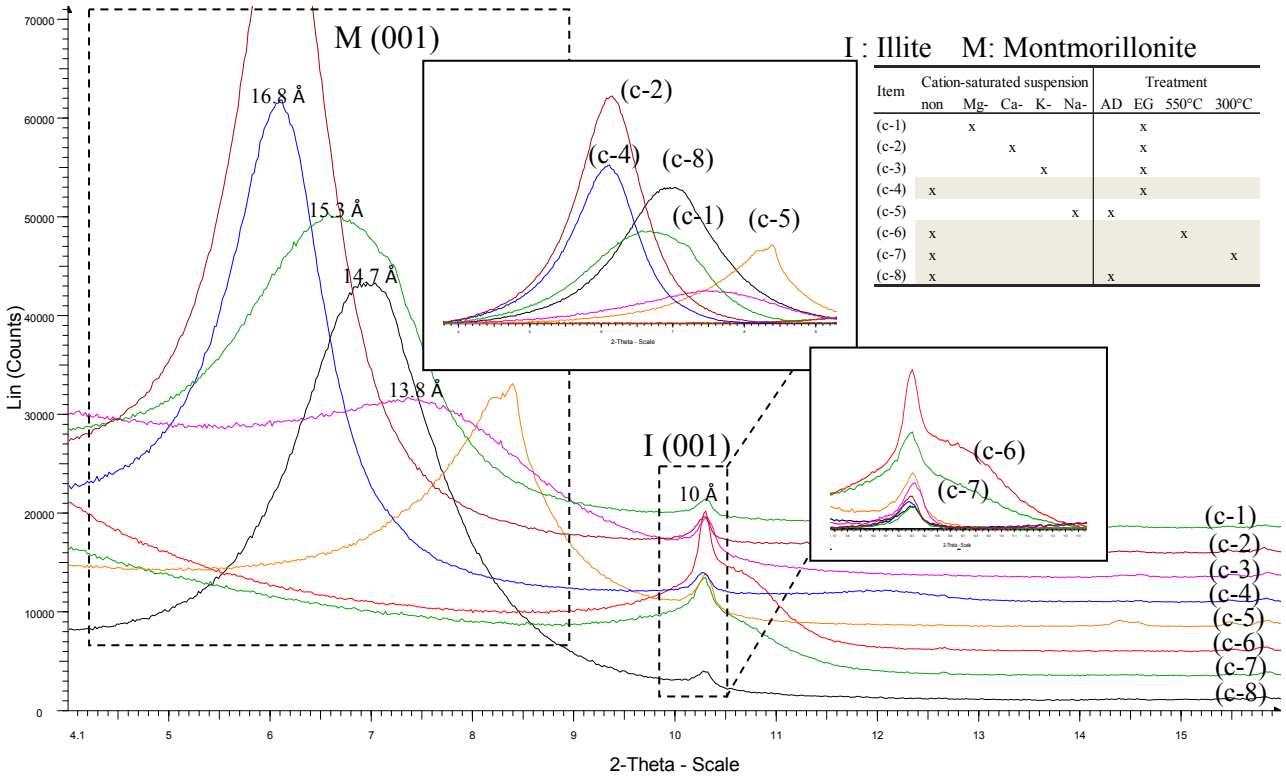

Figure 39 XRD patterns of extracted montm. in (c-1) Mg-, (c-2) Ca-, (c-3) K- and (c-4) non-cation exchanged-glass slides with EG treatment, (c-5) Na- glass slides with AD treatment and XRD patterns of extracted montm. heated up to at (c-6) 550 °C, (c-7) 300 °C and (c-8) non-heated glass slides with AD treatment (AD for air dried).

To conclude the extracted clays used to manufacture artificial sands were not pure clays but one type of clay was the main component. The polyphasic character of extracted clays increased the difficulty to validate the quantitative methods based on X-ray and applied on artificial sands. It came from the difficulty to find natural clays composed by just only one phase that could play the role of reference in mixtures.

3.1.1.2 Blends (artificial fine aggregates)

The artificial sands were manufactured by mixing extracted clay and washed sand. Then, the nature of the phases that composed the mixture is theoretically known. The mineral phases contained in 5 artificial fine aggregates noted S1-K3, S1-I13, S1-M2, S2-KI2 and S2-KI8 were identified to confirm expectations.

Quartz is the main detected component of analyzed mixtures and clays with high amounts were also detected on powder sample except montmorillonite on S1-M2 (Figure 40). Clay phases were successfully distinguished by the analysis of non-basal d (060) reflection between 70° to 75° 2θ on powder sample (Table 24) for all the samples except S1-M2. Regarding the detection limit of XRD, about 2% of the mineral content for mixed materials (*Dutrow and Clark 2015*), the 0.52 wt% of extracted montmorillonite added in S1-M2 was too low to overcome the background noise in the XRD pattern.

Such results pointed out a fact of importance: the identification and then quantification based on powder X-ray pattern was not possible when clays were in low content. It's the case of S1-M2 that contained a low

quantity of montmorillonite. Nonetheless such amount allowed to reach the MB threshold for qualified sand (the '2' in S1M2 indicated the value of MB). Rietveld methods will be limited in these conditions.

Table 24 Mineral phases of artificial fine aggregates identified from high reflection angles (Y denotes that the mineral phase was identified by the high angle reflection between 70° to 75° 2θ. Nd : non detected)

Sample	Mineral phases identified from 70° to 75° 2θ reflections, d (*060*)					
	Kao.	Illite	Montm.	V.or Chl.	Calcite	Quartz
S1-K3	Y	Y			trace	Y
S1-I13	trace	Y			Y	Y
S1-M2			Nd	Nd		Y
S2-KI2	Y	Y			Y	Y
S2-KI8	Y	Y			Y	Y

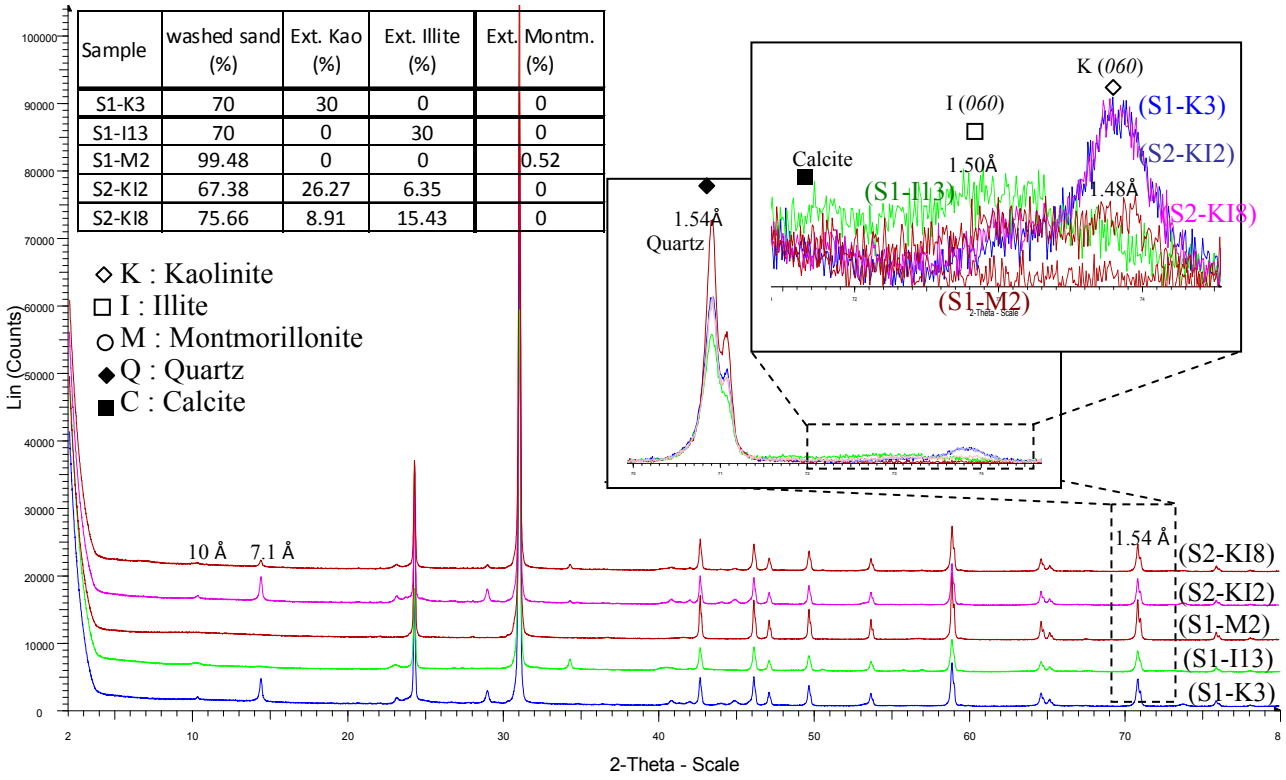

Figure 40 XRD patterns collected on artificial fine aggregates S1-K3, S1-I13, S1-M2, S2-KI2 and S2-KI8.

3.1.1.3 Unknown fine aggregates from quarries

The mineral phases of unknown fine aggregates noted A to E were analyzed using X-ray patterns on powder samples (Figure 41). Well-crystallized quartz with the strongest reflections at 3.34 Å was detected in the unknown sample A, C and D, whereas calcite with the strongest reflections at 3.03 Å was well-crystallized in unknown sample B and E. Hence, unknown sample A, C and D were considered as siliceous aggregates, whereas the unknown sample B and E were considered as calcareous aggregates.

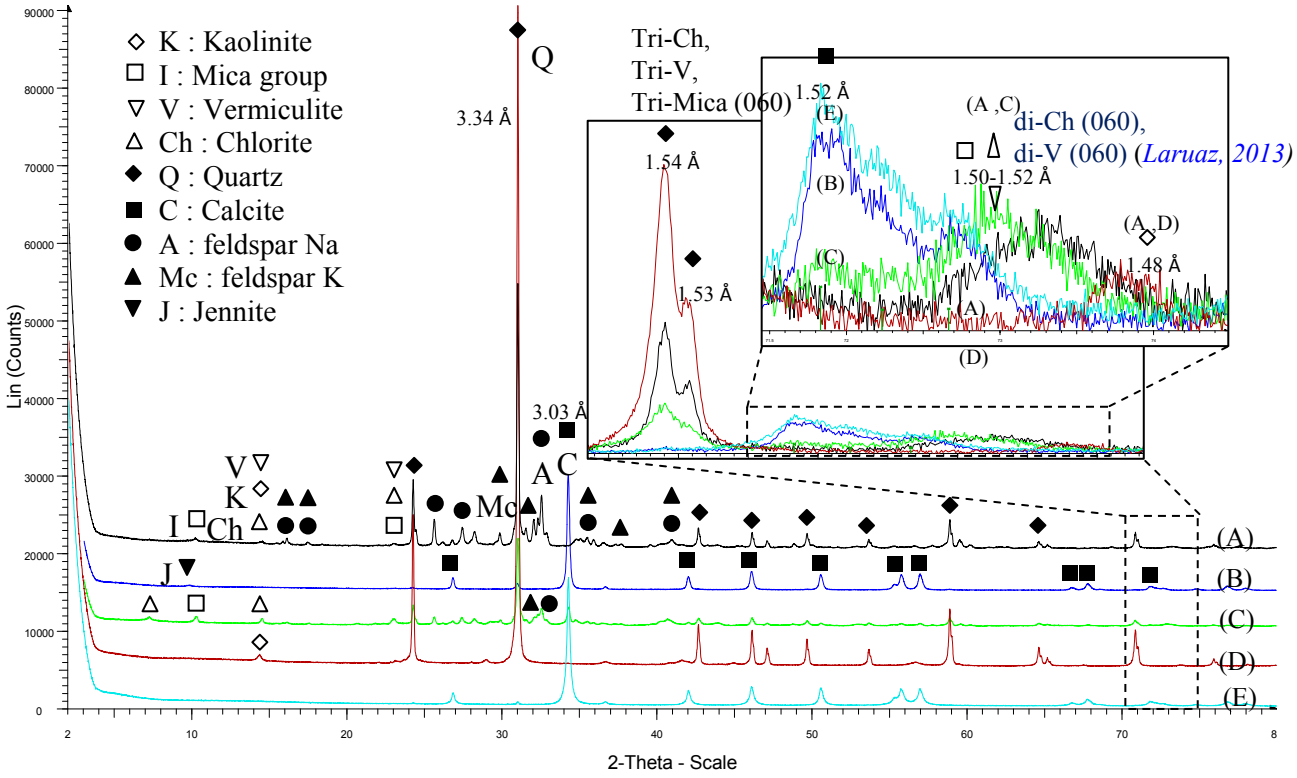

Figure 41 XRD patterns of sample of (A) unknown A, (B) unknown B, (C) unknown C, (D) unknown D and (E) unknown E in 32µm powder.

The identification of the whole mineral phases for unknown sample A to E was accomplished by using X-ray patterns on sample powder (Figure 41) combined with the analysis of treated oriented glass slides (Figure 42 to Figure 46). The images of sample analyzed from environmental scanning electron microscopy (ESEM) were associated for this X-Ray qualitative analysis as well (Figure 47). The reason is that the complexity of clay composition and the detecting limit of sample quantity which is the problem for X-Ray powder diffraction can be accomplished by X-Ray oriented sample diffraction. Results were synthesized in Table 25 and explained in the following paragraphs.

Table 25 Mineral phases of unknown fine aggregates A, B, C, D and E (grey box represented the main phase)

Unknown fine aggregate	clay minerals and related phyllosilicates					Other Minerals			
	Kaol.	Mica group	M. or V.	Chl.	Jennite *	Calcite	Quartz	K-Feldspar	Na-Feldspar
Unknown A	P, O	P O: Illite	P(poss.) O	P (poss.) O			P	P	P
Unknown B	O (low)		O (poss)		P, O	P	P (low)		
Unknown C		P, O	P (poss.) O	P (poss.) O		P (low)	P	P	P
Unknown D	P, O	O (low)					P (O)		
Unknown E	O	O	O (low)	O (low)		P	P (low)		

P, O indicate if the phase is present on powder sample and/or on oriented sample. Poss. possible
Chl. Chlorite, M. Montmorillonite, V: vermiculite, Mica group : illite/ muscovite.
*Jennite could be interpreted as attapulgite/palygorskite.

Unknown sample A

The unknown sample A (Figure 41) was a siliceous aggregate with quartz and minerals such as K-feldspar, Na-feldspar and clays. The composition suggested granitic affinities granite, gneiss. About clay fraction, the powder X-ray diffraction pattern can not differentiate chlorite and vermiculite (with a common peak around 14 Å) whereas kaolinite and a clay belonging to the mica group were identified.

The mineral identification from glass slides was necessary to go further. In the unknown sample A (Figure 42), **kaolinite** phase was easily identified from the disappearance of the 7 Å peak after the heating up to 550 °C, but it could not be used to validate the chlorite presence (A-4). As chlorite was unaffected by glycolation, the presence of peak at 14Å, 4.73 Å and 3.53 Å on EG-AD glass slide (A2) or Ca-EG glass slide (A-1) suggested the **chlorite** existence but such chlorite was affected by the heating up to 550°C with the disappearance of the peak at 14 Å on A-4. While it was not the usual behavior of chlorite, the disappearance of the peak after heating is possible yet as detailed in the following website (*http://www.axaa.org/clay-analysis-part-2.html*). The unchanged d (*001*) basal space at 10 Å before or after glass slide treatment (A-2, A-4, A-5) indicated an **illitic phase**. The existence of **vermiculite** was evidenced by the presence of its basal space at 14 Å, after EG treatment (A-2), but the space was increased after Ca^{2+} exchange on A-3 and it even became larger after EG treatment on A-1. Note that the high angle reflections on powder X-ray patterns (between 70° and 75° 2θ) measured on unknown fine aggregates (Figure 41) was not able to identify clearly all the clay types present in sample as it was done for artificial fine aggregates. The complexity (mixture of several phases) of mineral that composed the unknown sample A was probably at the origin of such problem.

Unknown sample B

The unknown sample B is a calcareous stone. Parallel to calcite, quartz is detected on powder X-ray diffraction pattern as well as a mineral characterized by a major peak located at 10,5Å. Such phase was first associated to palygorskite/attapulgite clay that is usually fibrous shaped clay. But no fiber was observed by scanning electron microscopy (Figure 47). Moreover, the presence of such clay type in calcareous sand was also doubtful because of the geological data. So, another phase was proposed such as Jennite ($Ca_9Si_6O_{18}(OH)_6•8(H_2O)$. Jennite is the late mineral stage in metamorphosed limestone and can be found also in concrete (Jennite belongs to Tobermorite group, the crystallized Calcium Silicate Hydrates or CSH that is layer shaped mineral).

Oriented glass slides (Figure 43) revealed the presence of kaolinite (small peak at 7 Å that disappeared after heating). Kaolinite phase might be missed if the glass slide sample was not applied as the kaolinite content was lower than the detection limit of XRD on powder sample (about 1-2%).

The mineral phase at 10.4Å was still present in the finest fraction deposed on glass slides manufactured from unknown sample B (such fraction is generally associated to clays). No change occurred after EG treatment while after heating at 550 °C, the mineral phase at 10.4 Å (associated to jennite) disappeared as commonly observed for cement hydrates destroyed at temperature higher than 130-150°C (note than the disappearance of the 10.4 Å peak at 550°C is also observed for palygorskite/attapulgite). Furthermore, an

amorphous-alike vermiculite phase with basal surface around 14.3Å was also detected. This poorly crystallized vermiculite slightly increased with EG treatment to 14.7-15.2Å and then collapsed to 9.9Å by losing water molecules.

Unknown sample C

Unknown sample C consisted of siliceous aggregates with quartz and minerals such as K-feldspar, Na-feldspar and clays (such as sample A). It suggested a granite or rhyolite rock.

The presence of chlorite in unknown sample C was confirmed by the d (*001*) and d (*002*) reflections at 14Å and 7Å on oriented glass slides on Figure 44 (no change after EG or heating treatment for the peak at 14Å), whereas illite was recognized by its basal space at 10Å that didn't change after any treatment. The discreet smectite and the discreet vermiculite were evidenced in unknown sample C by the increase of 14 Å basal space after EG treatment in not only the original sample (C-2) until 15.1 Å, but also its Ca^{2+} exchanged sample (C-1) until 16.6 Å (see appendix 1.1) (*Brown & Brindley 1984*). The shoulder observed on the 10Å peak corresponded also to the usual behavior of vermiculite after its lake of water molecule (the shift might go to until slightly lower than 10Å). Finally and surprisingly, calcite was also detected in powder sample. Geologically, the presence of a sedimentary mineral was unexpected. Several hypotheses were made: a contamination during lab preparation (it was doubtful with an amount higher 1-2% of $CaCO_3$, observable by XRD diffraction), the mixing of different geological formations in the quarry during sand elaboration, the nature of the sand (for example an aeolian sand), the application of lime treatment on sand (the calcite might be produced by contact between air and CaO). Unfortunately, all these hypotheses were refuted and no explanations were found until now.

Unknown sample D

The unknown sample D (identified as aeolian siliceous sand[10]) is mainly composed by quartz with kaolinite. The presence of kaolinite in clay fraction analyzed on oriented glass slides (Figure 45) was confirmed without any complexity with the disappearance of the kaolinite peak at 7Å after heating. The resistance of the peak at 10 Å corresponding to basal space of illite after EG or heating at 550°C treatments on glass slide confirmed illite mineral in Unknown sample D (Illite missed on powder X-ray diffraction pattern because of its low quantity in the whole sample).

Unknown sample E

The unknown sample E, as white calcareous is mainly composed by calcite and a very low content of quartz. No other phases (no clays) were observed on powder pattern. However, the existence of kaolinite and illite were evidenced on glass slides on Figure 46 by their basal space at 7Å and 10Å respectively. The trace of vermiculite was also found in the Ca^{2+} exchanged air dried samples and in non exchanged sample after EG treatment, moreover, the trace of chlorite may also be present.

[10] Sand formed and sharpened by wind activity

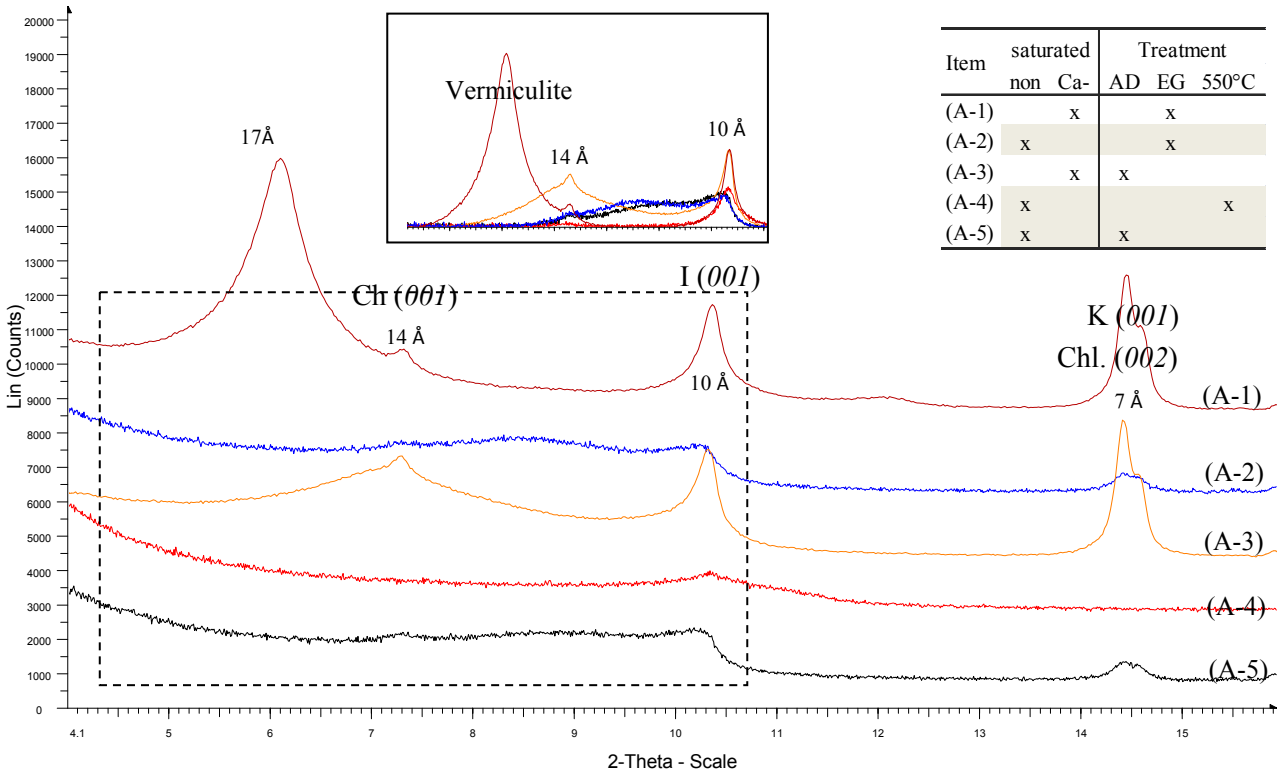

Item	saturated		Treatment		
	non	Ca-	AD	EG	550°C
(A-1)		x		x	
(A-2)	x			x	
(A-3)		x	x		
(A-4)	x				x
(A-5)	x		x		

Figure 42 XRD patterns of unknown fine aggregates A : (A-1) Ca-, (A-2) non-cation exchanged glass slides with EG treatment, (A-3) Ca-exchanged, (A-4) heated up to at 550 °C and (A-5) non-heated air dried (AD) glass slides

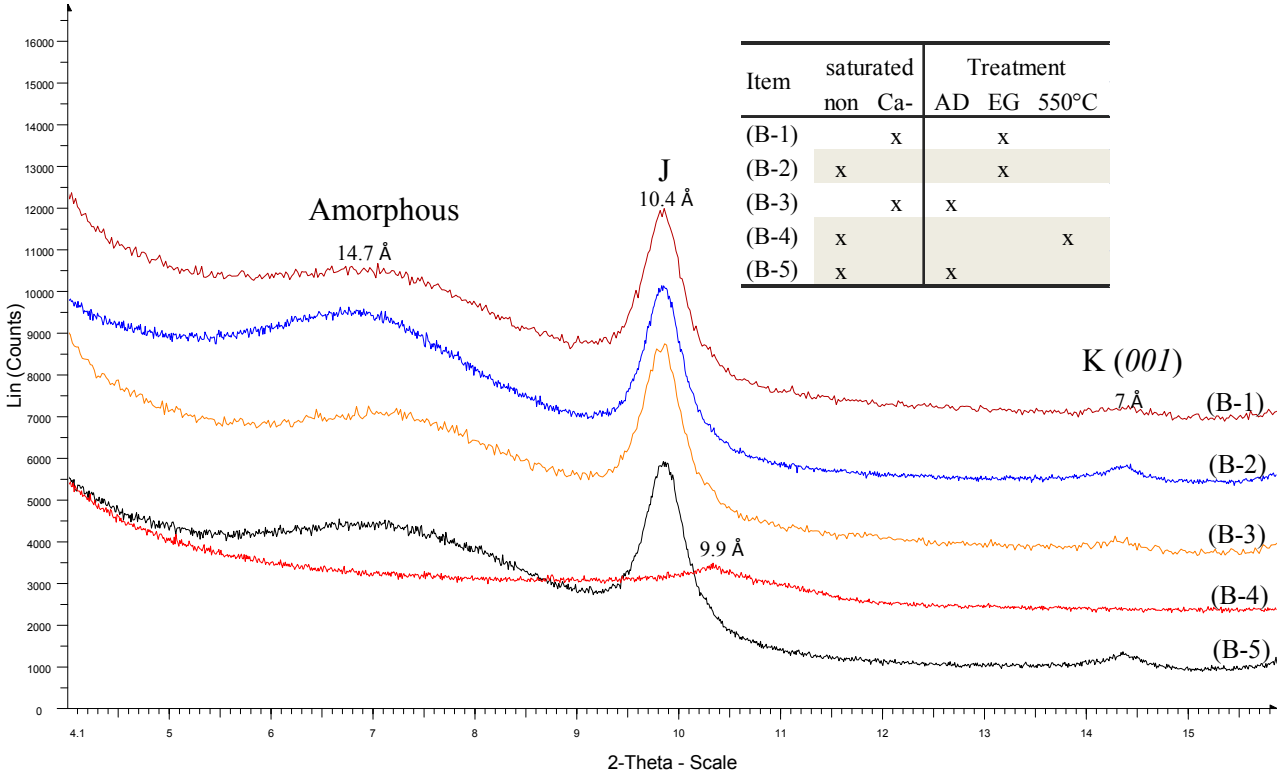

Item	saturated		Treatment		
	non	Ca-	AD	EG	550°C
(B-1)		x		x	
(B-2)	x			x	
(B-3)		x	x		
(B-4)	x				x
(B-5)	x		x		

Figure 43 XRD patterns of unknown fine aggregates B: (B-1) Ca-, (B-2) non-cation exchanged glass slides with EG treatment, (B-3) Ca-exchanged, (B-4) heated up to at 550 °C and (B-5) non-heated air dried (AD) glass slides

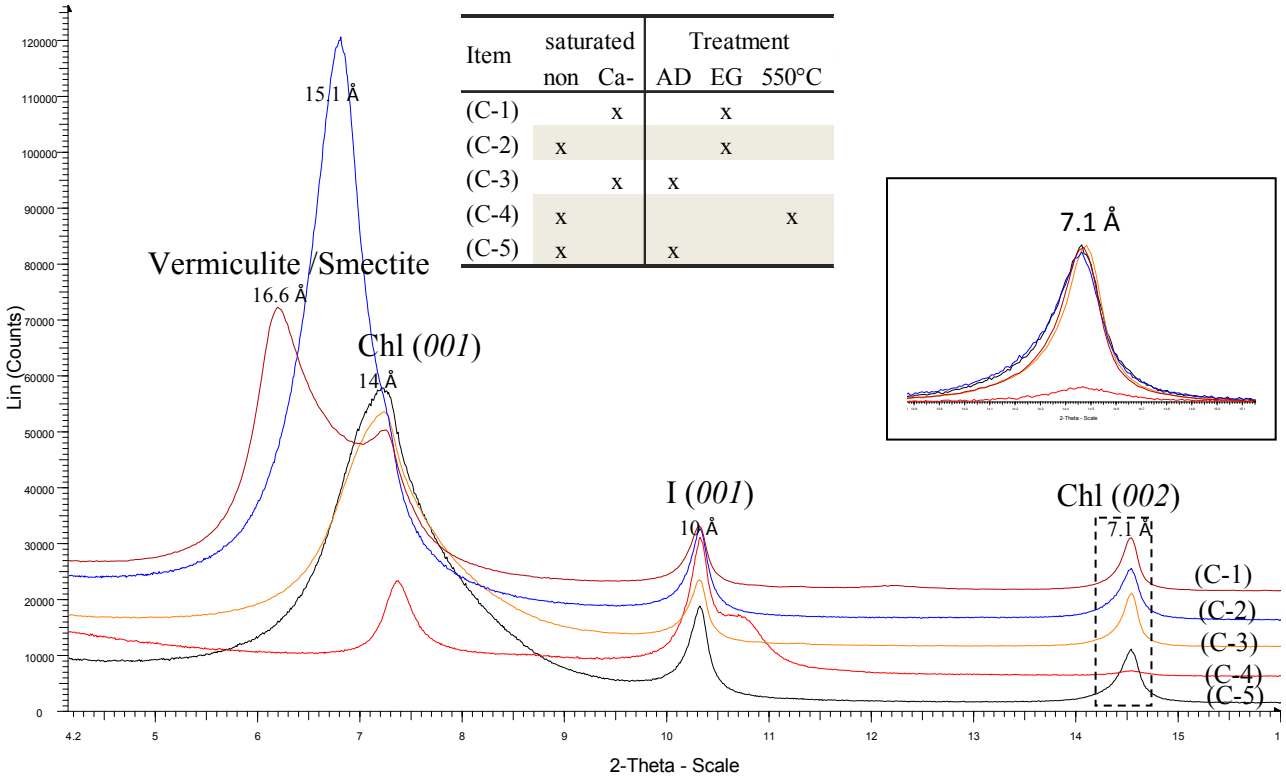

Figure 44 XRD patterns of unknown fine aggregates C: (C-1) Ca-, (C-2) non-cation exchanged glass slides with EG treatment, (C-3) Ca-exchanged, (C-4) heated up to at 550 °C and (C-5) non-heated air dried (AD) glass slides

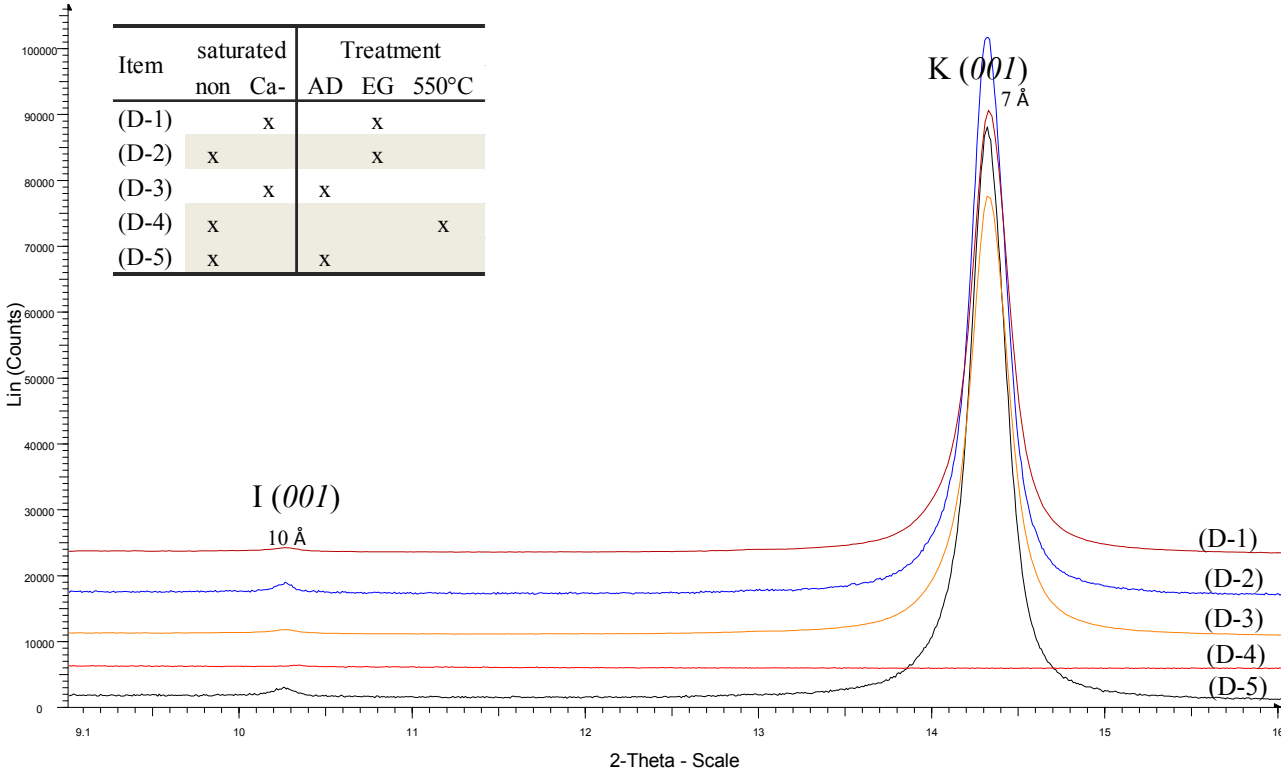

Figure 45 XRD patterns of unknown fine aggregates D : (D-1) Ca-, (D-2) non-cation exchanged glass slides with EG treatment, (D-3) Ca-exchanged, (D-4) heated up to at 550 °C and (D-5) non-heated air dried (AD) glass slides

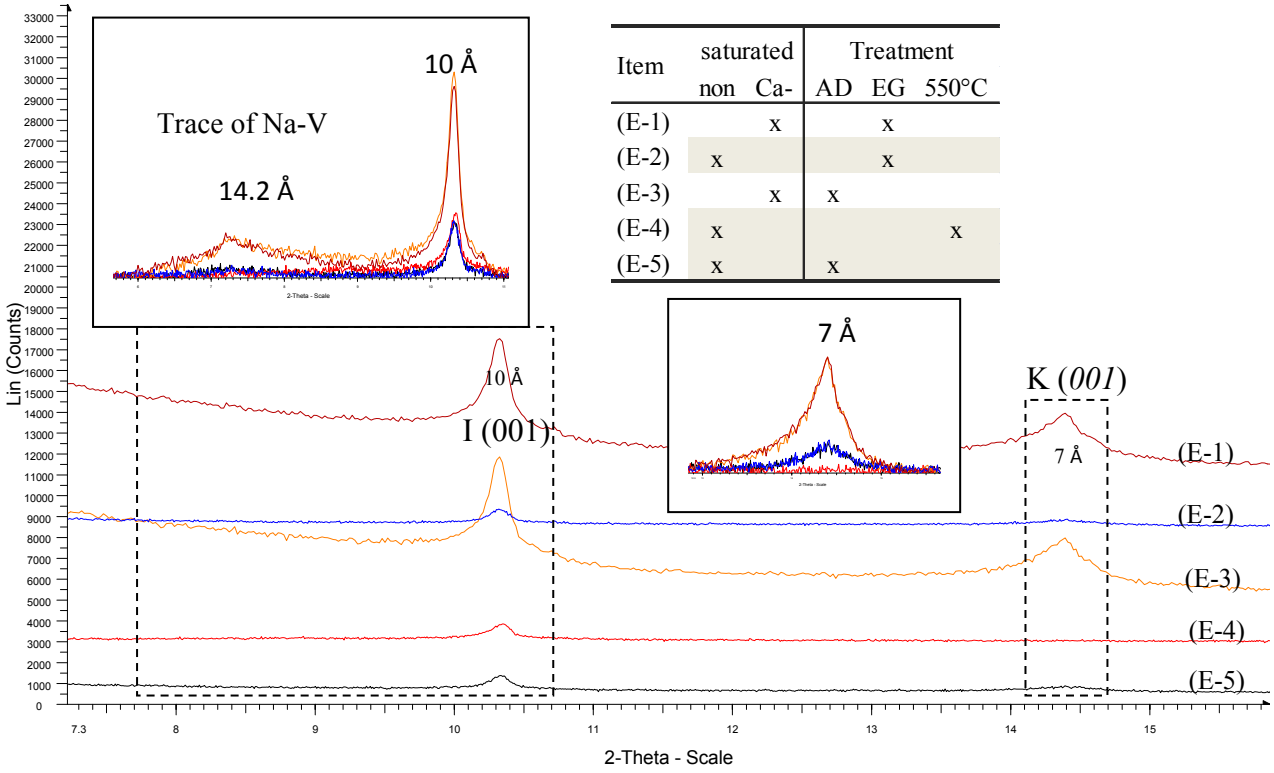

Item	saturated		Treatment		
	non	Ca-	AD	EG	550°C
(E-1)		x		x	
(E-2)	x			x	
(E-3)		x	x		
(E-4)	x				x
(E-5)	x		x		

Figure 46 XRD patterns of unknown fine aggregates E : (E-1) Ca-, (E-2) non-cation exchanged glass slides with EG treatment, (E-3) Ca-exchanged, (E-4) heated up to at 550 °C and (E-5) non-heated air dried (AD) glass slides

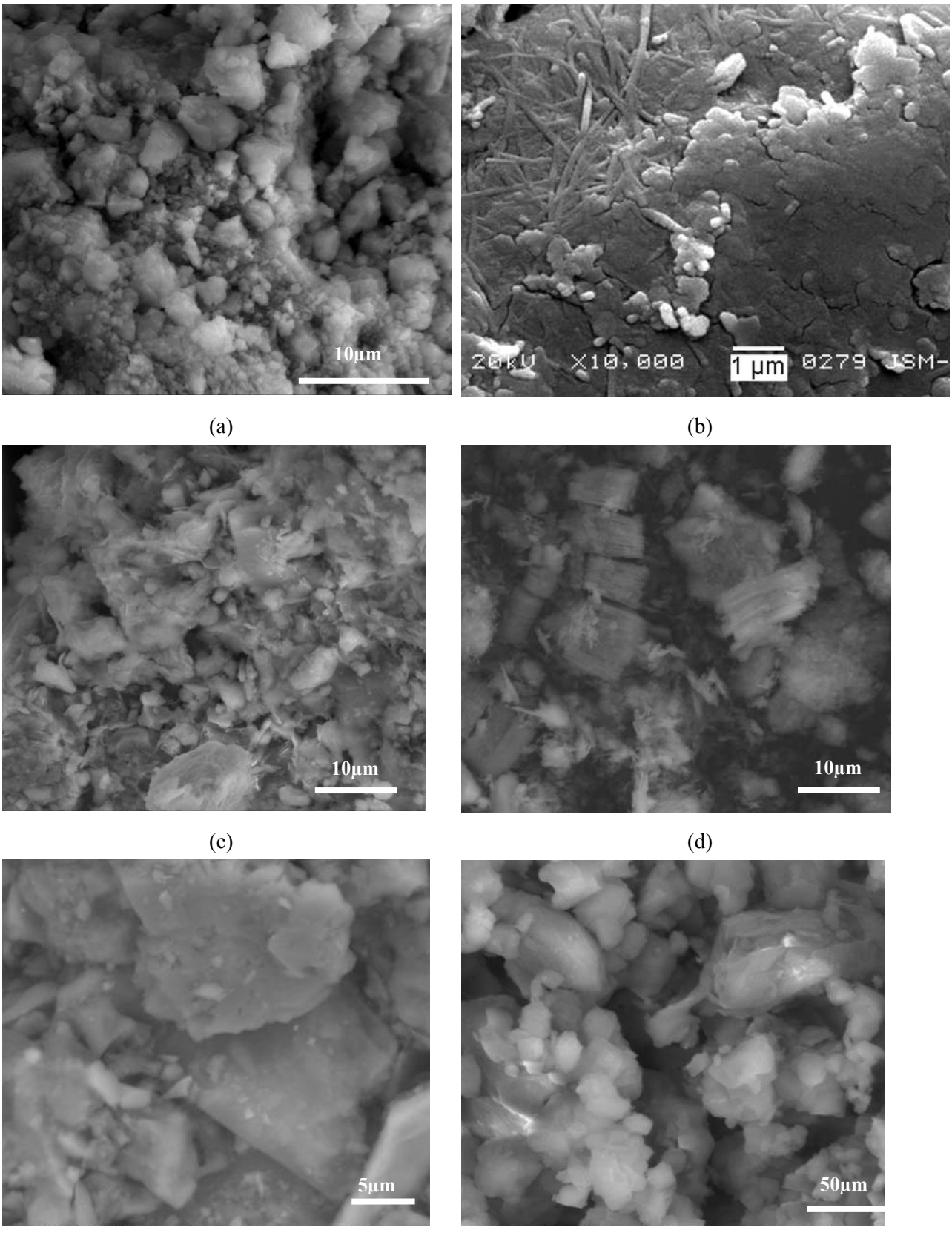

Figure 47 Images by environmental scanning electron microscopy in low vacuum mode on (a) unknown fine aggregates B, (b) Palygorskite fibrous particles from literature, (c) unknown fine aggregates C, (d) unknown fine aggregates D, (e) unknown fine aggregates E, (f) unknown fine aggregates A.

3.1.2 Quantification of mineral phases from X-ray diffractometer

The quantification of mineral phases from X-ray diffraction used in this study was based on **whole pattern methods** with the Reference Intensity Ratio (RIR) and Rietveld methods (using TOPAS software), and **single peak method** such as semi-quantification on oriented glass slide.

The accuracy of the methods was judged by comparing the designed proportions of extracted clays in artificial fine aggregates to the measured proportions as well as by comparing such measures with the results from complementary method taken as reference or validation (such method combined different techniques such as thermal analysis, Cation exchange capacity and chemical analysis). The results from unknown fine aggregates will indicate the capability to quantify the aggregates from quarry by using X-ray diffractometer.

3.1.2.1 Semi-quantification

The proportion of clay minerals in the fine fraction of sample is calculated by the Semi-quantification method using the mineral intensity factors or MIF (*Holtzapffel 1983*). Then, the results were combined to the particle size distribution of sample to obtain proportions on the whole sample.

Several drawbacks in semi-quantification were listed:

- The clay proportions were calculated with the assumption that only clays were present in the fine fraction on glass slides whereas other mineral may be present such as silica or colloidal particles. The bias caused by these miss-calculated minerals in fine fraction will raise clay quantity in whole sample by calculating through particle size distribution.
- The finer clay minerals will settle on the upper layer of sample on glass slide and then introduce the bias
- the protocol and operator for preparation of oriented glass slides may impact the results
- the quantity of clay in whole sample was difficult to approximate. The clay content was overestimated by the < 63 µm fraction while the < 2 µm fraction usually underestimated the clay fraction when clay dispersion was not complete in sedimentometric test even with dispersant agent (it's usually the case). This particular point is detailed in the following paragraphs.

Particle size distribution

The particle sizes of extracted clays, kaolinite, illite and montmorillonite, have been measured using laser size measurement compared to standardized sedimentometric test (Table 26). Comparing the quantity < 2 µm and < 63 µm fraction analyzed by laser size method or the conventional sedimentometric test (*XP P 94-041, NF P 94-057*), the effect of the method on the < 63 µm quantification is less noticeable than on the < 2 µm quantification. The < 63 µm fraction in montmorillonite measured by laser method is lower than the one evaluated by sedimentometric test. Results could be interpreted by a higher level of particle dispersion in sedimentometric test as in laser test (difference of protocol) but results were also directly impacted by the physical principal of the method (both impacts were coupled). In other words, the < 2µm

quantities detected by sedimentometric test were much higher than the quantities measured by laser test. The laser size particle distribution was definitely disregarded for further quantitative experiments.

Table 26 Size distribution of clays and washed sand (figure in appendix)

Material	Laser size distribution							French Std (*XP P 94-041* and *NF P 94-057*)	
	D_{10} (µm)	Mean (µm)	D_{90} (µm)	S.D.	layers per part. ($*10^3$)[a]	% < 63 µm	% < 2 µm	% < 63 µm	% < 2 µm
Ext. Kao.	2.3	9.7	19.9	8	14	100	7.7	100	83.7
Ext. Illite	1.5	5.4	10.8	5.2	4-5	100	19	100	75
Ext. Montm.	2.8	15.8	31.8	19.2	11	97	4.8	100	52
Montm. (comm.)	2.9	20.6	47.4	22.8	14	94.4	4.6	100	94

[a] Sheets per part.: average number clay sheets per particles. The calculation of number of clay sheet is the mean particle size divided by the thickness of single sheet.

To test the clay dispersion effect on measurement (and then to improve the accuracy on the < 2 µm quantification associated to clay fraction), four artificial fine aggregates S1-I13, S2-KI2, S2-KI8 and S3-3 were selected. European standard (*XP CEN ISO TS 17892-4*) and French standard (*XP P 94-041+NF P 94-05*) were applied on selected sands. Both methods are used in geotechnical engineering field and follow Stokes' law. The main differences between standards are the undried state of clay fraction at the beginning of sedimentometric test (after wet sieving in contact with hexametaphosphate) for European standard, whereas clay fraction is dried at 105 °C over a night from French standard after the wet sieving with water The particle size distributions curves were drawn in the appendix 5.1 and results were summarized in Table 27.

By comparing both methods, the idea was to evidence the influence of the drying onto the capability of clay to be dispersed (above all for montmorillonite swelling clay). It's why particle size distributions were previously measured on extracted and commercial products by the laser method (see Table 26). The commercial montmorillonite (drying at 230 °C by manufacturers) showed slightly larger particle size (around 20.6 µm) than the average size of particles in the never been dried over 40 °C extracted montmorillonite (around 15.8 µm). Extracted illite presented the smallest average particle size, whereas montmorillonite had the biggest average particle size (compared to illite and kaolinite). Considering the thickness of single layer of kaolinite, illite and montmorillonite (0.7, 1 and 1.47 nm respectively - 1.47 nm/layer referred to XRD results from air dried glass slide realized during this study), the number of layers per clay particles (with an average size) were around 14000, 4000-5000 and 11000 for extracted kaolinite, illite and montmorillonite respectively. According to the number of clay layers per particle from references (*Morel, 1996; Olphen, 1979; Eslinger, 1988*), all extracted clays from this study were aggregated in much bigger particle size than the reference one. The reason is that clay aggregation was unable to separate into indivisual clay particle even with the deflocculation reagent.

Keeping on testing the drying effect, European and French standards for sedimentometric test applied on selected artificial fine aggregates gave slightly different 2 µm fractions. European standard contributed to

increase the detected 63 µm fine fraction. The fine fraction was probably well dispersed from coarse fraction by the dispersing agent (hexametaphosphate). Surprisingly, the French standard gave higher content of particle size less than 2 µm than the non-dried European protocol, except for S2-KI8. It might be caused by the grounding of fine (< 63 µm) before the dispersion in water according to French standard (*XP P 94-041+NF P 94-05*). The particle size might no more follow its natural aggregation. However, the grinding was generally soft and such explanation was not convincing.

To conclude about the particle dispersion method before sedimentometric test, the size distribution resulting from non-dried sample used in the European standard (*XP CEN ISO TS 17892-4*) was taken into account in the semi-quantification method.

Table 27 Particles size distribution of artificial fine-aggregates (Figure in appendix 5.1)

Material	Sand (%)	Ext. Kao. (%)	Ext. Illite (%)	Ext. Montm. (%)	Protocol	Mean (mm)	% passing 63 µm	% passing 2 µm	Theoretical % passing 2 µm [c]
S1-I13	70.00	0.00	30.00	0.00	European Std. [a]	0.28	32	20.2	
					French Std. [b]	0.28	30.8	24.3	30-31.5
S2-KI2	67.38	26.27	6.35	0.00	European Std. [a]	0.27	34	6.3*	
					French Std. [b]	0.27	32.8	16.8	32.5-34
S2-KI8	75.66	8.91	15.43	0.00	European Std. [a]	0.31	25.1	17.9	
					French Std. [b]	0.31	24.8	14.5	24.4-25.8
S3-3	73.41	16.63	6.92	3.05	European Std. [a]	0.33	25.8	13.4	
					French Std. [b]	0.33	25.4	17.6	26.6-28

a: European standard, *XP CEN ISO TS 17892-4*, clay fraction has never been dried
b: French standard, *XP P 94-041+NF P 94-057*, clay fraction has been dried at 105 °C over night
c : Theoretical % passing 2 µm calculated by the addition of the clay content in sample (the < 2% coming from sand had to be added. It represented less than 2% of the sand content) * possible error

The size distribution of the five unknown fine-aggregates from quarries was also analyzed using the European standard. Results in Table 28 showed that unknown sample B had the highest average particle size with the lowest fine content passing 2 µm, whereas the unknown sample D had the lowest average particle size with the highest 2µm content.

Table 28 Size distribution of unknown fine-aggregates from quarries (see appendix 5.1). The measurements were done by the European standard (*XP CEN ISO TS 17892-4*).

Fine-Aggregate $D_{0/2}$ mm	Mean (mm)	% passing 63 µm	% passing 2 µm
Unknown A	0.42	25.9	3.85
Unknown B	0.49	21.5	2.2
Unknown C	0.47	28.8	10.8
Unknown D	0.36	16.7	10.1
Unknown E	0.39	27.3	7.4

With high amounts of fine content (< 63 µm), such fraction probably contained other phases as clays and clearly overestimated the clay fraction. Then, the < 2µm fraction may be chosen to represent the whole clay fraction in samples. It was not the case for quite pure clays (extracted clay) where the particles aggregation coming from the grinding of clay rock and their low dispersion in water allowed to prefer the < 63 µm instead of the < 2 µm fraction to approach the whole clay fraction in sample. The same conclusion

was done for artificial sand mixtures prepared with extracted clays. This was probably an effect induced by our manufacturing of sand (artificial sand didn't not behave as natural one which fine particles aggregated naturally).

Instead of choosing one fraction, semi-quantification was calculated using both fractions (< 2µm and < 63 µm) in order to overestimate or underestimate the whole clay fraction and the results were done as a range (in the practice, results are generally given 5% by 5% considering the error linked to the method)

Parallel to the optimization of the method to evaluate the whole clay fraction (from particle size distribution), preliminary tests were done by modifying the manufacturing of glass slide. Indeed, the traditional 1h40 sedimentation of sample suspension in order to extract the < 2µm fraction (considering the Stokes law), was not adapted to the samples with differential sedimentation. If clay particles were not well dispersed, the clay aggregates precipitaed more rapidly than expected which may conduct to underestimate a type of clay in sample composition (such phenomenon was observed above all for illite). The adapted protocol to elaborate glass slides (detailed in Chapter 2) resulted from these preliminary observations (on Table 29).

Table 29 The quantity of mineral phase derived from semi-quantification combined with < 63µm or < 2 µm fraction (given by the European standard *XP CEN ISO/TS 17892-4*). Comparison for two methods to manufacture glass slides.

Sample	Clay mineral	< 2 µm (%)	< 63 µm (%)	Calc. clay mineral content %[1]	Semi-quant. + < 63 µm (%)		Semi-quant. + < 2 µm (%)	
					Glass slide (t=0)	Glass slide (1h40)	Glass slide (t=0)	Glass slide (1h40)
S1-K3	Kao	25.1[3]	30[3]	22,4	26,5	26,9	22,2	22,5
	Illite			3,7	3,5	1,6	2,9	2,6
S1-I13	Kao	20.4	32	0.6	1,6	1,6	1,0	1,0
	Illite			21	25,2	17,8	16,0	11,4
	Montm[2]			0,0	5,3	12,6	3,4	8,0
S1-M12	Kao	4.5[3]	4.6[3]	0,3	0,6	0,6	0,6	0,6
	Illite			0,4	0,1	0,3	0,1	0,2
	Montm			4,05	4,4	4,2	4,3	4,1
S2-KI2	Kao	6.3*	34	19,7	26,4	25,0	13,0	12,4
	Illite			7,7	6,4	5,5	3,2	2,7
	Montm[2]			0,0	1,3	3,5	0,6	1,7
S2-KI8	Kao	17.9	25.1	7	10,9	11,1	3,5	7,9
	Illite			11,9	4,3	6,7	3,1	4,8
	Montm[2]			0,0	9,9	7,4	7,1	5,3
S3-3	Kao	13.4	25.8	12,7	16,0	13,7	8,4	7,2
	Illite			7,1	5,5	3,7	2,9	1,9
	Montm			2,6	4,4	8,4	2,3	4,4

[1] the calculated quantities taken as reference were the percentage of each extracted clay added to the artificial fine aggregates multiplied by the extracted clay composition given by Complementary method.
[2] the unexpected presence of montmorillonite was not explained.
[3] estimated value from calcutaion (calculated quantities of each extracted clay added to the artificial fine aggregates multiplied by the < 2µm or < 63µm quantities in extracted clays given French standard (XP P 94-041+NF P 94-05).

Finally, the whole clay fraction measurement was combined with X-ray results. The net areas of basal space of clay minerals were measured on X-ray diffraction pattern of EG treated-oriented glass slide (the protocol of glass slide manufacture was in chapter 2). By multiplying the measured net area by the mineral

intensity factor (MIF) from *Holtzapffel (1983)*, the semi-quantification of clay minerals were estimated (Table 30).

Calculations were done also with MIF factors proposed by other authors and a quite good agreement were obtained whatever the chosen MIF if the usual 5% inaccuracy associated to 'semi' quantification method was considered. Results in Table 30 will be discussed in details at the end of the chapter by comparing measured values with expected ones in artificial fine aggregates.

Table 30 The quantity of mineral phases derived from semi-quantification.

Samples	< 2 µm (%) [a]	< 2 µm (%) [c]	< 63 µm (%) [a]	< 63 µm (%) [c]	Clay minerals and related phyllosilicates (%)			
					Kao. 0.5 [b]	Illite 1 [b]	Montm. or V. 1.5 [b]	Chl. 1 [b]
Ext. Kao.	--	83	100	--	64 - 77.2	18. 9 – 22.8	--	--
Ext. Illite	--	75	100	--	4.5 -7	70.5 - 93	--	---
Ext. Montm.	--	52*	100	--	--	0.5-0.65 [e]	99.25-99.5 [e]	--
S1-K3	--	25.1[d]	--	30[d]	22.2-26.5	2.9-3.5	--	--
S1-I13	20.4	24.3	32	29.3	1-1.5	16.7-25.15	3.35-5.2**	--
S1M12	--	4.5[d]	--	4.6[d]	0.55	0.05	4.3-4.4	--
S2-KI2	6.3*	16.8	34	31.7	13-26.3	3.1-6.4	0.6-1.25**	--
S2-KI8	17.9	14.5	25.1	23.8	3.5-10.9	3-4.3	7.1-9.9**	--
S3-3	13.4	17.6	25.8	23.9	8.3-15.9	2.9-5.5	2.3-4.3	--
Unknown A	3.85	--	25.9	--	0.25-1.6	0.7-4.7	2.85-19.2	0.06-0.4
Unknown B	2.2	--	21.5	--	0.02-0.15	--	0.8-5.8 [V]	--
Unknown C	10.8	--	28.8	--	--	0.45-1.4	9.9-26.5 [V]	0.4-0.9
Unknown D	10.1	--	16.7	--	10-16.4	0.15-0.3	--	--
Unknown E	7.4	--	27.3	--	2.05-7.6	3.7-13.6	1.6-6.05 [V]	--

[a] results from European standard (XP CEN ISO TS 17892-4)
[b] (*Holzapffel 1985*) [c] results from French standard (XP P 94-041+NF P 94-05), [d] value estimated by calcuation, [e] calculated for < 63µm, V. vermiculite, * possible error : unused value, ** unexpected mineral in the mixture

3.1.2.2 Reference Intensity Ratio (RIR)

The method of Reference Intensity Ratio (RIR) for clay quantification was applied using X-ray powder diffraction on sample with 50 wt% added corundum. From each mineral phase, the net area of the peak with the strongest intensity was evaluated. Such areas were combined with the reference intensity ratio (RIR) from ICDD-PDF database for non-clay minerals and with the MIF associated to clays (from Holtzapfell, *1983)* for clay minerals. Such choice may appear surprising but in the absence of known RIR values for clay minerals, the MIF values gave against all odds some quantities not so far from the quantities estimated by other quantitative methods. RIR of 0.5 and 0.23 for kaolinite and illite respectively were given by *Hillier* (*2000*), but the method of sample preparation by applying air spray drying on powder made such factors incompatible with our measurements on sample prepared by using other method (note the similarity between RIR and MIF for kaolinite but it was not the case for illite). Then, MIF were chosen to approximate clay contents (in absence of other references).

The quantities of mineral phases were calculated by the have-known quantity of corundum in the sample (Table 31). Such method (as semi-quantitative method) remained inaccurate but might give a good order of

magnitude for the mineral quantities. Schroeder (*2015*) stated also that the application of the standardized RIR in ICDD-PDF database may generate an error up to 20%.

Finally, as expected from phase identification on sample powder X-ray diffraction pattern, the minerals with too low quantity couldn't be detected. It was the case of low amount of montmorillonite that governed the methylene blue adsorption quantities on sand.

Table 31 The quantity of mineral phase derived from RIR

Samples	clay minerals and related phyllosilicates (%)				Other Minerals (%)				
	Kao.	Mica group	Montm. or V.	Chl.	Calcite	Quartz	Feld. K	Feld. Na	Jennite
Parameters	**0.5** [a]	**1** [a]	**1.5** [a]	**1** [a]	**3.2** [b]	**3** [b]	**0.6** [b]	**0.6** [b]	**2.6** [b]
Ext. Kao.	82.6	2.8				14.6			
Ext. illite	13.1	68.1			13.7	5.1			
Ext. Montm.		M [c]	99.8		M [c]	0.2			
S1-K3	31.2	0.8				68.0			
S1-I13	3	6.1			2.8	88.1			
S1-M2		M [c]	M [c]		M [c]	100			
S2-KI2	24.2	0.6			0.3	75			
S2-KI8	10.2	1.2	*1.3**		1.00	86.3			
S3-3	14.6	0.7	0.2		0.3	84.2			
Unknown A	1.7	3.5	M [c]	1.3	1.05	51.2	11.8	29.4	
Unknown B	M [c]		M [c]		93.05	5.1			1.9
Unknown C		14.6	M [c]	13.4	7.2	52.2	2.3	10.3	
Unknown D	10.3	M [c]				89.7			
Unknown E	M [c]	M [c]		M [c]	99.7	0.3			

a clay intensity factor (MIF) from *Holtzapffel* (*1983*) [b] Reference Intensity Ratio from ICDD-PDF database
[c] the missing mineral phase considering the previous identification results
* possible contamination or error during the manufacturing

3.1.2.3 Rietveld method

The software named TOPAS (from Bruker) was used to quantify mineral phases by Rietveld method. The mineral structures were manually built or modified according to the qualitative results, then refined and quantified by TOPAS to reach the best fitting on X-Ray powder diffraction, typically the non-basal space d (*060*) reflections of clays. The goals were to be in accordance with mineral structure, chemical composition and particle size after refinement. The value of R-weight pattern (R_{wp}) was taken as a reference instead of an absolute judgment. Generally, except clay minerals and related phyllosilicates, the mineral phases of other silicates, oxides, hydroxides, carbonates, chlorides, fluorides, etc. were easily fitted. In this study, the difficulties in Rietveld method focused on clay minerals and the fitting of disorder kaolinite, the recognition of illitic polytypes, and the establishment of crystal structures for montmorillonite with various interlayer spaces and for the interstratified vermiculite-smectite mix layer.

In order to approach the reasonable quantities of mineral phases, the X-Ray powder diffraction from 50 wt% corundum added sample were performed and analyzed from Topas as well. Corundum was taken as reference in TOPAS calculation. The mineral phases quantified by TOPAS were shown in Table 32.

Table 32 The mineral phases of samples considered in the Rietveld method

Materials	Clay minerals				Other Minerals				others
	Kao.	Mica group	Montm. or V.	Chl.	Calcite	Quartz	K-Feld.	Na-Feld.	
Ext. Kao.	Y [a]	Y [a]				Y [a]			
Ext. illite	Y [a]	Y [a]			Y [a]	Y [a]	A [e]		
Ext. Montm.		M [c]	Y [a]		M [c]	M [c]	A [e]		M [d] *
S1-K3	Y [a]	Y [a]			M [c]	Y [a]			
S1-I13	Y [a]	Y [a]			Y [a]	Y [a]	A [e]		
S1-M12		M	Y [a]			Y [a]			
S2-KI2	Y [a]	Y [a]			Y [a]	Y [a]	A [e]		
S2-KI8	Y [a]	Y [a]	A [e]		Y [a]	Y [a]	A [e]		
S3-3	Y [a]	Y [a]	Y [a]		Y [a]	Y [a]	A [e]		
Unknown A	Y [a]	Y [a]	M [c]	Y [a]	Y [a]	Y [a]	Y [a]	Y [a]	
Unknown B	M_{low} [d]		M [c] **		Y [a]	Y_{low} [b]			Y [a] **Jennite**
Unknown C		Y [a]	**Y [a] Corrensite**		Y (low) [b]	Y [a]	Y [a]	Y [a]	
Unknown D	Y [a]	M_{low} [d]				Y [a]			A [e] Anatase
Unknown E	M_{low} [d]	M_{low} [d]	M_{low} [d]		Y [a]	Y_{low} [b]			

[a] mineral phase identified from both identification analysis and Rietveld method
[b] mineral phase assumed from Rietveld method with the low intensity of its reflection
[c] the **missing mineral** phase assumed after Rietveld method application
[d] the **missing mineral** phase in Rietveld method because of their too low quantity
[e] the **additional** mineral phase assumed from Rietveld method
V. vermiculite, Chl. Chlorite . Corrensite (interstratified vermiculite-smectite mix layer).
* inter-strat. clay ** amorphous clay X_{low}: low amount of mineral phase.

As for RIR method, some mineral phases noted M missed on X-ray powder pattern due to their low quantity. Parallel, additional mineral phases noted A appeared in order to allow a good fitting. Their real existence was still in debate. Regarding the mineral phases in extracted clays and its artificial fine aggregates, the additional feldspar K assumed in the extracted illite agreed with its presence in artificial fine aggregates S1-I13, S2-KI2 and S2-KI8. Interestingly, the corundum added S1-M2 sample showed montmorillonite phase whereas its low content (0.52 wt%) didn't allow its identification during previous analysis (montmorillonite had to introduced in TOPAS calculation to obtain the best fitting). On the other hand, the additional Feldspar K in extracted montmorillonite assumed by Rietveld method was not in agreement with artificial fine aggregate S1-M2 manufactured with extracted montmorillonite.

In unknown sample B, the TOPAS analysis was not possible assuming the presence of attapulgite or palygorskite (the structure of this mineral had to be searched in international mineralogical data base). The presence of Jennite (instead of attapulgite or palygorskite) gave a good fitting. In unknown sample C, the fitting was not possible for chlorite phase. However, the vermiculite/smectites structure in Topas was manually built with the consideration of corrensite structure $(Ca,Na,K)(Mg,Fe,Al)_9(Si,Al)_8O_{20}(OH)_{10}$),

which is ∝ 1:1 regular inter-stratification of trioctahedral chlorite and trioctahedral smectites allowed to fit well XRD powder pattern. The quantity of mineral phases in each material estimated by Rietveld method as well as the R factor (R-weight pattern - R_{wp}) is shown in Table 33.

Table 33 The quantity of mineral derived from Rietveld method

Material	Clay minerals (%)				Other Minerals (%)					R_{wp} [a]
	Kao.	Mica group	Montm. or V	Chl.	Calcite	Quartz	Feld. K	Feld. Na	Others	
Ext. Kao.	75.4	12.6				12				**8.27**
Ext. illite	15.4	70.1			8.7	0.2	5.6 (A)			**4.92**
Ext. Montm.		M	81.5		M	0.1	18.4 (A)		M *	**11.60**
S1-K3	25.1	6			M	68.9				**8.33**
S1-I13	5	19.7			3.1	63.7	8.45(A)			**4.40**
S1-M12		M	4.3			95.7				**2.27**
S2-KI2	20	7.7			0.9	67	4.3(A)			**6.15**
S2-KI8	3.9	16.4	1 (A)		1.4	76.4	0.9(A)			**4.80**
S3-3	10.9	10.5	4.3		1.5	71.4	1.4 (A)			**5.26**
Unknown A	1.8	5.7	M (V)	1.8	2 (A)	34.9	19.6	34.2		**6.38**
Unknown B	M		M **		95	3.9			1.05 **Jennite**	**6.95**
Unknown C		24.2	8.1 **Corrensite** [b]		8.5	25.5	12.75	21		**4.61**
Unknown D	11.1	M				87.8			1.15 **Anatase**	**5.96**
Unknown E	M	M	M (V)		99.4	0.6				**6.45**

[a] weighted pattern R factor, R_{wp} [b] corrensite (interstratified vermiculite-smectite mix layer).
(A) additional mineral phase assumed from Rietveld method , M: the missing mineral phase compared to identification (low amount or inadequation with Rietveld calculation) * inter-strat. clay ** amorphous clay

Difficulty to fit the disorder kaolinite appeared in non-basal space d (*060*) and difficulties also occurred with montmorillonite characterized by various interlayer space, reflected in the miss-fitting of its half cell in b axis d (*020*). Moreover, there was a miss-fitting in the unknown sample D without any suitable mineral phase. However, the R_{wp} found in this study were mostly lower than 10% (the threshold to estimate the quality of the fitting). The lower the R_{wp} is, the higher the quality is. In this case, the R_{wp} is not a good indicator to validate the presence or not of mineral phases (presence of feldspar for example). The 18.5% of K-feldspar quantified in extracted montmorillonite was also still doubtful considering the nature of the clay. The delicate sample preparation (responsible of the minerals quantification success when the preferential particle orientation is low) might play a major role in the quantitative errors.

3.1.3 Quantification of mineral phases from complementary methods

The most reasonable quantity of each mineral phase was approached by considering the results from chemical analysis, thermal analysis, calcimeter test and cation exchange capacity (CEC). The complementary method was applied on tested samples in order to compare results with quantifications from X-ray methods.

3.1.3.1 Results of complementary tests

The results of chemical analysis (Chem.), thermal analysis (Therm.), calcimeter (Calci.) and cation exchange capacity (CEC) measured on the different tested sands were shown in Table 34.

Table 34 The results of chemical analysis, thermal analysis, calcimeter and Cation exchange capacity for the complementary method

Tests	Param.	Ext. clays (%)			Artificial fine aggregates (%)					Unknown fine aggregates				
		kao. (%)	illite (%)	montm. (%)	S1-I13	S1-M12	S2-KI2	S2-KI8	S3-3	A	B	C	D	E
Chem	SiO_2	52.77	45.59	54.96	81.88	95.22	81.33	83.52	86.14	71.11	5.97	54.98	88.36	1.73
	Al_2O_3	32.26	18.69	21.37	5.52	2.78	8.89	5.79	6.62	15.49	0.44	15.38	4.07	0.43
	TiO_2	0.47	0.59	0.27	0.18	0.09	0.11	0.13	0.11	0.05	0.02	0.48	0.09	0.02
	Fe_2O_3	1.09	6.15	5.12	1.88	1.21	0.79	1.14	0.84	1.81	0.41	5.06	0.17	0.17
	CaO		6.12	2.94	1.93	0.23	0.37	0.88	0.46	0.65	54.21	4.92	0.03	54.63
	MgO	0.17	3.24	8.02	0.97	0.63	0.25	0.63	0.37	0.21	0.68	2.54	0.02	0.19
	Na_2O	0.22	0.16	0.11	0.05	0.03	0.03	0.03	0.02	3.75	0.03	2.74	0.01	0.04
	K_2O	1.05	6.08	1.99	1.56	0.18	0.65	0.83	0.58	4.72	0.06	4.92	0.03	0.09
	MnO									0.04	0.02	0.11		0.00
	P_2O_5										0.01	0.22		0.01
	Sum	88.03	86.62	94.78	93.97	100.38	92.43	92.96	95.14	97.83	61.85	91.35	92.77	57.32
Them.	H_2O	0.56	3.6	**14.39***	1.39	1.04	0.72	1.51	1.23	0.88	1.14	1.43	0.42	0.52
	OH and CO_2	10.55	9.1	4.54	1.89	0.26	3.64	2.56	2.53	1.34	40.66	5.63	1.77	42.58
	LOI	11.11	12.7	18.93	3.28	1.3	4.36	4.07	3.76	2.22	41.8	7.06	2.19	43.01
S = Sum + LOI		**99.14**	**99.32**	**113.7***	**97.25**	**101.7**	**96.79**	**97.03**	**97.9**	**100**	**103.65**	**98.41**	**94.96**	**100.42**
Calci.	$CaCO_3$	<0.1	5.8	0.2	3.09	0.47	1.71	1.41	0.97	8.68	103.24	20.47	11.94	95.65
CEC	cations	1.28	23.3	103.59	8.94	5.65	3.88	7.65	5.73	1.98	1.59	8.10	0.88	0.49

Chem.: chemical analysis by ICP/OES; Therm.: Thermal analysis TG/DTA, Calci. : calcimeter test; CEC: Cation exchange capacity via cobaltihexamine method. LOI : loss on ignition corresponding to H_2O + (OH and CO_2)
*modified value considering the high amount of water adsorbed by swelling clay.

For extracted clays, the high Al_2O_3 content of extracted kaolinite was caused by the high amount of aluminum octahedral from the 1:1 structure, whereas the high amounts of Fe_2O_3 and K_2O in extracted illite were due to the octahedral substitutions of Al^{3+} by Fe^{2+} and non exchangeable cations K^+ in illite structure. The highest water content obtained by thermal analysis characterized extracted montmorillonite that presented the highest CEC. As des-hydroxylation and decarbonation occurred in the same range of temperature (for particular clay), the quantity of OH and CO_2 were grouped. The high measured quantities corresponded to OH in kaolinite structure for extracted kaolinite and to CO_2 in extracted illite coupled to OH in illite structure. The quality of the measures was controlled by the term S corresponding to the loss of ignition added to the quantities of each element. S had to be the closest to 100% (if it's not the case, a lack of SiO_2 was generally observed linked to the uncompleted dissolution of siliceous phase). Finally, the high content of $CaCO_3$ in extracted illite from calcimeter result agreed with the high content of CaO from chemical analysis.

Regarding the artificial fine aggregates, the high SiO_2 content was caused by the siliceous sand in the mixtures, and the highest $CaCO_3$ value from S1-I13 could indicate the high calcite content in the sample.

Considering the chemical analysis of the unknown samples, the sample B and E significantly presented the composition of calcareous aggregates which contained high CaO with low SiO_2 and Al_2O_3 indicating a low clay content. The unknown sample D was assumed to be siliceous sand with quartz as main component because it mainly consisted of SiO_2. For the unknown sample A and C, high CEC value of sample A and their chemical composition indicated the complexity of their mineral phases. Generally, igneous or

sedimentary rocks which contained clay particles were suspected to belong to amphibole and mica group (*Deer et al. 1965*). The calcimeter test couldn't be considered for calcareous sand (the test was not accurate enough to evaluate the non calcareous fraction). The other samples that weren't sedimentary rocks showed more than 10% of phases sensitive to hydrochloric acid (associate to calcite). The presence of calcite didn't agree with the geological origin of sands. The acid reactivity of unknown sample A, C and D still remained unexplained. However, the calcimeter result wasn't considered in these cases.

3.1.3.2 Quantitative analysis

The quantities of mineral phases in extracted clays, artificial fine aggregates and unknown sand samples were shown in Table 35.

Table 35 The quantity of mineral phase derived from complementary method-chemical analysis

Material	clay minerals				Other Minerals					
	Kao.	**Mica group**	**Montm. or V**	**Chl.**	**Calcite**	**Quartz**	**K-Feld.**	**Na-Feld.**	Anatase	**Miscellany**
Ext. Kao.	74.6	12.4			0.3 [a]	12.2			0.50	
Ext. illite	2	70			12	15.4			0.60	
Ext. Mont.	*5*[a]	*8*	*84.85*		*0.05*[a]	*1.65*[a]			*0.25*	*0.25*[a] *(dolomite)*
S1 I13	3	21			3.5	72.32			0.18	
S1 M12	1	1	3.5			94.4			0.1	
S2-KI2	22	6			0.66	71.23			0.11	
S2-KI8	9	12			1.5	77.37			0.13	
S3-3	12	17	3		0.65	77.24			0.11	
Unknown A	0.2	2	7	0.35	1.15 [a]	32.05	27	30	0.05	0.20 (dolomite
Unknown B	0.1		2 (V)		90	4.6			0.03	1.20 (dolomite) 2 (Jennite)
Unknown C		3	12 (V)	3	7	26.5	26	20	0.50	2.00 (dolomite)
Unknown D	11	0.3			0.05 [a]	88.5			0.12	
Unknown E	0.8	1	0.3(V)		97	0.9			0.03	

[a] the additional mineral phase introduced in the calculation
[b] the missing mineral phase from chemical analysis compared to the identification results

In Table 36, Table 37 and Table 38, the composition correspond to the best fitting between calculated and measured chemical composition (each element was distributed between mineral phases previously identified by X-ray diffraction), thermal analysis and cation exchange capacity (< 63µm and < 2µm fractions from size distribution that represented the range of the whole clay quantity were also used to help the quantification work). Anatase appeared quite systematically in all samples to fit well the TiO_2 content from chemical analysis. Dolomite (in presence of calcareous sand) was also added to try to adjust MgO content.

In general, the complementary method is powerful but several difficulties still remained. On one hand, the low quantities of minerals might be evaluated (only if one element is assigned to only one mineral phase) but on the other hand, free chemical element as surface contaminants, the way of calculated CEC and the stoechiometry of minerals represent difficulties. The problem of free elements (that's to say the exchangeable cations or the elements present in the water surrounding the sand particle then on sand surface after drying) affected the quantification. For example, the fraction of CaO in crystalline structure of

mineral and the fraction of CaO as free cations remained unknown. After quantification, Na_2O, CaO or K_2O might remain without any mineral attribution.

The CEC value was a useful information but the calculated CEC remained an approximated value in several cases (see 2.2.2.3). Moreover, the minerals stoechiometry was not unique. If the quartz composition was fixed (corresponding to SiO_2), the clay composition varied not only from one type of clay to another but also from one clay to another clay within the same clay family. The case of extracted montmorillonite illustrated a typical case of stoechiometry (Figure 48). The quantification of montmorillonite calculated in 3 cases (calc1, calc2, calc3) depends strongly to the stoechiometry of montmorillonite mineral phase (the stoechiometry is given in Figure 48). The montmorillonite content may vary from 85% to 94% by varying the stoechiometry (note that the chemical, thermal characteristics of clay varied also in Table 36, as well as calculated CEC ranging between 115 and 161 meq/100g while the measured CEC is 103 meq/100g). For each material, the stoechiometry of clay mineral was adjusted in order to fit the measured parameters by respecting the mineralogical limit (for example the clay total layer charge range between 0.2 and 0.6).

	Calc1	Calc2	Calc3
quartz	1.5	2.25	2.25
Calcite/dolomite	0.25	0.5	0.5
Chlorite ?	--	1	1
Kaolinite ?	5	--	--
Montmorillonite	84.85	94	94
illite	8	1	1
Feldspath K (microcline)	--	1	1
anatase	0.25	0.25	0.25

SMECTITES with octahedral substitutions
Montmorillonite (Al2-xMgx)Si4(O10)(OH)2(CE)x
0,2 to 0,6 is the total layer charge par half cell

(Al2-0.5 Mg0.3 Fe0.2) Si4(O10)(OH)2 (CE)0.5
CE= Ca0.18 Na0.02 K0.05

Al2-0.5 Mg0,55 Fe0.25) (Si4) (O10)(OH)2 (CE)0.5
CE =Na0.02 K0.13 Mg 0.15 Ca0.2

Al2.5-0.8 Mg0,55 Fe0.25) (Si4-0.5Al0.5) (O10)(OH)2 (CE)1.3
CE =Na0.02 K0.13 Mg 0.15 Ca0.2

Tetrahedral substitution >>it missed 0.8 CE and max CE = 0.6

Figure 48 Complementary method applied on extracted montmorillonite: three propositions of calculated phase quantities (on the left with calc1, calc2 and calc3) corresponding to the three stoechiometries of montmorillonite clay and the measured/calculated chemical parameters in Table 36

If measured and calculated parameters agreed in quite all the case, difficulties remained especially with iron components. By comparing the chemical composition from estimated mineral phases with the measured one, unknown sample C showed a huge lack of iron (Table 38). It missed iron components in the proposed mineralogical composition of Unknown sample C. If in unknown samples A and E, iron oxides (goethite or hematite respectively) with a 2% or 1% content respectively may compensate the lack of iron, it's not possible with unknown sample C. The presence of another phase (such as Hedenbergite $CaFeSi_2O_6$ belonging to pyroxene family) had to be searched (in accordance with the geological origin of the sand which is the rhyolite rock). Such phase might partially overlap the calcite peak which presence in metamorphic rock was not explained initially. Augite $(Si,Al)_2O_6)(Ca,Mg,Fe,Ti,Al)_2$ that contained Fe (or diopside $CaMgSi_2O_6$ with magnesium) was also probably forgotten during the mineral phase identification in the unknown sample A which is gneiss and amphibolites. The petrographic identification using thin sections (Figure 49) helped to the presence of these additional mineral phases (such as iron oxides in unknown sample C)

Table 36 Comparison of measured and calculated characteristics of extracted clays used in the complementary method. Calculated parameters correspond to the quantities in Table 35

	Item	Ext. Kao.		Ext. Illite		Ext. Montm.			
		Measured	Calc[1,2]	Measured	Calc.[3]	Measured	Calc1	Calc2	Calc3
Chemical analysis (%)	Si	24.21	24.86	21.31	21.97	25.69	29.06	28.74	25.87
	Al	17.82	17.28	9.89	9.60	11.3	11.64	10.09	11.63
	Ti	0.30	0.30	0.35	0.36	0.16	0.15	0.15	0.15
	Fe	0.77	0.77	4.30	4.75	3.58	2.53	3.35	3.42
	Ca	0.14	0.12	4.37	4.81	2.10	1.65	2.04	2.08
	Mg	0.13	0.00	1.95	2.07	4.83	2.18	4.42	4.51
	Na	0.13	0.00	0.12	0.00	0.08	0.10	0.11	0.11
	K	1.50	1.18	5.05	6.65	1.65	1.01	1.43	1.45
Therm. anal. (%)	H_2O, OH and CO_2	10.55	11.08	9.10	8.62	4.77	5.24	4.66	4.76
CEC (meq/100g)	Exch. cations	1.28	3.01	23.30	17.01	103.6	115	158	161

[1]Kaolinite formula (on any material) : $Al2Si_2O_5(OH)_4$ with CEC= 0
[2]Illite formula in extracted kaolinite : $Al_2.08$ Fe0.46 Si_3,45 $(O10)(OH)_2K$
[3]Illite formula in extracted illite : (Al Mg0.5Fe0.5)$(Si_3Al)(O10)(OH)_2K$

Table 37 Comparison of measured and calculated characteristics of artificial fine aggregates used in the complementary method. Calculated parameters correspond to the quantities in Table 35

	Item	S1-I13		S2-KI2		S2-KI8		S3-3		S1-M12	
		Meas.	Calc.	Meas.	Calc.	Meas.	Calc.	Meas.	Calc.	Meas.	Calc.
Chemical analysis (%)	Si	38.27	38.76	38.02	39.31	39.04	40.58	40.27	40.74	44.51	45.53
	Al	2.92	3.38	4.71	5.39	3.06	3.46	3.50	3.84	1.47	0.67
	Ti	0.11	0.11	0.07	0.07	0.08	0.08	0.07	0.07	0.06	0.06
	Fe	1.31	1.43	0.55	0.41	0.80	0.81	0.59	0.67	0.84	0.21
	Ca	1.38	1.40	0.27	0.26	0.63	0.60	0.33	0.29	0.16	0.11
	Mg	0.58	0.62	0.15	0.18	0.38	0.35	0.22	0.36	0.38	0.18
	Na	0.04	0.00	0.02	0.00	0.03	0.00	0.02	0.03	0.02	0.02
	K	1.30	2.00	0.54	0.57	0.69	1.14	0.48	0.85	0.15	0.16
Thermal analysis (%)	H_2O and CO_2	1.89	2.87	3.64	3.62	2.56	2.44	2.53	2.44	0.26	0.34
CEC (meq/100g)	cations	8.94	5.1	3.88	1.45	7.65	2.91	5.73	9.4	5.65	8.90

Table 38 Comparison of measured and calculated characteristics of unknown samples used in the complementary method. Calculated parameters correspond to the quantities in Table 35

	Item	Unknown fine aggregates A		Unknown fine aggregates B		Unknown fine aggregates C		Unknown fine aggregates D		Unknown fine aggregates E	
		Meas.	Calc.	Meas.	Calc.	Meas.	Calc.	Meas.	Calc.	Meas.	Calc.
Chemical analysis (%)	Si	33.24	35.10	2.79	2.75	25.70	29.39	41.31	43.84	0.81	0.86
	Al	8.20	7.67	0.23	0.26	8.14	6.91	2.15	2.31	0.23	0.32
	Ti	0.03	0.03	0.01	0.02	0.29	0.30	0.06	0.07	0.01	0.02
	Fe	1.26	0.14	0.29	0.01	3.54	0.05	0.12	0.07	0.12	0.00
	Ca	0.47	0.46	38.74	36.72	3.52	2.80	0.02	0.02	39.05	38.71
	Mg	0.13	0.13	0.41	0.35	1.53	0.96	0.01	0.01	0.12	0.11
	Na	2.78	2.91	0.02	0.00	2.03	1.75	0.01	0.00	0.03	0.00
	K	3.92	3.98	0.05	0.00	4.08	3.88	0.02	0.03	0.08	0.07
Thermal analysis (%)	H_2O and CO_2	1.34	1.04	40.66	40.39	5.63	4.80	1.77	1.57	42.58	42.83
CEC (meq/100g)	cations	2.16	2.23	1.59	2.50	8.10	76.90	0.90	0.92	0.51	0.24

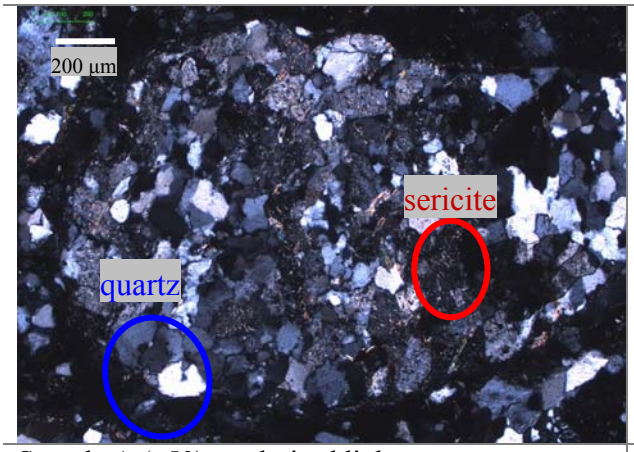

Samole A (x50) - polarised light.
Rock with a major fraction of siliceous sand grains (probably a gneiss). Presence of quartz and altered feldspars on sericite[11].

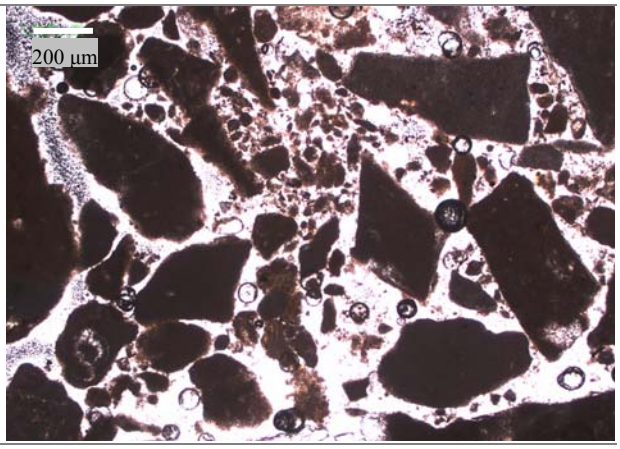

Sample B (x50) - natural light.
Crushed sand particles composed by calcareous stone with fine grain.

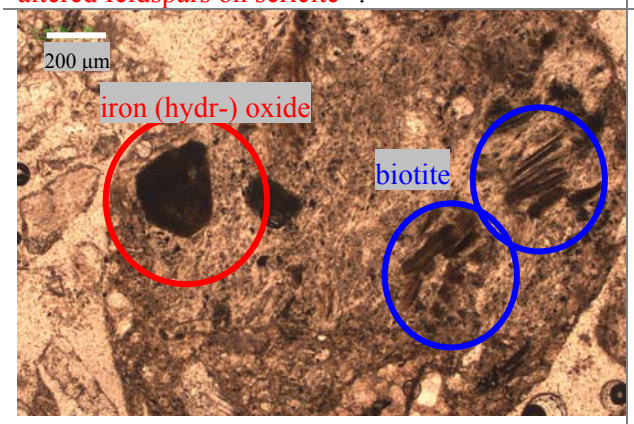

Sample C (x50) - natural light. Polyphasic grains containing iron (hydr-) oxide clusters and altered biotite.

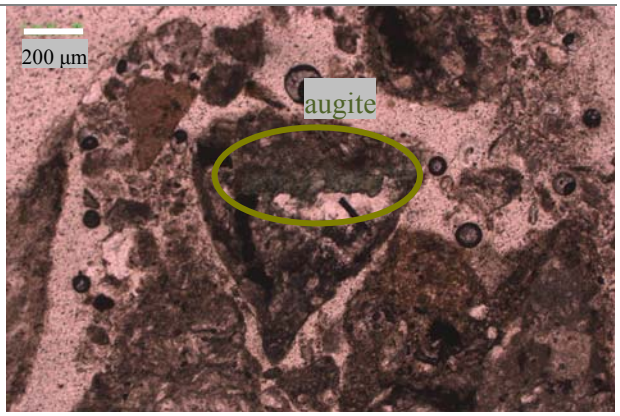

Sample C (x50) - natural light. Polyphasic grains containing pyroxène (augite in dark green).
Presence on other photos of iron oxide clusters.

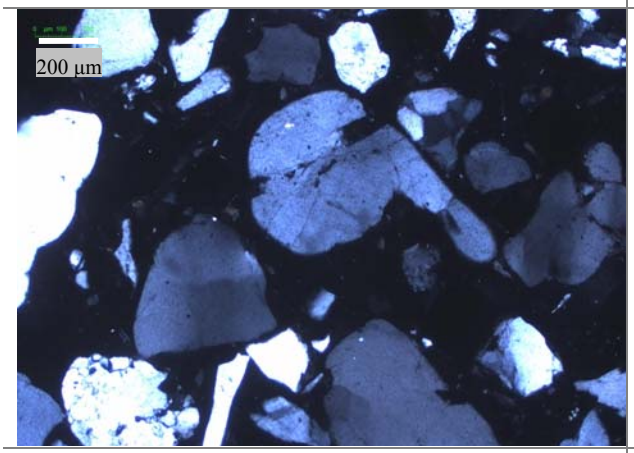

Sample D (x50) - polarised light.
Rounded grains indicating an alluvial or wind origin of the fine aggregate. The grains are mainly quartz.

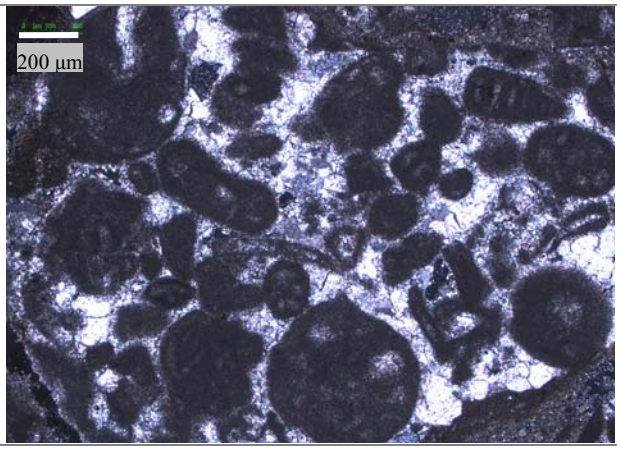

Sample E (x50) - natural light.
Oolitic limestone with sparitic cement (calcite crystals with a size greater than 50 µm. Wide variety of foraminifera fossil).

Figure 49 The thin section of unknown aggregates

[11] Fine fragments of mica (muscovite or paragonite) and common alteration mineral of orthoclase or plagioclase from feldspars

3.1.4 The comparison of quantitative results for aggregates by using X-Ray diffractometer

The quantities of mineral phases in extracted clays, artificial fine aggregates and unknown samples obtained by applying RIR, semi-quantification, complementary and Rietveld methods were compared in Table 39, Table 40 and Table 41 in order to evaluate the best quantitative method. As the quantification of mineral phases was used in this work to assess the harmfulness of clay particles in fine aggregates, the comparison of results focused on the clay quantities.

3.1.4.1 Extracted clays and artificial fine aggregates

The quantity of mineral phases in extracted clays was shown in Table 39. The accuracy of RIR, semi-quantification and Rietveld results were indicated by the relative deviation error to the complementary test results. The quantification result obtained from Rietveld indicated the best fitting by its lowest relative error except the kaolinite phase in extracted illite. However, as the results from all the tests presented large relative errors in the case of kaolinite phase in extracted illite, the error might be generated by the complementary test. Note that the semi-quantitative or RIR methods gave punctually results with less 10% of relative errors and the Rietveld method didn't allow the quantification of low amount of clay phases.

Table 39 The comparison of quantity from extracted clays derived by each quantitative method

Sample	Quantity	Clay minerals (%)			Relative error [a] (%)		
		Kao.	Mica group	Montm.	Kao.	Mica group	Montm.
Ext. Kao.	RIR	82.6	2.8	//	10.7	77.4	//
	Semi	64-77.2	18.9-22.8	//	3.5-14.2	52.4-83.9	//
	Rietveld	75.4	12.6	//	1.1	1.6	//
	Comp. [b]	74.6	12.4	//	--	--	--
Ext. illite	RIR	13.1	68.1	//	555	2.7	//
	Semi	4.5-7	70.5-93	//	125-250	0.7-32.8	//
	Rietveld	15.4	70.1	//	670	0.15	//
	Comp. [b]	2	70	//	--	--	--
Ext. Montm.	RIR	//	M	99.8	//	M	17.7
	Semi	//	0.5-0.65	99.25-99.5	//	91.9-93.7	17-17.3
	Rietveld	//	M	81.5	//	M	3.9
	Comp. [b]	5 (A)	8	84.8	--	--	--

[a] relative deviation error = | ((Comp.) - (measured value)) / (Comp.) |
[b] Comp. is the abbreviation of complementary test.
(A) additional phase (identification of the phase was not validated), M missing phases

For artificial fine aggregates (Table 40), the clay quantities in artificial fine aggregates measured by applying different methods were compared to expected quantities (the calculated quantities corresponded to the quantity of each extracted clay in mixture multiplied by the clay mineral quantity in each extracted clay from complementary method). The relative error was also calculated to evaluate the best method.

Both complementary and Rietveld measurements presented errors around 10-20% (but not in all the cases). RIR or semi-quantitative methods gave punctually good results too. The calculation of expected quantities based on complementary method applied on extracted clay probably contributed to the high relative error that appeared in Table 40. The highest relative errors were observed on the lowest clay contents as expected. Contrary to Rietveld method (or RIR method), the complementary method was able to give the

order of magnitude of the lowest clay content but such low clay fraction (except for montmorillonite) wouldn't have to play a major role on MB value adsorption or Duriez test.

Note that an extra montmorillonite phase was discovered by the Rietveld measurement in the sample of S2-KI8 (as well as in RIR method and semi-quantification). A mistake coming from operator during mixing might be able to explain these results (even if the mixing step was controlled by a second operator) or a contamination which origin was not identified.

Table 40 The comparison of quantity of artificial mixture derived by each quantitative method

Sample	Quantity from	Clay minerals (%)			Relative error [c] (%)		
		Kao	Illite	Montm	Kao	Illite	Montm
S1-I13	Design	//	30 [d]	//			
	calculation [a]	0.6	21	//			
	Comp. [b]	3	22	//	400.0	4.8	//
	RIR	3	6.1	//	400.0	71.0	//
	Semi	1-1.5	16.7-25.25	3.35-5.2*	**66.7**-150	20.2-20.5	*
	Rietveld	5	19.7	//	733.3	6.2	//
S1-M12	Design	//	//	4.77			
	calculation [a]	0.3	0.4	4.05			
	Comp. [b]	1	1	3.5	233.3	150.0	13.6
	Semi	0.55	0.05	4.3-4.4	83.3	87.5	6.2-8.6
	Rietveld	//	M	4.3	//	M	6.2
S2-KI2	Design	26.27 [d]	6.35 [d]	//			
	calculation [a]	19.7	7.7	//			
	Comp. [b]	22	6		11.7	22.1	//
	RIR	24.2	0.6		22.8	92.2	//
	Semi	13-26.3	3.1-6.4	0.6-1.25*	33.5-34.0	16.9-59.7	*
	Rietveld	20	7.7		1.5	0.0	//
S2-KI8	Design	8.91 [d]	15.43 [d]	//			
	calculation [a]	7	11.9	//			
	Comp. [b]	3.2	16		54.3	34.5	//
	RIR	10.2	1.2	1.3*	45.7	89.9	*
	Semi	3.5-10.9	3-4.3	7.1-9.9*	50.0-55.7	63.9-74.8	*
	Rietveld	3.9	16.4	1 A	44.3	37.8	*
S3-3	Design	16.63 [d]	6.92 [d]	3.05 [d]			
	calculation [a]	12.7	7.1	2.6			
	Comp. [b]	12	17	3	5.5	139.4	15.4
	RIR	14.6	0.7	0.2	15.0	90.1	92.3
	Semi	8.3-15.9	2.9-5.5	2.3-4.3	25.2-34.6	22.5-59.2	**11.5**-65.4
	Rietveld	10.9	10.5	4.3	14.2	47.9	65.4

[a] calculated quantity = (quantity of each extracted clay in mixture) × (clay mineral quantity in each extracted clay from complementary method) [b] Comp. : complementary test [d] Quantity of extracted clay in mixture - Design refers to the manufacture of artificial fine aggregates (see Table 14 in 2.1.2.1) [c] relative deviation error = | ((calculated quantity) - (measured quantity)) / (calculated quantity) | * unexpected mineral in the mixture

3.1.4.2 Unknown fine aggregates

The five unknown fine aggregates, unknown A to E samples, were examined by all the quantitative methods described previously (Table 41). For unknown fine aggregates, no reference quantities were available to compare the experimental results. The validation of the quantities might come from a good accordance between the results of the four methods. Samples A, D and E were in this case. The undetectable clay minerals from X-ray powder diffraction (noted M in the Table 41) in Rietveld and RIR methods agreed with the low quantities found by semi-quantification or complementary method. For samples A and C, the complexity of their mineralogical composition (higher number of phases) explained why results from the different methods were not coherent. The probable uncompleted identification (with the forgotten presence iron-rich mineral phase) might be at the origin of the differences as well as the non taking into account in Rietveld method of the amorphous clay considered as vermiculite in RIR and complementary method (for sample B), or the fitting of chlorite and vermiculite considered in RIR and Compl. method by corrensite in Rietveld method (for sample C). Finally, the quantification of unknown samples A and C remained unclear (no agreement between the four methods).

Table 41 The comparison of quantity of unknown fine aggregates

Material	Quantity from	Clay minerals and phyllosilicates			
		Kao.	Mica group	Vermiculite	Chl.
Unknown A	RIR	1.7	3.5	M	1.3
	Semi	0.25-**1.6**	**0.7-4.7**	2.85-19.2	0.06-**0.4**
	Rietveld	1.8	5.7	M	1.8
	Comp.	0.2	2	7	0.35
Unknown B	RIR	M	//	M*	//
	Semi	**0.02-0.15**	//	**0.8**-5.8	//
	Rietveld	M	//	M*	//
	Chem.	0.15	//	2	//
Unknown C	RIR	//	14.5	M	13.4
	Semi	//	0.45-1.4	9.9-26.1	0.4-0.9
	Rietveld	//	24.2	8.07 (Cor.)	//
	Chem.	//	3	12 (V)	3 (Chl.)
Unknown D	RIR	10.3	M	//	//
	Semi	**10**-16.45	**0.15-0.3**	//	//
	Rietveld	11.1	M	//	//
	Chem.	11	0.3	//	//
Unknown E	RIR	M	M	M	//
	Semi	2.05-7.6	3.7-13.6	1.6-6.05	//
	Rietveld	M	M	M	//
	Chem.	0.8	1	0.3	//

[a] Comp. : complementary test Chl : chlorite, Cor. : corrensite (interstratified vermiculite-smectite mix layer)
*amorphous clay considered as vermiculite in RIR and Complementary method

Considering that the Rietveld method was 'rapid' and capable to approach mineral composition in almost all the cases, the quantities estimated by Rietveld method could be used in the following chapters after a step of validation by using the calculation sheet developed for complementary method. The percentage of mineral phases given by Rietveld method should fit well enough the chemical, thermal and CEC value to be validated. The Table 42 presented the validation step by introducing Rietveld results in the chemical

calculation sheet used in complementary method. If the operator estimated that the calculated values were too far from experimental ones, the Rietveld method should be applied again.

Table 42 Comparison of measured and calculated characteristics of unknown samples. The mineral phase percentages found by the Rietveld method were introduced in the calculation sheet used for complementary method.

	Item	Unknown fine aggregates A		Unknown fine aggregates B		Unknown fine aggregates C		Unknown fine aggregates D		Unknown fine aggregates E	
		Meas.	Calc.	Meas.	Calc.	Meas.	Calc.	Meas.	Calc.	Meas.	Calc.
Chemical analysis (%)	Si	33.24	34.93	2.79	2.01	25.70	29.02	41.31	43.43	0.81	0.28
	Al	8.20	6.70	0.23	0.00	8.14	7.98	2.15	2.29	0.23	0.00
	Ti	0.03	0.02	0.01	0.02	0.29	0.30	0.06	0.69	0.01	0.00
	Fe	1.26	0.58	0.29	0.00	3.54	0.02	0.12	0.05	0.12	0.00
	Ca	0.47	0.80	38.74	38.38	3.52	3.40	0.02	0.00	39.05	39.67
	Mg	0.13	0.17	0.41	0.00	1.53	1.46	0.01	0.00	0.12	0.10
	Na	2.78	3.00	0.02	0.00	2.03	1.84	0.01	0.00	0.03	0.00
	K	3.92	0.03	0.05	0.00	4.08	3.62	0.02	0.00	0.08	0.00
Thermal analysis (%)	H_2O and CO_2	1.34	1.43	40.66	41.8	5.63	5.16	1.77	1.54	42.58	43.72
CEC *(meq/100g)	cations	2.16	2.40-5.25	1.59	0	8.10	1-2.18	0.90	0.33-1.67	0.51	0

*to simplify the CEC calculation and give a range of value instead of a fixed value, high and low CEC values are estimated using the CEC equal to 3-15 meq/100g for pure kaolinite, 10-40 meq/100g for pure illite and 100-150 meq/100 g for pure vermiculite (from literature)

3.1.5 Summary

The mineral phase identification and the evaluation of their quantities in fine aggregate were achieved by using X-ray diffraction. The clay identification remained the first step of the methodology of quantification. With adequate sample preparation (to lower the preferential orientation), the X-Ray powder diffraction pattern allowed the non clay mineral phase identification and their quantification by Rietveld method. However, when too numerous phases were present, some minerals could miss or the identification might remain unclear in presence of several minerals in low quantity, which peak might overlap. The geological expertise was needed to validate the mineral identification (petrographic study might be necessary as complementary method in the hardest sample identification).

The harmful clay minerals in fine aggregates (higher than 1%) could be also identified from X-ray powder diffraction pattern using high reflection angle d (*060*). But the analysis of clay fraction on oriented glass slides was still required in order to confirm results on X-ray powder pattern and to detect the harmful clay with extreme low quantity. The semi-quantitative method (X-ray diffraction combined with the < 63 µm and < 2µm measured in well dispersed fine aggregate suspension using preferentially European standard (*XP CEN ISO TS 17892-4*) as well as the RIR method gave first estimation of clay and non-clay minerals in tested samples.

Furthermore, the direct application of Rietveld method (in vogue today) might conduct to erroneous results for some complex geomaterials if a validation step is not applied. If the quantity of clay minerals was successfully obtained by applying Rietveld method (the quality of the fitting is shown by significantly low

R-weight pattern - R_{wp}), results needed to be validated by chemical, thermal and CEC measurements if it is possible. Considering experimental results, Rietveld method remained globally recommended for mineralogical analysis and the clay fraction measured by semi-quantification (combined to particle size distribution) had to be considered instead of Rietveld method when the clay quantities were too low. Such quantities when montmorillonite or vermiculite were concerned, should be evaluated with accuracy. The discussion chapter will cross-check the impact of low clay quantity on the mineralogical analysis of fine aggregates, the qualification of fine aggregates by using methylene blue test (*NF EN 933-9 2009*) and the water sensibility of AC mixture by applying Duriez test (*NF P 98-251-1 2002*).

3.2 Methylene blue (MB) test to assess the clay harmfulness

Interaction between MB molecules and clays was studied using UV-photometric measurement in order to clarify the parameters which impact on MB adsorption and the configuration of MB molecules.

Besides, the cation exchange capacity (CEC) measurement (applying the method using cobaltihexamine ions) was also done as a complementary test because it's a well-known parameters used by agronomists for a long time while MB value was chosen by geotechnicians. The threshold of qualification for artificial fine aggregates and unknown fine aggregates used in AC mixture, fixed to MB = 2 g/kg (for $D_{0/2\ mm}$ sample - *NF P18-545*), were examined and judged considering the MB variation with impacting parameters.

3.2.1 MB value, CEC measurement and configuration of MB molecules on extracted clay

The extracted kaolinite, illite and montmorillonite were tested to measure their MB adsorption and CEC value. The impact of MB initial concentration (MB solution added to the suspension) was discussed as a key parameter that may impact on MB value. The MB configuration measured by UV-spectrophotometry on MB solutions and MB-clay suspensions were collected as well. Based on MB value and the evolution of MB-clay suspensions spectrum versus contact time, general tendency of MB adsorption on clay can be preliminarily glanced.

3.2.1.1 Configuration of MB molecules measured in MB-clay suspension and in MB solution after clay removing

Using UV-spectrophotometer, the configuration of MB molecules in MB-clay suspension and in solution was measured after a 2 hours contact under continuous agitation. On one hand, the measurement on MB-clay suspension needs a low concentration of clay in suspension (approximately $7x10^{-2}$ g/l of clay) in order not to have an expected absorbance (Abs). The MB concentration is adjusted according to the mineralogy of the clay not to exceed Abs = 1 at the end of the contact time. On the other hand, the configuration of MB molecule in solution after clay contact (noted MB-clay solution) was measured after clay particles separation from suspension by centrifugation after the two hours contact.

The configurations of MB-kaolinite, MB-illite and MB-montmorillonite solutions (Figure 50a) presented the same type of MB molecules aggregations. Molecules gathered to form H-dimers and monomers characterized by peaks wavelength at around 613 nm and 664 nm respectively (see Table 7).

At the opposite, the configuration of MB-montmorillonite suspensions presented the additional H-aggregate configuration but not in MB-kaolinite or MB-illite suspensions (Figure 50b). Estimating that the 2h contact allowed the MB molecules re-arrangement on clay surface, the presence of H-aggregates still after 2h indicated that the tested montmorillonite had a high layer charge as the results presented in the literature review 1.2.3.2 (*Bujdak et al. 2002, Miguel et al. 2002, Pentrák et al.2012, Yenera et al. 2012*). Indeed, the d (*001*) spacing of EG treated K-saturated montmorillonite is clearly shown its high layer charge as well (C3 in Figure 39). In the case of MB-kaolinite and MB-illite suspensions, MB molecules mainly presented in monomer and dimer configurations because of the lower layer charge of clays.

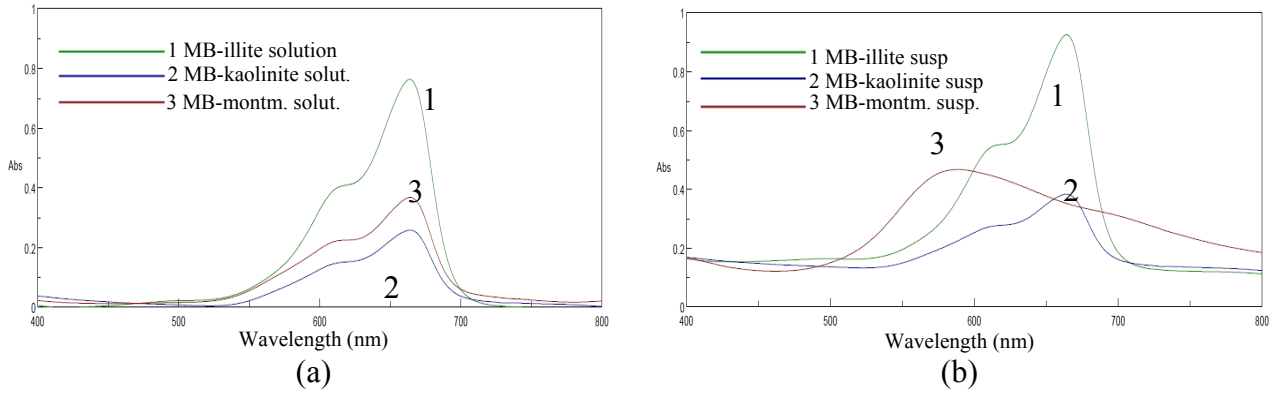

Figure 50 UV-visible spectra (absorbance versus wavelength) showing the configuration of MB molecules in MB-kaolinite, MB-illite and MB-montmorillonite (a) solutions coming from suspension after clay extraction and (b) suspensions after a 2h agitation.

3.2.1.2 MB adsorption and CEC measurements

Methylene blue adsorption (MB) and cation exchange capacity (CEC) on extracted and commercial clays and washed sand were measured by UV-photometric method presented in Chapter 2. Both types of material varied by their preparation (the drying at 40°C was controlled for extracted clay while the commercial products were extracted and dried thanks to industrial processes).

The results in Table 43 showed that the extracted clays have the higher adsorption for both methylene blue and cobaltihexamine ion than the commercial clays, except the MB value from illite. Such result agrees with the idea that the drying process before adsorption impacts strongly the phenomenon. The effect of the drying temperature before measurement will be discussed in further paragraphs.

Table 43 CEC and MB values of extracted and commercial studied clays (S.D. standard deviation)

Material Resource		MB adsorption (g/kg) (UV-photometric method)					CEC (cobaltihexamine method)	
		MB value (g/kg)	S.D.	MB $_{init.}$ % [b]	Abs. [c]	MB $_{fin.}$ % [d]	CEC value (meq/100g)	S.D.
Kao.	Ext.	6.40	0.30	154.1	0.51	153.9	1.28	0.28
	Comm.	4.62	0.14	266.6	1.19	265.3	0.54	0.24
Illite	Ext.	46.30	1.90	62.5	1.80	62.1	23.30	0.09
	Comm.	48.90	0.18	82.80	1.55	82.3	18.58	0.06
Montm.	Ext.	304.00	12.70	92.3	1.05	91.7	103.59	4.32
	Comm.	295.13	3.39	92	1.43	91.5	100.80	1.74
Sand	Washed	0.30	0.00	--	--	93.8	0.06	0.01

[a] Cation exchange capacities measured by cobaltihexamine method
[b] Initial MB covering percentage [c] Abs. is an abbreviation for absorbance [d] Final MB covering percentage

Comparing the results of CEC values from extracted clays to the literature (see the Table 44 taken from literature review), extracted kaolinite had slightly lower CEC values than references, whereas CEC of extracted illite and montmorillonite were in agreement with the references. Kaolinite and illite had much less exchangeable cations than montmorillonite, because of the absence of substitutions in crystal cell for kaolinite (the total layer charge is almost zero) or a partial permanent compensated charge by K^+ for illite. Both clays had lower exchange cation capacity (CEC) and lower specific surface area accessible to methylene blue molecules for adsorption than montmorillonite. The extremely high CEC values of

montmorillonite indicated the high sensitivity to water (swelling property). The MB values followed the same tendency as CEC but the comparison of measured MB values with literature review (see Table 44) couldn't be done easily because, even after unit conversion, the protocols of measurement were not the same.

Table 44 Usual CEC and MB values of different clay groups.

Type of pure clay	MB (g/kg)	CEC (meq/100g)	SSA (m^2/g)
Kaolinite	1.5-6.4	3-15	5-20
Illite	9.5-16	10-40	50-200
Mont.	19-96	70-120	700-800
Vermiculite	--	100-150	--
Chlorite	9.5-16	10-40	--
Sepiolite/ Palygorskite	--	20-30	--

Knowing that cobaltihexamine ions (used for CEC measures) doesn't aggregate (presence of just only one peak on UV-visible spectrum) and based on the assumption that the adsorption equilibrium is reached after 2 h, CEC is used as a reference value. Then, the comparison of MB and CEC values was used to discuss the rate of MB aggregation. Note that cobaltihexamine ions have not the same chemical affinity towards clay surface because of their valence or the same ability to reach clay surface because of their size as MB molecule. In other words, one cobaltihexamine ions (valence: 3+) can not be generally replaced by 3 MB molecules (valence :1+) (without the consideration of aggregation). The high affinity of cobaltihexamine and its ability to reach the entire clay surface reinforced the choice of CEC as reference to discuss MB value. So, the notion of "MB covering percentage" was introduced. The 'final MB covering percentage' corresponds to the ratio between MB value (MB adsorption) and the CEC value. It is calculated by:

$$\mathrm{MB_{Fin.}}\% = \frac{MB_{adsorbed}(g/kg)}{M_{MB}(g/mol)} \times \frac{1}{CEC(meq/100g)} \times 100$$

where M_{MB} = 319.9 g/mol

Furthermore, it's known from literature review (1.2.3.2) that MB molecule configuration may vary with the "initial MB covering percentage". Such parameter corresponds to the comparison of MB quantity initially added to the clay suspension to CEC value. Initial MB covering percentage is calculated by the following formula:

$$\mathrm{MB\ _{Init.}}\% = \frac{V_{MB\,added}(L) \times [MB](g/L)}{M_{MB} \times m_{clay}(kg)} \times \frac{1}{CEC(meq/100g)} \times 100$$

Initial MB covering and final MB covering percentages as well as absorbance of MB solution after clay extraction from suspension were presented in Table 43 corresponding to the MB adsorption measurement after 2 hours of agitation.

The final MB covering percentage on extracted kaolinite (153.9%) indicated the higher adsorption of MB molecule compared to cobaltihexamine ions, probably because of the MB-MB interaction on kaolinite surface. Moreover, the absorbance from final covering percentage on kaolinite was much lower than the case of extracted montmorillonite. Even if the initial MB covering percentage is high, absorbance of

solution extracted from suspension after MB-clay contact remained quite low (around 0.5) confirming the high amount of MB aggregates on kaolinite surface.

The final MB covering percentage on extracted illite was 62.1 % with 1.8 of absorbance. It indicated the lower adsorption of MB molecule after 2 hours of agitation compared to cobaltihexamine adsorption as the result from extracted montmorillonite. The reason was that the lower valence number of MB molecule (+1) and its size compared to cobaltihexamine ions size contributed to lower its capacity to enter into the clay internal space (longer time may impact on clay hydration and the entry into interlayer. Such aspect will be discussed below). MB molecules were not able to reach the whole illite surface above all if MB molecules are aggregates and if clay particles still formed big aggregates (2 hours of agitation was probably not enough to segregate illite into small pieces for revealing the entire illite surface).

In the case of montmorillonite, the final MB covering percentage ($MB_{fin.}$%) equal to 91.7% and the solution absorbance to 1.05 showed that the MB-montmorillonite suspension apparently behaved as illite or potentially hadn't reached the equilibrium yet during the testing time.

3.2.1.3 Impact of initial MB covering MB adsorption

To better understand MB-clay interaction, the role of the initial MB covering percentage on MB adsorption (linked to initial MB concentration or clay concentration in suspension - *Carter et Wilde, 1972*), the initial MB covering percentage on extracted montmorillonite were varied.

All the tests followed the standard of UV-photometer method for MB adsorption (that's to say the measure of the remained MB concentration in solution after a 2 hours contact of 35 ml of MB solution at 1 g/L with various quantities of clay). The Table 45 showed that MB value (or MB_{fin}%) behaved in accordance with the initial $MB_{init.}$% . The correlation between covering percentage, absorbance and MB adsorption onto extracted montmorillonite was shown in Figure 51.

Table 45 The MB adsorption on extracted montmorillonite related to the initial MB covering percentage.

Sample [a]		Added MB		Measured MB in solution		MB value	
no.	Clay quantity (g)	(ml)	$MB_{init.}$ % [b]	MB solution abs.[c]	MB concentration using calibration curve	MB (g/kg)	$MB_{fin.}$ % [d]
1	0.124	35.0047	85.22	0.31	1.14	282.08	85.12
2	0.120	35.0101	87.68	0.51	1.88	290.03	87.52
3	0.116	35.0256	91.43	0.57	2.11	302.36	91.24
4	0.112	35.1329	94.40	**0.96 (Abs =1)**	3.69	311.68	94.05
5	0.111	35.2457	95.84	1.96	8.21	315.00	95.06
6	0.106	35.0325	99.32	2.06	8.74	326.26	98.45
7	0.105	35.0086	100.94	3.46	18.31	328.38	99.09
8	0.102	35.0709	103.86	3.63	20.19	**337.21**	**101.76**
9	0.104	35.0164	101.57	3.77	22.17	**329.11**	**99.31**
10	0.103	35.0042	102.67	3.75	21.88	332.80	100.43
11	0.098	35.0052	107.90	3.55	19.34	350.64	105.81
12	0.093	35.0005	113.02	3.40	17.74	367.87	111.01

[a] The cation exchange capacities (CEC) is 103.6 meq/100g. [b] Initial MB covering percentage
[c] Abs. is an abbreviation for absorbance [d] Final MB covering percentage

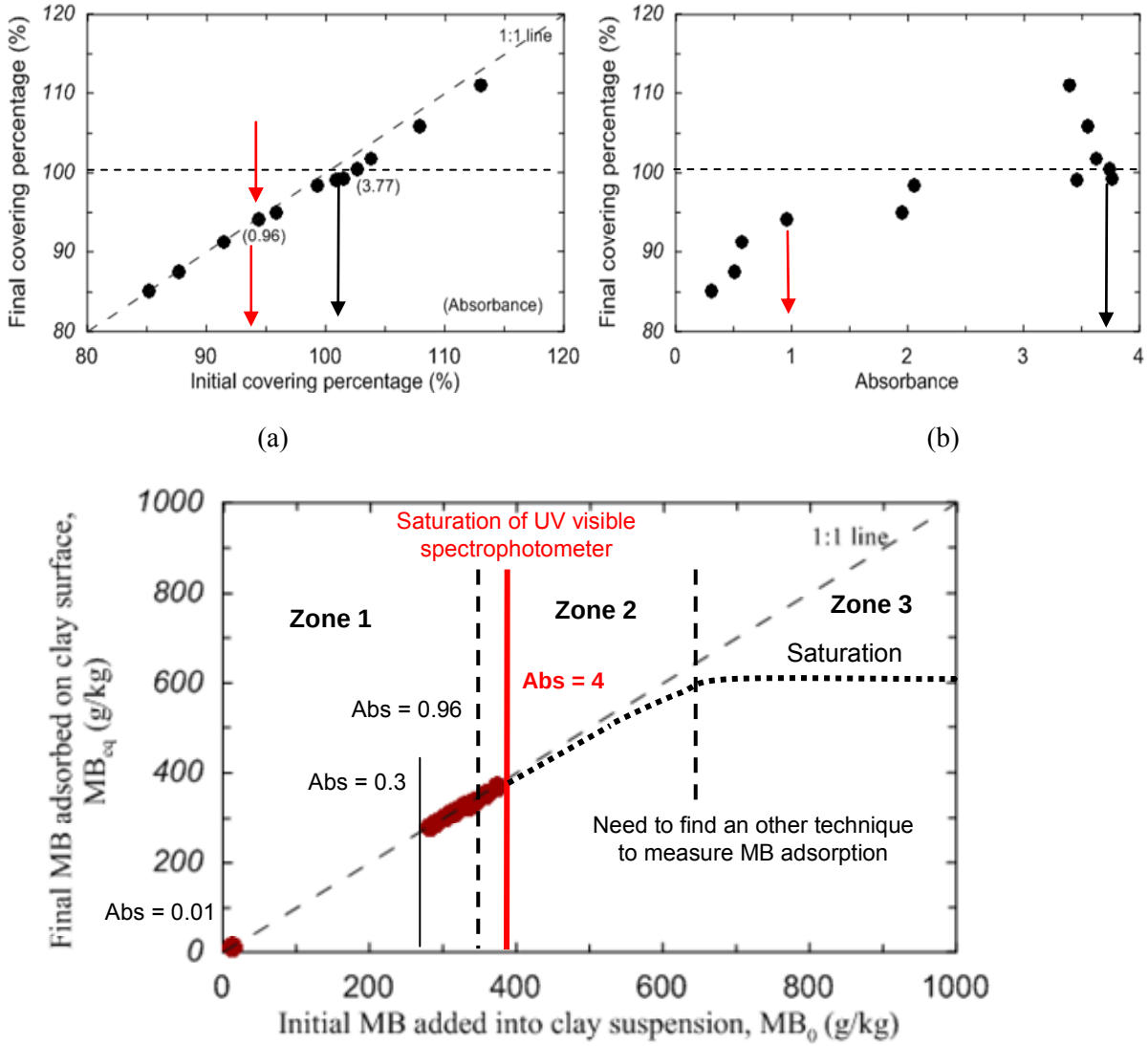

Figure 51 Final MB covering percentage on extracted montmorillonite versus (a) the initial MB coverage percentage or (b) absorbance. (c) Assumption of complete MB isotherm adsorption.

The initial MB covering percentage perfectly corresponded to the final covering percentage on montmorillonite surface until an absorbance equal to 0.96 (Figure 51b). A good fitting with 1:1 line was observed in the 0.01 to 0.96 range of absorbance. It corresponded to 94% of both initial and final covering percentage (Figure 51a).

The initial covering percentage higher than 95% produced slight lower final covering percentage on montmorillonite surface. However, adsorption kept on increasing with the increase of the initial MB concentration. The curve of MB adsorption didn't reach saturation that's to say a constant value. The MB aggregation occurring at high MB covering was probably at the origin of such behavior. If the initial covering percentage was higher than the available space for MB molecules on clay surface over 100%, MB-MB interactions mainly controlled the final covering percentage. The threshold at 94% of final covering percentage was probably caused by the fact that MB-clay suspension needed longer time of agitation to reach 100% of final covering percentage because of the arrangement of MB molecules on clay surface. The rectangular MB molecules initially were tilted with various configurations on clay surface (*Hähner et al 1996, Kobayashi 1996, Hang 1970, Kaneko, Bujdak J. 2003, 2008, Umemura 2003,*

Bodenheimer 1968), and the orientation of MB molecules took bigger space and longer time (than cobaltihexamine ions) was needed to adjust MB molecules the ones with the others on clay surface.

These considerations on initial MB covering percentage explained why spectrophotometric method is so tricky and why the absorbance value and initial MB covering percentage were systematically observed meticulously to control the quality of the measurement and to compare series of MB values. This strong impact of initial MB covering percentage on MB-montmorillonite adsorption is supposedly impact on MB-illite and MB-kaolinite adsorption as well. The irregular behavior of isotherms of MB adsorbed onto kaolinite, illite and montmorillonite also an evidence for this hypothesis (Figure 52).

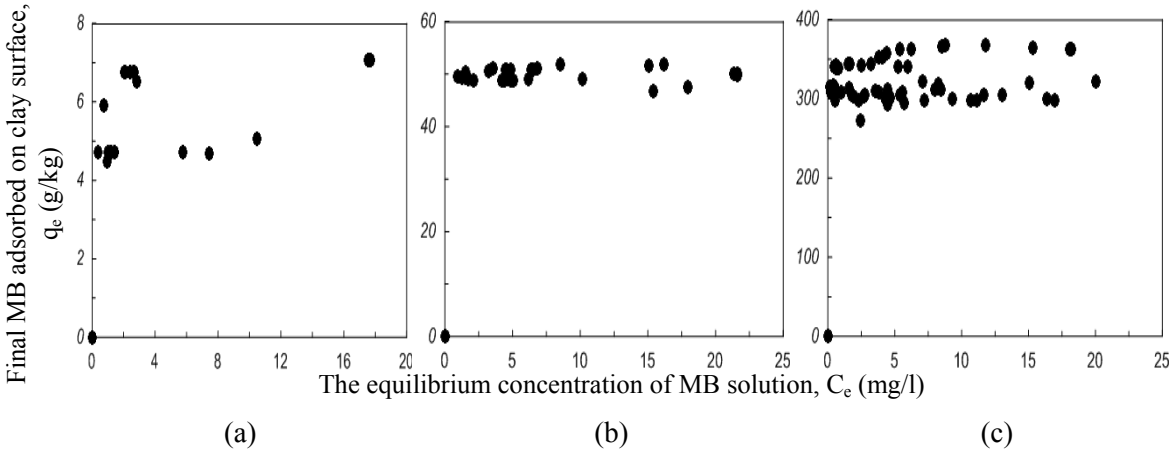

Figure 52 Adsorption of isotherms of MB onto (a) kaolinite, (b) illite and (c) montmorillonite

3.2.1.4 The impact of contact time on MB adsorption

As well as initial MB covering percentage, the time of contact between clay and MB solution may impact MB adsorption. The extracted clays were tested over a month of agitation. As the final MB covering percentage is in relation with MB adsorption and CEC value, the final MB covering percentage in the following formula was used in Figure 53 to follow MB adsorption (absorbances of MB solution extracted from suspension were also drawn).

$$\mathrm{MB_{Fin.}}\% = \frac{MB_{adsorbed\ at\ t}\ (g/kg)}{M_{MB}} \times \frac{1}{CEC_{measured\ at\ t=2h}(meq/100g)} \times 100$$

$\mathrm{MB_{fin.}}\%$ after 2 hours of MB-clays agitation have been found to be 154% on kaolinite surface, around 61% on illite and around 92% on montmorillonite surface (see Table 43). During one month of shaking, kaolinite was over covered by MB molecules (covering higher than 100%) constantly. Illite progressed the first few hours and remained at final covering percentage around 68% during the month of contact. Montmorillonite had the same trend with a slower increase of final covering percentage. It reached 100% of the surface covering between 25 hours to 48 hours of contact between MB and montmorillonite.

The evolution versus time contact of MB adsorption (proportional to the final MB covering percentage) had to be discussed also considering the various initial MB covering percentage (or called MB density). Based on Figure 51, the initial and final MB covering were linearly linked for montmorillonite and similar behavior were recorded on illite and kaolinite (see Figure 53). The absorbance from each sample at a

particular contact time was introduced by the empty symbols (each point corresponded to one tested suspension).

For MB-kaolinite adsorption, the final covering percentage seemed to be more correlated to the $MB_{init.}$% in solution than time. High MB densities were needed to allow the MB adsorption measurement with a final absorbance lower than 1. This high MB density oversaturated kaolinite suspension because of MB-MB interaction. The maximum value at around 160% of final covering is obtained for absorbance between 0.5 and 1 at long time contact. The tested point with the $MB_{init.}$% around 176% against 166% for the other points generated an 3.5 absorbance and a higher final MB covering percentage equal to 169%. This observation confirmed that MB adsorption is $MB_{init.}$% dependent. Considering time effect, kaolinite reached MB adsorption equilibrium after 2 hours. The MB aggregation on kaolinite surface is high and produced a great adsorption compared to cobaltihexamine ions adsorption.

For illite, MB-adsorption remained stable with time at long time contact on Figure 53 whereas the $MB_{init.}$% varied linearly with $MB_{Fin.}$% as demonstrated for montmorillonite in Figure 51. Note that absorbance of final solutions after clay extraction remained between 1 and 2 at long time contact while absorbance varied for short time contact.

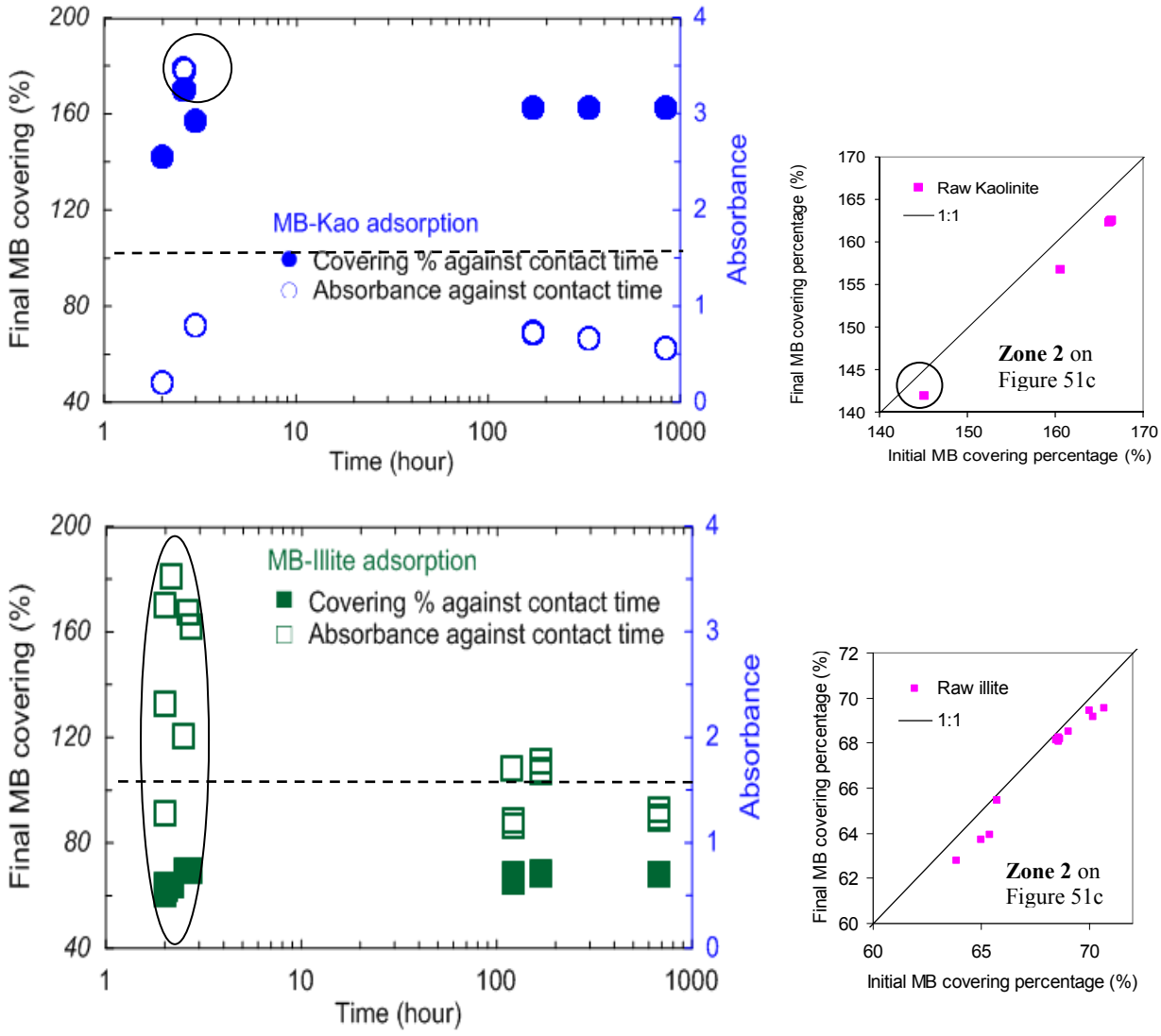

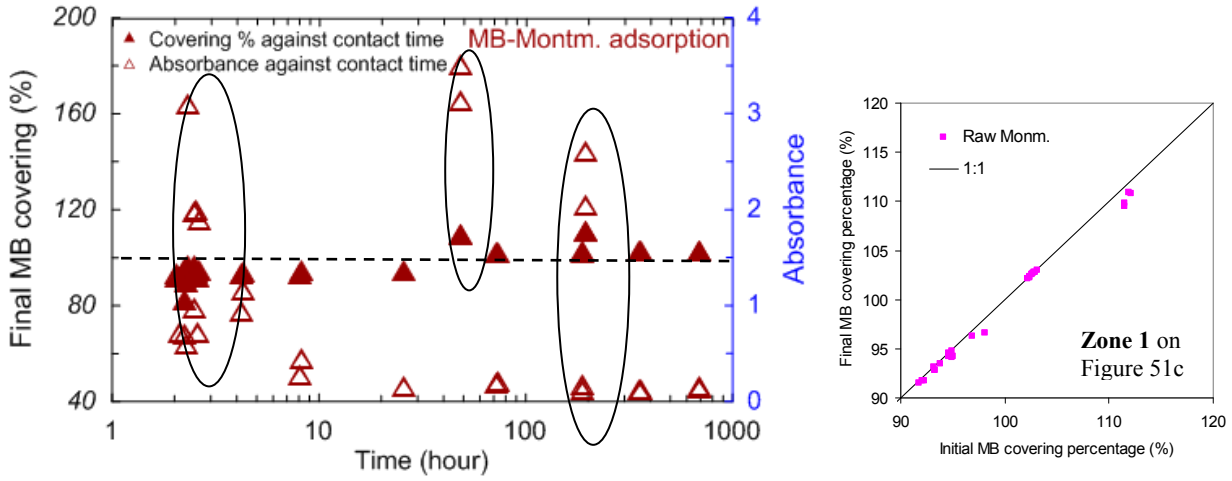

Figure 53 The final MB covering percentage (%) or absorbance on extracted kaolinite, illite and montmorillonite versus the contact time between MB and clay in suspensions

A correction of the $MB_{Fin..}$% was applied to compensate the $MB_{init..}$% variation to clearly see the time effect on MB adsorption. For each point x, the ratio $a_x = (MB_{Fin..}\%)_x/(MB_{init..}\%)_x$ was calculated and $MB_{Fin..}$% cor is calculated by the following way :

$(MB_{Fin..}\%\ cor)_x = a_x \times (MB_{Init..}\%)_{long\ time}$ with $(MB_{Init..}\%)_{long\ time}$ corresponded to the initial MB covering percentage taken as common reference. The corrected curves were done on Figure 54. After correction, the rapid kinetic to reach equilibrium is confirmed for kaolinite and MB adsorption on illite appeared to be stabilized after the first 2 hours of contact. The 68% final MB covering on illite surface agreed with the explanation that illite particles remained in non-dispersible big aggregates even after long time. The low affinity of MB molecule was not able to reach the whole illite surface by time (even with high MB initial density).

Regarding the MB adsorbed on montmorillonite with time and its absorbance on Figure 53, the final MB covering percentages reached over 100 % after 48 hours of agitation for all the absorbance values even high absorbance between 2 and 4. Considering the Figure 51, the final MB covering percentage variation for Abs between 0.3 and 3.5 ranged from 85% to 110%. The variation observed on Figure 53 agreed with such range. Now after correction on Figure 54, previous conclusion, which was the impact of time on MB-montmorillonite adsorption, was evidenced. MB-montmorillonite adsorption shall be measured not before 10 hours of contact time instead of 25-48 h as addressed previously. The increase of MB final covering percentage on montmorillonite within 10 hours probably causes by the dispersion of montmorillonite aggregation associated with water. This result partially agreed with the 18 hours suggested MB-montmorillonite agitating time by Bujdak *(2001)*.

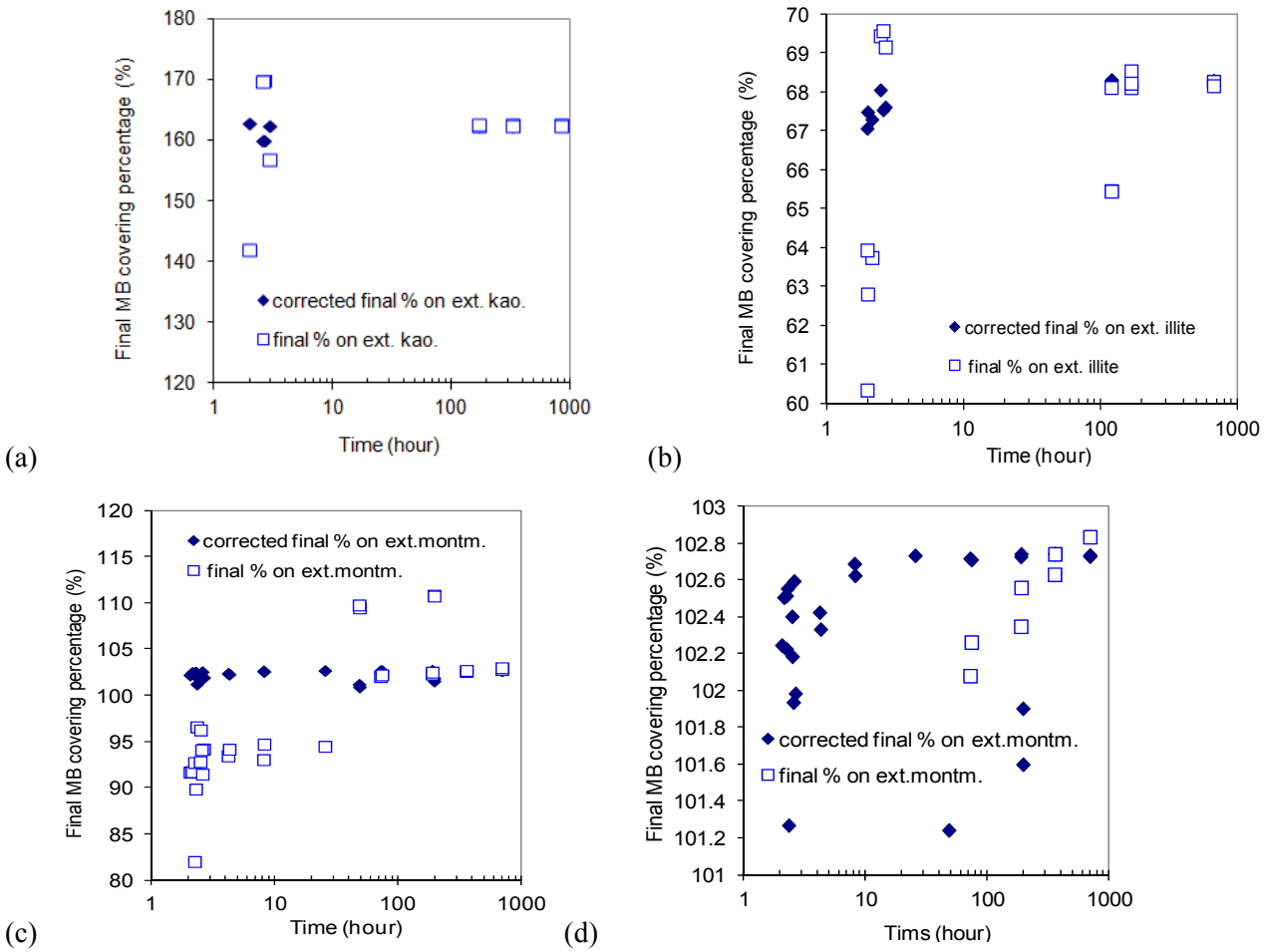

Figure 54 The final MB covering percentage (%) with and without correction on extracted (a) kaolinite, (b) illite and (c) montmorillonite ((d) a zoom of (c)) versus the contact time between MB and clay in suspensions.

In summary, there was no impact of time on MB-kaolinite- and MB- illite adsorptions after the first 2 - 3 hours contact, whereas adsorption onto montmorillonite had to be measured after more than 10 hours of agitation. The MB density (absorbance) adsorption had to be controlled for obtaining 'reasonable' MB value.

3.2.2 The impact of clay layer charge on MB adsorption

The effect of clay layer charge on MB adsorption and swelling property are well-known (*Komadel 1996, Bujdak et al. 2002, Miguel et al. 2002, Pentrák et al.2012, Yenera et al. 2012*) and introduced in the literature review (1.2.3.2 with detail shown in appendix 2.1) but the result of MB adsorption still be questioned.

The layer charge effect on MB adsorption was studied by using reduced-charge montmorillonite (RCMs) samples. The MB molecule configuration in MB-RCMs suspension, the MB adsorption (MB value) and the swelling properties of RCMs were investigated. Then, the link between the layer charge of clay impacting on MB adsorption (and then on MB value used as key parameter by geotechnicians) and the harmfulness of clay in civil engineering will be able to be considered.

3.2.2.1 The MB adsorption measured on reduced-layer charge montmorillonite (RCMs)

Samples of reduced-charge montmorillonite (RCMs) were prepared by following a protocol implying Li^+ saturation and different drying temperature between 25°C (ambient temperature) and 200°C (see chapter 2 - *Greene-Kelly, 1953*).

Table 46 Name of MB-RCMs suspension
(the numbers 105, 120, 140, 180 and 200 indicate the drying temperature)

N°	Name
1	Extracted montm.
2	RCMs (or 25-RCMs)
3	105-RCMs
4	120-RCMs
5	140-RCMs
6	180-RCMs
7	200-RCMs

The MB adsorption on xxx-RCMs clays were evaluated using the UV-visible photometric method at 663 nm (monomers peak) with an absorbance of MB solution after clay contact and centrifugation between 0.01 and 1 (close to 1) (see chapter 2). The MB adsorption on RCMs was measured after a contact of 30 min and a contact of 2 h. MB values after 30 min and 2h contact were compared with the CEC measure on the same material after a 2h contact with cobaltihexamine. Initial and final covering percentages are given in Table 47. If the same MB $_{init}$% is targeted for each tested clays (similar test conditions to test only the effect of layer charge), it was difficult to satisfy experimentally such conditions because the final absorbance needed simultaneously to range between 0.01 and 1 (close to 1). It explained why MB $_{init}$% varied in Table 47. Except for RCMs and 120-RCMs samples, the other samples had quite similar high initial MB covering.

Table 47 The CEC and MB adsorption onto xxx-RCMs (MB absorption is measured by UV-photometric method and the cation exchange capacities (CEC) is measured using cobaltihexamine coupled with spectrophotometer). Measurements after 30 min and 2h were done on different samples. S.D. standard deviation from 3 tests.

Sample	CEC (2hrs)		MB (30mins)				MB (2hrs)			
	CEC value (meq/100g)	S.D	MB value (g/kg)	S.D.	MB $_{Init.}$ %	MB $_{Fin.}$ %	MB value (g/kg)	S.D.	MB $_{Init.}$ %	MB $_{Fin.}$ %
Raw. montm	145.87	1.63	341.58	35.96	80.07	73.20	312.81	12.00	74.78	67.03
RCMs	144.19	8.91	516.98	138.69	160.46	112.08	469.91	50.59	127.45	101.88
105-RCMs	104.76	5.50	246.42	10.64	81.27	73.53	255.13	1.63	84.59	76.13
120-RCMs	80.11	3.34	125.69	9.02	55.82	49.05	165.41	2.66	70.75	64.55
140-RCMs	63.27	0.81	104.61	9.26	67.11	51.68	161.90	6.56	93.77	79.99
180-RCMs	34.78	2.39	68.75	6.50	75.89	61.78	97.64	1.69	98.40	87.75
200-RCMs	22.76	7.36	52.14	5.59	87.54	71.61	67.83	3.35	102.38	93.16

As expected, results in Table 47 showed that the MB measured on RCMs suspensions decreased with the heating temperature that's to say with the layer charge measured by CEC. The decrease of the layer charge

is linked to the decrease of the total layer charge[12]. The relation addressed by Christidis *(2003)* between the basal space from EG treated K-saturated clay determined by X-Ray diffraction and the total layer charge of montmorillonite clay was used to prove it. The Figure 55 presented the relation between basal space from EG treated K-saturated RCMs deposit on glass slide linked to the total layer charge, and MB and CEC values (RCMs sample was not considered in this figure).

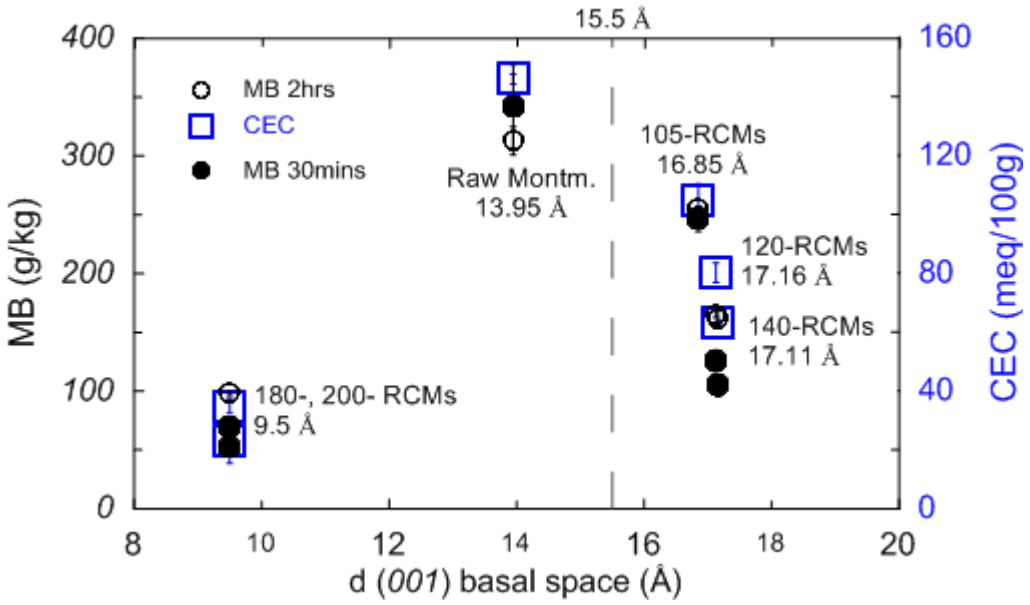

Figure 55 MB and CEC adsorptions versus clay interlayer space measured by XRD on EG-treated K-saturated xxx- RCMs clay deposit on glass slide.

The extracted montmorillonite belonged to the high total layer charge montmorillonite because d (*001*) reflection was smaller than 15.5 Å, whereas the other samples were low total layer charge montmorillonite *(Christidis et al. 2003)*. Among montmorillonite, the decrease of total layer charge yielded to the increase of d (*001*). Both MB and CEC values were intensively decreased when d (*001*) went from 13.95 Å of raw montm. to around 17 Å for the 105-, 120-, 140-RCMs samples. These low total layer charge montmorillonite favoured the ability of big molecule to intrude the interlayer.The intrusion of EG molecule was then easy whereas the swelling property of such clays was strongly reduced because swelling property implied the intrusion of water in interlayer using hydrated ions attracted by clay total layer charge. In the case of the lowest total layer charge montmorillonite, 180-RCMs and 200-RCMs, the smallest d (*001*) at 9.5 Å were due to the full collapse of montmorillonite interlayers. Thus, no more EG molecule could allow entering into their interlayer (*Green-Kelly 1953*). In summary, the low value of MB adsorption is in accordance with low total layer charge of clay and low swelling property. With low layer total charge, MB molecule would have been able to intrude the interlayer (it was not a size problem) but the charge that had to be compensated was too low.

Coming back to Table 47, the raw Montm. presented lower MB that RCMs (Li^+ exchanged raw montmorillonite). Such effect may come from the nature of the cation on clay. Furthermore, Table 47

[12] The total layer charge is the calculated charge by half crystal cell from mineralogical structure. It is different from the layer charge measured by CEC because some high total layer charge may be permanently and partially compensated as for illite. For such clay, total layer charge is high whereas CEC is medium/low. For too low or too high total layer charge, the swelling property is almost zero.

showed that the MB measured on RCMs suspensions agitated during 2 hours (the usual time in our method) gave higher MB adsorption than MB-RCMs suspensions agitated during 30 min except for the raw montm. (after extraction) and RCMs. It was probably caused by the lower MB_{init}% used for the 2 hours contact compared to the MB_{init}% used for the 30 min contact. The other measurements were done with higher MB_{init}% (2h) than MB_{init}% (30 min). Such results pointed out the difficulties to interpret results considering that it's almost impossible to vary experimentally only one parameter. Moreover, we are limited technically by the range of MB concentration analyzed by UV-photometer. Despite these considerations, tendencies could be observed on CEC and MB adsorptions values from tested RCMs clays on Figure 56 (datas from Table 47).

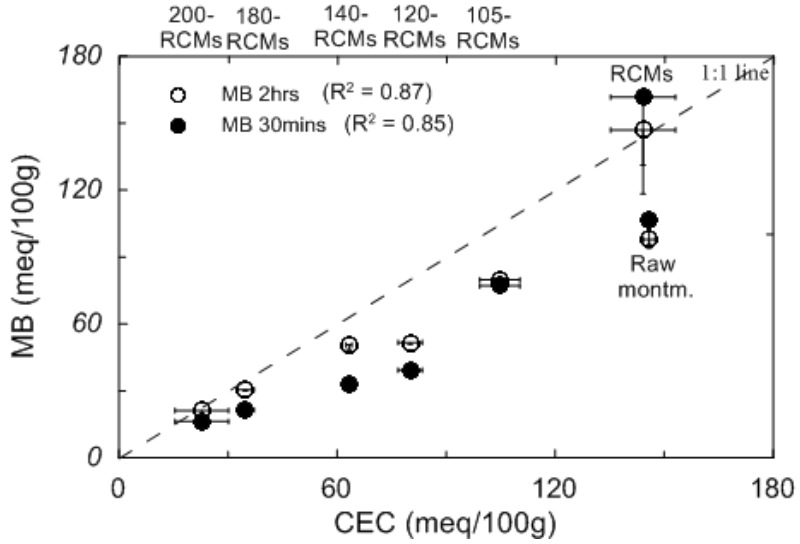

Figure 56 The CEC and MB adsorption onto RCMs clays (both value are compared with the same unit value)

If raw Montm. and RCMs clay presented more or less the same CEC adsorptions, the MB values associated to these samples behaved differently. If RCMs sample were ignored, the xxx-RCMs samples and raw Montm. gave MB values systematically lower than CEC values. Now, the MB values of low layer charge montmorillonite (200-RCMs and 180-RCMs) were close to CEC values. For low layer charge, this result meant that in such conditions the difference of chemical affinity and molecular size between methylene blue and cobaltihexamine ion seemed to be negligible. For higher layer charge, the low MB values compared to CEC values should be probably linked to MB aggregation. On one hand, if MB aggregated molecules adsorbed onto clay increased (on dimmer, H-aggregates or J-aggregates forms), then the remaining quantity of MB molecules in solution quantified by UV photometric method is low, which corresponds to a increase of MB value (because it is calculated by subtraction of the initial and final MB concentration in solution before and after clay contact). MB value higher than CEC might be expected (it's not the case). On the other hand, when aggregates occurred, their size might limit the access to interlayer space which decreased the adsorbed MB quantity.

To better understand the MB adsorption and aggregation phenomenon, UV-visible spectra were recorded on MB-xxx-RCMs suspensions. If MB adsorption considered the quantity of monomers in solution (after clay centrifugation), the UV-visible spectrum of MB suspension brought more information. For example,

MB adsorption measurement couldn't distinguish the configuration of adsorbed MB molecules and if molecules are aggregated or not.

3.2.2.2 The configuration of MB molecules measured on reduced-layer charge montmorillonite (RCMs)

Configuration of MB molecules for high initial MB covering percentage

The configuration of MB-RCMs suspensions with high initial MB covering percentage (necessary to measure MB adsorption presented in Table 47) are shown in Figure 57.

The main MB configurations on raw Montm. were dimer and monomer. The configuration was stable during the MB adsorption value measurement in 2 hours. The same behavior is observed for the low layer charge montmorillonite samples in contact with MB molecules except for MB-RCMc suspension and MB-105-RMCs suspension. For both suspensions, the presence of H-aggregates was confirmed at 577 nm.

The positions of the peaks associated to the different type of aggregates were stable. No shift with time contact indicating a re-arrangement of MB molecule was observed. The difference of peak intensity is not discussed as measurement on Figure 57 (a), (b) and (c) were done not on the same suspension followed during time (30 min, 2 hours and 5 hours).

Finally, the surprise came from the absence of visible H-aggregates on raw-Montm as previously expected from bibliography. It may come from the high MB molecule concentration in suspension to reach high initial MB covering percentage to measure MB value. Sprectra on Figure 57 showed the MB molecule in solution and onto clay (not just the absorbed fraction). To decrease the effect of MB molecule in solution, the UV visible spectra on xxx-RMCs suspension at low initial MB covering percentage were tested.

Configuration of MB molecules for low initial MB covering percentage

After Li^+ treatment and heating, dried RCMs clays were put in contact with water to obtain a 0.4w% water-RCMs suspension. Suspensions were stocked until measurement under agitation (during several days and weeks). The UV-visible spectra acquired on low MB_{init}% MB-xxx-RCMs suspensions were performed using the protocol previously described for MB-clay suspensions in 3.2.1. MB molecules were added to the suspension to obtain finally a maximum absorbance Abs < 1, while clay content in suspension is approximately 7.10^{-2} g/L (the initial MB covering percentage is between 2 and 15% in this case). The spectra were collected immediately after MB addition to xxx-RMCs suspensions and after 27 days of agitation.

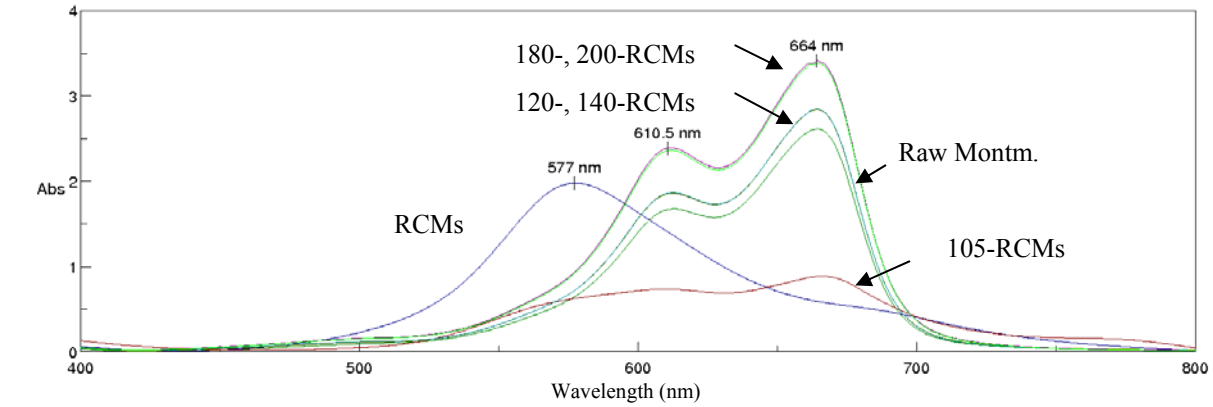

(a)

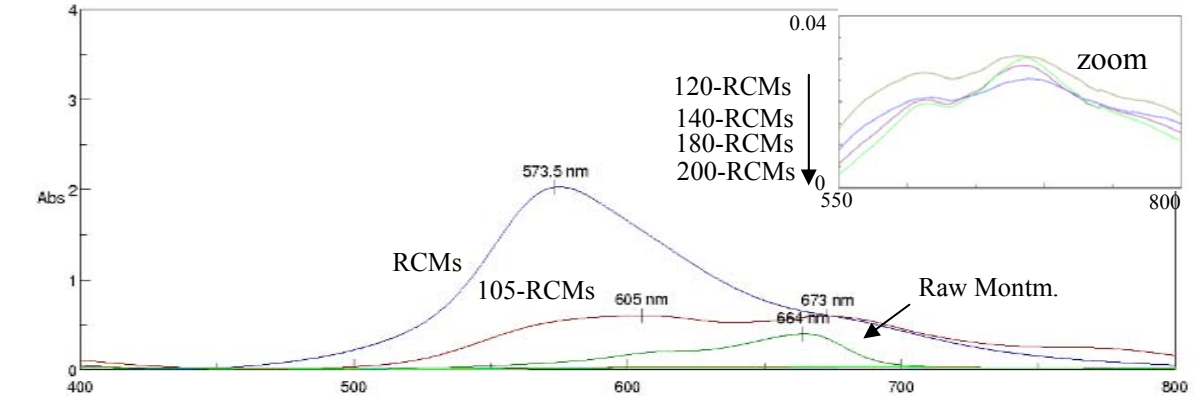

Wavelength (nm)

(b)

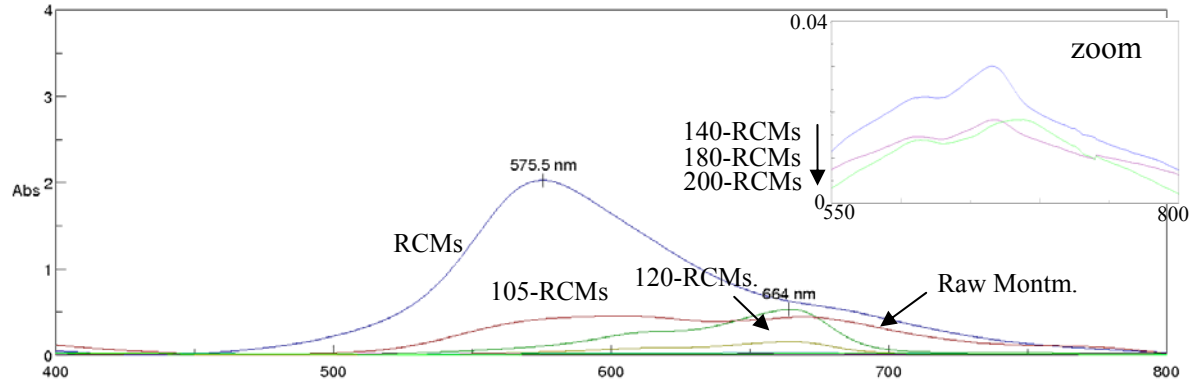

Wavelength (nm)

(c)

Figure 57 The configuration of MB-RCMs suspension in high MB covering
(a) after 30 min MB addition to clay suspension and (b) after 2h of contact (c) after 5 hours of contact

The spectra of MB-xxx-RCMs suspensions measured just after the MB addition were shown in Figure 58. The H-aggregate configuration rapidly appeared in MB-raw montmorillonite as well as in MB-RCMs or in MB-105-RCMs suspensions. The presence of H-aggregates measured on these 3 suspensions is consistent with high layer charge clays (see Table 47) as expected from literature. H-aggregates were probably present in Figure 57 (a) in the foot of the dimmer peak but its low quantity didn't allow to identify clearly

its presence. Moreover on Figure 58, MB-105-RCMs suspension was also characterized by J-aggregate, a low energy form of MB aggregation. Such result agreed with *Bujdak (2001)*'s statement, that the layer charge reduction favor the monomers and J-aggregates form of MB agglomeration compared to higher charged form such as H-aggregates.

For the MB-120-RCMs, MB-140-RCMs, MB-180-RCMs or MB-200-RCMs suspensions, characterized by lower layer charge (because of the strong heating after Li-exchange), the configurations of MB molecules were mainly H-dimer and monomer as for MB-illite and MB-kaolinite suspensions mentioned in Figure 50. The disappearance of J-aggregate was the consequence of a lower water auto-ionization and/or the non appearance of J-aggregates at the clay surface because of the low charge density (*Bujdak et al. 2001*).

Even Bujdak (*2001*) stated that the equilibrium of MB distribution is achieved after 18h of agitation, the MB configuration in MB-xxx-RCMs suspensions were followed until 27 days in this study, in order to confirm the final state of MB molecules. After 27 days of contact (Figure 59), Raw-Mont. and MB-RCMs suspensions (with quite similar layer charge and the highest values given by their CEC in Table 19) presented H-aggregate configuration with quite exactly the same absorbance as seen after short time contact on Figure 58 (that's to say the same height of the peak). H-aggregates present on high layer charge RCMs, essentially positioned on clay external surface, disaggregated neither into monomer nor into J-aggregates during the contact period, in agreement with Neunann (2002)'s results. Note also that the slight difference of behavior between Raw-Mont. and MB-RCMs suspensions (with similar layer charge measured by CEC) may come from the nature of the cation present at the clay surface (Li^+ for RCMs cay and Ca^{2+}, K^+ and Na^+ for - see the 3.2.4 for extended explanation).

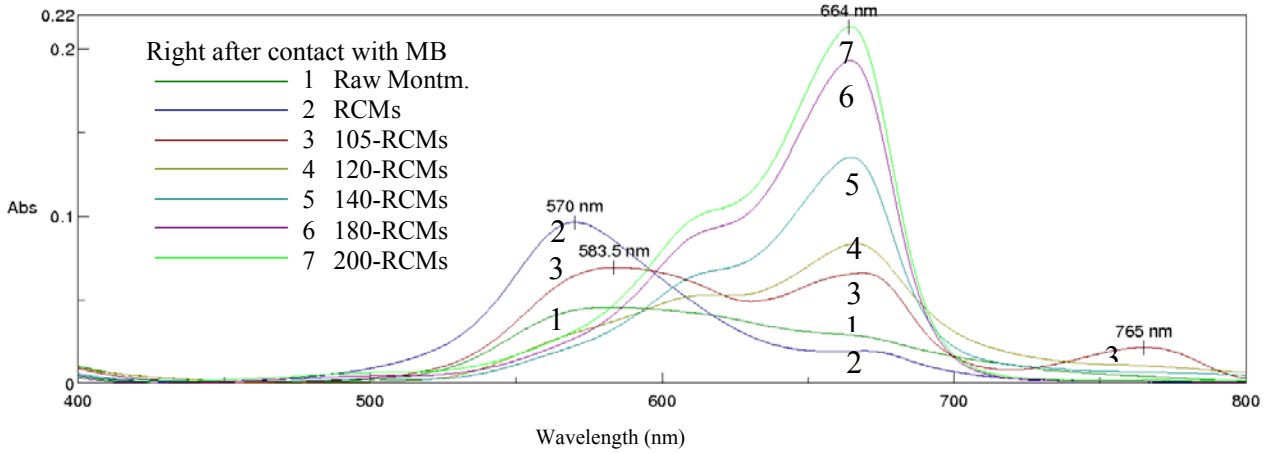

Figure 58 UV-visible spectra showing the configuration of MB-xxx-RCMs suspensions just after MB addition to the clay suspension.

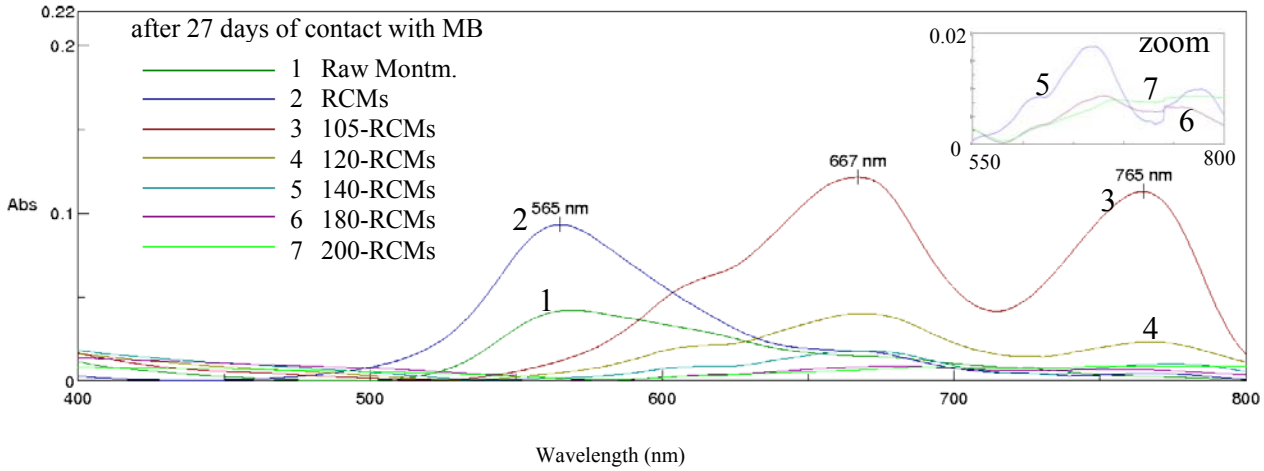

Figure 59 UV-visible spectra showing the configuration of the configuration of MB-xxx-RCMs suspension after 27 days of shaking

For MB-105-RCMs suspension, the evolution of MB configuration can be explained by the Cione (*2002*)'s statement. With a lower layer charge (compared to RCMs clay), H-aggregates on 105-RMCs clay surface disappeared (disaggregation) and the released MB molecules were distributed into dimer, monomer and J-aggregates configuration after long time contact. Such change with the appearance of J-aggregates showed that clay interlayers are touched during MB molecule re-arrangement. Indeed, aggregates are positioned on internal or external surface (Figure 60). Monomers and J-aggregates (with small sizes) may intrude or may be formed more easily into clay interlayer compared to H-aggregates (according to *del Monte, 1999* and *Cione, 2000*),. Not only the MB molecule interaction with clay impacts on MB aggregates but also the accessibility of clay surface to MB molecules and the layer charge of clay impacts on particle-particle interaction (as well as the quantity of MB molecule added to the suspension).

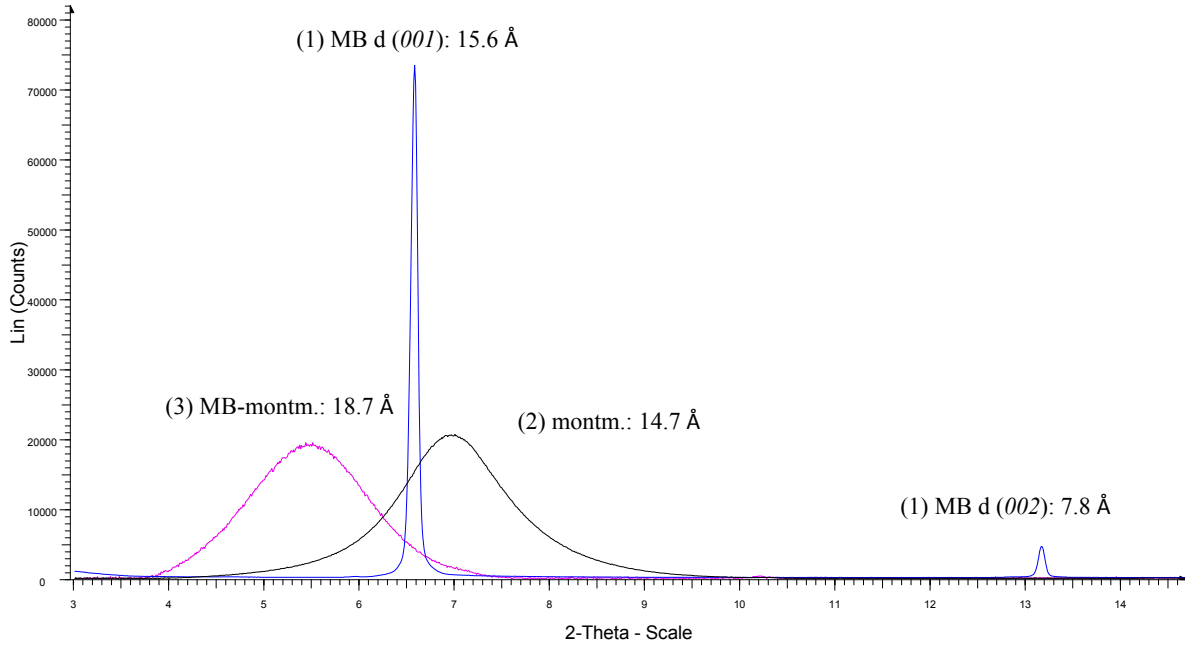

Figure 60 XRD patterns of (1) MB (2) montmorillonite and (3) MB-montmorillonite glass slides

For MB-120-RCMs, MB-140-RCMs, MB-180-RCMs or MB-200-RCMs suspensions, dimer and monomer were still present after a long contact time. The behavior is in agreement with the conventional hypotheses related to MB interaction with low layer charge clay (from *Jacobs and Schoonheydt 2001, Bujdák et al., 1998, 2002*): firstly, MB aggregation (high energy aggregates) instantaneously occurs in the vicinity of clay colloid particles within the electric double layer on clay surface and then, the decomposition of dye aggregates starts simultaneously (it's why H-aggregates are in low content appearing in the left foot of the dimmer peak around 570 nm on Figure 58). After 27 h, monomers and dimers remains stable configuration but their peak absorbance intensity decreased with time (spectra on Figure 58 and Figure 59 were obtained on the same suspension at different time). Such decrease was not clearly explained until now (technical problem links to UV-spectrophotomer, side chemical reaction with MB or between particle…). No peak decrease with time was clearly observed in literature, signifying the disappearance of MB molecule or their lack of absorbance properties by degradation. One aggregate configuration may decrease but another one has to increase if the quantity of MB molecule in contact with clay remains constant between t=0 and t=27h. The particle-particle interaction during a long time contact with MB solution (clay particle re-arrangement) may impact by modifying turbidimetric properties of suspension (depending on particle size or rate of aggregation). A decrease may be linked to the better dispersed suspension. Particle- particle arrangement also may impact on the MB molecules entering in the clay interlayer. In this case, the monomer peak is shifted as described in literature (Table 7) but no decrease of intensity is mentioned. A fall down of the peak intensity should imply the modification of the MB molecule electronic structure as met in photolysis reaction (in presence of UV-visible light) or in photocatalytic degradation (clay may play the role of catalyzer but the presence of H_2O_2 is required for example). But the presence of MB molecule in MB solution after centrifugation allowing the measure of low MB value on low layer charge RCMs clay indicated that the MB molecule were not degraded but they were like 'screened'.

If monomer and dimer remained stable configurations on MB- raw Montm. and MB-RCMs suspension, 120-RCMs suspension which had a relatively high layer charge (see Table 47) compared to RMCs clays heated at higher temperatures, could form J-aggregates after 27 days of contact with MB molecules. As J-aggregates were only formed in the clay interlayer, the non-appearance of J-aggregates in MB-140-RCMs, MB-180-RCMs or MB-200-RCMs suspensions probably resulted from their very low layer charge, too low to attract MB molecule into interlayer. The low layer charge is accompanied also by low swelling of RCMs clays which contributes to decrease the ability of aggregates to penetrate into interlayer.

3.2.3 The impact of pH value on MB adsorption

The impacts of pH value on MB adsorption were investigated because of the unclear explanation from literature (*Gurses et al. 2006; Ghosh and Bhattacharyya, 2002)*. The evolution of MB-clays suspensions with various pHs, between pH 1 and pH 13, was evaluated from MB configuration in clay suspension. Furthermore, MB adsorptions variation with pH value and MB covering percentage (related to CEC) were measured as well, in order to evidence the links between MB configuration change with pH and MB adsorption variation. Such considerations will be interesting to better understand for example the change of MB value after lime treatment.

3.2.3.1 The MB configuration measured in MB-clays suspension at various pH

Similar volume of 0.4wt% extracted kaolinite-, illite- and montmorillonite- suspensions (in water) were dropped into the same volume of HCl or NaOH solutions (with various pH). Suspensions at variable-pH were agitated during 24 hours. After measuring the suspension pH value (between pH1 and pH13), a controlled quantity of concentrated MB solution (1g/L) was added into the variable-pH clay suspensions in order to reach a final absorbance no higher than 1. The configurations of MB-pH clay suspensions were measured just after the addition of MB solution and after 5 days of agitation (Figure 61).

Previously, the MB configuration in MB solution at various pH was observed. If stable monomer and dimmer existed around neutral pH, alkaline pH favored the appearance of H-aggregates at longer time, while acidic pH favored slight shift of the dimmer and monomer peak wavelength and the appearance of J aggregates or in this case to bivalent protonated forms of MB (or MBH^{2+})(*Cenens, 1988; Schoonheydt and Heughebaert 1992*). Note that the saturation of the bivalent MB peak intensity on Figure 61 with abs =7 wasn't a problem for interpretation.

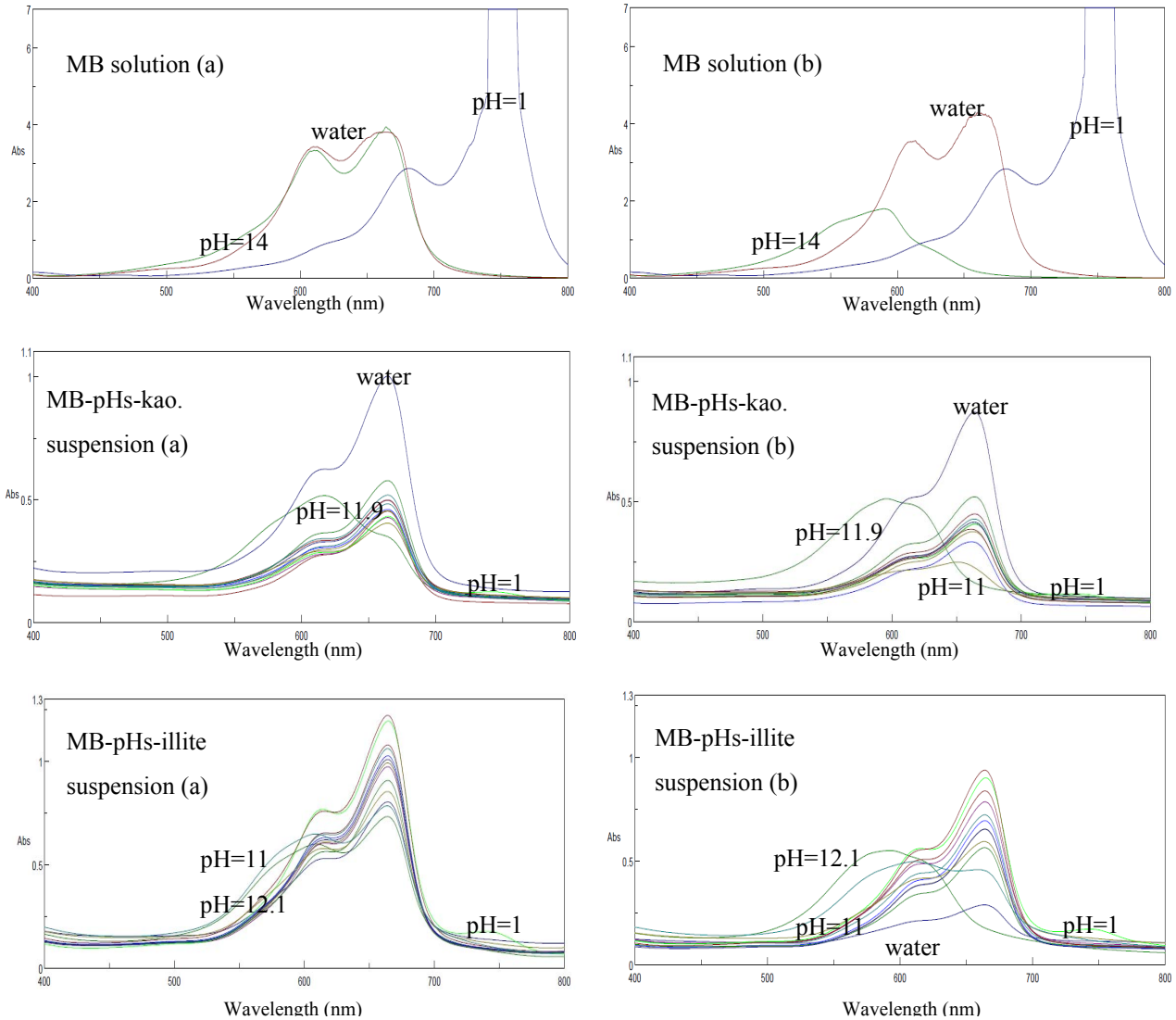

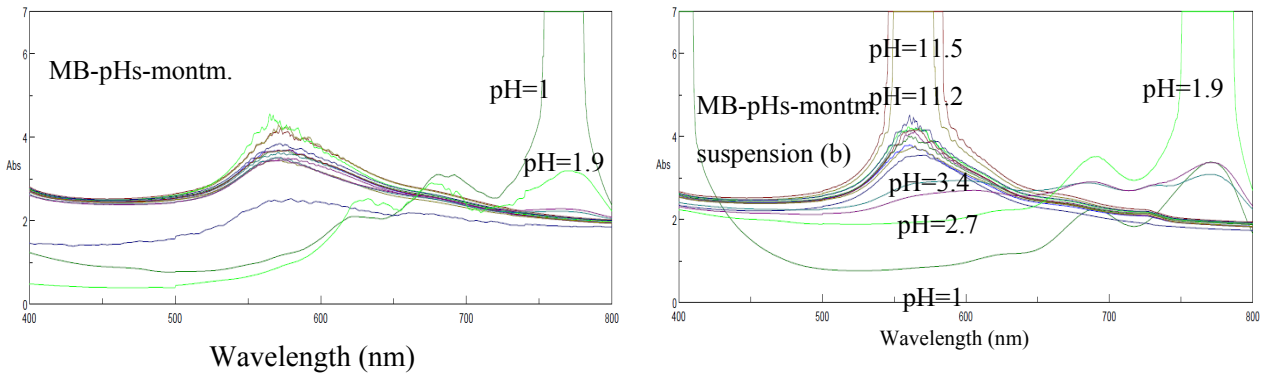

Figure 61 The configurations of MB solution, MB-pH-kao suspension, MB-pH-illite suspension and MB-pH-montm. measured (a) just after the MB addition and (b) after 5 days of agitation

By observing the main configurations just after the addition of MB solution in pHs-clay suspensions and after 5 days of agitation in Figure 61, pHs-MB clay suspensions seemed to behave quite similarly as pH-MB solution. The MB configurations on kaolinite and illite suspensions were characterized by dimer and monomer forms when pHs was between pH2 to pH10. The high layer charge MB montm. suspension (at low initial covering) produced stable H-aggregates forms when pHs was between pH4 to pH10. This behavior (in presence of Ca^{2+} with low amount of K^+ and Na^+ exchangeable cations) from montmorillonite was similar to the MB-RCMs (in presence of Li^+ exchangeable cation).

In high pH environment (pHs>12), the H-aggregates peak intensity seemed to increase on all the three clays. The reason could be that the high density of OH^- in suspension at pHs>12 played the role of bridge for MB molecules (MB molecules were attracted the one to each other and agglomerating into high energy configuration such as H-aggregates could be favored).

In the acidic environment, J-aggregates occurred at pH lower than 2 on illite and kaolinite MB suspension with quite no shift in peak wavelengths contrary to MB-montm. suspension that formed additional MB configurations between monomer and J-aggregates (as in MB solution) when pHs were lower than 3.4. It was caused by the bivalent protonated MB cations occurrence.

3.2.3.2 The MB adsorption in varying pHs value and mineralogical composition

The MB-pHs-clay suspensions whose MB configurations were investigated at low initial MB covering were also used for MB adsorption measurement after 5 days of agitation to let the time to montmorillonite to reach equilibrium. $MB_{Init.}$ % and $MB_{Fin.}$ % were calculated using the CEC value measured at natural pH (around neutrality) and after 2h of contact. The change of CEC value with pH is not considered in such part even if the pH-dependence of CEC is known (*Maes and Cremers 1979*) for a long time. The final covering percentage on Figure 62 was then directly correlated to MB value variation (see value in appendix 5.2).

The results on Figure 62 showed a clear increase of final MB covering percentages on kaolinite and illite in alkaline medium (from pH 10 for both) while MB adsorption remained stable up to Ph5 and slightly increased between pH 5 and 8 (the lowest MB adsorption were reached for pHs around 3.2 to 3.6). This tendency caused by the impact of zeta potential of illite and kaolinite on their MB adsorption. MB adsorption on illite seemed also abruptly to increase at pH 1 but such tendency should be confirmed. Such evolution is confirmed by Figure 63 that demonstrated the non linear dependence between initial and final

MB covering percentage. In other words, the variation of MB absorbance is not only linked to the variation of $MB_{Init.}$ % as it seemed to be the case for montmorillonite (1:1 linear correlation between $MB_{Init.}$ % and $MB_{Fin.}$ %). These results for illite and kaolinite were in agreement with the literature review proposing as explanation that pH modifies the particle size of clay and the configuration of MB molecules in MB solution which induces the variability of MB adsorption (*Gurses et al.2006 Zhang et al. 2013*, *Ghosh and Bhattacharyya, 2002*).

While considering the effect of $MB_{Init.}$ %, MB adsorption onto montmorillonite at different pHs didn't depend clearly on pHs value (even if the MB aggregation in clay suspension changed with pH on Figure 61). The main observed differences were attributed to variable initial MB covering percentage. On Figure 63, a group of 3 points were characterized by MB_{init} % = 91.5-93% and the other points by $MB_{Init.}$ % = 77.5-80% except one medium point at 83,5%. The different groups of points were easily distinguished on Figure 62. MB adsorption onto montmorillonite seemed to behave as zeta potential (a surface charge measurement) versus pH that's to say no change with pH .

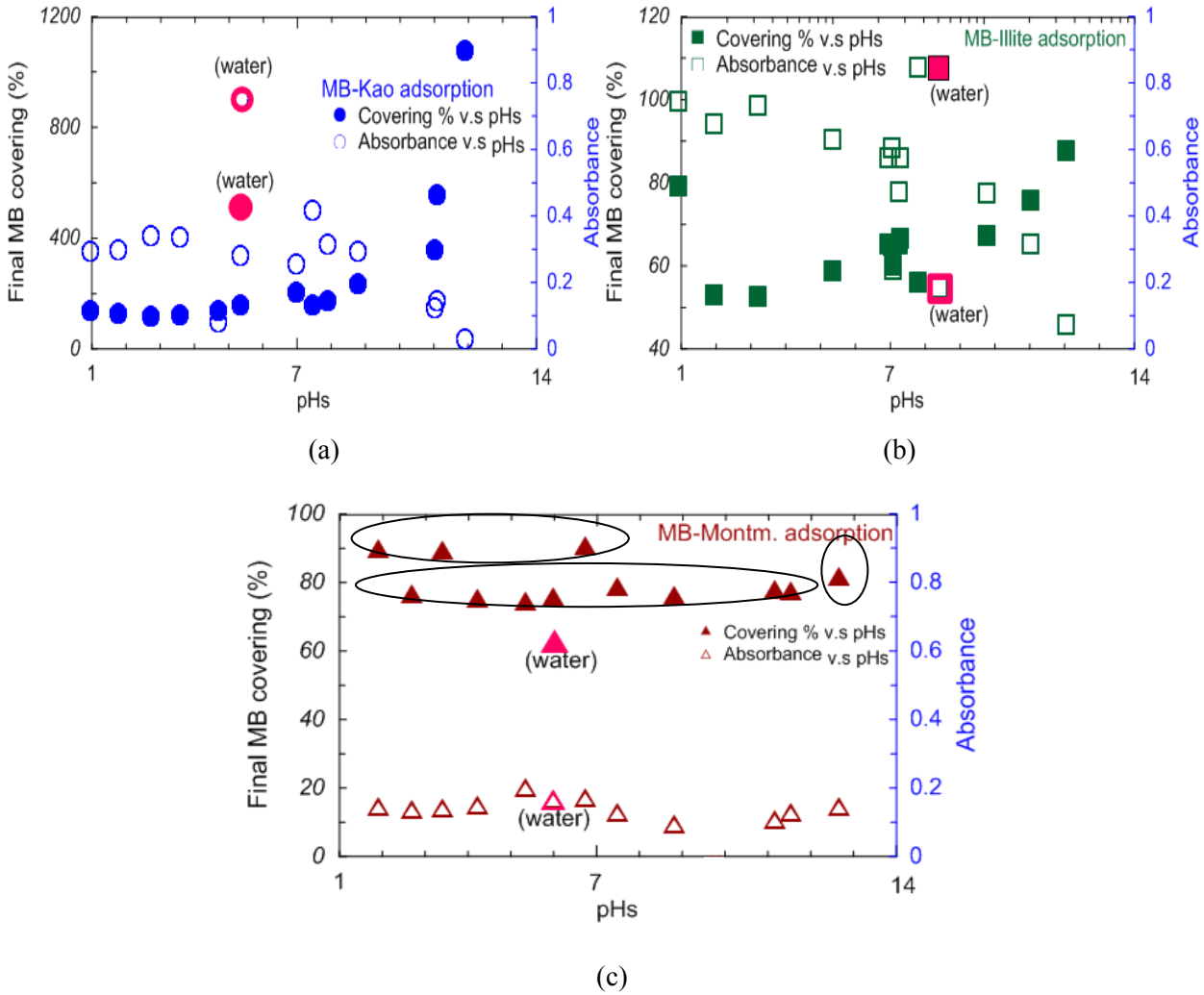

Figure 62 Final covering percentages and absorbance after the 5th day of contact versus pHs of MB kaolinite, illite and montmorillonite.

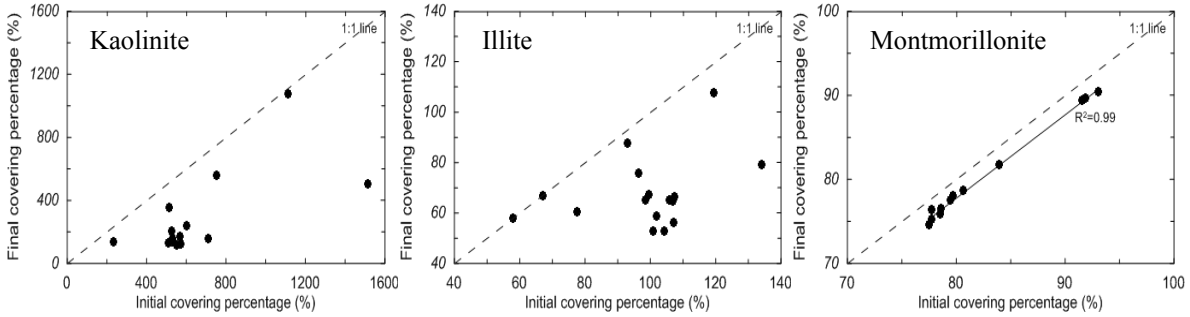

Figure 63 Final MB covering percentage on extracted kaolinite, illite and montmorillonite after the 5th day of contact versus initial MB covering

To explain the MB^+ adsorption behavior, several processes had to be considered:

- The change of MB aggregate configuration in solution under pH effect (as for very high or low pH) might impact the MB adsorption onto clay. The appearance of stable 'big' aggregates of MB molecules favored by pH may decrease their ability to intrude in clay interlayer space and then the clay potential MB adsorption. At the opposite if big MB aggregates were formed as at 580 nm on Figure 61 and adsorbed on external surface instead of monomer or dimer, MB adsorption might increase. It may explain why MB adsorption increased in alkaline or acidic medium for kaolinite or illite (where interlayer spaces were not or low accessible).

- The potential dissolution of clay at pH > 10-10.5 and pH< 3-3.5. In alkaline medium, silica tetrahedral layers might be attached and in acidic medium octahedral layer might be dissolved partially. The release of cations from clay dissolution allowed for example the Al^{3+} or Mg^{2+} adsorption onto clay surface and the dissolution was also at the origin of the decrease of specific surface so the decrease of charge surface site. Dissolution was in favor of the fall of MB^+ adsorption, as water was taken as reference suspension, the addition of acid or base introduced ions in solution and increased the ionic strength of the solution in contact with clay and MB. Such parameter might impact MB adsorption as well as cations speciation above all in high pH medium (for example Mg^{2+} became $Mg(OH)^+$).

- The control of edge surface charge of clay by pH: it was well known that when pH decreased, the positive charge increased (then the neutral and negative decreased) which induced the fall of the MB adsorption value (or CEC value). Indeed the hydroxylated surface sites ≡SOH (with S = Al, Si, Mg or Fe generally) evolved from alkaline to acidic medium by the following reaction:

  $$\equiv S - O^- + H^+ \Leftrightarrow \equiv S - OH + H^+ \Leftrightarrow \equiv S - OH_2^+$$

  The increase of MB adsorption in alkaline medium for illite and kaolinite might be attributed to such process. The zeta potential curve or the surface charge measured by titration on clay suspension versus pH would be able to confirm this assumption,

Finally, the presence of H^+ in high concentrated acidic medium was at the origin of a competition between H^+, the natural exchangeable cations onto clay and MB^+ on site with permanent surface charge (on basal surface). The evaluation of the exchange constant between MB^+ and the different cations (especially H^+)

would help to understand the MB adsorption onto clay. A decrease would be expected if exchange is in favour of H^+.

In summary the impact of pHs on MB adsorption was occurring on the kaolinite- and illite- suspension, whereas there was no impact on MB-pHs-montmorillonite (variations were still controlled by MB initial MB covering percentage).

3.2.4 The impact of the nature of clay exchangeable cation onto clay on MB adsorption

The effect of Li^+ exchange on montmorillonite behavior has been preliminarily glanced by analyzing the MB adsorption on RCMs (that's to say the Li^+ exchanged montmorillonite sample without any heating). Previous result showed that H-aggregates were constantly formed on MB-RCMs suspension with no time evolution. The extremely high MB adsorption (around 516 g/kg in Table 47) derived from MB concentration in solution (after clay extraction). In presence of Li^+ onto montmorillonite, MB adsorption was increased compared to the adsorption on montmorillonite with its natural cations (Ca^{2+} with Na^+ and K^+).

In order to understand the cation impact on MB adsorption, extracted montmorillonite was exchanged by other cations than Li^+. Most of cations in natural sand are Ca^{2+} and K^+, Na^+ can be found also but more rarely. The other cations are really rare except Mg^{2+} that may come from magnesian clay or magnesium oxide dissolution for example. Calcium may also come from an additional lime treatment (as done in USA).

A mean to discriminate the nature of the cation is interesting because cations impact potentially on clay harmfulness in contact with bitumen in presence of water. Considering the physico-chemical properties of cation (size, valence, hydration enthalpy…), cations may contribute to change the water resistance of asphalt concrete mixture as it was shown for calcium. If chemical analysis of extracted cobaltihexamine solution after contact with clay is a direct way to identify and quantify the nature of exchangeable cation, this paragraph showed if UV-visible spectrum on exchanged montmorillonite suspension may discriminate the nature of cations. The estimation of MB absorption variation with the nature of clay cations were not done in this work. Assumptions were proposed and will have to be validated.

The cation exchanged montmorillonite, noted CEMs, were exchanged by Li^+, Na^+, K^+, Mg^{2+}, Ca^{2+}, Cs^{2+}, La^{3+} cations. Figure 64 a and b showed the MB configurations in CEMs suspension just after MB contact and after the 28^{th} days of agitation, respectively.

The comparison of MB configuration on Li^+ exchanged montmorillonite from RCMs (experiments with MB low initial covering percentage on Figure 59) and Li-CEMs showed that, both suspensions formed H-aggregates (as main MB configuration). Absorbance peaks intensity on Li-RCMs underwent slight decrease with time. The same trend was observed in Na^+-, Mg^{2+}-, Ca^{2+} and La^{3+}-CEMs suspensions (H-aggregates were stable with a low decrease of absorbance with time) while a slight increase of J aggregates at 723 nm instead of 765 nm as seen for K^+or Cs^+-CEMs occurred.

On the other hand, the K^+-CEMs and $Cs^{+`}$-CEMs suspension presented initially H aggregates but also high amount of monomers, dimer and J-aggregates. A tremendous evolution in these three forms of aggregates significantly occurred while H-aggregates decreased. These results agreed with the statement from literature that not only the layer charge of montmorillonite controlled MB adsorption onto CEMs

(*Czímerová et. al 2004, Neumann et. al. 2002*) but also the cations (with various sizes and valences) (*Neumann et. al. 2002, Dzene et al. 2015*).

K^+-CEMs and Cs^+-CEMs that behaved differently from Li^+, Na^+-, Mg^{2+}-, Ca^{2+} and La^{3+}-CEMs suspension presented the lowest valence (1+) with the bigger crystal ionic radius (size without hydration water) and the lowest hydration energy (ability to loose their water hydration) (Table 75). Regarding MB-CEMs adsorption, K^+-CEMs and Cs^+-CEMs performed also the lowest MB adsorption value according to *Myers (1999) and Zhang et al. (2013*).

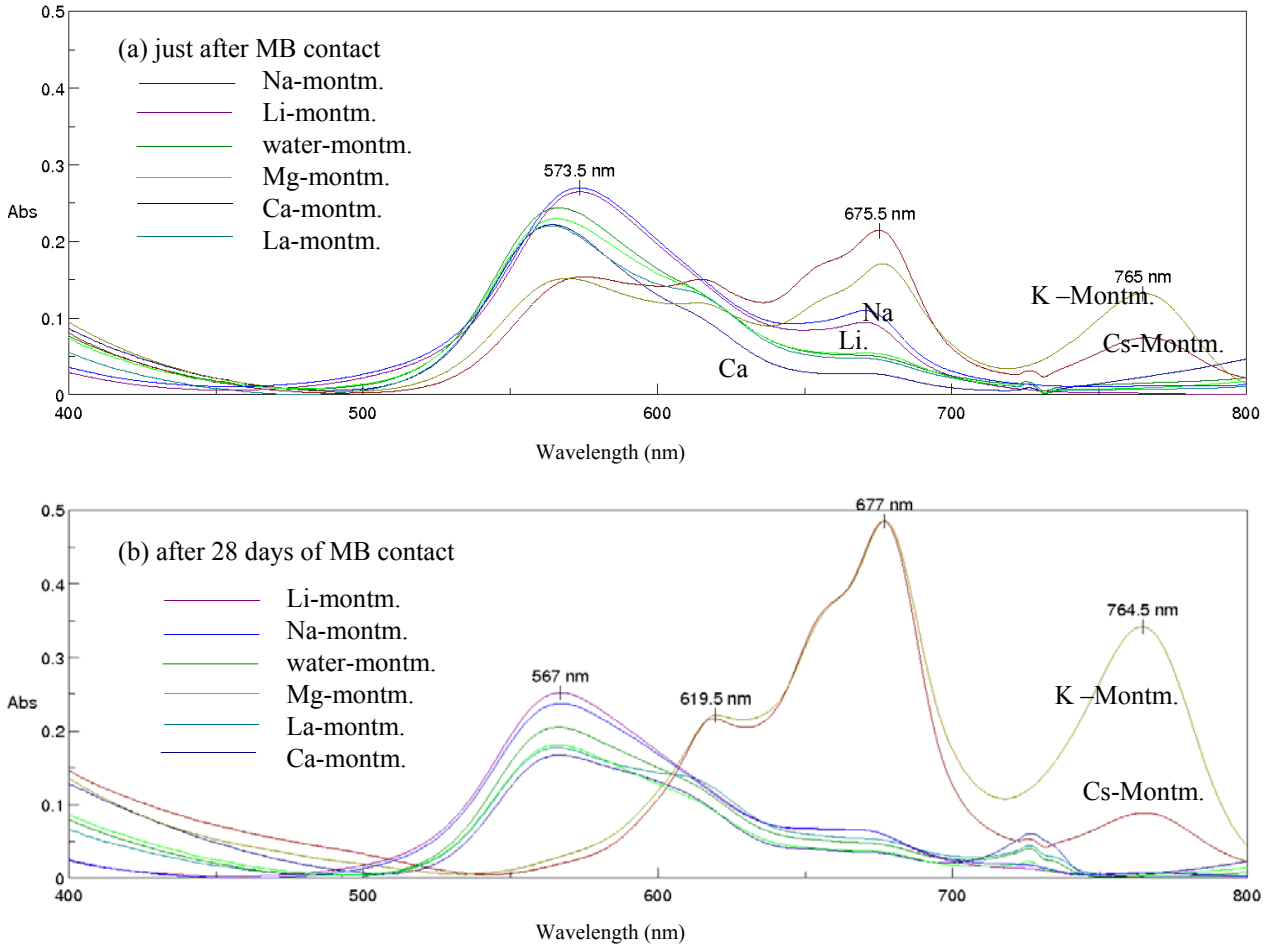

Figure 64 UV-visible spectra showing the MB aggregates configurations in MB-CEMs suspension (a) just after the addition of MB solution and (b) after 28 days of contact between clay and MB.

Table 48 Properties of ions (*Tansal et al. 2006* cited by *Conway, 1998*; Hydration energy : enthalpy of hydration of gaseous ions from Smith (*1977*); http://www.elementschimiques.fr/?fr/proprietes/chimiques/rayon-ionique, http://www.lenntech.com/periodic-chart-elements/density.htm)

Cations	Radius (nucleus) (Å)	Crystal ionic radius (Å)	Hydrated radius of ions (Å)	Hydration energy[a] $\Delta H_h°$(kJ/mol)
Li (+)	1.23	**0.60**	3.4	-515
Mg (2+)	**--**	**0.78**	**3.00/ 4.28**	**-1926**
Na (+)	1.57	**0.95**	1.78 / 3.58 / 2.76	-405
Ca (2+)	**--**	**0.99**	**2.6/4.12**	**-1579**
K (+)	2.03	**1.33**	2.01/ 3.31	-321
Cs (+)	2.35	**1.69**	3.29	-268
La (3+)		**1.15**	**4.52**	**-3278**

On the other hand, MB – (Na^+-, Li^+-, Mg^{2+}-, Ca^{2+} or - La^{3+}) - CEMs suspensions with cations characterized by high hydrated energy and small radius (except La^{3+}) presented H-aggregate configuration. The configuration was stable with time contact.

Note that the presence of H-aggregates didn't allow to determine if MB adsorption globally increased or decreased. Spectra were not enough to conclude. Indeed, the MB aggregation increased the number of adsorbed molecules but aggregates adsorbed preferentially probably on external surface that represented a low percentage of the whole clay surface. If MB molecules were gathered on external surface in H-aggregates for (Na^+-, Li^+-, Mg^{2+}-, Ca^{2+} or - La^{3+}) CEMs, MB molecules in presence of K^+-CEMs and Cs^+-CEMs formed dimmer, monomer or J-aggregates able to penetrate the interlayer shown in Table 7 (the presence of aggregates is not the proof of their adsorption onto clay).

Measures of MB adsorption will have to order the quantities of adsorbed MB on various cation exchanged high or low layer charge montmorillonite (or on other types of clay such as illite even if the major cations are potassium on illite).

It was expected that MB adsorption varied with :

- the effect of cations on particle – particle interaction that's to say the swelling properties of clay impacting on the ability of MB to intrude the interlayer

- the effect of cations on MB molecule aggregation in solution because of the nature of the cation (valence) and the change in ionic strength. Indeed, MB molecule interacted with clay by cation exchange reaction producing the release of cations in solution that increases the ionic strength. According to *Neumann et. al (2002) or Cione et al.(2000),* the impact of cation on UV-visible spectrum on clay suspension is negligible if cation concentration (in the case of Na^+) is not higher than 0.15M.

The effect of the cation nature on MB/cation exchange onto clay surface. A competition exists between cation Cat^{n+} and MB^+ on clay surface sites (as mentioned in the chapter dealing with the pH effect). The edge surface sites are characterized by a pH dependent charge. The nature of the cation impact the electric double layer on clay surface and then adsorption. But the charge generated by edge surface sites is very low compared to the permanent charge on basal surface in the case of montmorillonite. The role of edge surface will be considered as minor compared to ion exchange that occurs on basal surface. Ion exchange process is described by the following equation:

$$Mont - Cat^{n+} + nMB^+ \Leftrightarrow n(Mont - MB^+) + Cat^{n+}$$

with $k_{Catn+/MB+} = \dfrac{[n(Mont - MB^+)][Cat^{n+}]}{[Mont - Cat^{n+}][MB^+]}$ k is the ion exchange constant

The evaluation of cations affinity compared to MB^+ affinity towards clay surface should allow to explain the difference in MB adsorption. No literature deals clearly with the ability of MB molecule to replace one type of cation. Pedologists proposed on montmorillonite the following series (the series may vary with the clay mineralogy):

$Na^+ < K^+ < H^+ < Mg^{2+} < Ca^{2+} < Ba^{2+}$ (the cations on right may displace the cation on left)

The validation of such series with the addition of Cs^+ and La^{3+} need further measures. The goal is to position the MB^+ molecule ability to replace cations (Figure 65).

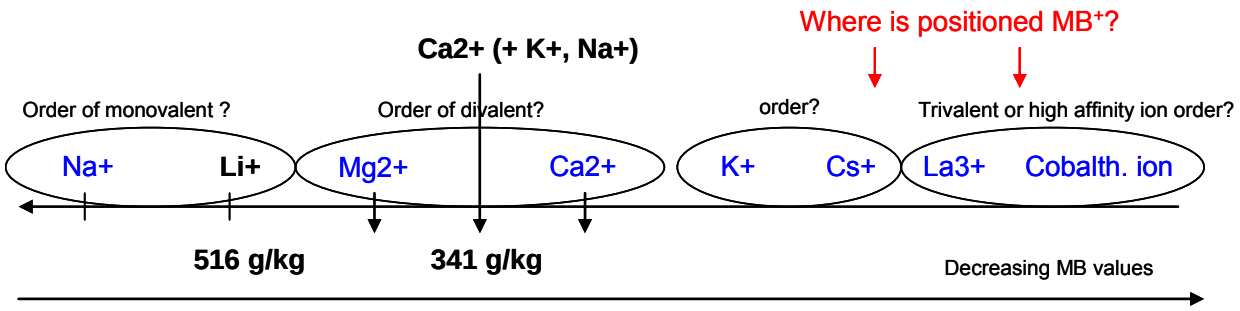

Figure 65 Assumptions on the order of cation exchanged (high layer charge) montmorillonite capability to fix MB molecules based on the ion exchange.

For comparison, the retention of organic molecule "quinalizarin" by bentonite saturated with different cations showed that more quinalizarin (organic compound with formula $C_{14}H_8O_6$) is adsorbed by homoionic smectite made with various mono, di and trivalent cations (except by smectite homionic to potassium) (Ayari et al., 2007 cited by Liu and Zhang 2007). The sequence of adsorption onto homoionic smectite was (from high amount towards low amount): $Al^{3+}>NH_4^+>Na^+>Fe^{3+}>Li^+>Ca^{2+}>Mg^{2+}>K^+$.

A specific behavior of potassium is pointed out in such work. The potassium ions suppressed quinalizarin adsorption to smectite, probably by collapsing the clay lattices and preventing the expression of the interlayer-derived cation-exchange capacity, according to the authors's statement. Such explanation would not agree with the presence of monomer, dimer and J-aggregates in K^+-CEMs. In such case, K^+ acts directly on MB aggregation letting free the interlayer.

In summary, the impact of cation on MB adsorption onto montmorillonite is governed by the nature of the cation but such behavior may be modified by the clay layer charge. In our case, **the higher layer charge of clay** combined with big cation radius / high hydration energy (as well as low mobility) such as K^+ and Cs^+ would present the lower MB adsorption (UV-visible spectrum are in accordance with *Czímerová (2004)*'s results for a montmorillonite with CEC = 110 meq/100 g)**,** whereas the cations with small radius and high hydration energy would increase MB adsorption. The **low layer charge montmorillonite** such as SWy-1 **(**CEC= 79 meq/100 g) studied by *Neumann (2002)* agree with this assumption. The determination of the cation series on low layer charge montmorillonite should have to confirm if the order of the series related to MB adsorption is changed or not.

3.2.5 The impact of drying temperature of sample before MB adsorption measurement

The commercial clays coming from the quarries at the origin of the studied extracted clays were used to study the impact of drying temperature on MB adsorption. The extracted clays from producer were rapidly dried by passing in a drying drum. The temperature of drying was no more 230 °C while extracted clays in lab were dried at temperature no higher than 40°C. Theoretically, there was no chemical component used during the manufacturing of commercial products. The mineralogical composition of commercial product and extracted clays in the lab was confirmed by X-Ray diffraction. The use of commercial products instead

of prepared materials from raw natural rocks allowed not only to save time, but also to produce results that can be compared with literature. Indeed, commercial products on powder form (such as clay) are usually used in scientific work without consideration of the potential influence of the industrial preparation step (above all on surface site reactivity).

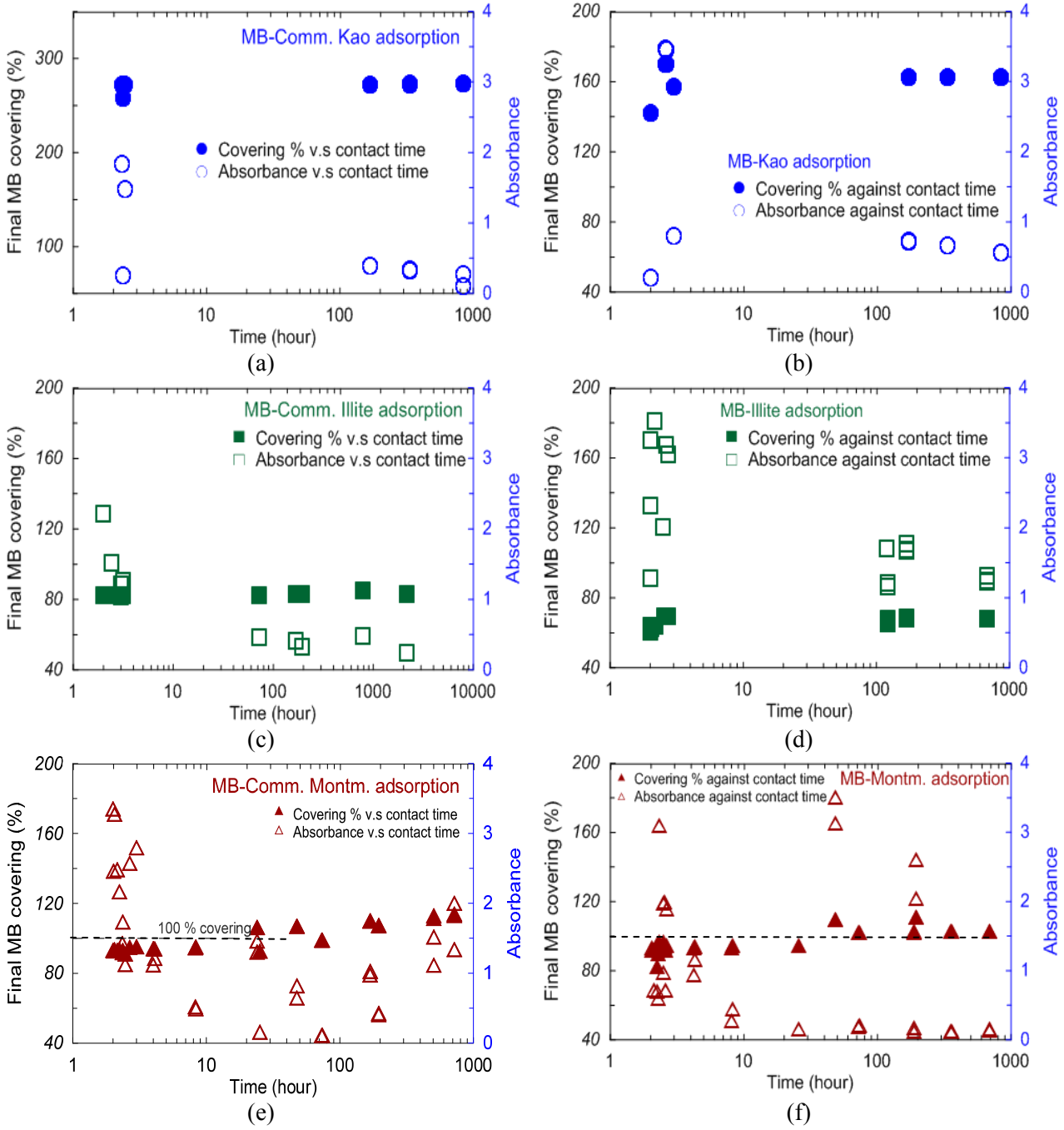

Figure 66 Final MB covering (%) and its absorbance on commercial (a) kaolinite, (b) illite and (c) montmorillonite and extracted (d) kaolinite, (e) illite and (f) montmorillonite related to the contact time of MB-clay suspension

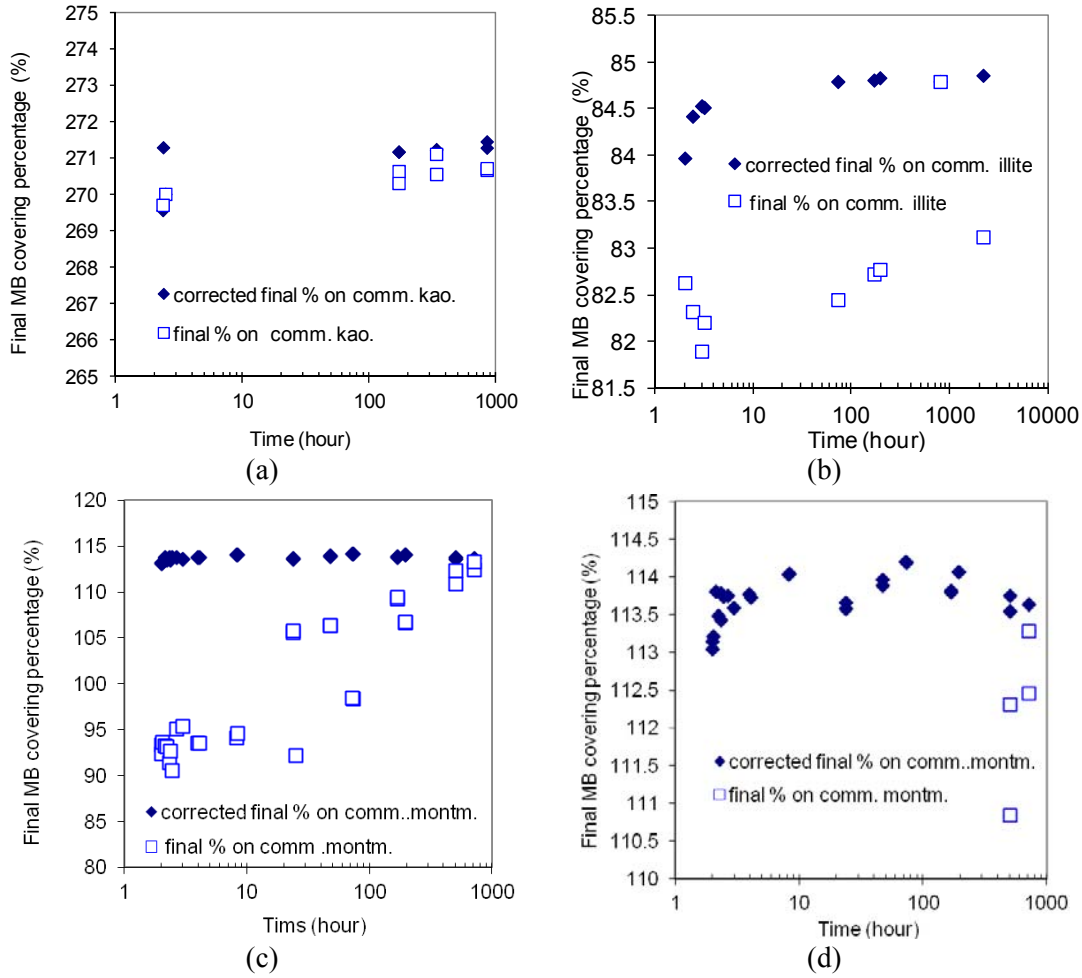

Figure 67 Final MB covering (%) with and without correction from initial MB covering effect on commercial (a) kaolinite, (b) illite and (c) and (d) montmorillonite ((d) is a zoom of (c)) related to the contact time of MB-clay suspension.

The results of MB and CEC values from extracted and commercial clays after 2 hours of agitation were done in previous Table 43. In order to better understand the drying effect, the effect of contact time on MB value measured on extracted and commercial clays were also studied (Figure 66). The evolution of final MB covering percentage measured on MB-clays versus time revealed that long time contact didn't impact on MB value on both extracted and commercial kaolinite or illite (CEC were measured after the usual 2h contact) whereas montmorillonite adsorption kept on varying revealing that the dried montmorillonite equilibrium in contact with MB is not reached after a long time contact. The Figure 67 showing the corrected MB_{fin}% from the impact of initial MB covering percentage proved that MB_{fin}% on extracted or commercial montmorillonite behaved similarly. The MB adsorption on extracted montmorillonite dried at 40°C seemed to reach equilibrium in 10 hours, and it was much shorter than the commercial montmorillonite, which was dried at 230 °C. The conclusions from results on Figure 66, Figure 67 and Table 43 concerning the quantity of adsorbed MB molecules were:

- Kaolinite after short drying at no more 230°C showed lower MB adsorption than extracted kaolinite, even with $MB_{fin.}$% equal to 265%. The increase of the percentage of final covering while the MB value decreased revealed a temperature effect on MB adsorption. Note that not only MB value decreased but also CEC, which value varied from 1.28 to 0.54 (while the mineralogical compositions of materials were closed). The lower MB adsorption from commercial kaolinite was due to the less surface of kaolinite for

MB covering after drying (a longer hydration time on Figure 66 didn't seem to help commercial material to reach the surface reactivity of raw material),

- Industrially-dried illite compared the extracted one absorbed higher amount of MB molecules, producing the rise of the final MB covering percentage for a lower final absorbance of MB solution extracted from suspension. In this case, it was difficult to say if the increase was related to MB density (MB_{init} %) or to the drying temperature. Note that the usual effect of the drying is a reduction of MB value. Indeed, the reduction of the accessibility to the interlayer space may be permanent (at high temperature of drying like a heating) or temporary if reversible dehydration is admitted (rehydration may be delayed with the increase of the drying temperature but no time effect was observed on Figure 67 compared to Figure 54). The increase of final MB covering percentage of commercial illite up to 82% could also be explained by the increase of the surface area (the decrease of particle size) which might affect MB adsorption. The particle size of commercial illite (20-40µm) was globally lower than the one of extracted clay prepared in lab because of the high efficiency of industrial grinder (and perhaps the use of chemical reagent as dispersing agent as illite rock was particularly difficult to disperse even after several days of agitation in contact with water.

- No significant evidence of difference between MB adsorption on commercial and raw montmorillonite was found after a 2 hours contact (initial and final covering percentages were almost the same). The slight reduction of MB value is more attributed to the lower initial MB covering percentage than to the drying temperature of clay before analysis.

In summary, above all kaolinite (a non-swelling clay) is impacted clearly by drying process. MB adsorption from heated kaolinite is decreased. For montmorillonite, the hydration process taking more than 10 hours didn't seem to be modified and the conclusion with a slight decrease of MB value associated to MB_{init}% variation. MB adsorption onto illite after a drying at higher temperature than 40°C remained unclear (the initial MB covering percentage kept on disturbing results and the difference of particle size may control the accessibility to surface charge). The MB change by varying the agitating time didn't clearly validate that the equilibrium status was reached more or less rapidly according to the temperature of the drying. Indeed, high temperature might induce non reversible dehydration and the temperature of 105°C used usually for water content measurement is considered as a usual threshold (upper than this temperature material properties - as hydration with the occurrence of the surface charge - may be degraded with no possibility to reach the initial state even after long contact with water).

3.2.6 The impact of methods on MB measurement

The extracted clays, kaolinite, illite and montmorillonite, were also measured by the standardized method from the NF EN 933-9 (2013) French standard, which is named 'drop method' in this study. MB adsorption of 2 g/kg measured by drop method is considered as the threshold for fine aggregates ($D_{0/2mm}$) qualification. All the manufacturers of aggregates in France measured the fine aggregates characteristic by using drop method. Therefore, the impact of the methodology to measure MB adsorption had to be cleared. By comparing the results and protocols from drop and UV-photometer methods and using the knowledge acquired in previous paragraphs, the impact of MB test methodology was analyzed.

3.2.6.1 MB adsorption measured by UV-photometer and drop methods

UV-photometer method is commonly used in the research domain for MB adsorption study, whereas the drop method is used in the engineering domain for the friendly use of operator. MB adsorption on extracted kaolinite, illite and montmorillonite measured by drop method were compared to their MB and CEC value in Table 49.

Table 49 The MB value of extracted clays measured by drop method and UV-photometer method

Material	CEC [a] (meq/ 100g)	MB value (standardized drop method)			MB value (UV-pho. method)		
		$MB_{first\ drop.}$ [c] %	MB (g/kg)	$MB_{Fin.}$ [d] %	$MB_{Init.}$ [b] %	MB (g/kg)	$MB_{Fin.}$ [d] %
Ext. kao.	1.30	119.1	9.7 ±0.4	233.2	154.1	6.4 ±0.3	153.9
Ext. illite	23.30	0.6	42.6 ±0.9	57.2	62.5	46.3 ±1.9	62.1
Ext. montm.	103.60	0.1	236.1 ±8.5	71.2	92.3	304 ±12.7	91.7
Sand	0.10	3012.5	0.4 ±0.1	125.0	87.3	0.3 ±0.0	93.8

[a] Cation exchange capacities measured by cobaltihexamine method [b] Initial covering percentage after the addition of the first drop of MB solution at the beginning of the test. [c] Initial covering percentage [d] Final MB covering percentage

The measurements of MB values from both methods behaved globally similarly. The MB adsorption on extracted kaolinite measured by drop method was higher than the value measured by UV-photometer, whereas the values of extracted illite and montmorillonite measured by drop method were lower than the value measured by UV-photometer. Such variation didn't change the clay classification (kaolinite with the lower MB value to montmorillonite with the higher one).

For the samples with low swelling potential, indicated by MB < 40 g/kg (*Cokca, 1991*), MB value measured by UV-photometer was lower than the value measured by drop method (it's the case for kaolinite but not for illite). Yukselen (*2008*) also illustrated the same phenomena by calculating the specific surface area (SSA) of samples from MB value: the calculated SSA_{MB} measured by UV-photometer was also lower than the value measured by drop method from the low swelling potential samples.

As MB adsorption threshold for fine aggregates was fixed to 2 g/kg (exceeding of this value is forbidden), the better understanding of the differences observed between MB values measured by the two methods may help to decide if MB_{drop} or $MB_{Phot.}$ is better or not correlated to stripping phenomenon when clayey sand is introduced in bitumen.

3.2.6.2 The impact of methods on the measurement

The differences between drop and UV-Photometer methods were compared in Table 50. The initial concentration, the quantity of sample, the procedures and the end points were all different. The concentration of prepared MB solution from drop method was higher than UV-photometer method. The gradually added MB solution into 500 g of water from drop method gave lower initial concentration than the UV-Photometer method (the covering is gradually increased).

The **contact time** of MB-clay suspension in the drop method varied with the quantity and the property of samples. It was different from the contact time imposed in UV-Photometer method which was fixed to 2 h but it should be adjusted to the sample nature to reach final targeted absorbance (more than 2h for montmorillonite).

In order to determine the impact of methods on MB adsorption, the initial and final MB covering percentages were given in Table 49.

The **initial MB covering** from the drop method applied on extracted clays (it corresponded exactly to the final MB covering considering the method) were higher (for kaolinite and sand) and lower (for illite and montmorillonite) than the initial MB covering applied in UV-Photometer method.

Table 50 Comparison of differences between drop method and UV-Photometer method

	Drop method (*NF EN 933-9, 2013*)	UV-Photometer method
Concentration of MB solution added	10g/L (small addition)	1g/L (high fixed amount)
Quantity of material	200g of $D_{0\text{-}2}$mm sample in 500g of water (30g, 20g and 10g for extracted kaolinite, illite and montmorillonite)	Depending on sample nature 50 mg to10 g (pure clay) to 10 g for sand in 35 to 50 mL MB solution
Initial MB covering	Low (it increases during the test after each MB solution additions)	High but close to the final MB covering test (it decreases during the test)
Procedure (impact of the time contact)	1.Initial addition of 5ml MB solution in the suspension and agitation 1mins. 2. No halo appearing >>> addition of 5ml MB solution and agitation 1mins 3.Halo appearing: addition of 2 ml MB solution if halo disappeared in 4 mins	1. MB-sample suspension in agitation during 2 hours 2.extraction of solution from suspension by 20-30 min of centrifugation 3.Measure of the solution absorbance by UV-Photometer after calibration
	Variable time contact from 1h to several hours	Fixed time contact (2h)
End point	Halo persists for 5 minutes It depends on operator (eye sensitivity)	The absorbance of solution has to be around 1 (if not the test is done again). It depends on the spectrophotometer sensitivity
Final MB covering	--	Close to initial one

The **higher MB adsorption on extracted kaolinite and sand** measured from drop method were due to the higher initial MB covering on their surface compared to the initial covering applied in UV photometer method. This 'overestimation' of kaolinite and sand MB values with drop method was generated by the lower sensitivity of operator's eyes compared to UV-visible spectrophotometer apparatus (the concentration of MB solution had to be higher than 40 mg/L in order to generate a visible blue halo while spectrophotometer was able to detect lower concentration until 0.1 mg/L). Moreover, the personal judgment to localize the end point with drop method (that's to say the persistence of a blue halo for 5 minutes) induced the MB adsorption variability as well.

The **lower MB adsorptions on illite and montmorillonite** measured by drop method compared to the value measured by than UV-Photometer method were due to the impact of contact time and particle size. The short operating time applied in drop method was not enough to reach the equilibrium. It's also the case for the UV-photometer method that imposed a 2 hours operating time. However, such period was generally longer than the period applied in drop method.

In summary, the MB adsorption of non-swelling material measured by drop method was increased while the MB adsorption on fine aggregates with big particles (hardly dispersible) and with high swelling property.

3.2.7 Methylene blue adsorption on artificial fine-aggregates

After the study of MB adsorption onto extracted clays, the MB adsorption on artificial fine aggregates made with siliceous cleaned sand and various quantities of extracted clays, were measured and compared to expected values. The expected MB adsorptions onto artificial fine aggregates were calculated by following the additivity-law that's to say the MB adsorption value of a mixture corresponded to the sum of the weighted MB value of each pure components. By comparing the measured and calculated MB adsorption, the possibility to estimate the MB adsorption by additivity-law can be analyzed.

3.2.7.1 MB adsorptions and CEC values

The MB and CEC value of artificial fine aggregates (mixtures between extracted clays and washed sand) were measured by the drop method and the UV-photometer method (Table 51). The repetition of MB value measurement by UV-photometer method was varying because large amounts of tests failed before approaching the final value with Abs less than 1 and the quantity of sample was limited.

Table 51 CEC and MB values of artificial fine aggregates made by ext. clays (all the sand clay mixtures detailed in chapter 2 were not tested by both methods but all were characterized by drop method).

Material	Washed sand	Ext. Kao.	Ext. Illite	Ext. Montm.	CEC (meq/100g)		MB adsorption (g/kg)			Abs	$\%MB_{Init.}$[d] (%)	$\%MB_{Fin.}$[d] (%)	
	(%)	(%)	(%)	(%)	Value	S.D	Drop	UV-Pho.	S.D.	UV-Pho	UV-Pho	Drop	UV-Pho.
S1-K3	70	30	0	0	1.17	0.49	2.2	2.04	0.15[e]	1.26	57.03	58.78	54.50
S1-I4	92.78	0	7.22	0	1.67	0.01	4.7	3.30	-[c]	0.96	61.95	87.98	61.77
S1-I9	80	0	20	0	4.23	0.06	11.2	7.72	0.15[e]	0.48	57.12	82.77	57.05
S1-I13	70	0	30	0	8.94	0.05	19.6	16.53	-[c]	0.37	57.85	68.53	57.80
S1-M2	99.48	0	0	0.52	0.86	0.02	2.2	1.84	-[c]	0.40	66.97	79.97	66.88
S1-M4	98.63	0	0	1.37	1.83	0.02	5	4.53	-[c]	1.23	77.66	85.41	77.38
S1-M12	95.23	0	0	4.77	5.65	0.13	16.1	9.99	-[c]	0.05	55.30	89.08	55.27
S2-KI2	67.38	26.27	6.35	0	3.88	0.07	9.7	5.61	-[c]	0.10	45.23	78.15	45.20
S2-KI8	75.66	8.91	15.43	0	7.65	0.03	20.3	13.31	-[c]	0.08	54.41	82.95	54.39
S2-IM6	88.21	0	7.47	4.31	6.28	0.08	18.1	11.48	-[c]	0.22	57.19	90.10	57.14
S2-KM3	69.86	27.24	0	2.9	4.46	0.21	12.2	9.57	-[c]	1.52	67.40	85.51	67.08
S3-3	73.41	16.63	6.92	3.05	5.73	0.05	12.5	10.35	0.00[f]	0.43	56.55	68.19	56.46

[a] 3 tests of repeatability [b] 2 tests of repeatability (lack of sample) [c] No repeatability (lack of sample). The repeatability of MB measurement demonstarted that the coefficient of variation is lower than 5% for UV-Photometer method and lower than 10% (with ponctually 20%) for drop méthod. Range of error agreed with interlaboratory tests on 0/2 mm sands realized in 2011 (the coeficient of variation was around 14.3%).
[d] Final MB covering percentage on clay surface [e] 3 tests of repeatability with various initial MB covering percentages, [f] 2 tests of repeatability with various initial MB covering percentages.

Globally, MB adsorptions measured by the two methods presented on Figure 68 were following the same trend as CEC results. The results measured from UV-photometer presented a better correlation coefficient to CEC than results from drop method.

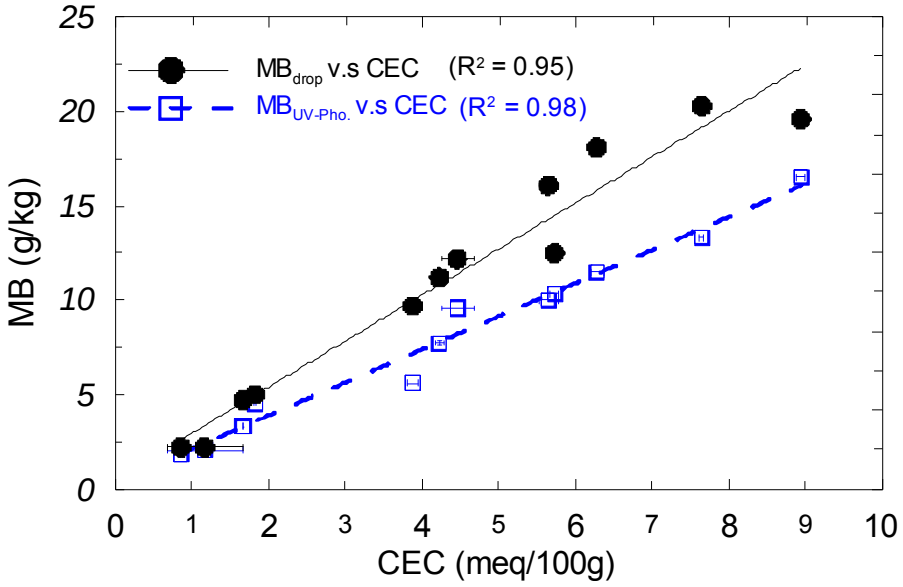

Figure 68 The CEC and MB values of artificial fine aggregates measured by drop and UV-Phot. methods

By observing the final MB covering percentages from both methods in Table 51 and Figure 69, none of the sample reached the oversaturated state that's to say MB_{fin}% over 100% (measures ranged between 45 to 77% MB_{fin}% with initial MB covering percentage close to the final one - except for one point). The final and initial MB covering were quite the same for drop method and the final MB covering percentage were systematically lower by UV-Photometer method compared to drop method. Such behavior disagreed with raw illite and montmorillonite trends as seen in Table 49). It came probably from the presence of high amount of sand in mixture. Artificial fine aggregates presented the irregular high covering percentage from drop method measurement, even higher than the final covering percentage measured on mother raw clays.

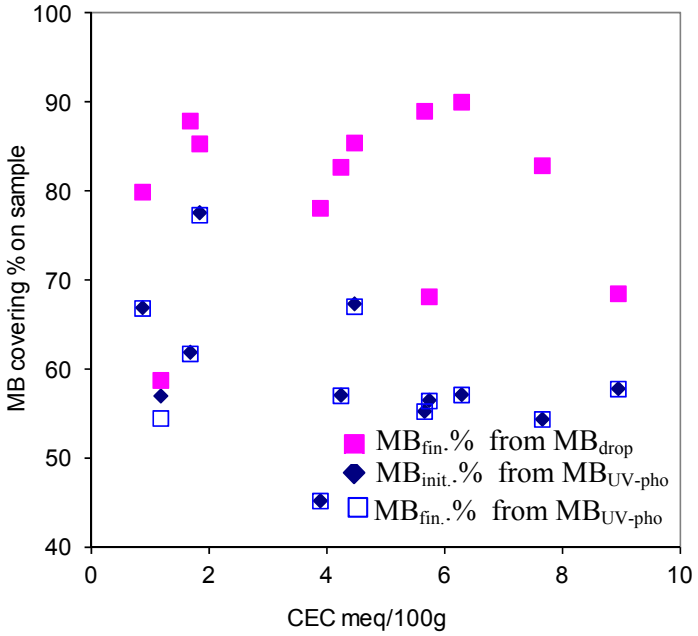

Figure 69 Initial or final MB covering percentage on artificial fine aggregates measured by drop and UV-Phot. Methods versus CEC.

3.2.7.2 Estimation of MB adsorption by additivity-law

As all the MB adsorption on extracted clays and artificial fine aggregates varied with the initial MB covering percentage, the correlation between measurement and estimation by additivity-law were estimated from $MB_{drop,}$ $MB_{Phot.}$ and CEC measurements (Table 52). The MB_{CEC} was introduced and it corresponds to: MB_{CEC} (g/kg) = CEC (meq/100g) x 319.85 /100 (with M_{CEC} = 319.85 g/mol, the molar mass).

Table 52 The comparison of MB adsorption between measurement and additivity-law for MB_{CEC} value (g/kg) and for MB value (g/kg). The measures on pure materials are : MB_{CEC} ext. kaol = 4.16 g/kg, MB_{CEC} ext. illite = 74.54 g/kg, MB_{CEC} ext. montm. = 331.42 g/kg, MB_{CEC} pure sand = 0.32 g/kg)

Artificial fine aggr.	Washed Sand (%)	ext. Kao. (%)	ext. Illite (%)	ext. Montm. (%)	MB_{CEC} (g/kg)		$MB_{Phot.}$ (g/kg)		MB_{Drop} (g/kg)	
					Measure	Add. law	Measure	Add. law	Measure	Add. law
S1 K2	78.56	21.44	0.00	0.00	--	--	--	1.61	2.20	2.39
S1-K3	70.00	30.00	0.00	0.00	3.74	1.47	2.04	2.13	2.20	3.19
S1-I4	92.78	0.00	7.22	0.00	5.34	5.68	3.30	3.62	4.70	3.45
S1-I9	80.00	0.00	20.00	0.00	13.53	15.16	7.72	9.50	11.20	8.84
S1-I13	70.00	0.00	30.00	0.00	28.60	22.59	16.53 [c]	14.10	19.60	13.06
S1-M2	99.48	0.00	0.00	0.52	2.75	2.04	1.84 [c]	1.53	2.20	1.63
S1-M4	98.63	0.00	0.00	1.37	5.85	4.86	4.53 [c]	3.53	5.00	3.63
S1-M12	95.23	0.00	0.00	4.77	18.07	16.11	9.99 [c]	11.55	16.10	11.64
S2-KI2	67.38	28.05	8.62	0.00	12.41	6.04	5.61 [c]	5.99	9.70	6.66
S2-KI8	75.66	10.54	16.94	0.00	24.47	12.11	13.31 [c]	8.75	20.30	8.54
S2-IM6	88.21	0.00	7.81	4.66	20.09	20.13	11.48 [c]	14.89	18.10	14.69
S2-IM10	90.28	0.00	3.79	6.39	--	--	--	17.11	20.60	17.06
S2-KM3	69.86	28.05	0.00	3.98	14.27	10.97	9.57 [c]	11.41	12.20	12.41
S2-KM11	88.14	4.69	0.00	7.86	--	--	--	19.12	19.40	19.36
S3-2	69.35	29.08	2.20	0.94	--	--	--	5.31	5.80	6.26
S3-3	73.41	18.47	8.62	3.98	18.33	16.19	10.35 [b]	14.80	12.50	15.16
S3-5	81.60	10.54	3.79	6.39	--	--	--	17.76	15.10	18.05

The Figure 70 showed that MB_{CEC}, MB_{drop} and $MB_{Pho.}$had different levels of correlation between calculated and measured MB or MB_{CEC} values. The coefficient of determination of linear fit was 0.78 for MB_{CEC} compared to 0.71 for MB_{drop} and 0.75 for MB_{Phot}. The highest dispersion was globally obtained for drop method. However, UV-photometer method as well as drop method demonstrated a good linear fit until MB equal to 6 (low MB values that characterized the usual clayey sand used in asphalt concrete mixture). For high MB, measured MB_{drop} are quite systematically higher than calculated one except for 3 points and measured MB_{Phot} are quite systematically lower (except for 3 points). The chapter dealing with the impact of the method that differ by different time contact, initial/final MB covering percentage and the sensitivity of operator to detect blue halo or the sensitivity of apparatus may explain the difference between results.

The CEC measurement compared to MB adsorption avoided the impact of time contact, particle size (with a high affinity of cobaltihexamine for clay surface) and MB density (initial covering percentage). As expected calculated MB_{CEC} values were better correlated to CEC measured as MB_{drop} or $MB_{Phot.}$ (Figure 70). For the most of artificial fine aggregates, calculated MB_{CEC} followed approximately the 1:1 line except for 3 samples, S1-I13, S2-KI2 and S2-KI8. The irregular correlation between adsorption measurement and additivity-law of S1-I3 and S2-KI8 were also observed on MB measurement by both methods. Note that MB_{CEC} values from S1-I13 and S2-KI8 took the highest and second places from all the samples and gave

also the highest MB adsorptions measured by UV-photometer and drop methods respectively compared to the expected calculated values. Such results suggested that result probably came from errors during the artificial fine aggregates manufacturing by operators. After exchange with operator supervised by other person who controlled each addition and weight, no errors were done during this step. No other explanation was found except the presence in each mixture of illite that was not easily dispersed.

To conclude, it's not easy to evaluate if the presence of several clays may impact on MB adsorption compared to the case where just only one clay was present in high amount. The presence of sand (clay dilution in mixtures) seemed to impact the measures, an impact that varied with the method of measures.

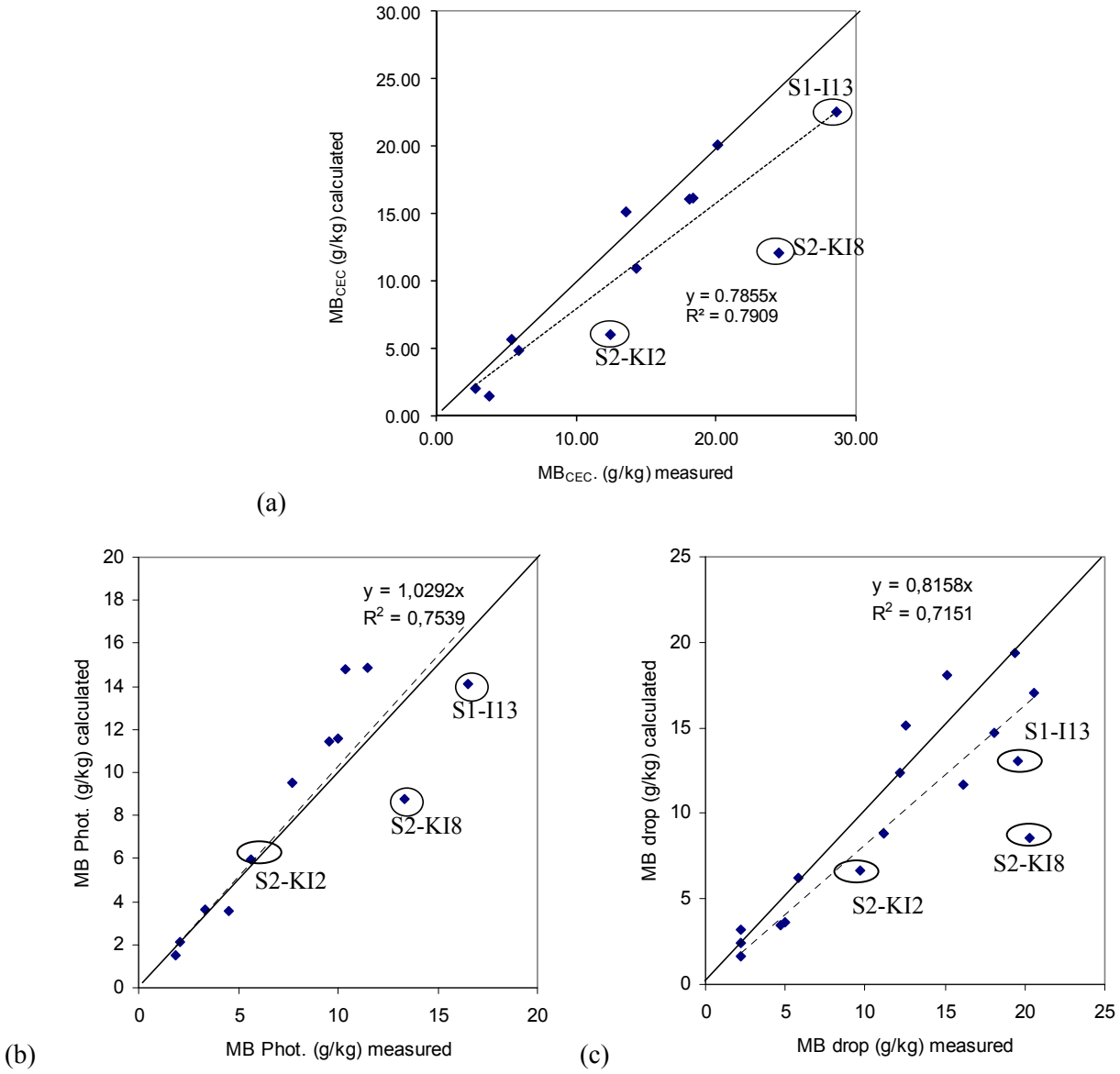

Figure 70 The correlation between measures and calculated values of (a) MB_{CEC} , (b) $MB_{UV\text{-}pho}$ and (c) MB_{drop} adsorption (g/kg). The calculated values were obtained by applying additivity-law

3.2.8 MB adsorption on unknown fine aggregates from quarries

The MB values of unknown fine aggregates were measured by drop and UV-Photometer methods, and their CEC values were measured for indicating their final MB covering percentages as well (Table 53).

The unknown sample C presented the highest CEC and MB value as well as unknown sample A. The rest of unknown sample, B, D and E, presented similar MB values lower than 2 g/kg. In the practical application, the unknown samples B, D and E, were qualified for the use of asphalt concrete pavement, whereas the unknown sample A and C were non-qualified. The use of photometer method instead of drop method didn't change the qualification of sand but closer to the threshold, it might happen.

Table 53 CEC and MB values of unknown fine aggregates.

Fine-Aggregate $D_{0/2}$ mm	% passing 2 µm	CEC (meq/100g) Value	CEC S.D.	MB adsorption (g/kg) Drop	MB adsorption S.D.	MB adsorption UV-Pho.	MB adsorption S.D.	$MB_{Fin.}$ (%) Drop	$MB_{Fin.}$ (%) UV-Pho.	Abs [a] UV-Pho	$MB_{Init.}$ (%) UV-Pho.
Unknown A	4.12	2.16 [b]	-	2.54 [a]	0.06	2.83	0.37 [c]	36.76	40.96	0.13-2.24	39.1-50.3
Unknown B	3.44	1.59 [a]	0.03	1.5 [a]	0	1.40	0.08 [c]	29.49	27.52	0.37-1,16	26.8-29.9
Unknown C	10.10	8.10 [a]	0.4	9 [a]	0.1	9.12 [b]	-	34.73	35.20	1.56	36.8
Unknown D	10.20	0.90 [b]	-	1.73 [a]	0	1.39	0.01 [c]	60.09	48.28	0.21-1.18	48.3-49.3
Unknown E	7.64	0.51 [b]	-	1.74 [a]	0.12	1.45	0.07 [c]	106.65	88.88	0.18-1.05	83.6-92.4

[a] : 3 tests of repeatability in the same conditions [b] : No repeatability because the limited amount of available material after the failure of several tests to find the adequate initial MB covering to obtain an absorbance around than 1.[c] 3 tests of repeatability with various initial MB covering percentages

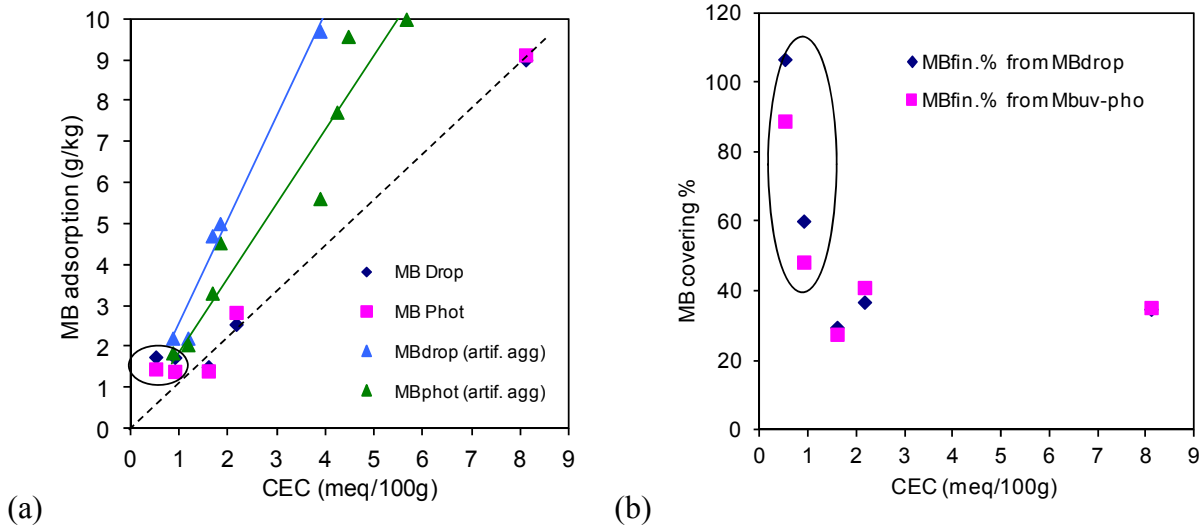

Figure 71 The correlation between CEC and (a) MB adsorption (g/kg) or (b) MBfin.% obtained by photometer or drop method on unknown fine aggregates (measurements are compared to the artificial sand aggregates in (a))

The correlation between CEC and MB (Figure 71) is not in accordance with the fitting of measures on artificial sand aggregates. If samples D and E (characterized by the highest MB final covering percentages and the presence of kaolinite or illite as main clay) were in quite good accordance with artificial sands at low MB, the samples A, B and C indicated low MB values compared to the MB values on artificial sands. Such trend was probably connected to the presence of swelling clay as montmorillonite/vermiculite and/or to the particle size (accessibility to reactive site) and the time contact too much short to reach equilibrium. The difference of total layer charge that impact also on MB aggregation as well as the presence of cations with different nature onto clays may be also at the origin of MB adsorption variation between unknown and artificial aggregates.

The impact of the total layer charge was estimated using the analysis of the basal space from EG treated K-saturated clay fraction using X-Ray diffraction. After EG treated K-saturated clay fraction, the unknown sample B, D and E did not show any diffraction greater than 10 Å (no swelling clays), whereas the unknown sample A and C consisted of the significant diffraction at 14.1 Å and 17.1 Å. As The threshold of high and low total layer charge of montmorillonite (swelling clay) being fixed at 15.5 Å (Christidis, *2003*), unknown sample C and unknown sample A belonged to high and low total layer charge of clay respectively (Figure 72). High total layer charge induced an increase of CEC and then the rise of MB adsorption. If the layer charge increased too much (like in the case of illite), the CEC might decrease because of the lower ability of MB molecule to reach interlayer space (permanent closure of the interlayer space). The total layer charge impacted also on MB aggregation with the presence of permanent H aggregates. Their presence should be validated by the collection of UV-visible spectrum.

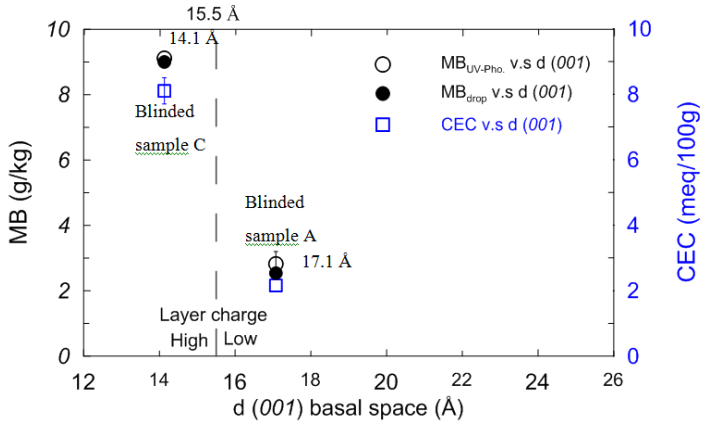

Figure 72 The d(*001*) spaces of unknown samples A and C versus MB and CEC adsorption

3.2.9 Methylene blue adsorption on clays: summary

MB adsorption measured by drop method is a standardized test commonly used in France and Europe in the aggregates field. The qualification threshold is 2 g of methylene blue adsorbed per kg of aggregates. Even though this standard has been established over 40 years, literature review and experimental results demonstrated how several parameters (initial MB covering percentage, clay layer charge, contact time, test method…) may impact on the measurement of MB value. Results illustrated the effect of MB aggregation in MB solution and MB suspension, how absorbance has to be used in MB measurement, the impact from particle size of sample, pH value, various cations and time contact. All of these impacts alter the evaluation of MB adsorption. Then MB may not be sufficient to judge the sample harmfulness.

The cation exchange capacity (CEC) used by pedologists is clearly correlated to methylene blue value but methylene blue and cobaltihexamine ions (the two chemical compounds used to evaluate clay surface area and reactivity by both method) have not the same affinity towards clay surface varying with mineralogy. As cobaltihexamine ion (responsible of orange color in solution) is more stable in solution as MB with the appearance of aggregation and with a higher affinity for clay surface compared to MB, CEC may be also a good indicator to replace MB. The comparison of the correlation between MB and Duriez test as well as CEC and Duriez test will reveal in the following chapter if such proposition can be seriously considered.

3.3 *The water-bitumen-clay interaction from micro aspects*

This section investigates from a micro-scale point of view the interactions between clay thin films and bitumen in the presence of water molecules. As surface energy refers to the predominant theory invoked to explain bitumen/aggregate interaction (*Terrel and Shute 1989*), the components of surface energy, polar forces and dispersive forces, are calculated in order to assess the stripping potential of the bitumen-clay binding. For this purpose, contact angle measurements are performed using the static sessile drop method. Then, the role played by the nature of clay exchangeable cation on the stripping resistance at bitumen-clay interface is investigated. Eventually, the compatibility between bitumen and clay is examined.

3.3.1 Determination of contact angle from static sessile drop test

Assessment method

Figure 73 depicts the variations of contact angle, volume, area, and diameter of bitumen drops deposited on a glass substrate and on thin sections of extracted kaolinite, extracted illite and extracted montmorillonite as a function of time.

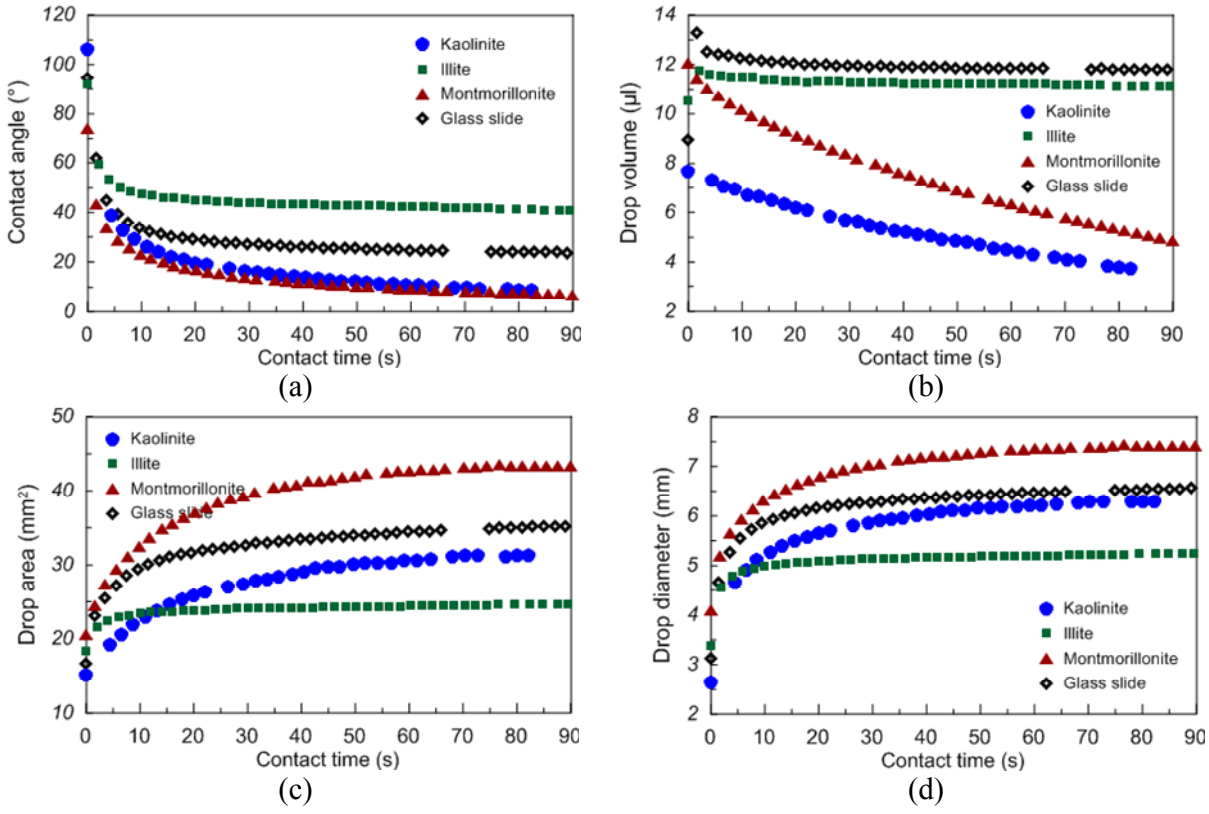

Figure 73 (a) Contact angle, (b) drop volume, (c) drop area, and (d) drop diameter as a function of time determined by static sessile drop method.

The measurement period is every 0.06s. Contact time is initialized when the drop has just hit the surface and is no more in contact with the micro-syringe needle. The drop then adapts its geometry to achieve energetic equilibrium, thus causing contact angle decrease as well as drop diameter and area increase.

Meanwhile, observe that the drop volume decreases on kaolinite and montmorillonite film, indicating that bitumen penetrates into the pores of the colloid film, whereas the drop volume remains more or less constant on glass or illite films. As a consequence, contact angle measurements were performed as far as possible when the drop area, drop diameter and contact angle itself stabilize, but before any significant decrease of drop volume as such a decrease biases contact angle readings (*Shang et al, 2008*).

Influence of the surface roughness of clay thin films

In general, surface roughness is known to affect contact angle determination due to part of the liquid penetrating into the surface porosity (*Cheng, 2002; Graf, 1986; Bahia, 1999*). However, *Meiron et al. (2004)* have evidenced that a surface roughness as low as R_a=1.3 µm doesn't affect contact angle determination with reference to a perfectly smooth surface. Furthermore, the surface roughness of kaolinite, illite and montmorillonite has been reported to have little influence on contact angle measurement from dynamic sessile drop method (*Shang et al. 2008*). Hence, it was decided to assess the surface roughness of the tested commercial clays thin films.

For this purpose, a laser scanning profilometer was used to measure surface roughness from 2D profiles and 3D surfaces. For each clay, Figure 74 summarizes the values of surface roughness parameters recommended by *Zahouani et al (2000)*, arithmetical mean height within a definition area (S_a), arithmetic mean deviation of the vertical profiles (R_a) and root-mean-square gradient of surface slope (S_{dq}).

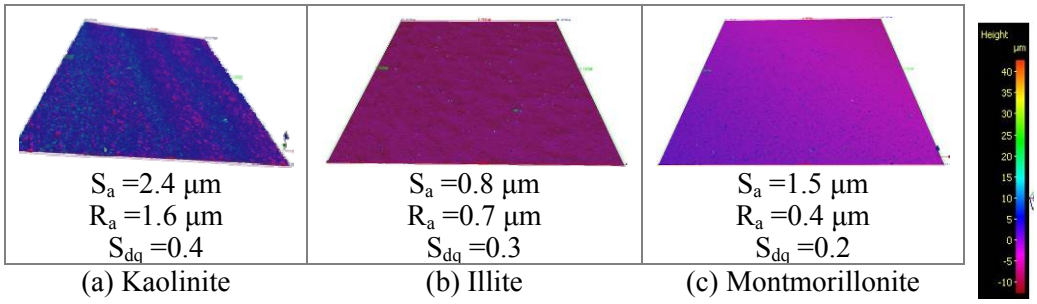

Figure 74 The arithmetic mean deviation of the vertical profile (Ra), average height of selected area (Sa) and root-mean-square gradient of surface slope from select area (Sdq) of commercial (a) kaolinite, (b) illite and (c) montmorillonite thin film

With higher S_a values, these results evidence that kaolinite forms a thicker film than montmorillonite, and much thicker than illite. With higher R_a values, kaolinite also shows rougher surface than illite, and much rougher than montmorillonite. The values of corresponding root-mean-square gradient of surface slope agree with this roughness ranking. As clay thin films were all made from suspensions having the same concentration of clay, the thickness and roughness differences between clay thin films may be explained by different numbers of sheets per clay particle and different aggregation modes between particles (*Morel 1996, Bentahar et al. 2010*). Kaolinite has the highest thickness and roughness among clays, which suggests random orientation between big kaolinite particles. Contrariwise, clays such as montmorillonite having a low number of sheets per particle more easily disperse in suspension, thus forming a smoother surface through preferred orientation of particles on glass slides.

As the roughest clay thin film of the present study corresponds to R_a=1.6 µm (kaolinite), it seems likely that the surface roughness of commercial clays thin films only moderately affected contact angle measurements.

Contact angle values

The results of contact angle measurements performed with four different liquids at ambient temperature and 60% ~ 75% relative humidity are shown in Table 54. Except illite, these results compare fairly well with those obtained by *Shang et al (2010)* on similar clay types tested with water and diiodomethane at 20°C and 33% relative humidity. The deviation observed with illite may result from differences in clay moisture content, which will be discussed again in the next section.

Table 54 Contact angles measured from static sessile drop tests on various surfaces

Material		Contact angle (°)							
		Water	S.D.	**Ethylene glycol**	S.D.	**Glycerol**	S.D.	**Diiodo-methane**	S.D.
Glass slide		31.4	8.0	27.6	3.4	39.2	5.8	44.3	2.8
Kao	Comm.	13.4	1.0	15.6	2.8	39.4	2.2	24.7	0.9
	Ext.	16.8	0.7	29.5	2.1	52.3	2.3	29.1	0.9
	Shang et al. (*2010*)	16.9	0.7	-	-	-	-	21.8	1.7
Illite	Comm.	7.2	0.6	10.7	1.9	9.8	2.4	18.3	2.0
	Ext.	14.9	2.9	51.7	4.9	51.7	4.9	30.3	1.4
	Shang et al. (*2010*)	34.2	0.9	-	-	-	-	27.6	1.2
Montm.	Comm.	16.4	6.4	12.3	2.1	16.7	3.9	42.5	0.5
	Ext.	40.1	7.1	49.3	3.0	48.5	2.5	41.8	0.8
	Shang et al. (*2010*)	23.8	1.7	-	-	-	-	42.1	2.5

Contact angle differences may be observed between commercial and extracted clays as shown in Figure 75, in which bitumen contact angle values have also been represented. In particular, the contact angle of bitumen on extracted illite is significantly smaller than the one on commercial illite; conversely, the contact angle of water on extracted montmorillonite is significantly higher than the one on commercial montmorillonite. The smaller particle size distribution of commercial illite compared to that of extracted illite could explain the lower contact angle value of the latter (*Graf, 1986; Bahia, 1999*), whereas montmorillonite differences could arise from different exchangeable cations between commercial and extracted batches, the former being washed during its manufacturing process.

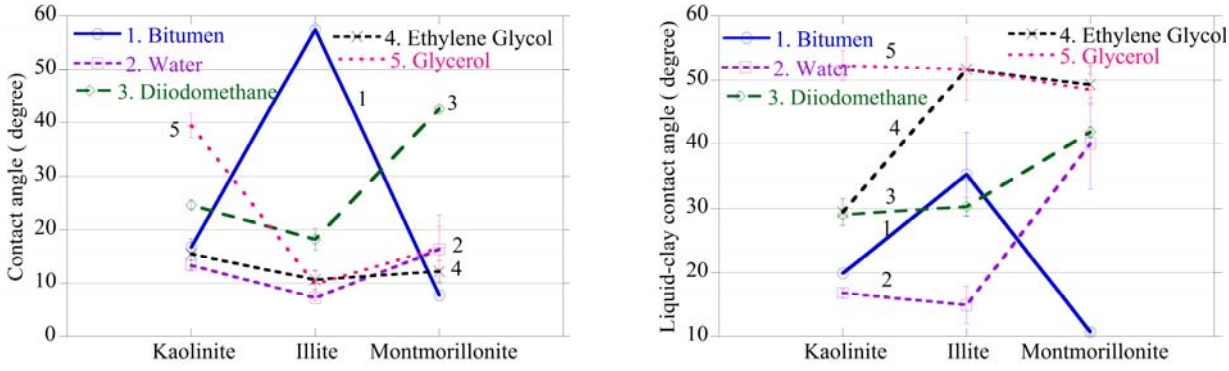

Figure 75 Contact angles between liquids (bitumen, water, diiodomethane, Ethylene glycol and Glycerol) and clays (kaolinite, illite, and montmorillonite) from (a) commercial products and (b) extracted clays

3.3.2 *Surface energy calculations*

The polar forces (γ_S^P), dispersive forces (γ_S^D) and surface energy ($\gamma_S = \gamma_S^P + \gamma_S^D$) of commercial clays, extracted clays and glass substrate were determined from previous contact angle measurements upon performing linear fits using the Owens-Wendt model (Eq. 13 in 1.4.1.2).

Table 55 shows the polar forces, dispersive forces, and surface energy of (1) the four liquids (*Strom 1987, Yu et Dekker 1982*) and (2) glass slide substrate, commercial and extracted clays. The coefficients of determination (R^2) of the regression fits as well as the pH value of suspensions are also depicted in Table **55**. With all coefficients of determinations over 0.9, fits quality is very good. Table 55 also shows that the kaolinite suspension appears slightly acid, whereas illite and montmorillonite suspensions are slightly basic.

Table 55 Surface energy values of tested liquids and clays

Material	Type		Polar forces (mJ/m^2)	Dispersive forces (mJ/m^2)	Surface energy (mJ/m^2)	R^2 [e]	pH [f]
(1) Liquids	Water [a]		51.0	21.8	72.8		
	Ethylene glycol [a]		16.8	30.9	47.7		
	Glycerol [a]		26.4	37	63.4		
	Diiodo-Methane [b]		6.7	44.1	50.8		
(2) Materials	Glass slide		50.7	11.3	62.0	0.99	-
	Kao	Comm.	55.0 (48.9) [d]	12.9 (20.4) [d]	67.9 (69.2) [d]	0.96 (1) [d]	6 [g]
		Ext.	56.5	9.8	66.3	0.92	4.5
	Illite	Comm.	54.5 (37.7) [d]	16.0 (23.7) [d]	70.5 (61.4) [d]	0.97 (1) [d]	7-8 [g]
		Ext.	58.9	8.6	67.5	0.92	9.5
	Montm.	Comm.	59.7 (51.3) [d]	11.5 (16.3) [d]	71.2 (67.5) [d]	0.99 (1) [d]	7-8 [g]
		Ext.	43.7	10.7	54.4	0.94	8.3

[a] *Strom, 1987* [b] *Yu et Dekker, 1982* [c] *Somé, 2012* [d] *Shang et al. 2010*
[e] Coefficient of determination from Owens and Wendt *(1969)* fit
[f] pH value of clay suspension used for making the clay thin film
[g] *Pham, 2008*

The surface energy of clays seems to be primarily of polar origin and the results compare reasonably well with *Shang et al. (2010)*, except in the case of illite for which these authors reported a high dispersive component. According to literature review, Ca-montmorillonite shows higher polar forces than dispersive forces when its water content is higher than 48% (Figure 18 from literature review, *Chassin 1986).* Hence, with a relative humidity between 60% ~ 75% in the laboratory where slides were air-dried at room temperature and tested for contact angle measurements, it seems reasonable to consider that clays have high residual water contents, justifying higher polar forces than dispersive forces as depicted in Table 55. Besides, extracted montmorillonite evidences lower polar forces than commercial one, which might derive from exchangeable cations and particle size of clay generated by different methods of clay extraction between laboratory and industry *(Chassin 1986).* Last, the high polar forces of glass slides may result from their non-regular SiO_2 structure and Na^+/Al^{3+} additions used to increase the glass toughness and photosensitivity (*Trukhin et al. 2009*).

3.3.3 *Water-clay and bitumen-clay work of adhesion*

According to the theory of surface energy, the work of adhesion between solid and liquid, W_{ad}, may be derived either from known surface energy of the liquid and measured contact angle θ, or from known surface energy of both the solid and liquid. Equations Eq.11, Eq.14 and Eq. 23 were used to calculate the work of adhesion in each case, with the last two equations allowing comparison between the Fowkes *(1964)* and *Wu (1973)* expressions of polar adhesion forces. The measured contact angle and surface energy values used to calculate the Wad of bitumen-clays and water-clays are depicted in Table **56**.

Table 56 Measured contact angle and surface energy values to calculate the work of adhesion

Material	Type		Contact angle (°)		Surface energy (mJ/m²)		
			Bitumen	Water	Polar forces	Dispersive forces	Surface energy
Water [a]	Distilled				51.0	21.8	72.8
Bitumen [b]	35/50 at 140°C				5.0	23.0	28.0
Solids	Glass slide		32.5	31.4	50.7	11.3	62.0
	Kao	Comm.	16.8	13.4	55.0	12.9	67.9
		Ext.	19.9	16.8	56.5	9.8	66.3
	Illite	Comm.	57.5	7.2	54.5	16.0	70.5
		Ext.	35.3	14.9	58.9	8.6	67.5
	Montm.	Comm.	7.7	16.4	59.7	11.5	71.2
		Ext.	10.7	40.1	43.7	10.7	54.4

[a] *Strom, 1987* [b] *Somé, 2012*

$$W_{ad} = \gamma_L (1 + \cos\theta_{SL}) \qquad \text{Eq 11}$$

$$W_{ad} = 2(\sqrt{\gamma_S^P \gamma_L^P} + \sqrt{\gamma_S^d \gamma_L^d}) \qquad \text{Eq 14}$$

$$W_{ad} = 2\sqrt{\gamma_S^d \gamma_L^d} + 4\frac{\gamma_S^P \gamma_L^P}{\gamma_S^P + \gamma_L^P} \qquad \text{Eq 23}$$

The results of W_{ad} calculations at bitumen-clay and water-clay interfaces are shown in Table 57. These results have been supplemented with calculated values of the work of adhesion at bitumen-glass slide and water-glass slide interface. Whatever the calculation method, water-clay interfaces have much higher work of adhesion values than bitumen-clay interfaces, confirming a much higher affinity of clays to water than to bitumen and consequently predicting a high risk of adhesive failure at the bitumen-clay interface in the presence of water. High W_{ad} values between water and solids derive from highly polar surface forces, which could be explained by the persistence of residual moisture on solids surface while air-drying at ambient temperature and 60% ~ 75% relative humidity in the laboratory. The more or less similar W_{ad} values between water-glass slide and water-clays tend to confirm this hypothesis.

Table 57 Work of adhesion between bitumen / water and materials

Material	Type		Wad of bitumen-solid (mJ/m²)				Wad of water-solid (mJ/m²)			
			1 (Eq. 11)	2 (Eq. 14)	3 (Eq. 23)	Variation [a] (%)	1 (Eq. 11)	2 (Eq. 14)	3 (Eq. 23)	Variation [a] (%)
Solids	Glass slide		51.6	64.1	50.4	2%	135.0	133.1	133.1	1%
	Kao	Comm.	54.8	67.6	52.8	4%	143.6	139.5	139.4	3%
		Ext.	54.3	63.7	48.5	12%	142.5	136.6	136.5	4%
	Illite	Comm.	43.1	71.4	56.7	-24%	145.0	142.8	142.7	2%
		Ext.	50.8	62.5	46.6	9%	143.2	137.0	136.7	5%
	Montm.	Comm.	55.7	67.0	50.9	9%	142.6	142.0	141.7	1%
		Ext.	55.5	60.9	49.3	13%	128.5	124.9	124.6	3%

[a] (Eq.11-Eq.23)/Eq.24 *100%

Note that W_{ad} calculations using contact angle and liquid surface energy values (Eq 11) range between those calculated using exclusively surface energy values and Wu's expression (Eq 23) and those using exclusively surface energy values and Fowkes' expression (Eq 14), except for commercial illite-bitumen interface for which a surprisingly low work of adhesion value was calculated from Eq 11. Furthermore, note that Eq 11 and Eq 23 give fairly similar values, except for commercial illite-bitumen interface

3.3.4 Water-clay and bitumen-clay interaction as a function of exchangeable cations

Exchangeable cations on clay surface affect bitumen-clay interaction, and this effect may be detected by the sessile drop method (*Ishai and Craus 1977*). Therefore, suspensions of cation-exchanged extracted clays (CEECs) were prepared and, once air-dried in the same laboratory conditions as for the previous thin sections, the work of adhesion between thin clay film and water or bitumen drops was determined. Subsequently, each thin section of cation-exchanged extracted clay covered with a bitumen drop was immersed in a water container with the intention of observing the occurrence of stripping phenomena.

3.3.4.1 Contact angles of cation-exchanged extracted clays

Table 58 depicts the mean and standard deviation values of contact angles measured on water or bitumen drops deposited on the surface of cation-exchanged extracted clays. As for the previous thin sections, bitumen contact angles on the various clay surfaces were measured at 140 °C in a heating chamber. Each value in Table 58 was calculated from at least three measurements.

Table 58 Contact angles of static sessile drop on cation-exchanged extracted clay surface

Material	Contact angle (°)											
	Water						Bitumen					
	Kao	S.D	Illite	S.D	Montm.	S.D	Kao	S.D	Illite	S.D	Montm.	S.D
Comm.	13.4	1.0	7.2	0.6	16.4	6.4	16.8	0.1	57.5	0.6	7.7	0.2
Ext.	16.8	0.7	14.9	2.9	40.1	7.1	19.9	0.1	35.3	6.5	10.7	0.4
Li-Ext.	20.6	0.4	21.3	2.6	27.7	2.5	19.1	0.7	46.7	0.2	11.4	1.5
Na-Ext.	21.1	2.1	21.1	2.7	31.4	11.0	19.5	0.3	48.2	0.1	11.7	1.1
K-Ext.	15.5	0.7	20.7	2.6	60.2	1.6	18.0	0.4	48.4	0.1	11.1	0.8
Cs-Ext.	17.1	4.2	16.7	1.1	43.5	3.1	17.8	0.4	49.8	0.5	10.6	1.0
Mg-Ext.	17.4	3.7	17.6	1.2	- [a]	- [a]	19.9	0.1	49.3	0.2	10.4	0.7
Ca-Ext.	19.3	0.9	20.9	3.1	54.9	5.7	19.9	0.1	48.8	0.4	25.3	3.6
La-Ext.	14.0	0.6	17.6	1.7	61.5	2.1	19.9	0.6	49.9	0.1	10.8	0.3

[a] Experimental failure

Figure 76 facilitates the comparison between contact angles measured on bitumen and water drops deposited on the various CEECs. This figure shows that bitumen-clay as well as water-clay contact angles are not significantly affected by cation substitution, which is consistent with *Shang et al. (2010)*, except in the case of montmorillonite, whose hydrophobic behavior tends to increase namely with potassium, calcium or lanthanum substitutions. A possible explanation of this hydrophobic behavior could be the collapse of the basal space of Ca^{2+}- and La^{3+}- montmorillonite because of the high valence and small crystal ionic radius of these cations (*Conway 1998, Tansel et al. 2006*). Furthermore, as already observed with commercial and extracted illites, Figure 76 also confirms that bitumen drops deposited on cation-exchanged illites have significantly higher contact angle values than bitumen drops deposited on other CEECs. Last, bitumen drop on Ca^{2+}- montmorillonite shows a significantly higher contact angle than bitumen drop deposited on any other cation-exchanged montmorillonite.

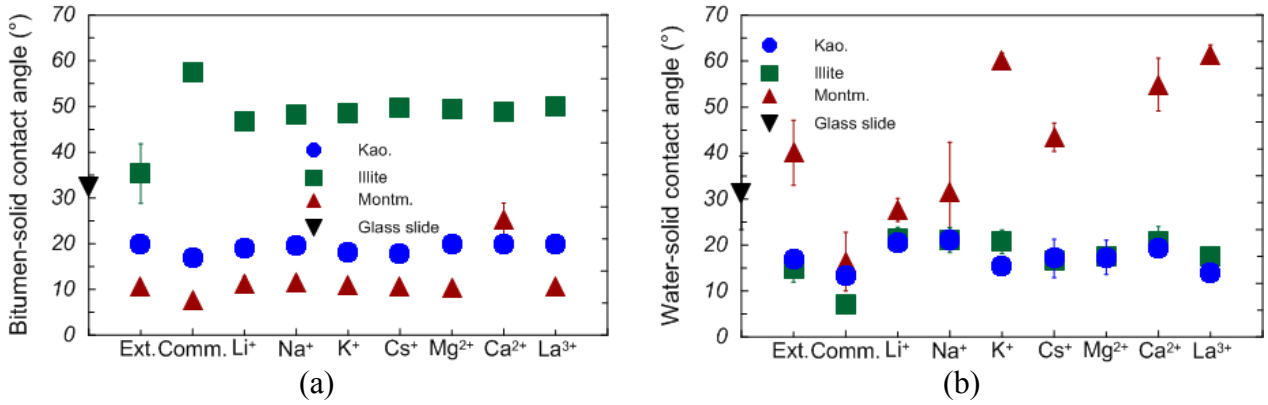

Figure 76 Contact angles determined from (a) bitumen and (b) water drops

3.3.4.2 Work of adhesion of cation-exchanged extracted clays

As for commercial and extracted clays, the surface energy of CEECs may be calculated from measured contact angles using water and bitumen drops. Then, corresponding bitumen-CEEC and water-CEEC work of adhesion values may be calculated in order to predict the stripping potential of bitumen-CEECs.

However, observing that CEECs were prepared as suspensions subsequently air-dried at laboratory temperature with a relative humidity between 60% ~ 75%, and that water drop contact angle measurements were performed in the same conditions, it was further considered that a hydration water film was still present on clay surface at the time of measurement and that ambient relative humidity caused water vapor molecules to adsorb on clay surface and exert a non-zero spreading pressure π_E . Note that such a spreading pressure is zero with bitumen drops for which contact angle measurements are performed in a controlled atmosphere at 140 °C.

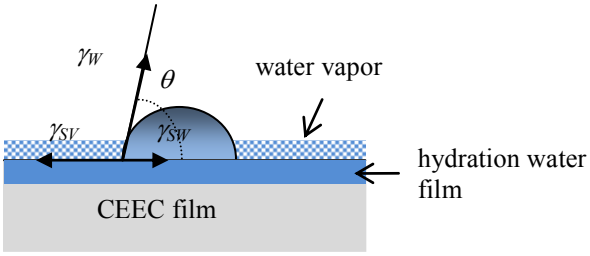

Figure 77 Equilibrium state for a CEEC-water drop-water vapor system inspired from *Janczuk et al (1989).*

Young's equation summarized in the literature review rewrites as follows (*Janczuk et al. 1989*):

$$\gamma_{SV} = \gamma_S - \pi_E = \gamma_{SW} + \gamma_W \cos\theta_W \quad \text{for the water drop} \quad \text{Eq 32}$$

$$\gamma_S = \gamma_{SB} + \gamma_B \cos\theta_B \quad \text{for the bitumen drop} \quad \text{Eq 33}$$

Upon assuming that the water vapor is close to saturation, *Janczuk et al. (1989)* suggested the following expression of the spreading pressure:

$$\pi_E = \gamma_S - \gamma_W \quad \text{Eq 34}$$

The work of adhesion at water/CEEC and bitumen/CEEC interfaces rewrite (see equations 20, 21 and 23 of the literature review):

$$W_{SW} = \gamma_S + \gamma_W - \gamma_{SW} = 2\sqrt{\gamma_S^d \gamma_W^d} + 2\sqrt{\gamma_S^P \gamma_W^P} \quad \text{for water/CEEC} \quad \text{Eq. 35}$$

$$W_{SB} = \gamma_S + \gamma_B - \gamma_{SB} = 2\sqrt{\gamma_S^d \gamma_B^d} + 2\sqrt{\gamma_S^P \gamma_B^P} \quad \text{for bitumen/CEEC} \quad \text{Eq. 36}$$

Substituting interaction energy terms of equations 35 and 36 with their expression from equations 32 to 34 yields the following system of equations:

$$\gamma_S^d + \gamma_S^P - 2\sqrt{\gamma_S^d \gamma_W^d} - 2\sqrt{\gamma_S^P \gamma_W^P} + \gamma_W \cos\theta_W = 0 \quad \text{Eq. 37}$$

$$\gamma_B^d + \gamma_B^P - 2\sqrt{\gamma_S^d \gamma_B^d} - 2\sqrt{\gamma_S^P \gamma_B^P} + \gamma_B \cos\theta_B = 0 \quad \text{Eq. 38}$$

with θ_W and θ_B given by Table 59 for each CEEC. Solving this system of equations yields CEEC surface energy values, from which the work of adhesion at water/CEEC and bitumen/CEEC interfaces may be calculated using equations 34 and 35.

Table 59 Surface energy and work of adhesion values, in mJ/m², of bitumen/CEEC and water/CEEC interfaces

Material	kaolinite					illite					montmorillonite				
	γ_s^P	γ_s^d	W_{SB}	W_{SW}	S[b]	γ_s^P	γ_s^d	W_{SB}	W_{SW}	S[b]	γ_s^P	γ_s^d	W_{SB}	W_{SW}	S[b]
Comm.	38.9	7.6	54.3	114.0	S	37.5	6.0	50.8	109.3	S	9.1	19.2	55.5	71.8	S
Ext.	39.9	7.7	54.8	115.4	S	34.5	3.1	43.1	98.7	S	40.5	8.1	55.7	116.8	S
Li-Ext.	34.1	8.7	54.5	109.3	S	35.6	4.6	47.2	103.8	S	19.5	13.8	55.5	91.2	S
Na-Ext.	31.9	9.2	54.4	106.8	S	39.5	3.7	46.7	107.1	S	15.7	15.4	55.4	84.7	S
K-Ext.	41.5	7.2	54.6	116.6	S	39.9	3.7	46.6	107.4	S	1.3	27.7	55.5	54.0	**NS**
Cs-Ext.	38.8	7.8	54.7	114.3	S	37.8	3.7	46.1	104.9	S	7.2	20.6	55.5	67.5	S
Mg-Ext.	38.9	7.6	54.3	114.0	-[a]	36.2	4.1	46.3	103.5	S	-[a]	-[a]	-[a]	-[a]	-[a]
Ca-Ext.	39.2	7.5	54.3	114.3	S	38.6	3.8	46.5	106.0	S	2.5	23.2	53.3	54.5	S
La-Ext.	36.2	8.2	54.3	111.4	S	36.6	3.9	46.0	103.7	S	1.0	28.3	55.5	53.6	**NS**

[a] Experimental failure
[b] Stripping (S) or no stripping (NS)

Table 59 yields surface energy values which are 20 to 30% lower than the ones reported in Table **56** on raw and commercial clays, and this reduction applies essentially to the polar component. Furthermore, it should be noted that the surface energy values of Table 59 are reasonably constant for kaolinite and illite whatever the exchanged cation, whereas this cation plays a major role on the surface energy polar component of montmorillonite. Besides, with kaolinite and illite, Table 59 shows that the calculated bitumen/CEEC work of adhesion values are smaller than corresponding water/CEEC work of adhesion values, confirming the prediction of a high risk of adhesive failure at the bitumen/CEEC interface in the presence of water as pointed out for raw and commercial clays. However, this prediction no more holds with montmorillonite as, at least for K^+- and La^{3+}-montmorillonite (see shaded cells of Table 59), the calculated work of adhesion values predict stripping resistance. Moreover, the Ca^{2+}-montmorillonite may resist stripping as W_{SB} and W_{SW} are almost identical within the experimental deviation.

3.3.4.3 Experimental stripping resistance of bitumen-CEEC samples immersed in water

In order to simulate the impact of water-bitumen-clay interaction on sand-oil recovery, *Basu (1996, 1998, 2000, 2004)* immersed bitumen-glass slides in a clay suspension. Similarly, the original intention in the present study was to simulate clay-induced stripping upon immersing bitumen/clay thin sections in a water cell at controlled temperature and continuously record the gradual change of bitumen-clay contact angle using a camera (see a and b in Figure 78).

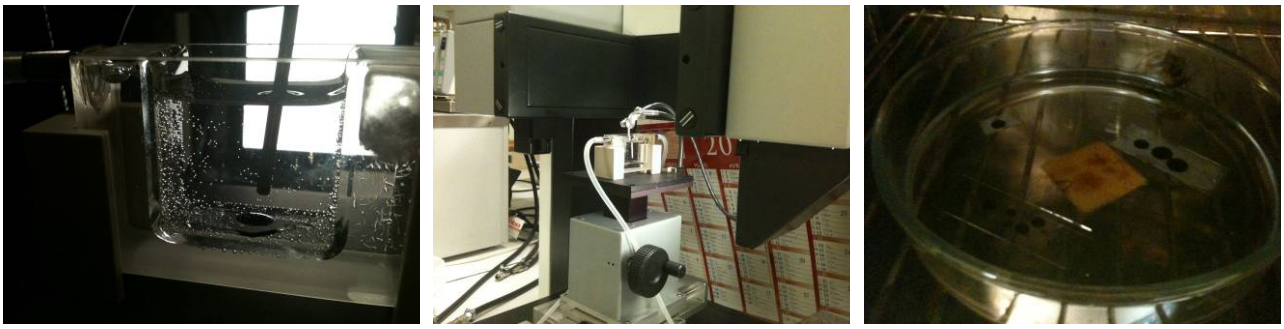

(a) (b) (c)

Figure 78 The bitumen-clay sample (a) in the presence of water and (b) continuously recorded the evolution of its contact angle and (c) the alternative method without recording

Though this experimentation had been tested for feasibility, it could not be implemented since the water cell was accidently broken and the new one received from manufacturer was not appropriate. As a consequence, an alternative method illustrated by picture c on Figure 78 was adopted. Thin sections made of bitumen drops deposited on extracted clays, commercial clays and CEECs were immersed in ultra pure water and left in the oven at 60 °C for 3 days without recording.

The results of this alternative experimentation are shown in Figure 79. This figure shows that the bitumen-kaolinite and bitumen-cation exchanged kaolinite interfaces were still bound on their corresponding glass slides, though volcano-like patterns were visible on bitumen drop surfaces. Furthermore, the density of these volcano-like patterns tends to decrease with increasing atomic weight of exchanged cation. On the other hand, bitumen-illite, bitumen-montmorillonite and their bitumen-CEECs had all detached from glass slides except bitumen-La^{3+}-illite and bitumen-La^{3+}-montmorillonite (Figure 79). Moreover, the detached bitumen drops were floating in the water cell with a flat shape.

Work of adhesion calculations performed in Table 59 could predict the stripping of bitumen/illite and bitumen/montmorillonite thin sections as well as the non-stripping of bitumen/La^{3+}-montmorillonite thin section. However, they could not predict the non-stripping of bitumen/kaolinite and bitumen/La^{3+}-illite thin sections. However, volcano-like patterns suggest weakened bitumen/kaolinite interfaces under a reverse emulsion effect, which was not further investigated within the present study.

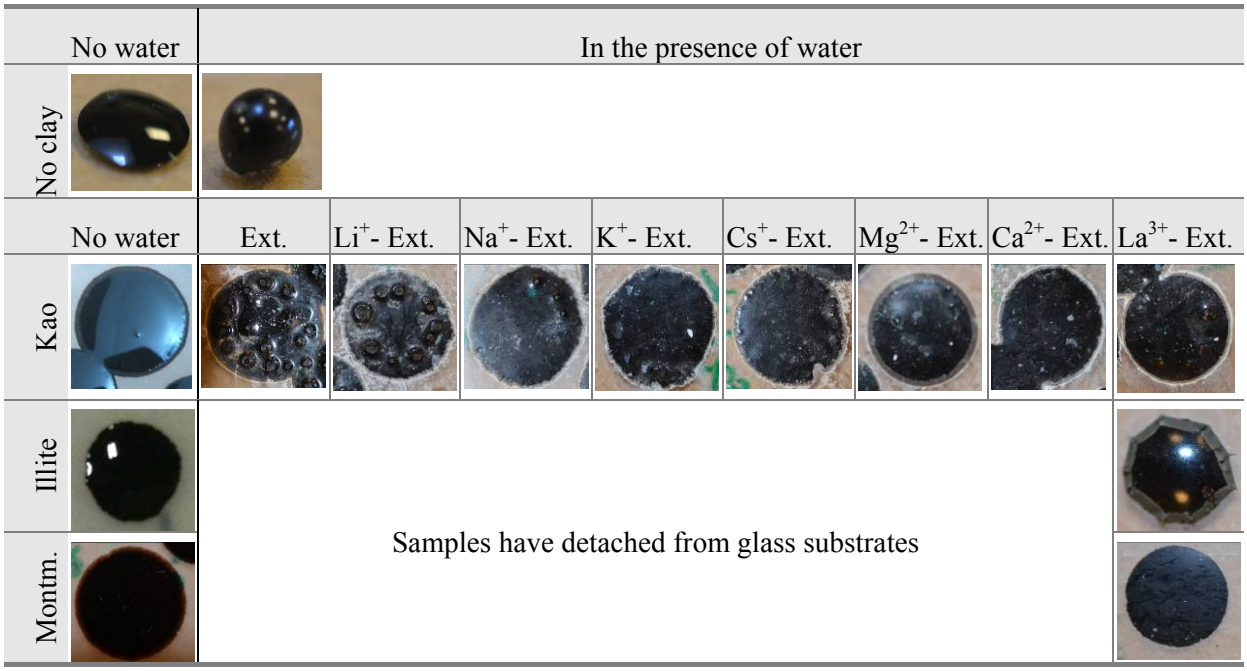

Figure 79 Screenshots of bitumen/clay thin sections after immersion for 3 days in ultra-pure water at 60°C (alternative test procedure).

3.3.5 Bitumen-clay compatibility (Oliensis spot test)

The compatibility of bitumen and clay was assessed from the degree of development of an oily ring surrounding a bitumen drop deposited on commercial clay thin films. Bitumen drops of constant volume and temperature (6 μ l $\pm$ 1.1; 140°C) were deposited on each clay thin film, kaolinite, illite, and

montmorillonite, and then immediately moved back into the oven at 140°C for 4 hours. Figure 80 shows the Oliensis test results on each clay type.

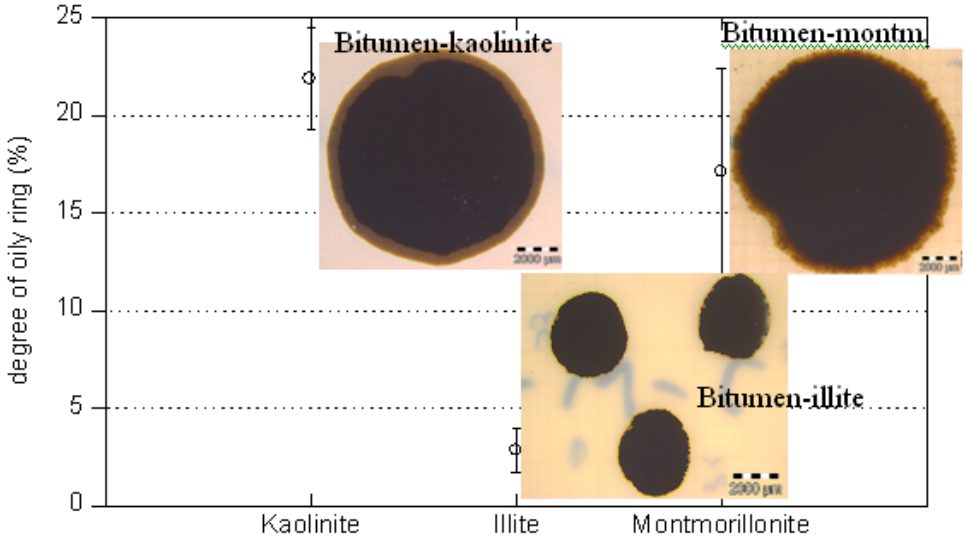

Figure 80 Screenshots of bitumen-commercial clay spots and calculated degree of Oliensis (ratio of the oily ring width to whole spot radius)

Whereas an oily ring is visible around the central drop on kaolinite and montmorillonite thin sections, evidencing segregation between bitumen compounds, no such phenomenon is visible on bitumen-illite thin sections. Furthermore, this segregation of bitumen tends to be concomitant with the development of a much larger contact area at bitumen-kaolinite and bitumen-montmorillonite interfaces when compared to that at bitumen-illite interface. In other words, kaolinite and montmorillonite surfaces have a better bitumen-wettability than illite surface.

Additional investigations have been carried out to explain bitumen segregation and bitumen-clay contact area differences evidenced on Figure 80. The negligible segregation of bitumen and the small contact area at bitumen-illite surface reflects poor affinity between bitumen and illite, which is consistent with the higher contact angle and the lower work of adhesion values depicted on Table 57 and Figure 75 (Eq.11) respectively. This is in agreement with the lower contact angle between illite and water compared to other clays (Figure 75).

The straw color of clear oil ring formed around the bitumen-kaolinite drop was determined to belong to the Saturates group. Such a high degree of segregation was probably due to the residual vapor-phase reaction of tetrahydrothiophene from saturates group which was catalyzed by alumina from kaolinite surface, whereas the large contact area might result from the low molecular weight of Saturated group contributing to their high mobility in a low pH environment (protonation) (*Masson and Collins 2008; Allsop et al. 1995*).

The acidic components from Asphaltenes and Resins such as anhydride and carboxylic acid seem to be responsible of the wide bitumen-montmorillonite contact area. Indeed, these acidic components are prone to bind with exchangeable cations upon losing their hydrogen (*Allsop et al. 1995; Bukka et al. 1994*). Accordingly, the large black bitumen-montmorillonite contact area reflects the spreading of high molecular

weight and high viscosity groups of bitumen, which were Asphaltenes and Resins, over the montmorillonite surface. Simultaneously, the expandable interlayer of montmorillonite facilitated the diffusion of low molecular weight and low viscosity groups of bitumen, causing the segregation of Saturates from bitumen which explains the straw color around bitumen-montmorillonite spots.

3.3.6 Summary

The interactions between clay thin films and bitumen in the presence of water molecules have been investigated from a micro-scale point of view. It was observed that contact angle measurement on clay surface using the static sessile drop method had to be performed with care, at least before significant drop volume change but once the drop diameter and area had stabilized. The impact of roughness on contact angle measurements was found negligible for the commercial clays. Furthermore, measured contact angles using water and diiodomethane were found to compare well with *Shang et al. (2010)* results, except for illite which was found more polar. Referring to *Chassin (1986)*, the high polarity of tested clays was found consistent with the laboratory conditions in which thin sections had been prepared and analyzed (60 – 75% relative humidity).

This study also provided useful information to explain water-bitumen-clay interaction from micro-aspect point of view. According to work of adhesion calculations, high risks of adhesive failure at bitumen-clay interface have been predicted, and cations substitutions were found inefficient to improve the binding except in the case of lanthanum, potassium and calcium. Stripping experimentations on thin sections confirmed predictions from calculations except for kaolinite. Explanations were suggested, in particular the modification of clay structure by Ca^{2+} and La^{3+} to prevent montmorillonite stripping or a reverse emulsion effect to explain binding persistence with kaolinite thin sections.

Finally, oliensis tests revealed large bitumen-clay contact area concomitant to bitumen segregation with montmorillonite and kaolinite, but no such phenomena with illite. Chemical explanations were suggested to explain these observations.

3.4 The water-bitumen-clay interaction from macro-aspects

3.4.1 Detecting stripping in AC mixtures from MB chemical probe

Seven specimens were prepared to investigate water intrusion into AC mixtures incorporating montmorillonite. To shorten the time needed for sample preparation, commercial montmorillonite was used. A reference specimen (N°1) made of pure bitumen was prepared, as well as a mastic specimen (N°2) made of 50% bitumen and 50% montmorillonite. The remaining five specimens comprised sand and coarse aggregates further to bitumen and clay (Figure 83), and they all had the same composition and mass, so that they only differed in terms of montmorillonite location in the AC mixtures (see Table 16 in chapter 2 for the detailed composition of the specimens):

- N°3: sand was coated with montmorillonite
- N°4: diorite (coarse fraction) was coated with montmorillonite
- N°5: diorite, sand and montmorillonite were separated during mixture processing (no coating)
- N°6: montmorillonite was aggregated to form montmorillonite-balls
- N°7: sand was coated with montmorillonite and then marinated with 3% quicklime, CaO (*National lime association from America, 2003)*.

These seven specimens were separately immersed in a MB solution and the residual MB concentration was measured every day. Then the residual compressive strength of AC mixtures was measured after 23 days in contact with the MB solution.

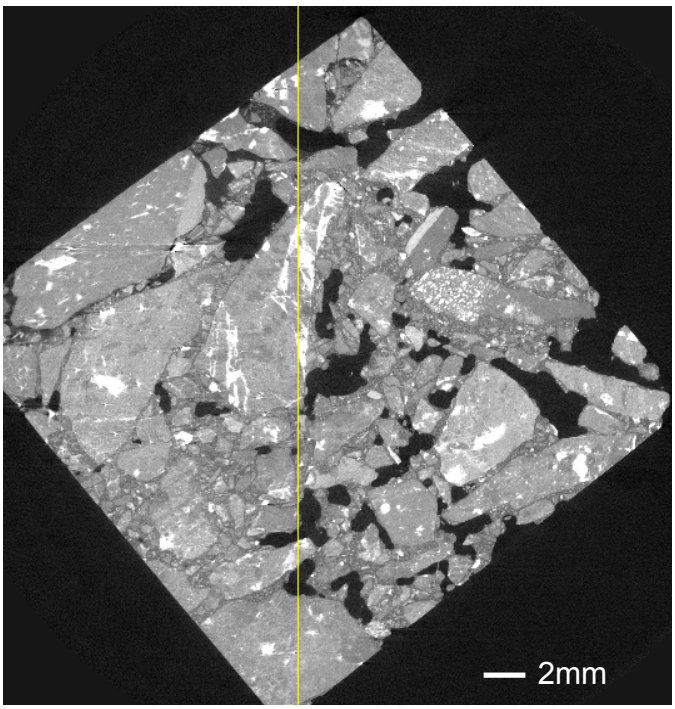

Figure 81 A image of AC mixture reconstructed by tomography. The sample was prepared as N°3

3.4.1.1 Degree of water intrusion

The MB adsorption value of each specimen was calculated from measured concentration and expressed as a percentage of the maximum MB adsorption value achieved among all specimens, this maximum being achieved by sample N° 6. Figure 80 depicts the MB adsorption curve of each specimen tested as a function of time. This figure shows that no MB adsorption occurred with pure bitumen (N°1), whereas montmorillonite-mastic (N°2) only moderately adsorbed MB molecules. Then, specimens N°3, N°5 and N°7 were found to adsorb more or less the same MB quantities, although specimen N°7 had been obtained from the lime-treatment of specimen N°3. Eventually, the specimen incorporating montmorillonite balls (N°6) had the highest MB adsorption, and the one with montmorillonite coated on coarse aggregates (N°4) ranked as the second highest MB adsorption. Hence, this MB adsorption experiment evidences that water may intrude into AC mixtures and that montmorillonite location impacts their water sensitivity.

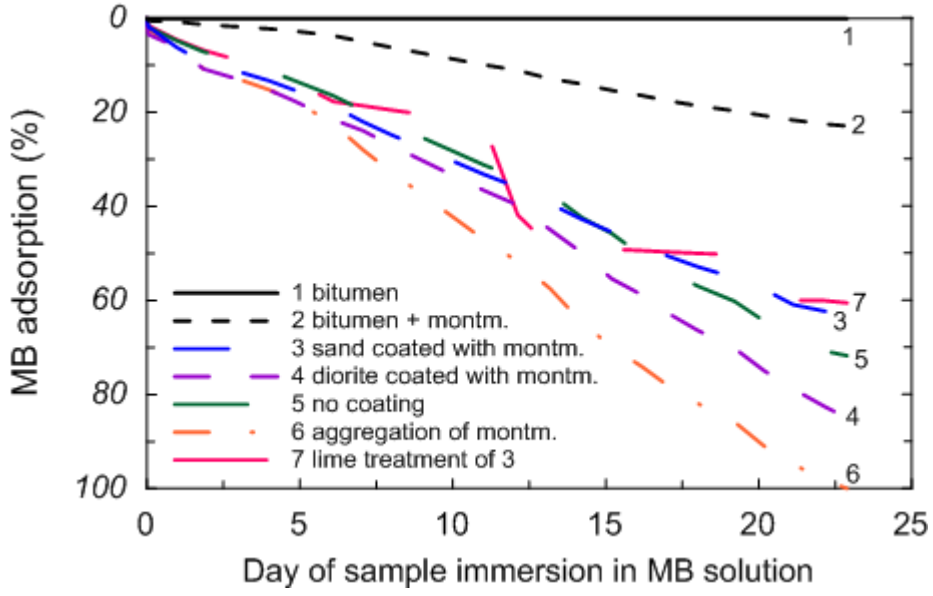

Figure 82 MB adsorption of various bituminous specimens as a function of time

The intrusion of water detected by MB adsorption in this study may be explained by (1) the non-perfect coating of aggregates with bitumen (*Frouin, 1989*) and (2) the development of channels at the interfacial zone between coarse aggregates and the fine aggregate matrix (FAM) through which water may circulate (*Arambula et al. 2010).* Indeed, bitumen non-perfect coating accelerated the water adsorption by the specimen with montmorillonite aggregated as balls (N°6), whereas water channels developing at the continuous interfacial zone accelerated the adsorption of water by the specimen in which montmorillonite is coated on coarse aggregates (N°4). Further to good binding properties between bitumen and mineral phases, a low viscosity of bitumen is necessary to improve its coating on mineral phases, which requires high temperature and low fines content.

Besides, AC mixture containing lime marinated fine aggregate (N°7) performed much higher MB adsorption than expected. After 4 days of immersion, the MB spectrum of specimen N°7 appeared to be shifted from 664 nm to 586 nm, and the color of the MB solution turned from blueish to purplish (Figure 83). The same peak shift phenomenon was observed and used to detect the synthesis of calcium hydrated silicate (C-S-H) in cement hydration reaction (*Beaudoin et. al. 2011*). In fact, the reason for this peak shift

is the impact of lime high pH value on MB molecules, which caused their aggregation to form high energy H-aggregates and biased the measurement of MB adsorption on sample N°7. Further details regarding these experimental results may be found in 3.2.3.

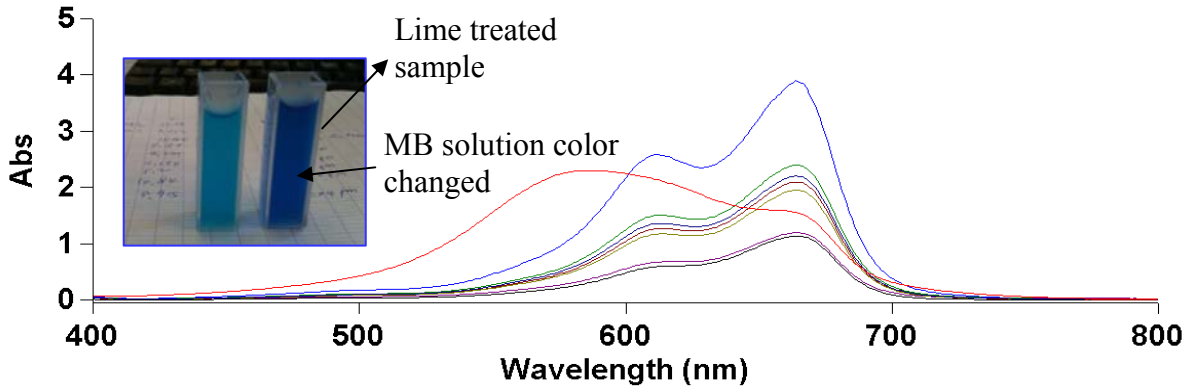

Figure 83 The H-aggregation formed in MB solution after 4th day of contact with lime treated sample.

3.4.1.2 Residual strength

After 23 days of immersion in the MB solution, the water sensitivity of AC specimens N°3 to N°7 was determined by measuring their compressive strength and calculating their I/C Duriez ratio (Figure 84). The I/C ratio was calculated from the residual compressive strength measured on immersed specimens divided by the compressive strength measured on non-immersed ones. The I/C ratio and standard deviation of specimens N°4, N°5, N°6 and N°7 were obtained from 2 repetitions, whereas the ratio of specimen N°3 resulted from 5 repetitions. Figure 84 shows that specimens N°3 to N°6 have more or less the same I/C ratio, which is much lower than that of specimen N°7.

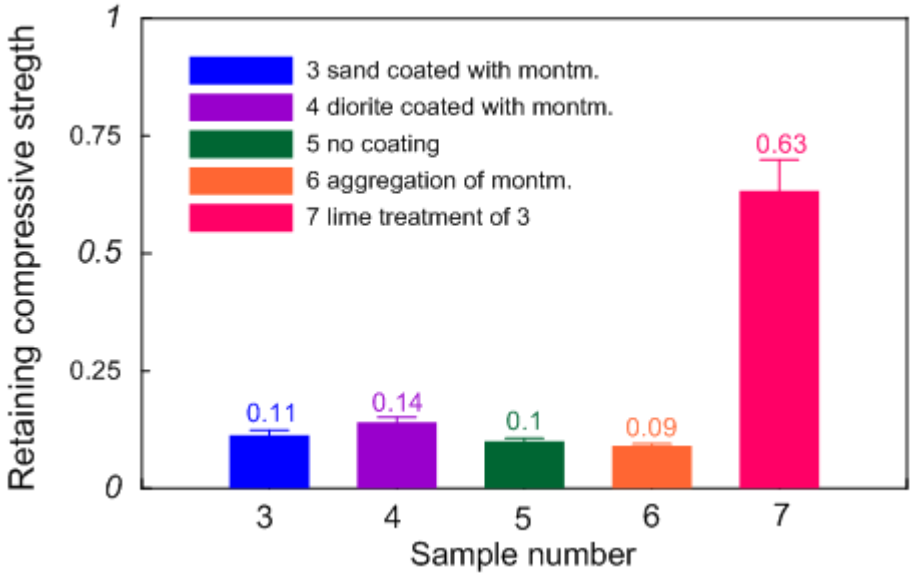

Figure 84 The retaining compressive strength of the AC mixture with various montmorillonite locations

The ranking of specimens N°3, N°5 and N°6 was found consistent with their ability to adsorb MB molecules, with specimen N°6 suffering both the highest MB adsorption and the lowest I/C ratio. However, a significantly high I/C ratio was observed with lime-treated specimen N°7. This result confirms that lime

used as an addition improves the mechanical behavior of AC mixtures immersed into water (*Tarrer and Wagh 1991*, *Lesueur et al. 2013).*

3.4.2 Water resistance related to the mineral composition of fines

The water sensitivity of AC mixtures comprising controlled quantities of well identified clay types have been assessed from Duriez tests. By analyzing the results, correlations were expected between clay composition and the water sensitivity of AC mixtures incorporating clay minerals.

3.4.2.1 The moisture susceptibility of AC mixture related to single type of clay in aggregates

Various quantities of extracted clays, kaolinite, illite and montmorillonite, were incorporated to AC mixtures having identical grading curves and bitumen film thickness (same richness modulus K, see Table 16 in chapter 2 for the details). Initially, the water sensitivity of AC mixtures containing a single clay type was measured using the Duriez test, and the resulting I/C values were analyzed to find correlations. For each AC mixture tested, Table 60 summarizes the composition of its 0/2 mm fraction, the proportion of clay in the 0/2 mm fraction and in the total mixture, the measured void ratio and Duriez value. Appropriate quantities of limestone filler were added to the AC mixtures to achieve 9% fines in total mixture.

Table 60 Clay mineralogy and quantity in AC mixtures, measured void ratio and water resistance.

Mixture	Composition of the 0/2mm fraction (%)				clay in 0/2mm fraction [b] (%)	Clay in total mixture [c] (%)	Void ratio of AC mixture (%)	Duriez (I/C)	S.D.
	sand	kao	illite	montm					
Reference	100.0	0.0	0.0	0.0	0.0	0.0	9.9	1.00	0.07
S1 K2	78.6	21.4	0.0	0.0	21.4	4.4	-[a]	0.94	0.03
S1 K3	70.0	30.0	0.0	0.0	30.0	6.9	-[a]	0.87	0.04
Max. Kao	65.4	34.6	0.0	0.0	34.6	8.5	12.5	0.74	0.06
S1 I4	92.8	0.0	7.2	0.0	7.2	1.2	-[a]	0.89	0.03
S1 I9	80.0	0.0	20.0	0.0	20.0	4.0	10.3	0.77	0.03
S1 I13	70.0	0.0	30.0	0.0	30.0	6.9	10.0	0.60	0.03
Max. Illite	63.9	0.0	36.1	0.0	36.1	9.0	9.3	0.56	0.03
S1 M2	99.5	0.0	0.0	0.5	0.5	0.1	11.1	0.90	0.05
S1 M4	98.6	0.0	0.0	1.4	1.4	0.2	11.2	0.87	0.14
S1 M12	95.2	0.0	0.0	4.8	4.8	0.8	11.6	0.75	0.05
Max. Montm	65.1	0.0	0.0	34.9	34.9	8.6	9.5	0.11	0.01

[a] the void ratio was not reported
[b] limestone filler (< 0.063 mm) is added to achieve 36% fines in the 0/2 mm fraction
[c] total mixture includes clay, filler, sand and diorite

The water sensitivity of AC mixtures was successfully observed in this study and the selected void ratios were among the most critical values inducing stripping, 6% and 14% (*Bahia, 1999; Birgisson et al 2003, Kandhal and Rickarda, 2001, Terrel and Shute 1994*). Duriez ratio was calculated from compressive strength values measured after 28 days of immersion in water. As shown in Table 60, the reference AC mixture containing no clay yielded a Duriez ratio of one, evidencing the absence of water sensitivity

(*Cheng et al, 2002*). For a given clay type, the water resistance of AC mixtures was found to decrease with increasing clay quantity.

For each clay type, Figure 85 depicts the variations of clay content and Duriez values. According to French practice, water resistant AC mixtures have their Duriez ratios in excess of 0.8 ($ITSR_{80}$, *Delorme and Wendling 2007*). Figure 85 shows that clay-rich AC mixtures have Duriez ratios below 0.8, meaning that the presence of clay decreased their water resistance. Given the location of clay at the aggregate-bitumen interface, stripping was responsible of the Duriez value decrease, and void ratio had negligible effect. Furthermore, the water resistance of AC mixtures varies with clay mineralogy, kaolinite-AC mixtures being less affected than illite- and far less than montmorillonite-AC mixtures.

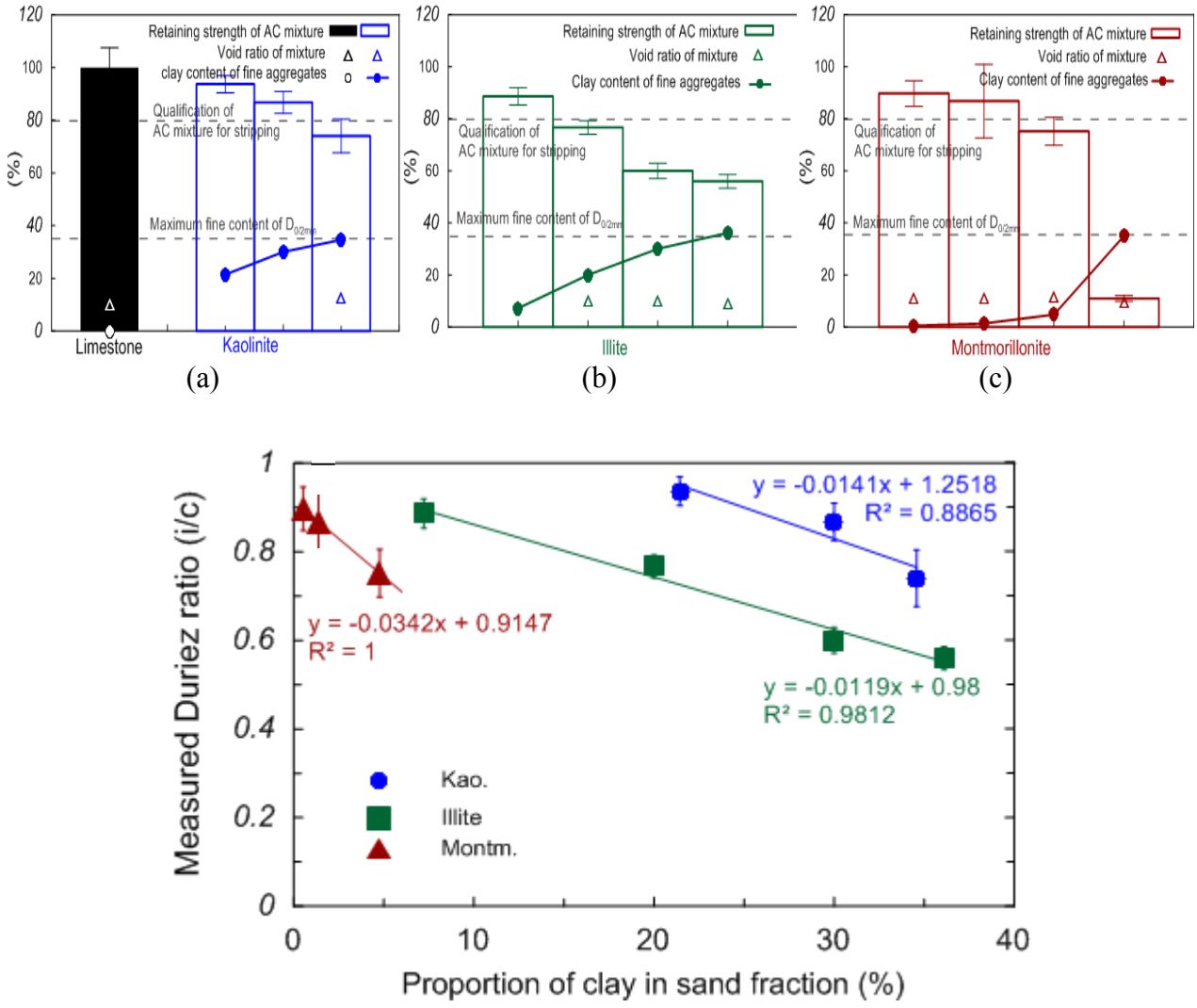

Figure 85 Duriez ratios measured on AC mixtures as a function of clay content of the fine aggregate fraction for (a) kaolinite, (b) illite and (c) montmorillonite.

Eventually, the following three experimental linear regressions have been calculated from Duriez ratios represented as a function of the kaolinite content (x), illite content (y) or montmorillonite content (z) of the sand fraction (expressed as a percententage):

I/C = 1 if $x \leq 18$ and I/C = -0.0141x +1.25 if x>18 ($R^2 = 0.89$)

I/C = -0.0119y +0.98 ($R^2 = 0.98$)

I/C= -0.0342z +0.91 ($R^2 = 1$)

Note that at least 18% of kaolinite is required in the fine aggregate fraction to decrease the Duriez value below 1.

3.4.2.2 The water sensitivity of AC mixtures related to clay content of fine aggregates

Figure 86 depicts the Duriez ratio measured for all series tested (S1, S2 and S3) as a function of clay content in the fine aggregate (sand) fraction. The design of these artificial fine aggregates incorporating known quantities of up to three clay types as well as corresponding AC mixture design is detailed in appendix 5.3. The void ratio of AC mixtures was measured following the Duriez protocol and it was found fairly constant between all tested samples (in the range 9 to 12 %). Figure 86 evidences significant differences between Duriez ratios from one sample to another.

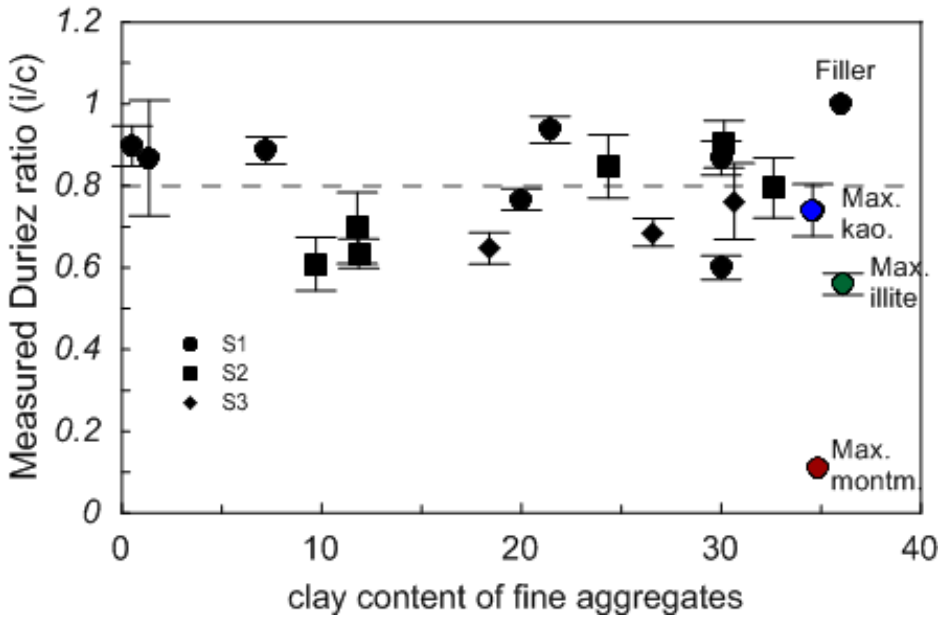

Figure 86 Duriez ratios of AC mixtures as a function of clay content of the fine aggregates fraction

3.4.2.3 Assessment of Duriez ratios from combination-law

Regression laws experimentally determined in paragraph 3.4.2.1 were used to predict the Duriez ratio of S2 and S3 AC mixtures knowing the clay composition of their fine aggregates. For this purpose, a Duriez ratio was calculated from the proportion of each clay type in the fine aggregate fraction as if it were the only one present, and the product of these Duriez ratio was performed to assess the Duriez ratio of the AC mixture. Calculated and measured Duriez ratios of S2 and S3 series have been summarized in Table 61.

Table 61 Comparison between calculated and measured Duriez values for S2 and S3 series incorporating 2 and 3 clay types respectively

Sample	clay content of sand fraction (%)			Duriez calculation from regression and combination law				Measured Duriez	
	kao	illite	montm	i/C-kao	i/C-illite	i/C-montm	combination	(i/c)	S.D.
	(x)	(y)	(z)				i/C= i/C-kao· i/C-illit· i/C-montm.		
S2-KI2	26.3	6.4	0.0	0.88	0.90	1	0.80	0.79	0.07
S2-KI8	8.9	15.4	0.0	1	0.80	1	0.80	0.85	0.08
S2-IM6	0.0	7.5	4.3	1	0.89	0.76	0.68	0.70	0.09
S2-IM10	0.0	3.6	6.2	1	0.94	0.70	0.65	0.61	0.07
S2-KM3	27.2	0.0	2.9	0.87	1	0.81	0.70	0.90	0.06
S2-KM11	4.3	0.0	7.5	1	1	0.65	0.65	0.63	0.04
S3-2	28.4	1.6	0.7	0.85	0.96	0.89	0.72	0.76	0.09
S3-3	16.6	6.9	3.1	1	0.90	0.80	0.72	0.69	0.03
S3-5	9.6	3.2	5.6	1	0.94	0.72	0.68	0.65	0.04

Estimated Duriez ratios of S2 and S3 series of AC mixtures have also been represented as a function of corresponding measured Duriez ratios (Figure 87). Most samples show fairly good relation between measured and estimated Duriez ratios except for S2-KM3. This good comparison between measured and estimated Duriez value suggests that the moisture susceptibility of AC mixtures may be assessed from precise knowledge of the clay composition of fine aggregates. However, the small scattering on Duriez value may derive either by the approximated clay content used to estimate Duriez value (the true clay content calculated from clay mineralogy of raw material was not applied here) or by the experimental standard deviation of measured Duriez results.

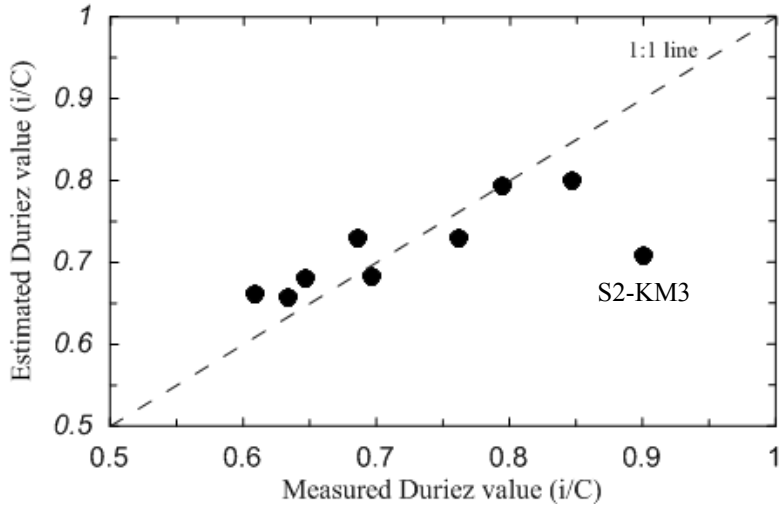

Figure 87 Comparison between calculated and measured Duriez ratios of AC mixtures containing several clay types (S2 and S3 series)

3.4.3 Summary

The water resistance of AC mixtures incorporating clay in their fine aggregate fraction was studied from a mineralogical perspective. These AC mixtures were prepared under the same conditions but with variable contents of extracted kaolinite, illite and montmorillonite.

The water sensitivity of AC mixtures incorporating montmorillonite was first studied using MB as a chemical probe. According to the results, water intruded into AC mixtures through interfacial zone and transitional channels. The lime treated fine aggregates suffered the lowest water sensitivity whereas its high pH biased the MB adsorption.

Then, Duriez tests were performed on AC mixtures incorporating known quantities of various clay types. Tests performed on AC mixtures incorporating known quantities of a unique clay type allowed to determine simple relations between Duriez ratios and clay quantities, which were further combined to predict the Duriez ratios of AC mixtures incorporating known quantities of up to three clay types. Predicted results were found in fairly good agreement with measured Duriez ratios. The water resistance of AC mixtures was found to vary with clay mineralogy, kaolinite-AC mixtures being less affected than illite- and far less than montmorillonite-AC mixtures. On the other hand, Duriez values bore no relation to the global fines content in aggregates if no attention is paid to their mineralogy.

The identified regressions and combination law could be a means to evaluate the Duriez value if the quantity of each clay type was known. Hence, establishing a fast and accurate mineralogical analysis method for fine aggregates will be the next priority.

Chapter 4 Discussions

In the discussion part, the correlations between the different characteristics measured on artificial and unknown fine aggregates will be discussed and then a new methodology for sand qualification will be exposed based on experimental results obtained in this study.

4.1 Correlations between mineralogy, Duriez test, surface energy measurements, cation exchange capacity and methylene blue value,

4.1.1 The correlation between MB adsorption, cation exchange capacity and clay mineralogy in fine aggregates

The correlations between CEC or MB and mineralogy have been well known for a long time. CEC or MB are considered until now as good indicator of clay mineralogy even if they remained "global" indicator used in several classifications (CEC and MB were global characteristics based on the surface reactivity of fine aggregates particles in contact with different chemical probes). To validate the good correlation between CEC or MB and mineralogy, the characteristics of artificial and unknown fine aggregates were crossed. The correlations were discussed from the experimental results in Table 62 and the localization of the different tested materials in Figure 88 and Figure 89.

The clay quantity in each sample was estimated using TOPAS method or complementary method. In order to increase the number of point to better correlate the fine aggregate properties, the clay composition in the artificial fine aggregates was calculated using the percentage of extracted clay in the mixture and the mineralogical composition of extracted clays measured by (a) complementary method or (b) Topas method.

Globally, the Figure 88 and Figure 89 demonstrated that for artificial fine aggregates, the kaolinite content didn't govern the MB_{phot}, MB_{drop} or MB_{CEC} evolution. MB_{CEC} (g/kg) instead of CEC (meq/100g) was introduced in this chapter. It corresponded to the equivalent mass of adsorbed MB^{+} calculated from the quantity of negative surface charge measured by the cobaltihexamine test for CEC measurement.

$$MB_{CEC}\ (g/kg) = CEC\ (meq/100g) \times 319.9/\ 100$$

with 319.9 g/mol = the molar mass of methylene blue compound.

The kaolinite content had a low impact on the measured parameters as fine aggregates with high or low MB_{phot}, MB_{drop} or MB_{CEC} might have high or low kaolinite content too. It seemed not to be the case for illite and montmorillonite that can appear only in a limited zone (delimited by a dashed line). Such limit is correlated to the MB or CEC of raw extracted clay used to prepare mixtures. Indeed, experimental results demonstrated that MB or CEC followed quite well a additivity law that's to say:

$$X = X_{pure\ illite}\,(\%illite) + X_{pure\ kaolinite}(\%kaolinite) + X_{pure\ montm.}(\%montm.)$$

with X = MB, CEC… and (%phase i) the quantity of phase i in the mixture

Table 62 CEC and MB adsorption on fine aggregates and Duriez test on associated AC mixture

Mixture	Calculated quantities (compl. method)[a]			Measured quantities (compl. method)			Calculated quantities (TOPAS method)[a]			Measured quantities (TOPAS method)			Measured CEC (meq/100g)	MB adsorption (g/kg)		MB $_{CEC}$ (g/kg)	Duriez (i/C)	
	kao	illite	montm	kao	illite	montm	kao	illite	montm	kao	illite	montm		Drop	UV-Phot.		value	S.D
Sand	0.00	0.00	0.00				0.00	0.00	0.00	0.00	0.00	0.00	0.00			0.32	1	0.07
S1 K2	15.99	2.66	0.00				16.16	2.71	0.00					2.20			0.94	0.03
S1 K3	22.38	3.72	0.00				22.62	3.79	0.00	25.13	5.99	0.00	1.17	2.20	2.04	3.74	0.87	0.04
Kao-ref.	25.79	4.29	0.00				26.07	4.37	0.00	26.07	4.37						0.74	0.06
S1 I4	0.27	4.90	0.00				1.11	5.06	0.00				1.67	4.70	3.30	5.34	0.89	0.03
S1 I9	0.74	13.59	0.00				3.09	14.02	0.00				4.23	11.20	7.72	13.52	0.77	0.03
S1 I13	1.11	20.39	0.00	3.00	22	0.00	4.63	21.03	0.00	4.96	19.73	0.00	8.94	19.60	16.53	28.57	0.60	0.03
Illite-ref.	1.34	24.53	0.00				5.57	25.30	0.00								0.56	0.03
S1 M2	0.03	0.04	0.44				0.00	0.00	0.42				0.86	2.20	1.84	2.75	0.90	0.05
S1 M4	0.07	0.11	1.16				0.00	0.00	1.12				1.83	5.00	4.53	5.85	0.87	0.14
S1 M12	0.24	0.38	4.05	1.00	1	3.50	0.00	0.00	3.89				5.65	16.10	9.99	18.06	0.75	0.05
Mont-ref.	1.75	2.79	29.62				0.00	0.00	28.44								0.11	0.01
S2-KI2	19.83	7.57	0.00	22.00	6	0.00	20.79	7.77	0.00	20.02	7.74	0.00	3.88	9.70	5.61	12.40	0.79	0.07
S2-KI8	7.22	11.59	0.00	3.20	16	0.00	9.10	11.94	0.00	3.94	16.39	0.99	7.65	20.30	13.31	24.45	0.85	0.08
S2-IM6	0.49	5.42	3.66				1.15	5.24	3.51				6.28	18.10	11.48	20.07	0.70	0.09
S2-IM10	0.44	2.91	5.23				0.55	2.49	5.02					20.60			0.61	0.07
S2-KM3	20.47	3.61	2.46				20.54	3.44	2.36				4.46	12.20	9.57	14.25	0.90	0.06
S2-KM11	3.61	1.14	6.38				3.27	0.55	6.12					19.40			0.63	0.04
S3-2	21.30	4.64	0.56				21.68	4.68	0.54					5.80			0.76	0.09
S3-3	12.81	7.01	2.58	7.00	15	2.60	13.61	6.95	2.48	10.87	10.48	4.31	5.73	12.50	10.35	18.31	0.69	0.03
S3-5	7.57	3.82	4.73				7.74	3.47	4.54					15.10			0.65	0.04
A				0.20	2.00	7.00				1.80	5.70		2.16	2.54	2.83	6.90	0.85	--
B				0.15	0.00	2.00				0.00	0.00	0.00	1.59	1.50	1.40	5.08	0.83	--
C				0.00	3.00	12.00				0.00	24.21	8.07	8.10	9.00	9.12	25.89	0.64	--
D				11.00	0.30	0.00				11.10	0.00	0.00	0.90	1.73	1.39	2.88	1.03	--
E				0.80	1.00	0.30				0.00	0.00	0.00	0.51	1.74	1.45	1.63	0.93	--

[a] The mineralogical composition of artificial fine aggregates is calculated using the percentage of extracted clay added in the mixture and the mineralogical composition of extracted clays measured by complementary method or Topas method. [b] MB $_{CEC}$ (g/kg) = CEC (meq/100g) x 319.9 / 100

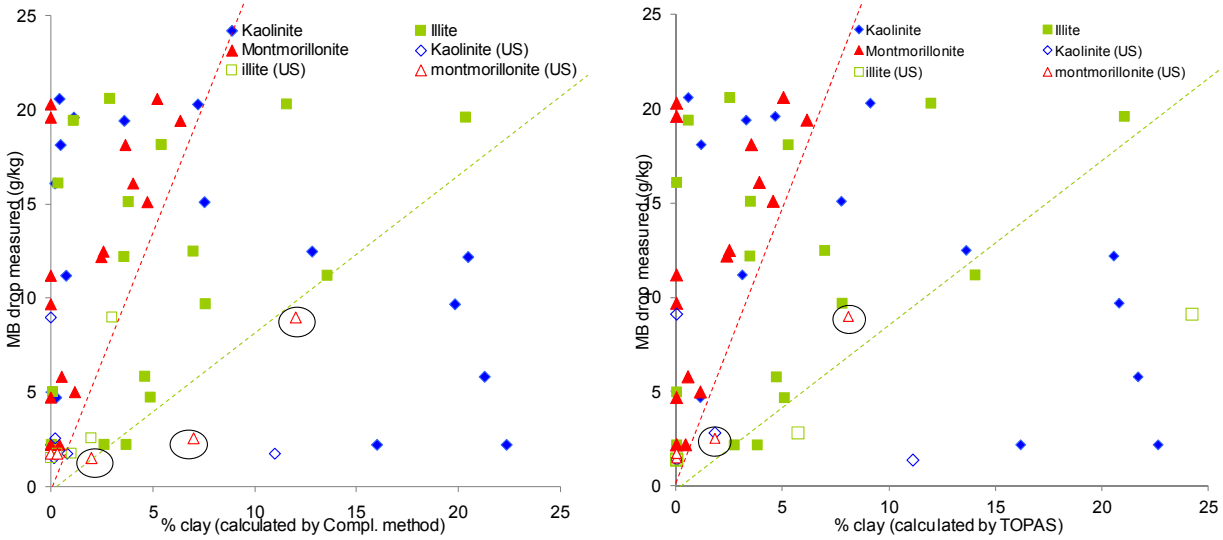

(a) (b)

Figure 88 MB_{drop} versus the mineralogical composition of fine aggregates. The mineralogical composition of artificial fine aggregate is calculated using the percentage of extracted clay in mixture and the mineralogical composition of extracted clays measured by (a) complementary method or (b) Topas method. The mineralogical composition of unknown fine aggregates (noted US for unknown sand) is evaluated experimentally by (a) complementary method or (b) Topas method.

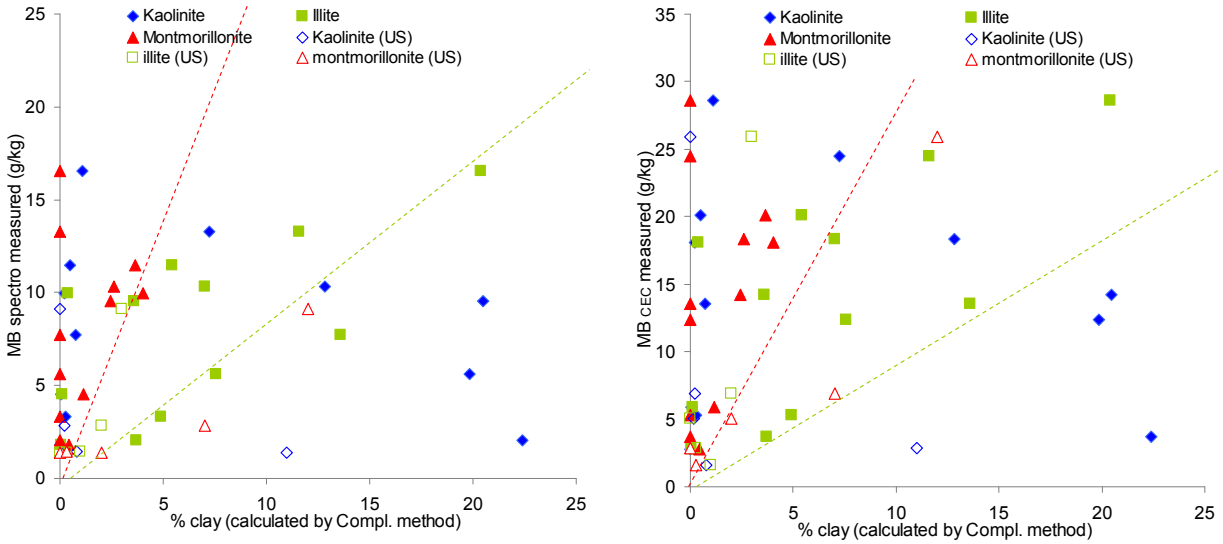

(a) (b)

Figure 89 (a) MB_{Phot} and (b) MB_{CEC} versus the mineralogical composition of fine aggregates. The mineralogical composition of artificial fine aggregate is calculated using the percentage of extracted clay in mixture and the mineralogical composition of extracted clays measured by complementary method. The mineralogical composition of unknown fine aggregates (noted US for unknown sand) is evaluated experimentally by complementary method.

A more general delimitation of the illite or montmorillonite zone needed the test of the widest set of pure clays or the use of the range of CEC (and MB) given in literature review. As the CEC values measured on extracted clays used in this work (in Table 63) didn't reach the lowest value of the CEC range for kaolinite or illite given in literature, a larger illite or montmorillonite was expected (in other words, the

slope of the dashed line had to decrease to take into account all the types of illite or montmorillonite clays).

Table 63 Average CEC values for pure clays from literature and CEC valued measured on extracted clays.

Type of clay	Range of CEC (meq/100g) from literature	Measured CEC of extracted clays (meq/100g)
Kaolinite	3-15	1.3
Illite	10-40	23.3
Mont.	70-120	103.6
Vermiculite	100-150	--

The observations on artificial fine aggregates agreed with the results from Lautrin (1987) in Figure 90. Author studied several types of soil (composed by pure clay or several phases). The standardized measurements of MB value (noted VB in soil domain) were correlated to the clay mineralogy in soil. Only the montmorillonite content seemed to control the VB value and not the illite content as observed on our results. Note that the scale of observation as well as the number of tested soils impacted the results (the MB values met in aggregates domain was generally lower than the VB met in clayey soils).

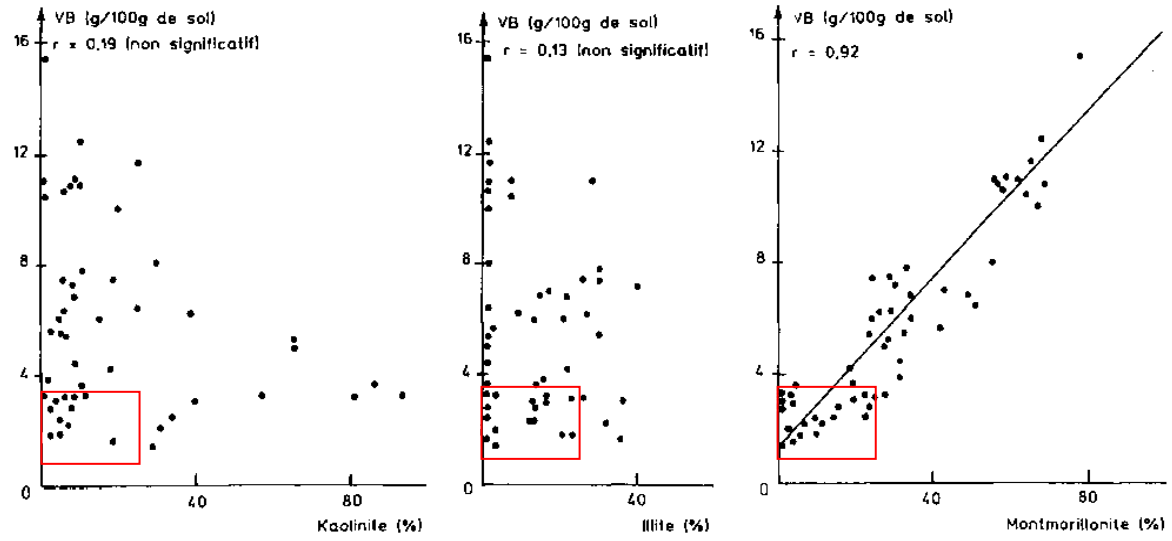

Figure 90 Correlation between MB_{drop} (from the standardized MB test in soil domain *NFP18592 (1980)* applied on the 0-400µm fraction of soil with probably no drying before test) and mineralogy of the tested soil (*Lautrin, 1987*). The red box gives an indication of position of studied artificial fine aggregates (even if the direct comparison is not possible because of the difference in the protocol of MB measurement).

Now, the Figure 88 and Figure 89 revealed that the unknown fine aggregates didn't behave as expected from artificial fine aggregates. Their content of vermiculite (drawn in place of montmorillonite because of its high CEC near 100-150 meq/100g) should have imposed a higher MB or CEC. Such behavior might confirm that the slope of the dashed line had to be decreased considering the nature of the swelling clay present in the unknown fine aggregates. It might come also from an inaccuracy in quantification (quantitative results from the different applied methods varied) but a other explanation might be

proposed. As it concerned above all the samples A and C that's to say the gneiss or rhyolitic sands, the lower MB or CEC might come from the nature of the coarse grains in sand. The petrographic study revealed their alteration and the probable presence of clay phases inside the coarse grains. Such clays were quantified by X-ray diffraction after the 32 µm grinding, while MB or CEC ignored them if the covering of only coarse grains external surface was taken as hypothesis. Such aspect should be investigated in next studies on natural sands by the quantification of clay phases on several size fractions (separated by grinding and then ground for X-ray analysis).

4.1.2 The correlation between Duriez value and mineralogy of clays in fine aggregates

The water sensitivity (stripping) of AC mixture induced by clays was studied by testing filler, kaolinite, illite and montmorillonite mixed with bitumen. The water resistance of AC mixtures triggered by clay (results see 3.4.2) may be examined as a function of clay composition in light of test results, water-bitumen-clay interactions from micro-aspects (3.3) and water intrusion tests (3.4.1). In the case of kaolinite-AC mixtures, the waterproof bitumen-kaolinite binding probably consists, on the bitumen side, of dispersive compounds and, on kaolinite side, silanol groups on kaolinite surface. After the system in contact with water, the acidic components segregated from bitumen-kaolinite binding interacted with water on bitumen side, which is the cohesive failure. Then, the lowest diffusion coefficient from pure bitumen in AC mixture indicated the low contribution of moisture susceptibility from bitumen-kaolinite interaction. On kaolinite-glass side, the far less exchangeable cation from kaolinite (CEC=1.3 meq/100 g) than illite and montmorillonite constrained water molecules diffusing through kaolinite particle and interlayer. Therefore, the water resistance of AC mixture was less affected by kaolinite presenting in AC mixture than illite and montmorillonite.

The bitumen binding with illite and montmorillonite occurred between acidic components from bitumen side and cations from clay side. The stripping occurred because work of adhesion from water-clay was much higher than the work of adhesion from bitumen-clay, so called adhesive failure. Even though illite was poorly coated with bitumen than kaolinite- and montmorillonite- bitumen coating due to its less segregation, the CEC value (23.3meq/100g) lower than montmorillonite derived the intermediate water resistance of illite-AC mixture. Water molecules were less adsorbed on illite particles than on montmorillonite. Consequently, the higher amount interfacial zone and transition water channels formed in montmorillonite-AC mixture than illite-AC mixture. Therefore, stripping depended on the capability of water to enter in AC mixture, either by following the continuous interfacial zone between bitumen-clay mastics and coarse grain surface (creating channels for water in AC mixture), either by diffusing within the bitumen-clay mastics.

The works of adhesions from bitumen-clay interaction are similar to each other and much lower than work of adhesion from water-clay interaction except K^+- and La^{3+}- montmorillonite. Regarding the low moisture susceptibility of kaolinite-AC mixture, the pinhole observed on bitumen-intact-kaolinite and bitumen-Li^+-kaolinite samples in the presence of water is the evidence of the cohesive failure from bitumen. The reason is that the emulsification of the polar components on bitumen side of bitumen-

kaolinite interaction loses the bonding strength by water hydrolysis (*Fromm, 1974*). The high water resistance of kaolinite-AC mixture derived from this non-polar interaction on bitumen-kaolinite interface with the non-swelling property of kaolinite constrains the water intrusion into the kaolinite-AC mixture. It is also evidenced by all the bitumen-kaolinite samples survive on the glass substrates in the presence of water, and kaolinite-AC mixture has the highest water resistance than other clays-AC mixtures according to Duriez results.

The bitumen-illite and bitumen-montmorillonite samples detach from their glass substrates in the presence of water except bitumen interacts with La^{3+}-illite and La^{3+}-montmorillonite samples, and it indicates that the stripping of illite-AC mixture and montmorillonite-AC mixture occurs along the interfacial zone between bitumen-clay mastics and the substrate. The reason is that La^{3+} not only contributes the lowest work of adhesion between water and clays, but also induces the collapses of the clay interlayer and blocks the water transitional channels. Therefore, the stripping of AC mixture containing swelling clays in fine aggregates is also related to their swelling properties presenting in the interfacial zone and the transitional channels apart from the water-bitumen-clay interaction. It is the reason why the decrease of Duriez values is in a good accordance with the increase of swelling properties of clays in AC mixture. Therefore, stripping can be judged either by Duriez value from AC mixture or by the mineralogy of clay in fine aggregates.

The AC mixture with calcareous filler added to aggregates showed a full water resistance, whereas the siliceous clays in fine aggregates induced various stripping in AC mixture in relation with the clay mineralogy. The Figure 89 presented the results of Duriez test (i/C) versus the mineralogical composition of fine aggregates.

Considering the 0.8 Duriez threshold imposed for fine aggregate qualification, high or low amount of kaolinite in aggregates might produce qualification or non qualification. Considering that the Duriez test applied on the kaolinite sand mixture with almost the highest permitted quantity of fine particles (around 26 %) gave 0.74 (close to 0.8), the clays other than kaolinite controlled the stripping phenomenon except when kaolinite was in high content. The bitumen-kaolinite interaction could explain the triggered stripping in AC mixtures because it didn't provide efficient interfacial zone or water channels in kaolinite-AC mixture. The non-swelling property of kaolinite and the cohesive failure are responsible for the kaolinite-AC stripping.

For illite in fine aggregates, a limit at 12.5% of illite in mixture seemed to appear on Figure 91. This limit of content divided illite sand mixtures into two groups, the first where Duriez value was systematically below the 0.8 threshold and the second one where Duriez value might be upper or lower than 0.8. Such limit was linked to the mineralogical characteristics of illite present in the tested extracted illite and had to be validated on natural sands and other type of illite. Then, a more general limit should be identified.

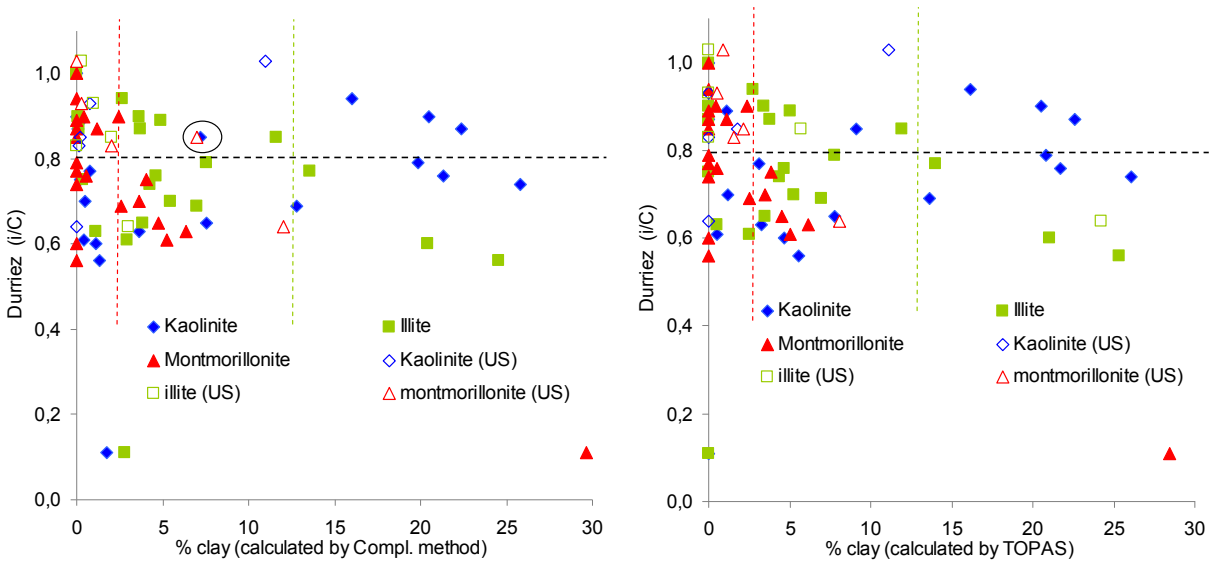

Figure 91 Duriez value (i/C) versus the mineralogical composition of fine aggregates. The mineralogical composition of artificial fine aggregate is calculated using the percentage of extracted clay in mixture and the mineralogical composition of extracted clays measured by (a) complementary method or (b) Topas method. The mineralogical composition of unknown fine aggregates (noted US for unknown sand) is evaluated experimentally by (a) complementary method or (b) Topas method.

Montmorillonite mixed with sand behaved as illite sand mixture. As expected, the limit for montmorillonite around 2.5% is lower than the limit with illite. The conclusions didn't vary with the method of clay quantification (complementary or TOPAS method) except for one natural sand (the circled point) that contained vermiculite instead of montmorillonite. The test of other natural sands should allow to better identify the highest montmorillonite content. The lower required quantity of montmorillonite to trigger stripping can be interpreted by the high efficiency of interfacial zone between coarse grain coated with montmorillonite particles to let water passing through AC mixture. The high swelling properties of montmorillonite probably contributed to enhance stripping phenomenon, whereas illite with lower swelling (water sensitivity) impacted more weakly on stripping.

Considering now the water/clay/bitumen interaction from surface energy point of view, the stripping in AC mixtures induced by clays was linked to bitumen-clay interaction in the presence of water. Clay mineralogy which affects the work of adhesion and the compactability governs the bitumen-clay interaction from clay side. Generally, clay surfaces are characterized by higher polar forces than dispersive forces (from surface energy measurement), and perform higher work of adhesion during water-clay interaction than bitumen-clay interaction. Therefore, clay is more sensitive toward water compared to bitumen and it triggers stripping in AC mixture. Moreover, at long time, kaolinite composition and montmorillonite properties may induce the segregation of bitumen components during their interaction. Bitumen-kaolinite binds with dispersive components of bitumen whereas bitumen-montmorillonite binds with the polar one. The segregated polar components of bitumen at bitumen-kaolinite interface attract water and induce the cohesive failure from bitumen side. The polar components at bitumen/montmorillonite interface trigger water adsorption on high swelling clay (such as

montmorillonite). Free cations onto clay surface affect the water-bitumen-clay interaction according to their hydration energy and by affecting also the clay surface energy and the clay swelling property.

4.1.3 Correlations between CEC value, MB value and Duriez test

In order to examine the MB or CEC values with the Duriez test results, Figure 92 depicts the correlated results from Table 62. An interesting trend was observed : AC mixtures with artificial fine aggregates, S1-K2, S1-K3, S1-I4, S1-M2, S1-M4, S2-KI8, S2-KM3 and unknown sample A presented qualifying Duriez values (i/C > 0.8) with non-qualifying MB_{drop} values (MB_{drop}< 2). It meant that these eight sands would be rejected actually considering the rules for fine aggregates qualification while experimental results in this study proved the possibility to use them for hot asphalt mixing.

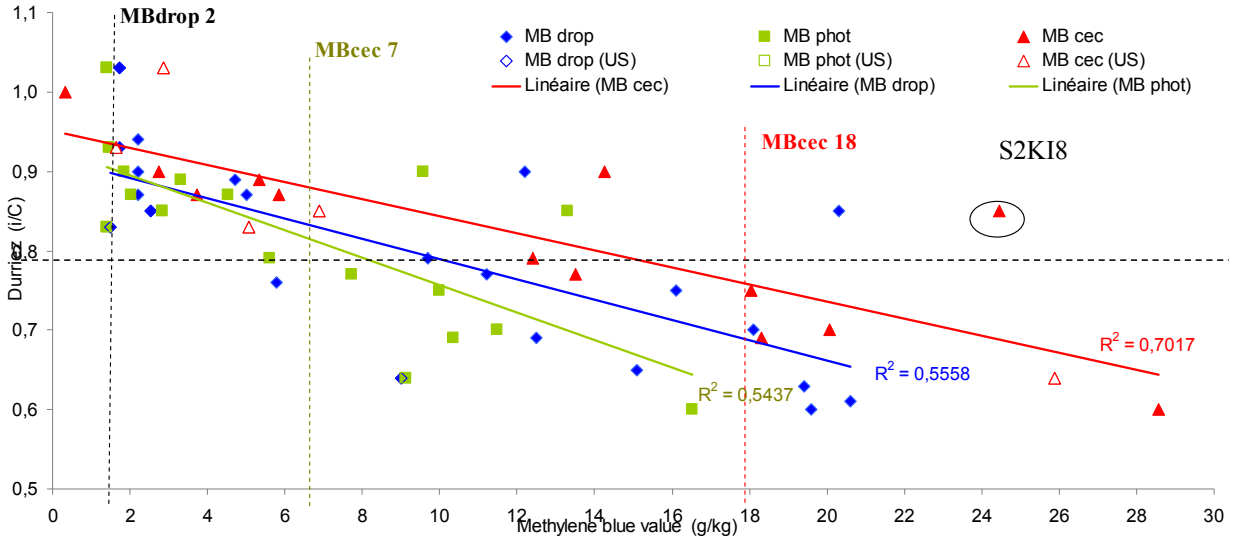

Figure 92 Correlation between Duriez value measured on AC mixtures (BBTM type) and MB_{drop} (g/kg) , $MB_{Phot.}$ (g/kg) and MB_{CEC} (g/kg) values measured on corresponding fine aggregates (with MB_{CEC} (g/kg) = CEC (meq/100g) x 319,85/100). US is for unknown fine aggregates while the other measurements came from artificial fine aggregates.

The possibility to push back the threshold to qualify fine aggregates appeared clearly by defining different zones using the localization of the points on Figure 92 (the points coupled Duriez values with MB_{phot} (for photometric method) or MB_{drop} (for standardized drop method) or MB_{CEC} (with MB_{CEC} (g/kg) = CEC (meq/100g) x 319,85/100).

To chose between these 3 parameters, the coefficient of determination from measured values (R^2 associated to the linear fit of each set of data) was observed. R^2 values demonstrated that Duriez results were better correlated to MB_{CEC} values (R^2 = 0.7) than MB_{Phot} (R^2 = 0.55) or MB_{drop} (R^2 = 0.54). Such results confirmed that the chemical probe used to investigate the clay surface charge was determinant. If MB value might vary with several parameters the effect of which were previously described in Chapter 3,

the methodology to measure CEC value was simpler because of the lower effect of contact time, the absence of cobaltihexamine ions aggregation effect (like MB molecule aggregation) and the non impact of initial ion covering percentage on CEC measure (contrary to initial MB covering percentage). The CEC measurement was an easy method (colorimetric method using UV spectrophotometer) applied by pedologists since 30 years with available standards. If the nature of the cations (except perhaps for cation with valence higher than 3) didn't impact on CEC value because of the strong affinity of trivalent cobaltihexamine ion to clay surface, CEC as MB value were submitted to the impact of suspension pH. The lower effect of almost all the experimental parameters on CEC measurement, as well as the operator error, explained why the Duriez values and MB_{CEC} were better correlated. Note that the correlations between Duriez values and MB_{phot} or MB_{drop} were really close. The use of a spectrophotometer for MB_{phot} measurement just improved slightly the coefficient of determination R^2 (the average standard deviation for MB_{phot} is close to 5% while the one for MB_{drop} was around 5-10% until 20%).

Secondly, several zones were observed considering the 0.8 Duriez threshold. The limit of the different zones might vary depending on whether MB_{phot}, MB_{drop} or MB_{cec} were considered

The first zone corresponded to AC mixtures with fine aggregates that gave a Duriez value systematically larger than 0.8 (qualified fine aggregates whatever the sand mineralogy). The MB_x2 limit (x for Phot, Drop or CEC) seemed to be extremely strict. Considering the better correlation between MB_{CEC} and the Duriez value, the limit might be extended to $MB_{CEC}7$. Such limit should be validated on a series of natural fines aggregated as large as possible with the highest variability in mineralogy and chemical nature of exchangeable cations. Such limit was validated by AC mixtures manufactured in this study and it depended on the type of used bitumen (other source of bitumen might behave differently) and the type of AC mixture (a BBTM6A from *Delorme* and Wendling *(2007)* used in this study*),* also called EB6 from European standard *NF EN 13108-1(2007)).* As such BBTM6A AC mixture formula produced medium porosity, such limit should be the most strict compared to the other formula (too much porous to keep water in contact with clay (porous Asphalt) or to much dense with a higher bitumen quantity to let the water intrude easily in AC mixture).

The second zone corresponded to AC mixtures with fine aggregates that might give a Duriez value randomly upper or lower than 0.8. Some fine aggregates were qualified whereas others with close MB_x values were not qualified after the application of Duriez test. As in literature (Figure 2 and Figure 3 in literature review), MB_x values were not sufficient to distinguish qualified and unqualified sands. In this case, the fine aggregates mineralogy was probably determinant as well as the nature of cations onto clay (the nature of cation was not clearly taken into account either by MB_{phot} or MB_{drop}, or by MB_{CEC}).

The third zone corresponded to AC mixtures with fine aggregates that gave a Duriez value systematically lower than 0.8. This zone would start from $MB_{CEC}18$. Certainly, both limit MB_{CEC} 7 and $MB_{CEC}18$ should be validated with the test of several natural clayey sands with various clay mineralogies.

4.2 A new methodology for qualification of fine aggregates for AC pavement

Experimental results in this study demonstrated clearly that clay mineralogy in fine aggregates impacted the water sensitivity of AC pavement indicated by Duriez value. Even if MB_{drop}, used in the usual practice for fine aggregates qualification, was linked indirectly to the clay mineralogy in fine aggregates (because swelling clays presented higher specific surface area), MB_{drop} presented a lack of correlation with Duriez test. MB_{drop} couldn't describe the water-bitumen-clay interaction as well as the cation nature onto clay surface. MB_{drop} couldn't also discriminate two sands with different mineralogical compositions but with the same global methylene blue adsorption.

So a mineralogical approach to better estimate the stripping in AC mixture was proposed and a new methodology was described in the following paragraphs. By this way, much more fine aggregates should be saved because the total (and not partial) distinction between qualified and non qualified fine aggregates should be improved (potentially without the systematic application of Duriez test).

The strategy to indicate the stripping in AC pavement induced by clays in fine aggregates is presented in four steps, detailed in the next paragraphs and justified by experimental results given in chapter 3 and the correlations evidenced in Chapter 4. The artificial and unknown fine aggregates were used to illustrate the application of this new method. The proposed methodology is summarized in Table 64.

Table 64 The proposed methodology to estimate the stripping of AC mixtures induced by clay in fine aggregates. AC mixture corresponds to a BBTM6A (*Delorme and Wendling 2007) or* EB6 from *NF EN 13108-1 (2007).* In green : qualified fine aggregates, in red : non qualified fine aggregates, in grey : not clear qualification.

Fine aggregates (D 0/2mm)	% passing 63 µm [a]	MB_{drop} [b] (g/kg)	MB_{CEC} [c] (g/kg)	Mineralogical analyses[d]: position compared to duriez0.8 surface[e]	Application of Duriez test [f] (i/C)	Water sensitivity of AC mixtures
	(optional)	Step 1	Step 2	Step 3	Step 4	
sample preparation and sub-sampling	< 3% or > 3%	< MB2				qualified
		> MB2	MBCEC < 7			qualified
			7< MBCEC < 18	Below Duriez0.8 surface		qualified
				Near Duriez0.8 surface	> 0.8	qualified
					< 0.8	Non-qualified
				Above Duriez 0.8 surface		Non-qualified
			MBCEC >18			Non-qualified

[a] European standard (*XP CEN ISO TS 17892-4),* [b]MB value measured by European standard *NF EN 933-9*, [c]MB_{CEC} (g/kg) = CEC (meq/100g) x 319,85/100) with the CEC measured by *NF EN ISO 23470 (2011*), [d]X-Ray powder diffraction analysis (TOPAS method on powder), [e]the building of Duriez 0.8 surface is detailed in further paragraphs. It corresponds to the mineralogical composition of clay mixtures in sand (in terms of illite, kaolinite and montmorillonite contents) that produce a Duriez value equal to 0.8 when mixed with bitumen, [f] European standard, *NF EN 129 12697-12.*

4.2.1 Previous step in the methodology: the measurement of < 63µm fraction, sample preparation and sub-sampling

According to European standard (EN13043), the preliminary regulation for fine aggregates qualification was the quantity of fine particles (D0/0.063 mm) in fine aggregates. No stripping of AC mixture was considered if the fine content in fine aggregates was less than 3%. French practice didn't

considered such threshold and methylene blue test was systematically applied on fine aggregates whatever the fine content. The tested artificial fine aggregates confirmed that sand with less than 3% of fine gave good Duriez values, even with 1.37% of montmorillonite as in S1M4 (Figure 93). The predicted Duriez value for a 3% montmorillonite fine aggregate was 0.8125 (the value was calculated using S1M2, S1M4 and S1M12 samples). The fact that Duriez value was close to 0.8 indicated that the 3% threshold might fail (in presence of pure montmorillonite which was exceptional in natural sand). So, the measure of the 63 µm passing was kept as indicative data.

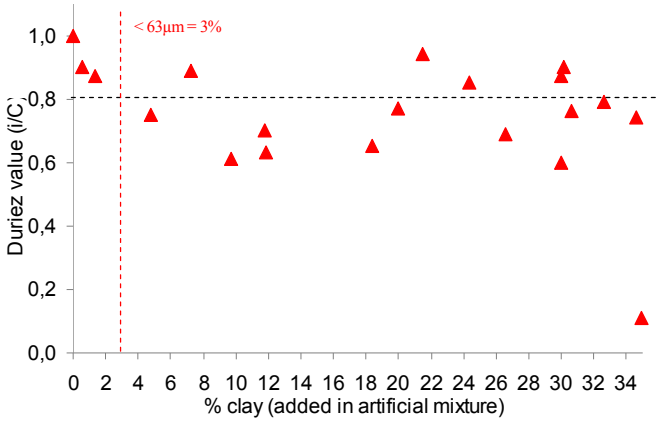

Figure 93 Duriez values versus % of clay content (clay added in mixture in chapter 2)

In order to improve the quality of measurement, the required quantity of fine aggregates for each measurement was sampled by using rotating sample divider to avoid the heterogeneity of clay content in subsample (the apparatus will be covered to avoid the lack of clay by particles flight, the sample will be wetted by spraying if the sample is too dried). Samples was never dried over 40°C to obtain representative test results (high drying temperature may collapse the clay interlayer and alter the clay reactivity in contact with methylene blue, cobaltihexamine ions or potentially with water when clay is mixed with bitumen). Moreover, at least 3 repetitions for each measurement were necessary to estimate the standard deviation.

4.2.2 Step 1 of the methodology: the measure of MB_{drop}

As MB test was quick, easy to operate and practiced by quarrymen to qualified fine aggregates, MB test using the drop method (European standard NF EN 933-9) was kept as a reference in the new methodology. It corresponded to the first step of the diagram in Table 64. As expected, all the fine aggregates with a MB_{drop} lower than 2 were qualified. No upper limit for MB_{drop} value appeared on Figure 92 (in other word, no MB drop above all the sand gave Duriez value lower than 0.8). For MB_{drop} higher than 2, the step two is required.

4.2.3 Step 2 of the methodology: the measure of MB_{CEC}

Fine aggregates with MB value higher than 2 were submitted to the CEC measurement and MB_{CEC} (g/kg) was calculated. Considering experimental results on tested fine aggregates in this study, fine aggregates might be classified considering upper and lower thresholds, corresponding to $MB_{CEC}7$ and $MB_{CEC}18$ respectively. Below $MB_{CEC}7$, fine aggregates were qualified while above $MB_{CEC}18$, no qualification occurred. The step 2 by using MB_{CEC} avoided the impact of operator and of the

methodological parameters on MB measurement (as met for MB_{drop}) which decreased the dispersion of MB values. By this way, fine aggregates initially rejected by MB_{drop} measurement could be saved. The better correlation between Duriez value and MB_{CEC} reinforced also the idea that the range of qualified sands might be extended and the step 1 could be became an optional step.

Furthermore, as the nature and the quantity of cations onto clays surface played a determining role on water-bitumen-clay interface, we suggested to measure by chemical method (as ICP/AES) the exchanged cation contained in the cobaltihexamine solution after clay contact at the end of CEC measure. The cation nature might indicate if the water resistance of AC mixture should be increased or decreased compared to the level of water resistance estimated just from mineralogy in the step 3. As Duriez tests were not applied on AC mixtures with fine aggregates containing exchanged clays (such as Ca-montm. or Na- montm. …), the cation nature were not used in present methodology (but this should be done after new tests).

4.2.4 Step 3 of the new procedure: introduction of mineralogical analysis

For samples with MB_{CEC} values ranging between 7 and 18, MB_{CEC} couldn't be used to discriminate clearly qualified and non qualified fine aggregates for AC mixture.

Mineralogical analysis of clay fraction in fine aggregates should help to identify the cases where stripping might occur. Then, the identification and quantification of clay in fine aggregates by X-ray diffraction is recommended. Samples were ground lower than 32 µm and were properly mounted by top loading with the cutting of the surface to avoid preferential orientation. The identification of clay fraction (using the main peak d(00l) for each clay mineral coupled to the d(060) peaks), and the quantification of such fraction (using Reitveld method with corundum addition as reference) could be done at the same time. The analyses of oriented glass slides were usually required to confirm clay identification and to detect the presence of low quantities of clay (above all the swelling clay). The too low quantities of clays couldn't be detected on X-ray powder diffraction patterns used in Reitveld method which might be a problem. Fortunately, experimental results demonstrated that when low fractions were not detected and quantified by Reitveld method, such quantities (even for swelling clay) seemed to impact slightly the Duriez test values. Pure montmorillonite mixed with sand needed to reach a content higher than 3% to decrease the Duriez value below 0.8 (considering the experimental results obtained in S1M4 and S1M12). The 3% content is the upper detection limit of XRD apparatus (around to 1-2%). So, only the 'detectable' clay fraction might clearly govern the Duriez value and allowed its decrease below the 0.8 threshold. The case of interstratified clays and clays with low crystallinity (often linked to low swelling properties in the case of montmorillonite and low X-ray diffraction peak intensity) should be more studied.

The other option for samples with MB_{CEC} ranging between 7 and 18 values was to apply directly Duriez test but such test was time consuming. Based on experimental results in this study, the Duriez results could be estimated from mineralogical analysis and then the qualification of fine aggregates is proposed based on the calculated Duriez.

The quantitative results from artificial fine aggregates noted S1 in Table 62 composed by a single type of extracted clay were used to established the iso-Duriez 0.8 surface versus the mineralogical

composition of fine aggregates (with x = kaolinite content, y = montmorillonite content and z = illite content).

This simple approach consisted to consider that Duriez value on fine aggregates containing a mixture of several extracted clays (close to pure clay minerals in this study) could be calculated by combining the weighted effect of separated extracted clays.

The quantities of each clay mineral in artificial fine aggregates (S1) were calculated by combining the quantities of extracted clays added in mixtures combined to the mineralogical composition of extracted clay measured by Rietveld method. To have the simplest correlation, only illite content in S1Ix, kaolinite content in S1Kx and montmorillonite content in S1Mx were considered. The cross effect between clay minerals was not considered. The regression fitting on these few points gave the relations written in Figure 94.

The following calculation for Duriez value using the clay mineral content

$(i/C)_{c1} = I_{c1} \times K_{c1} \times M_{c1}$ with

I_{c1} = [-0.00006 × (illite mineral %) ^{2} -0.0192× (illite mineral %) +1]

K_{c1} = [-0.0006 × (kaolinite mineral %) ^{2} -0.007 (kaolinite mineral %) +0.999]

M_{c1} = [-0.0546 (Montm. mineral %) +0.9532]

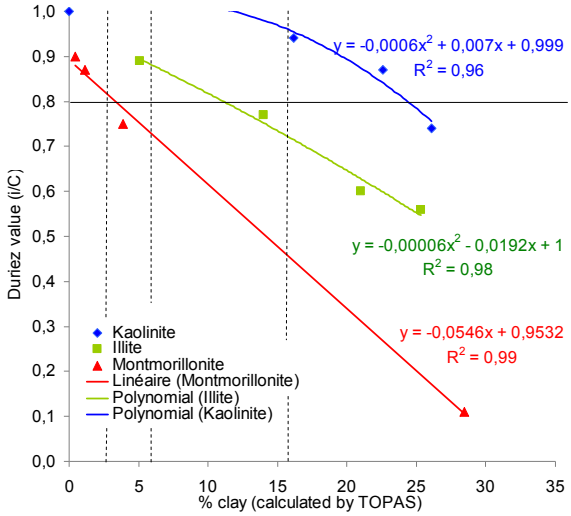

Figure 94 The regression fitting on Duriez values versus the clay content in artificial fine aggregate series S1 (kaolinite, illite and montmorillonite quantities were calculated using the mineralogical composition of extracted clays measured by Rietveld method).

Duriez values for AC mixtures incorporating the fine aggregates series S2, S3 as well as S1 were calculated using $(i/C)_{c1}$ formula and the results are given in Table 65. Boxes were colored in green for Duriez values higher than 0.8 and in pink for (i/C) lower than 0.8. Calculated Duriez value $(i/C)_{c1}$ compared to experimental Duriez value revealed a quite good accordance. If the goal of the calculation was first to fit well experimental Duriez value, the real goal was to be able to discriminate fine aggregates with experimental Duriez values higher than 0.8 from the others. It was the case for the

major part of tested artificial fine aggregates but results seemed to overestimate the decrease of (i/C) compared to the AC mixture with pure sand tested as reference that gave 1. $(i/C)_{c1}$ formula gave worse Duriez values as expected for four artificial fine aggregates in AC mixtures. These samples were characterized by high content of kaolinite (the kaolinite effect was overvalued).

Table 65 Measured and calculated Duriez values for fine aggregates series, S1 S2 and S3. Boxes were coloured in green for Duriez values higher than 0.8 and in pink for (i/C) lower than 0.8. * Duriez value < 0.8 (non realistic value). ** Duriez value just equal to the 0.8 threshold so it's difficult to state on the qualification or not of AC mixture.* high standard deviation**

Material	Calculated mineralogical composition (TOPAS)			Duriez value from experimental test (i/C)		Calculated Duriez Value $(i/C)_{c1}$	Contribution of each clay type to $(i/C)_{c2}$			Calculated Duriez Value $(i/C)_{c2}$
	Kaol%	Illite%	Montm.%	value	S.D.		K_{c2}	I_{c2}	$M_{c2.}$	
Non-clay ref.	0.00	0.00	0.00	1.00	0.07	0.88	1.00	1.00	1.00	1.00
S1-K2	16.16	2.71	0.00	0.94	0.03	0.79	0.96	1.00	1.00	0.96
S1-K3	22.62	3.79	0.00	0.87	0.04	0.67	0.86	1.00	1.00	0.86
Kao-ref.	26.07	4.37	0.00	0.74	0.06	0.59	0.78	1.00	1.00	0.78
S1-I4	1.11	5.06	0.00	0.89	0.03	0.81	1.00	0.90	1.00	0.90
S1-I9	3.09	14.02	0.00	0.77	0.03	0.67	1.00	0.74	1.00	0.74
S1-I13	4.63	21.03	0.00	0.60	0.03	0.57	1.00	0.62	1.00	0.62
Illite-ref.	5.57	25.30	0.00	0.56	0.03	0.50	1.00	0.55	1.00	0.55
S1-M2	0.00	0.00	0.42	0.90	0.05	0.87	1.00	1.00	1.00	1.00
S1-M4	0.00	0.00	1.12	0.87	0.14***	0.85	1.00	1.00	1.00	1.00
S1-M12	0.00	0.00	3.89	0.75	0.05	0.77	1.00	1.00	0.74	0.74
Montm-ref.	0.00	0.00	28.44	**0.11***	0.01	**0.10***	**1.00**	**1.00**	**-0.60***	**-0.60***
S2-KI2	20.79	7.77	0.00	0.79	0.07	0.65	0.89	0.85	1.00	0.76
S2-KI8	**9.10**	**11.94**	**0.00**	**0.85**	**0.08**	**0.70**	**1.00**	**0.78**	**1.00**	**0.78**
S2-IM6	1.15	5.24	3.51	0.70	0.09	0.72	1.00	0.90	0.76	0.69
S2-IM10	0.55	2.49	5.02	0.61	0.07	0.71	1.00	1.00	0.68	0.68
S2-KM3	20.54	3.44	2.36	0.90	0.06	0.66	0.90	1.00	1.00	0.90
S2-KM11	3.27	0.55	6.12	0.63	0.04	0.72	1.00	1.00	0.62	0.62
S3-2	**21.68**	**4.68**	**0.54**	**0.76**	**0.09**	**0.67**	**0.88**	**0.91**	**1.00**	**0.80****
S3-3	13.61	6.95	2.48	0.69	0.03	0.70	1.00	0.87	0.82	0.71
S3-5	7.74	3.47	4.54	0.65	0.04	0.72	1.00	1.00	0.71	0.71

To improve the calculation of the Duriez value, the idea was to impose a threshold. As observed on Figure 91, critical percentage for each clay mineral seemed to exist. Clay mineral content higher than such percentage produced a Duriez value higher than 0.8. Based on this idea, the effect of kaolinite, illite and montmorillonite in fine aggregates below these percentages were neglected. Then, clay behaved as filler without inducing water sensibility of AC mixture. The percentage threshold for kaolinite, illite, and montmorillonite in fine aggregates was 16.16%, 4.5% and 2.5% respectively. Such values were adjusted manually to fit the best possible experimental Duriez values.

The calculated Duriez value noted $(i/C)_{c2}$ is given by :

$(i/C)_{c2} = I_{c2} \times K_{c2} \times M_{c2}$ with

I_{c2} = 1 if (illite mineral %) < 4.5%, if not = $-0.00006 \times (\text{illite mineral \%})^2 - 0.0192 \times (\text{illite mineral \%}) + 1$

K_{c2} = 1 if (kaol. mineral %) < 16.16%, if not = [-0.0006 × (kaol. mineral %) ^{2} -0.007 (kaol. mineral %) +0.999]

M_{c2} = 1 if (Montm. mineral %) < 2.5%, if not = [-0.0546 (Montm. mineral %) +0.9532]

The Duriez value $(i/C)_{c2}$ in Table 66 compared to Duriez value $(i/C)_{c1}$ were close to the experimental measures of Duriez values.,. The adjusted thresholds improved above all the calculation of Duriez value for AC mixtures with fine aggregates containing kaolinite (such as S1K2, S1K3 and S2KM3).

However for AC mixture with the highest authorized content of 'pure' Montmorillonite (that's to say almost 30%), $(i/C)_{c1}$ was close to the experimental measure while $(i/C)_{c2}$ gave wrong value with a negative result. Nevertheless $(i/C)_{c2}$ (even negative) indicated that Duriez value was lower than 0.8.

The qualification of S3-2 with a calculated Duriez value $(i/C)_{c2}$ equal to 0.8 was not clear while the $(i/C)_{c1}$ Duriez value indicated first a non qualification. Note also that the standard deviation on experimental value of Duriez test (i/C) might impact the non qualification of sand. New measurements were needed to clearly position the behavior of S3-2 compared to the 0.8 threshold.

Results on S3-2 and Montm-ref demonstrated that the threshold on montmorillonite was a sensitive value (it should be improved). Finally, the behavior of S2-KI8 remained unexplained even if as for S3-2 the standard deviation on measures (i/C) reached 0.08 which might impact on the qualification of the fine aggregates. Indeed, experimental Duriez value qualified the fine aggregates (with a value equal to 0.85) while the calculated one didn't qualify it. No reason clearly identified explained why such mixture behaved differently but a clay contamination before mineralogical analysis and $MB_{Phot.}$ or MB_{CEC} was suspected (while S2KI8 fine aggregate sub-sampled for Duriez test was not affected by this contamination as test were done on a other site). Note that such sample didn't follow clearly the additivity law for $MB_{Phot.,}$ MB_{CEC} or MB_{drop} (in chapter 3).

If the Duriez calculations gave good results when artificial fine aggregates were quantified by Rietveld method, the complementary method can be used also (Table 66). Even if these two quantitative methods generally produced different quantitative values, calculated Duriez values from each sample were relatively close to each other. The fact that Rietveld method was not sensitive to low clay amount was not a problem because of the present thresholds on clay content to calculate $(i/C)_{c2}$ (note that $(i/C)_{c1}$ in this case is close to $(i/C)_{c2}$).

To go further, both quantitative methods were directly applied on a few set of artificial fine aggregates: S1I13, S1M12, SiKI2, S1KI8 and S3-3 (fine aggregates that presented unexpected MB or CEC behaviors). Instead of the calculation of clay content using the added quantity in the mixture combined to the clay quantity measured by Rietveld or complementary method, these quantities were directly measured by both methods. The limited number of tested samples didn't allow (unfortunately) to give a general trend. However, results in Table 66 showed that the use of Rietveld method for S1M12 produced an underestimation of the water sensitivity of AC mixture while calculated or measured clay content by both methods gave calculated Duriez value in accordance with measured one for S1I13, S3-3 or S2KI2 (the accordance meant higher or lower than 0.8). The case of S2KI8 was discussed previously and calculated or measured clay content by both methods allowed to reach the

same order of magnitude for Duriez value lower than 0.8 while measured (i/C) was higher than 0.8. At the opposite, the qualification of S3-2 was obtained by both methods (Rietveld or complementary method applied for clay quantification) whereas (i/C) was lower than 0.8 (that's to say 0.76 with a standard deviation equal to 0.09).

Table 66 Measured and calculated Duriez values for fine aggregates series, S1 S2 and S3 using [1] calc. mineral phase composition%. by compl. method, [2] measured mineral phase composition%. by compl. method [3] calc. mineral phase composition by Rietveld method, [4] measured mineral phase composition by Rietveld method. * Duriez value < 0.8 (non realistic value).

	Calculated Duriez value[1] Compl. meth	Calculated Duriez value[2] Compl. meth	Calculated Duriez value[3] TOPAS	Calculated Duriez value[4] TOPAS	Duriez test experimental results (i/C)	
					value	S.D.
Non-clay ref.	1.00		1.00		1.00	0.07
S1-K2	1.00		0.96		0.94	0.03
S1-K3	0.86		0.86		0.87	0.04
Kao-ref.	0.79		0.78		0.74	0.06
S1-I4	0.91		0.90		0.89	0.03
S1-I9	0.75		0.74		0.77	0.03
S1-I13	0.63	0.61	0.62	0.64	0.60	0.03
Illite-ref.	0.57		0.55		0.56	0.03
S1-M2	1.00		1.00		0.90	0.05
S1-M4	1.00		1.00		0.87	0.14
S1-M12	0.73	0.76	0.74	1.00	0.75	0.05
Montm-ref.	-0.66*		-0.60*		0.11	0.01
S2-KI2	0.78	0.77	0.76	0.77	0.79	0.07
S2-KI8	**0.79**	**0.71**	**0.78**	**0.70**	**0.85**	**0.08**
S2-IM6	0.68		0.69		0.70	0.09
S2-IM10	0.67		0.68		0.61	0.07
S2-KM3	0.90		0.90		0.90	0.06
S2-KM11	0.60		0.62		0.63	0.04
S3-2	**0.81**		**0.80**		**0.76**	**0.09**
S3-3	0.71	0.59	0.71	0.58	0.69	0.03
S3-5	0.70		0.71		0.65	0.04

4.2.5 Application of the proposed strategy on unknown fine aggregates

The qualification of fine aggregates seemed to be possible on artificial mixtures by using the new procedure that introduced a calculated Duriez versus the clay mineral contents. Now this approach had to be validated on the widest set of natural fine aggregates (by applying the same AC mixture regulation that's to say the BBTM6A/EB6 regulation).

The possibility to apply the procedure with the same parameters on other type of bitumen mixture or with a different source of bitumen should be validated. A series of Duriez test used as calibration (as done in this study) should be probably necessary. But even if a few number of Duriez test was

required to calibrate the new procedure, its application (after this preliminary step) to estimate the stripping in AC mixture was less time-consuming.

So, the new procedure was applied to qualify the unknown fine aggregates A to E that contained 16% to 28% of fine particles with various mineralogical compositions. Unknown sands A, C and D were siliceous aggregates whereas B and D were calcareous aggregates. The results to apply the procedure was gathered in Table 67.

As all the unknown fine aggregates contained more than 3% of fine particle, the MB_{drop} measurement were applied (in France the MB_{drop} test is applied whatever the fine content). Then, unknown fine aggregate E, D and B was qualified by following the usual procedure (MB_{drop} value is less than 2). The unknown sample A and C, with high MB values had to be judged by MB_{CEC}. The unknown sample C was then definitely non-qualified because MB_{CEC} was higher than 17.

The unknown sample A remained and needed the use of calculated Duriez value to clearly establish its qualification. The calculated Duriez value (i/C)c2 (from Rietveld method in Table 68) gave 0.89 which is higher than 0.8 and qualified the unknown sample A and qualified the unknown sample A. unfortunately by using the complementary method (in Table 69), the $(i/C)_{c2}$ gave 0.57 which is lower than 0.8. The experimental Duriez value (i/C) equal to 0.85 validated the qualification of unknown fine aggregates A (whereas MB_{drop} unqualified it). The use of Rietveld method seemed to reach a better fit of the water sensitivity of fine aggregates. All the results of qualification coming from such quantitative method were validated by experimental Duriez values (i/C). Note that globally, $(i/C)_{c2}$ might not to fit well (i/C) but it allowed to discriminate the experimental values above or below 0.8.

Table 67 The new procedures for fine aggregate qualification applied on unknown fine aggregates. In pink : non qualifying conditions and in green : qualifying conditions

Unknown fine aggregates	% passing 63 um [a]	MB_{drop} value	MB_{CEC} [b] (g/kg)	Calculated Duriez Value $(i/C)_{c2}$ (from: TOPAS)	Estimated moisture susceptibility	Duriez value from experimental test (i/C) Validation
A	25.9	2.55	6.9	0.89	Qualified by By Duriez test	0.85
B	21.5	1.5	5.1	1.00	Qualified by MB_{drop}	0.83
C	28.4	9.0	25.9	0.29	Non-qualified by MB_{CEC}	0.64
D	16.7	1.7	2.9	1.00	Qualified by MB_{drop}	1.03
E	27.3	1.75	1.6	1.00	Qualified by MB_{drop}	0.93

[a] European standard, *XP CEN ISO TS 17892-4*, [b] MB_{CEC} (g/kg) = CEC (meq/100g) x 319.58 /100 final MB

Table 68 Calculated Duriez values (i/C)c1 and (i/C)c2 using the equation defined from the series of artificial fine aggregates and by using the clay mineral contents given by Rietveld method

Material	Duriez value from experimental test (i/C)	Calculated Duriez Value $(i/C)_{c1}$	Contribution of each clay type to $(i/C)_{c2}$			Calculated Duriez Value $(i/C)_{c2}$
			K_{c2}	I_{c2}	M_{c2}.	
Unknown A	0.85	0.80	1.00	0.89	1.00	0.89
Unknown B	0.83	0.88	1.00	1.00	1.00	1.00
Unknown C	0.64	0.38	1.00	0.57	0.51	0.29
Unknown D	1.03	0.88	1.00	1.00	1.00	1.00
Unknown E	0.93	0.88	1.00	1.00	1.00	1.00

Table 69 Calculated Duriez values (i/C)c1 and (i/C)c2 using the equation defined from the series of artificial fine aggregates and by using the clay mineral contents given by complementary method.

Material	Duriez value from experimental test (i/C)	Calculated Duriez Value $(i/C)_{c1}$	Contribution of each clay type to $(i/C)_{c2}$			Calculated Duriez Value $(i/C)_{c2}$
			K_{c2}	I_{c2}	M_{c2}.	
Unknown A	0.85	0.66	1.00	1.00	0.57	0.57
Unknown B	0.83	0.82	1.00	1.00	1.00	1.00
Unknown C	0.64	0.52	1.00	1.00	0.30	0.30
Unknown D	1.03	0.87	1.00	1.00	1.00	1.00
Unknown E	0.93	0.86	1.00	1.00	1.00	1.00

In summary, results demonstrated clearly that clays in fine aggregates were strongly correlated to the stripping of AC mixture, so the introduction of mineralogical content to estimate Duriez value seemed to be necessary. As a proof, the water resistance of AC mixtures was estimated successfully using the clay mineralogy (from Rietveld method) for either siliceous or calcareous mineralogical formations. The water resistance of kaolinite-, illite- and montmorillonite- AC mixtures may be overestimated without the use of a threshold value linked to the idea that a certain quantity of clay was required to trigger the stripping in AC mixture. Moreover, each clay behaved differently at water-bitumen-clay interface according to surface energy calculation (the nature of the cations onto clay was not taken into account in the new proposed procedure but the role of the calcium compared to other usual mono- or divalent cations on clay surface was put in evidence in this study). Finally, the application of this new procedure to qualify fine aggregates to avoid stripping phenomenon allowed to extent the range of qualified fine aggregates compared to the regular standard using MB_{drop} test. Such approach should be applied on other types of AC design, bitumen type and natural aggregates to confirm its capability to predict Duriez value.

For example, the drawing of iso – Duriez 0.8 surface versus the clay mineralogical composition in fine aggregates (Figure 95) showed clearly that MB value (iso-MB line were drawn also on the surface) fixed to MB2 don't allow to judge the qualification of AC mixture.

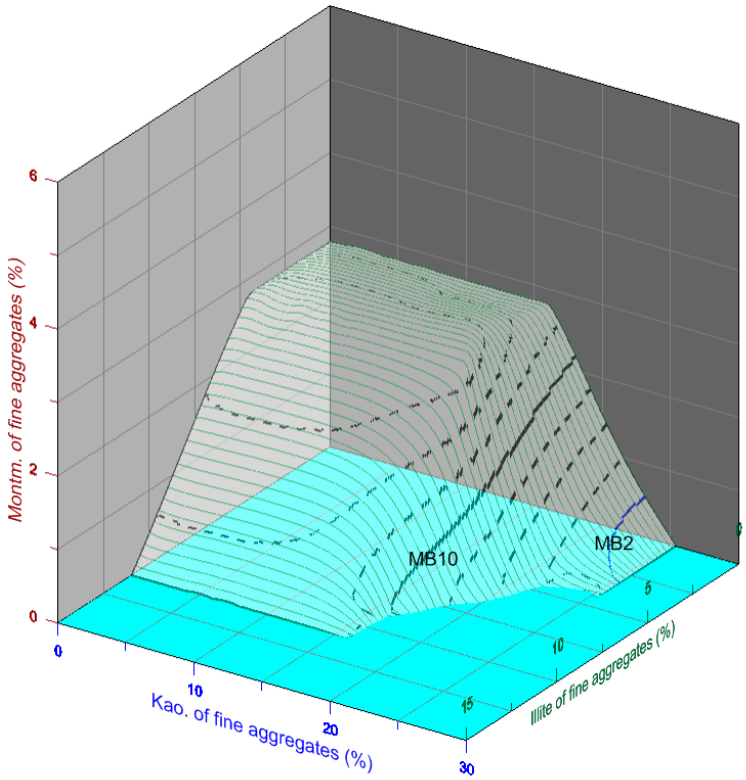

Figure 95 The iso-Duriez0.8 surface versus clay mineralogy.
On this mapping the iso-MB lines were drawn.

Such method presented advantages but also drawbacks. It required a single apparatus (X-Ray diffractometer) to apply directly the step 3 of the method (without the step 1 and 2 using standardized method with a manual titration and a colorimetric test with a spectrophotometer, respectively). The X-ray diffractometer (available now on a compact and easy to use desk form) was until now used not exclusively but above all in academic field and it needed technicians with good skill in X-ray diffraction pattern analysis to reach the trustful quantitative result by Rietveld method. The cost for mineralogical analysis and the lack of standard for the operating process will be a serious challenge to be solved before applying the new proposed strategy by the aggregates producers. However, after a step of mineralogical characterisation of the fine aggregates produced in a quarry (identification and quantification with an evaluation of the variability of the composition) and the implementation and validation of the new proposed method by applying a series of Duriez test, the procedure might become a real usual test on production line.

Chapter 5 General conclusions and perspectives

The natural resources are faced to scarcity and the possible use for AC pavement of fine aggregates not qualified by MB_{drop} test offers a way to save material. Indeed, the MB_{drop} test, which is the engineering rapid test applied by aggregates producers to qualify fine aggregates for AC pavement, is not systematically in accordance with Duriez test for the water sensitivity of AC mixture. This observation gave the idea that the MB2 threshold for fine aggregates qualification might be extented if the mineralogical composition of clay was taken into account. The goal of the present study was to improve the knowledge about the stripping of AC mixture triggered by clay mineralogy in fine aggregates. The fine aggregates characterization and the physical-chemical interactions at water-bitumen-clay interface were combined to the engineering behavior of clay-rich AC mixture, in order to reach our goals. The main contributions of this study were listed below.

First, Duriez test, Surface energy measurement and Oliensis test allowed to better understand the links between clay mineralogy and the stripping phenomenon in AC mixture.

- The mineralogical composition of siliceous fines (as clays) considering their various water sensitivity impacts bitumen-clay interaction in presence of water. Water may intrude AC mixture by diffusion into pore (channels) at aggregates -mastic interface or into bitumen-clay mastic. When clay is reached, the stripping may occur. The worse situation producing the highest damage is the presence of clay clusters.
- The kaolinite-AC mixture performs the highest water resistant through cohesive failure, and it yields higher Duriez value than illite-AC mixture, and much higher than montmorillonite-AC mixture. The kaolinite, a non-swelling clay which bonds studied bitumen by their non-polar components, induces stripping in AC mixture by the interaction of polar components between water and bitumen. The studied bitumen interacts with low swelling and high swelling clays, illite and montmorillonite, induces stripping of AC mixture along the interfacial zone between bitumen-clay mastic and clay, and then create the water channels in the AC mixture. Moreover, the cation with low mobility and high affinity in the interlayer of swelling clay is efficiently reducing the stripping by decreasing of not only the work of adhesion between water and clay, but also the swelling property of clay.
- The lime treated clay-rich fine aggregates reduced the stripping of its AC mixture, and it is caused by calcium that enhanced the bitumen-aggregates interaction at high pH and reduces the swelling property of clay. The lime-treated clay yields acceptable Duriez values because Ca-clay/bitumen bonding is stronger and opposes stripping.

To avoid the damage generated by the water sensitivity of clays in fine aggregates, the qualification of materials is required. However, the standardized MB_{drop} test remains questionable:

- The MBdrop test was useful to qualify fine aggregates when MBdrop value was lower than MB2 or very high. Between these values, uncertainties remained on the level of qualification of fine aggregates.

- Several factors might affect the MB adsorption onto clay. The UV-visible spectrophotometric measurements on MB-clay suspension confirmed that MB molecules might aggregate in various configurations (and orientation) onto clay surface. MB adsorption was sensitive to clay layer charge (for swelling clays), the pH value of the clay suspension and the nature of the exchangeable cations onto clay. If the UV visible spectrum of MB-clay suspension was affected, the effects of the different parameter were not clearly evidenced on MB value measurement by drop method or UV-phot. method (except when lime is added to fine aggregates which induced a great variation of pH which is the desired effect). Tests showed also that the drying of fine aggregates before test had an impact. Material had to be never dried over 40 ° C before test in order to avoid a change of the clay specific surface area (drying might change the clay surface reactivity).
- MBdrop value was sensitive to operator who defined the end point of the test, compared to MBphot value that varied strongly with the initial MB covering. Considering the numerous factors that impacted MB value, the use of the cationic exchange capacity (CEC) was proposed instead of MB adsorption. With a lower standard deviation, CEC value (or MBCEC assessed from CEC measurement multiplied by methylene blue molar mass) might save material during the qualification process. MBCEC correlated better with the clay mineralogy than MBdrop or MBUV-Phot.

A new methodology was proposed to qualify fine aggregates for AC pavement. It allows figuring out erroneously disqualified fine aggregates due to $MB_{drop} > 2$ g/kg. It combines MB adsorption (step 1), cation exchange capacity or MB_{CEC} (step 2) and mineralogical quantitative analysis of fine aggregates (step 3). The last step is the experimental measure of Duriez value (when results from step 3 are not clear).

- The X-Ray powder diffraction coupled with Rietveld method allowed the clay identification and gave reasonable quantitative results. However, it needed a delicate step of sample preparation to lower the preferential orientation of powder particles and X-Ray diffraction on orientated glass slide remained useful to validate the clay identification above all when clays were in low content. The complementary method based on chemical and thermal analysis coupled with CEC developed in this work, validated in most cases the quantitative measures given by Rietveld method.
- In the new methodology, the calculation of Duriez test is based on the combination of the effect of illite, kaolinite and montmorillonite determined on single clay AC mixtures. The introduction of thresholds in the calculation improves the matching between calculated and measured Duriez values. The thresholds are associated someway to the required amount of kaolinite or illite or montmorillonite to trigger stripping in AC mixture were 16.16%, 4.5% and 2.47%, respectively. The decrease of the required quantity for each clay mineral is in accordance with the increase of their swelling properties. The presence of thresholds allows to neglect the low clay content (even the montmorillonite content) that are not detected or quantified from powder XRD patterns (by Rietveld method).

- The clay mineralogy given by X-Ray diffraction (Rietveld method) is able to predict directly (without step 1 and 2) the stripping in AC mixture.
- The new strategy to predict the water sensitivity of AC mixture (for the model of BBTM6A/EB6 AC mixture) was validated not only on the tested artificial fine aggregates (a combination of siliceous sand with montmorillonite, kaolinite and illite) but also on natural calcareous or siliceous sands.

Finally the use of unqualified fine aggregates (when $MB_{drp} > 2$ g/kg) in AC pavement was checked. Regarding that the fine aggregates abandoned aside in a quarry in France might reach 50% of the production, the new methodology proposed in this study might conduct to properly use the natural resources, which should allow not only to protect environment but also to the increase the benefits of aggregate producers.

However, several limitations remain and perspectives for future work include :

- The new methodology was validated on a limited number of natural fine aggregates. The test of a great number of natural fine aggregates with a wide range of mineralogical composition is necessary to reinforce the validation.
- the methodology takes into account illite kaolinite and montmorillonite but other type of clay has to be tested (such as palygorskite which particle shape as needle impact strongly AC mixture according to litterature (*Huet, 1989*)).
- The new strategy to predict the water sensitivity of AC mixture was developed for the model of BBTM6A/EB6 AC mixture (the most sensitive to water effect). Other bitumen type and other model of AC mixture should be tested too. The principle of the methodology remains probably valid but the parameters have to be adjusted based on Duriez values measured on single clay-sand mixtures used for calibration.
- Even if MB adsorption is not able to predict in all the case the level of stripping in AC mixture, MBdrop standardized test remained a simple and rapid preliminary test, available in all the quarries. By adopting the new methodology based on mineralogy (even if this study proved it's capability to predict stripping in AC mixture), the use of X-ray diffraction needs expensive apparatus and technicians with adequate skill compared to the simple MBdrop test.
- The nature of the cations onto clay was not taken into account in the new methodology and needs to be introduced in an improved version, by using the chemical analyses of cobaltihexamine solution at the end of CEC measure. Cations may favor or prevent (in the case of Ca2+) stripping in AC mixture. Duriez test with cation exchanged clays are required to evaluate the cation effect.
- The direct evidence, which bridges micro- and macro- aspects of clay inducing AC stripping, still remains unsolved. The impact of surface energy and compatibility on bitumen-clay bonding, and the interaction of bitumen-clay in the presence of water have to be scientifically verified and indicated to the water resistance of AC mixture. However, the identification of bitumen interacting with a nano-, poro- and swelling- mineral, clay, is a great challenge.

- Regarding the quantification of clay mineralogy, the complementary method has to be applied to validate the quantitative results from Rietveld method (calculated and measured chemical composition of fine aggregates has to match the best possible). The clay mineralogy has to correspond to the mineralogical composition of fine aggregates related to the geological formation and the location of quarry. A complementary petrographic study helps the identification.
- Considering that the grinding of the whole fraction of the natural fine aggregates may release clays contained inside altered coarse grains (it's not the case with all the sands), the methodology could be tested on a sieved fraction (the particle size limit should to be chosen after several tests). With the hypothesis that the coarse fraction doesn't impact on the Duriez value (it is characterised by a small specific surface and clays inside grain are not in contact with bitumen whereas they are quantified by X-Ray diffraction if the whole fraction is ground), the clay quantification on sieved fraction should be drawn versus experimental Duriez value. Results should demonstrate if the correlation between Duriez value and mineralogy should be improved or not by this way. It depends on the amount of clays inside coarse grains compared to the free clay in the fine fraction.
- The last question is to know if the Duriez test is the best indicator of AC mixture water sensitivity, given that no traffic-simulating load is applied to test specimens during immersion.

As soon as the complementary tests will be done, the easy, accurate and efficient new methodology to estimate the stripping of AC pavement induced by clays will have a chance to be commonly applied by the aggregates producers.

Appendix 1 X-Ray diffraction

1.1 Mineralogical qualitative analysis by X-Ray diffraction

Table 70 Spacing in Å, and intensities for preliminary identification of clay minerals (*Brindley & Brown 1980a*)

Minerals	*d* (001)	*I* (00*l*) *l* = 1	2	3	4	5	*d* (060)
Kaolinite group	7·15–7·20	100	90	15	10	4	1·489
Mg-serpentine	7·25–7·35	100	100	—	20	20	1·536–1·540
Fe-serpentine / Berthierine	7·04	100	100	—	—	5	1·555
Pyrophyllite	9·20	80	30	100	5	10	1·493
Talc	9·35	vs	w	s	vw	m	1·527
Smectites							
(dioctahedral)	← variable →						1·49–1·50
(trioctahedral)	← variable →						1·52–1·54
Vermiculite	14·3	100	10	15	30	40	1·541
Muscovite	10·0–10·05	>100	55	>100	20	75	1·499
Phlogopite	10·0–10·05	>100	20	>100	30	65	1·538
Biotite	10·0	100	20	90	10	10	1·530
Celadonite	9·95	50	—	70	—	10	1·510
Glauconite	9·95	100	—	60	—	20	1·511
Paragonite	9·62	30	20	100	—	30	1·481
Chlorites (magnesian)	14·15–14·35	70	100	50	80	30	1·549
Chlorite (iron-rich)	14·10–14·25	20	100	20	50	10	1·560

Sepiolite $d(110) = 12·1–12·3$, $I = 100$; $d(131) = 4·30$, $I = 25–40$.
Palygorskite $d(110) = 10·4–10·5$, $I = 100$; $d(121) = 4·25$, $I = 10–30$.

Table 71 Effect of some diagnostic treatments on spacing of first low angle reflection of clay minerals; spacings in Å are approximate (*Brindley & Brown 1980a*)

Mineral	Air-dried	Ethylene glycol	300–350°C	500–600°C	Reflection disappears at	Remarks	Reference
Imogolite	20–12 Å (B)	20–12 Å (B)	19	Disappears	300–450°C	20–12 Å band replaced by sharp intense 19 Å reflection at 100–200°C; reversible in moist air	
Kaolinite	7	7	7	Disappears	500–550°C	Occasionally weak broad band at 12–14 Å at 500–550°C	
Dickite	7	7	7	Disappears	550–650°C	Usually broad reflection *c.* 14 Å at 550–700°C	(1)
Nacrite	7	7	7	Disappears	550–650°C		
Kaolinite, disordered	7	7	7	Disappears	500–550°C		
Halloysite-7 Å	7	7	7	Disappears	450–520°C		
Halloysite-10 Å	11	10	7	Disappears	450–520°C	Dehydrates, usually irreversibly to 7 Å form at 50–100°C	
Serpentine	7	7	7	Disappears	575–700°C	Broad reflection 11–14 Å region at 550–650°C; forms olivine and enstatite at 650–700°C	(2, 3)
Nepouite	7 (B)	7 (B)	7 (B)	Disappears	550–600°C	Broad reflection 11–14 Å at 550–650°C; amorphous 550–800°C; NiO-like phase 800–1000°C	(3, 4)
Berthierine (ferrous)	7	7	7	Disappears	450–500°C	Oxidized to ferric form 350–450°C	(5)
Berthierine (ferric)	7	7	7	Disappears	450–500°C	Forms hematite + spinel 650–1000°C	(5)
Cronstedtite	7	7	7	7		Spinel-like phase with 7 Å reflection persists to >700°C	(6)
Amesite	7	7	7	Disappears	550–600°C		(7)
Mica	10	10	10	10	800–1000°C+		
Kerolite–pimelite	10 (B)	10 (B)	10 (B)	10 (B)	700–800°C	Transformed to enstatite 700–800°C	(4)
Smectite, Mg, Ca	15	17	10	10	700–1000°C	Trioctahedral varieties more stable in 700–1000°C range	
Smectite, Na	12·5	17	10	10			
Vermiculite, Mg, Ca	14·5	14·5	10	10	700–1000°C		
Vermiculite, Na	12·5	14·5	10	10			
Chlorite (magnesian)	14	14	14	14	800°C	14 Å intensity increased at 500–600°C; forms olivine at about 800°C	(8)
Chlorite (iron-rich)	14	14	14	14	600°C	14 Å intensity much increased 500–600°C; forms olivine at 600–700°C	
Swelling chlorite	14	16–17	14	14			
Palygorskite	10·5	10·5	10·5 + 9·2	9·2	700°C	Marked increase in 10·5 Å intensity at 150°C	(9)
Sepiolite	12·2	12·2	12·2 + 10·4	10·4	700°C		

Temperature at which thermal changes occur are affected by size of crystals and duration of heating; larger crystals require higher temperature and longer time for reaction.
(B) = broad reflection.
References: (1) Hill (1955); (2) Brindley and Zussman (1957); (3) Brindley and Wan (1975); (4) Pham Thi Hang and Brindley (1973); (5) Brindley and Youell (1953); (6) Steadman and Youell (1957); (7) Brindley, Oughton and Youell (1951); (8) Brindley and Ali (1950); (9) Nathan (1970).

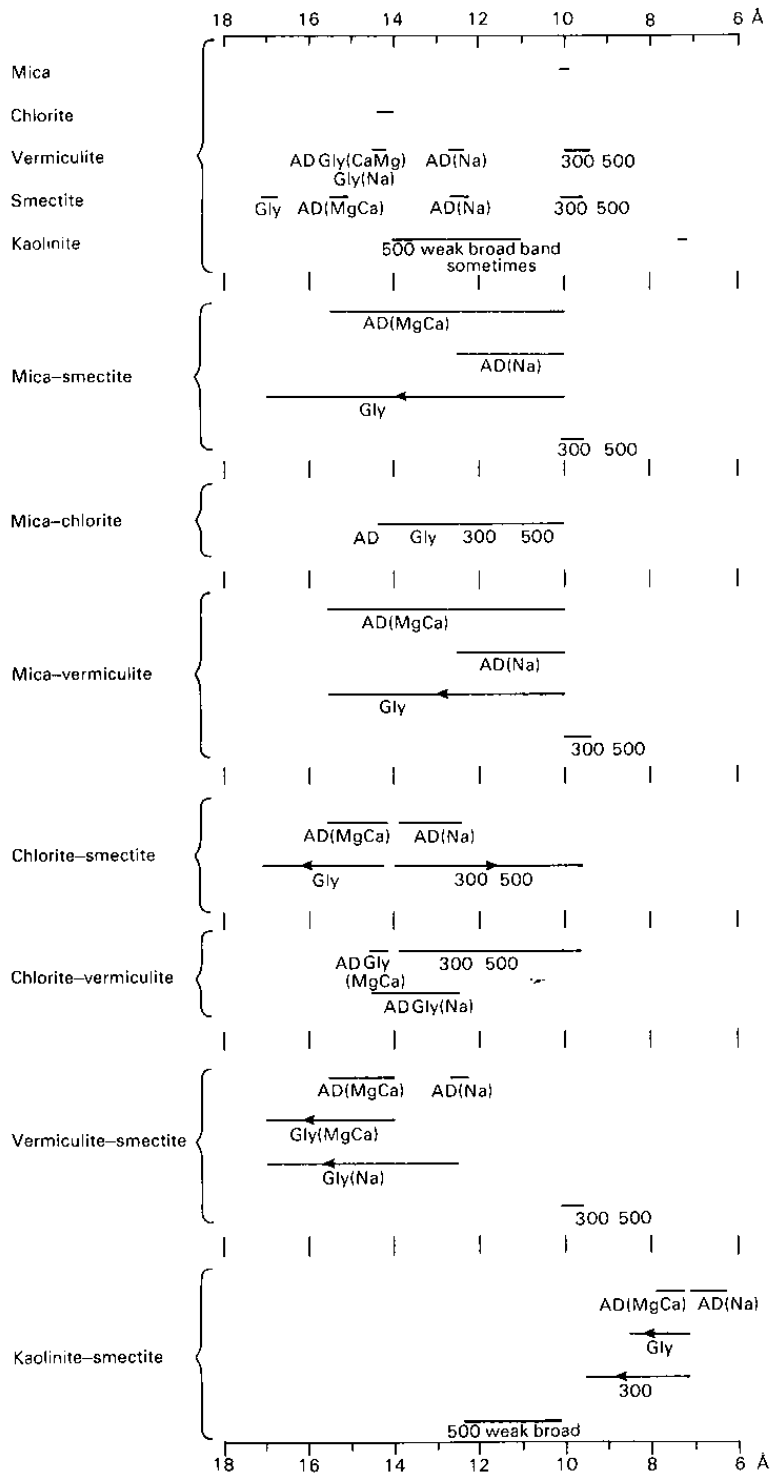

Figure 96 Guide to range of equivalent d in Å (indicated by horizontal line) of first basal reflection from some irregularly interstratified minerals after various diagnostic treatment. Position of maximum along line depends on proportion of components. Positions of the reflection from pure components are also shown. The exchangeable cations of expanding components are given when they affect position of the reflection. When direction in which the reflection moves after treatment is not obvious an arrow shows direction of shift from position for air-dry specimen. Treatments are denoted: AD = air-dry, Gly = ethylene glycole, 300 = heated to 300 °C, 500 = heated to 500 °C (*Brindley & Brown 1980a*).

Figure 97 Identification of clay minerals by X-Ray powder and oriented glass slide diffraction (*Laruaz et al. 2013*)

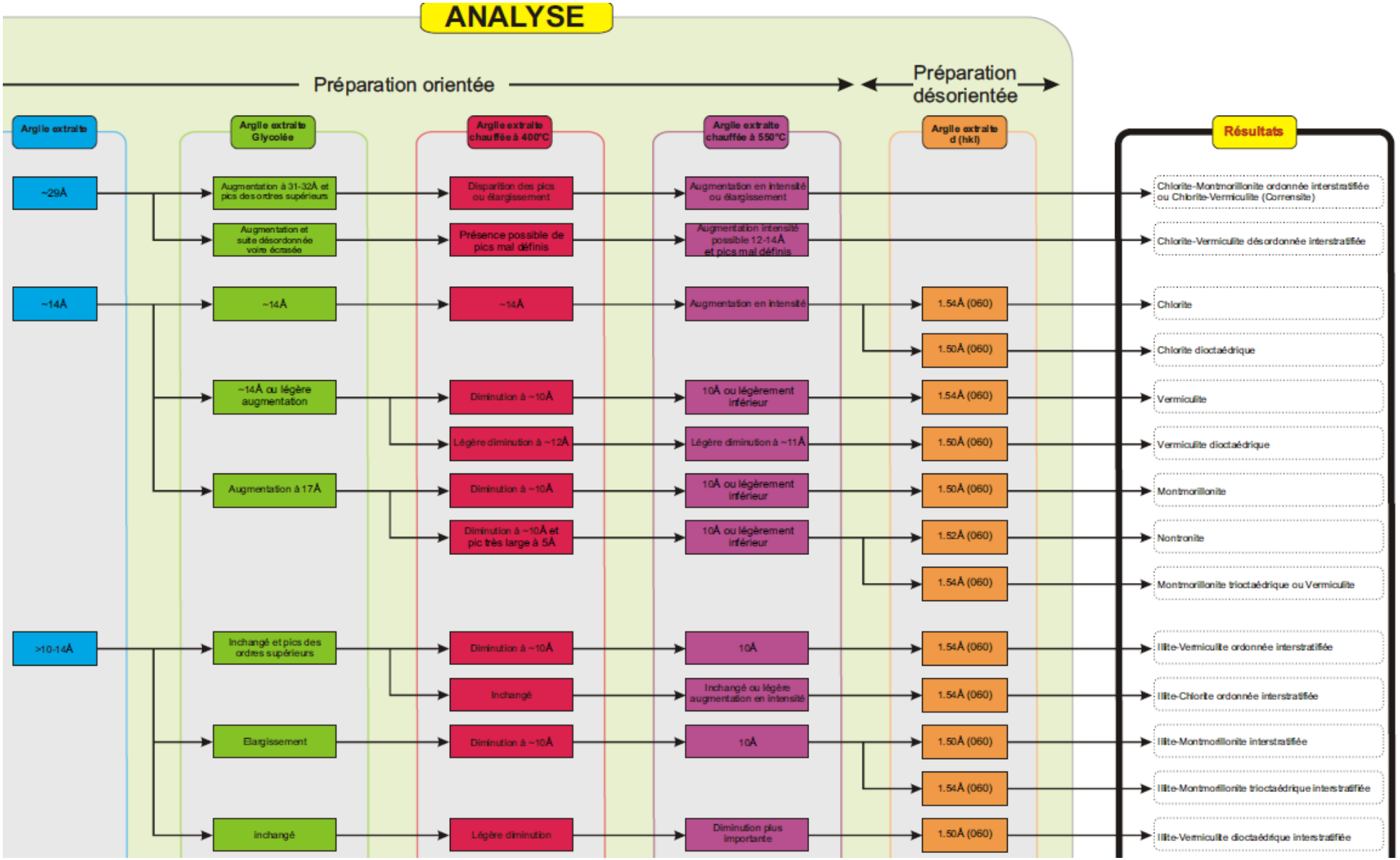

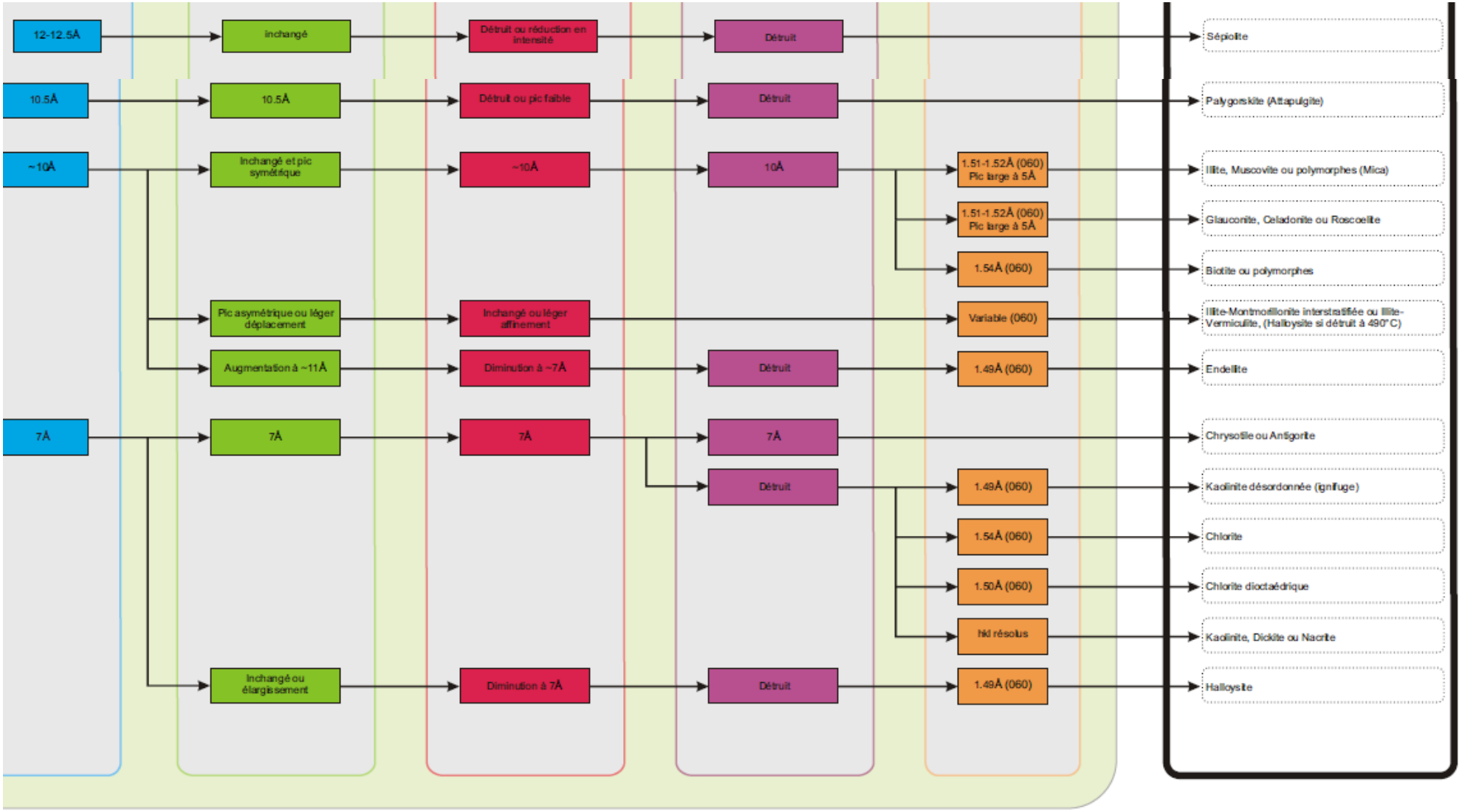
12-12.5Å
Inchangé
Détruit ou réduction en intensité
Détruit
Sépiolite
10.5Å
10.5Å
Détruit ou pic faible
Détruit
Palygorskite (Attapulgite)
~10Å
Inchangé et pic symétrique
~10Å
10Å
1.51-1.52Å (060) Pic large à 5Å
Illite, Muscovite ou polymorphes (Mica)
1.51-1.52Å (060) Pic large à 5Å
Glauconite, Celadonite ou Roscoelite
1.54Å (060)
Biotite ou polymorphes
Pic asymétrique ou léger déplacement
Inchangé ou léger affinement
Variable (060)
Illite-Montmorillonite interstratifiée ou Illite-Vermiculite, (Halloysite si détruit à 490°C)
Augmentation à ~11Å
Diminution à ~7Å
Détruit
1.49Å (060)
Endellite
7Å
7Å
7Å
7Å
Chrysotile ou Antigorite
Détruit
1.49Å (060)
Kaolinite désordonnée (ignifuge)
1.54Å (060)
Chlorite
1.50Å (060)
Chlorite dioctaédrique
hkl résolus
Kaolinite, Dickite ou Nacrite
Inchangé ou élargissement
Diminution à 7Å
Détruit
1.49Å (060)
Halloysite

1.2 Mineralogical quantitative analysis

Statistical report of applied quantitative methods

Table 72 is the statistic report from the international quantitative competition of sedimentary rock, Reynolds Cup, since 2002 (*The clay mineral society 2013*). There are more than 97% participants applied XRD technical to analyze clay quantity and confirmed by associated techniques, such as chemical analysis (XRF, ICP, neutron activation), FT-IR, VNIR reflectance, and so on. Moreover, the Rietveld method is majorly applied from X-ray diffraction technical

Table 72 Statistical report of applied quantitative methods from Reynolds cup (*The clay mineral society 2013*)

Primary quantification technique (>97%)	Other techniques	Ancillary techniques
XRD: • Single peak methods (21.0%) - Matrix flushing - NEWMOD - RIR ICDD-PDF • Whole pattern techniques (19.5%) - Arquant - Fullpat - Hillier - Quanta - Rancourt and Dang - RockJock - X-LS Mineral • Rietveld method (57.0%) - AutoQuan/BGMN - Fullprof - GSAS - HighScore Plus - Jade - Maud - Quanto - RIQAS - SIROQUANT - Topas • Educated guess (2.5%)	• IR • FT-IR • Raman spectroscopy • SEM/TEM • Mossbauer	• Chemical analysis - XRF - ICP - neutron activation • FT-IR • VNIR reflectance • DTA-TGA-DSC • Electron microscopy - SEM - TEM-EDX • Wet chemistry • CEC • Carbonate analysis • Surface area • Optical microscopy • petrography • Mossbauer • Ion chromatography

Single-peak method

Typically, clay mineral analysis involves the separation of a clay sized fraction (usually < 2 micron) from the sample (*http://www.claysandminerals.com/methods/xrd*). Once obtained the clay fraction is prepared by collecting it and transferring the layer of clay to a glass slide substrate. These oriented samples are run on the diffractometer (air-dried) and then run again following various treatments such as solvation with ethylene glycol, and heating to specified temperatures for specified times. Other treatments may be appropriate for the identification of some clay minerals. Peak positions, shapes and intensities and changes in these between treatments are diagnostic for the identification of different clay minerals. Following identification, quantitative analysis may be made by an intensity ratio method on glycolated glass slide whereby the integrated intensity (peak area) of selected clay mineral peaks is related to their weight fraction in the mixture by means of a predetermined constant of proportionality termed mineral intensity factors

(MIF or mineral intensity factor established for clays, Table 73) or more generally known as Reference Intensity Ratios (RIR). These are most readily determined from calculated one dimensional X-ray diffraction patterns, using for example the NEWMOD program as described in *Moore and Reynolds (1997).*

Table 73 Factors of surfaces area from clay peaks according to various authors and semi –quantification from Holtzapfell (*1985*)

	Montmorillonite 001	Illite 001	Kaolinite 001	Chlorite 002
Biscaye (1965)	1	4	2	2
Hay et al (1991)	1	3	2	2
Schultz (1964)	1	1.2	1,1	1.5
Holtzapfell (1983)	1,5	1	0,5	Chlorite 001: 1
Simulations NEWMOD				
Moore et Reynolds (1989)	Montmorillonite 003: 1,2	Illite 002: 2,0	Kaolinite 001: 0,5	

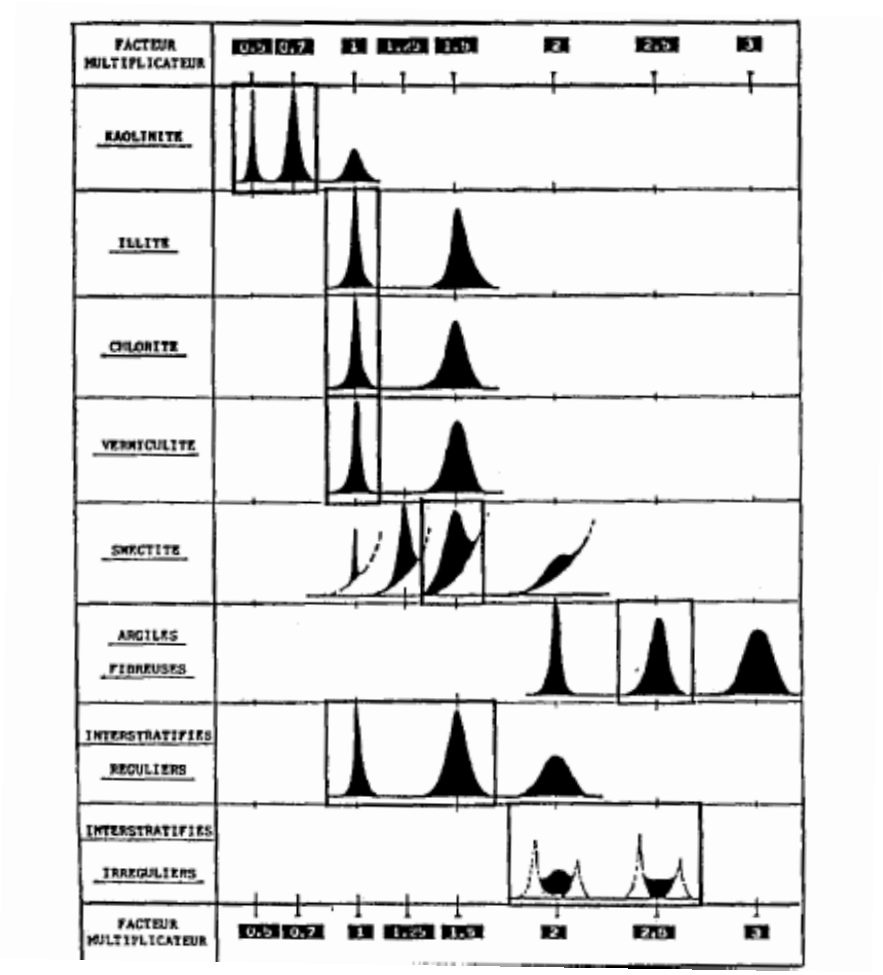

Complementary method : the developed excel sheet for calculations.

		résultats % massique		coef ox-element		% massique élémentaire mesuré	% massique élémentaire : les cations en solution (CEC)
analyse ICP	SiO2	51,79		0,467465468	Si	24,21	
	Al2O3	33,68		0,529227148	Al	17,82	
	TiO2	0,5		0,599348942	Ti	0,30	
	Fe2O3	1,1		0,699436443	Fe	0,77	
	CaO	0,2		0,714693295	Ca	0,14	0
	MgO	0,22		0,60307616	Mg	0,13	0
	Na2O	0,18		0,74185221	Na	0,13	
	K2O	1,81		0,83014862	K	1,50	1,235502206
	SO3			0,400524541	S	0,00	
	MnO			0,774457288	Mn	0,00	
	P2O5			0,43638157	P	0,00	
	tot	89,48			tot	45,02	
	perte au feu 1100°C	11,68					
	tot	101,16	calcul				
analyse thermique	H2O basse T°C	0,56					
	H2O haute T°C		10,39855104				
	CO2	11,12	0,131881307	11,13043235			

duc: Ca = cations en solution ou calcite (voir pic en ATD et perte de masse en CO2)

duc: cation K en solution calculé à partir des rapports Na/K (mesure de la CEC)

duc: pas de phase porteuse de Na > Na = cation

duc: Mg dans le réseau de l'illite en substitution de Al ou bien Mg cation

	% massique élémentaire calculé	comments	différence calculé - mesuré
Si	24,48		0,27
Al	17,86		0,03
Ti	0,30		0,00
Fe	0,66		-0,10
Ca	0,12	0,3% de calcite ou bien Ca en solution	-0,02
Mg	0,08		-0,05
Na	0,00		-0,13
K	1,29		-0,21
S	0,00		0,00
Mn	0,00		0,00
P	0,00		0,00
tot masse	44,79271421		

illite : hypothèse 1K sur 10 s'échange en moyenne / kaolinite pas de contribution

		1,3 meq/100g
CEC mesurée	1,3E-05	mol/g
CEC calculée	3E-05	mol/g

< 2 µm	< 63 µm	
82,00%	100,00%	taille max 40µm

calcul

argile	arg + felds
88,60%	88,60%

granulométrie

total 1

pour 1 gramme de matériau humide

				Masse molaire élémentaire (g/mol)		28,09	26,98	47,87	55,85	40,08	24,31	22,99	39,1	32,07	35,45	54,94	30,97	16	1	12
minéral identifié par DRX		pourcentage massique = masse en g	formule	Masse molaire (g/mol)	nombre de mole n du minéral	Si	Al	Ti	Fe	Ca	Mg	Na	K	S	Cl	Mn	P	O	H	C
quartz	tr	0,106	SiO2	60,09	0,001764021	1												2		
			mole			0,001764021	0	0	0	0	0	0	0	0	0	0	0	0,00353	0	
			masse			0,04955134	0	0	0	0	0	0	0	0	0	0	0	0,05645	0	
calcite		0,003	CaCO3	100,09	2,9973E-05					1								3		
						0	0	0	0	2,9973E-05	0	0	0	0	0	0	0	9E-05	0	3E-0
						0	0	0	0	0,001201319	0	0	0	0	0	0	0	0,00144	0	0,0003
dolomite			MgCO3	84,32	0						1							3		
						0	0	0	0	0	0	0	0	0	0	0	0	0	0	
						0	0	0	0	0	0	0	0	0	0	0	0	0	0	
kaolinite	xxx	0,746	$Al_2Si_2O_5(OH)_4$	258,14	0,002889905	2	2		0									9	4	
						0,005779809	0,0057798	0	0	0	0	0	0	0	0	0	0	0,02601	0,01156	
						0,162354846	0,1559393	0	0	0	0	0	0	0	0	0	0	0,41615	0,01156	
montmorillonite	x, Cat		(Al2-xMg ou Fex) Si4(O10)(OH)2(Ca, Na, K)x, nH2O	404,6617	0	4	2,9		0,25	0,08	0,1	0,02						12	2	
						0	0	0	0	0	0	0	0	0	0	0	0	0	0	
						0	0	0	0	0	0	0	0	0	0	0	0	0	0	
illite	R,x	0,14	(Al1,75Rx) Si3,5 Al0,5 (O10)(OH)2K0,75	423,6048	0,000330497	3,54	2,54		0,36		0,1		1					12	2	
muscovite			Al2(Si3Al)(O10)(OH)2K			0,001163958	0,0008395	0	0,000118979	0	3,3E-05	0	0,000330497	0	0	0	0	0,00397	0,00066	
			(Mg,Fe)y(Si4-xAl2+x-y) (O10)(OH)2Kx+y avec x+y=0,75 à 1			0,032864132	0,0226487	0	0,006644967	0	0,000803	0	0,012922422	0	0	0	0	0,06346	0,00066	
chlorite			$(Fe,Mg,Al)_6(Si,Al)_4O_{10}(OH)_8$	591,22	0	1	3				1							18	8	
						0	0	0	0	0	0	0	0	0	0	0	0	0	0	

Appendix 2 Impacts of different parameters on methylene blue adsorption

Several parameters may impact on the MB value measurement. The clay layer charge impacting on aggregation and the orientation of adsorbed MB molecule was previously mentioned and is more detailed here, as well as the concentration of MB solution, the pH value and the salinity of MB-clay suspension, the time contact, the clay particle size and the temperature.

2.1 Layer charge of clay

As explained in previous paragraphs, MB molecules on the highest layer charged clay tend to form H-aggregates rather than monomers. These H-aggregates are also formed in the presence of lower layer charge of clay, but the H-aggregation of MB molecules will disintegrate by time to form H-dimers and especially monomer which presents in the low energy of wavelength (*Neumann. et al., 2002*). Hence, MB value is underestimated on the clay minerals with high layer charge when the peak attributed to monomer is considered at 664 nm by UV photometric measures. The non-expandable minerals which layer charge is negligible as kaolinite are mostly characterized by H-dimer and monomer formation of MB molecule. So comparable MB value is obtained (still based on the measurement of the 664 nm UV-visible photometric peak. Regarding the relationship between the extent of MB agglomeration and the layer charge density, the spectrum of MB-clay adsorption can be a sensitive method for characterizing the layer charge distribution of swelling clay (*Komadel, 1996 394 /id).* The differences in MB sorption observed within individual series of minerals can be ascribed directly to the differences in the layer charge *(Bujdak, 1997, 1998, 2001, 2002, 2003, 2006, 2008; Czímerová, 2004, 2006; Hillier, 2000; Li, 2011; Pentrák,, 2012; Yenera et al. 2012; Neumann, 2002)*. The Table 74 lists the correlation between the layer charge of clay, some clay properties and the MB aggregation on clay surface.

Table 74 MB molecules configurations on mineral surface

	Layer charge of clay mineral	
	High	**Low**
Mineral particle size	larger	Small
CEC value	High (Montmorillonite) Medium (Illite)	Low (kaolinite)
MB absorption capacity	high	Low
Type of MB molecular aggregates	All	Monomer and H-dimmer
Arrangement of MB molecules on mineral surface	Ordered (tilted)	Disordered (island; tilted; perpendicular)
Wavelength of the peak associated to MB aggregates	550-700 nm	600-765 nm
Aggregation of MB molecular energy	High	Low
MB molecular evolution	May migrate/disaggregate with time contact (low charged mont.) or keep staying in H-aggregate (high charged mont.)	Rapid migration/disaggregation

2.2 The effect of the concentration of MB solution

The concentration of MB solution used to measure MB value can alter the configuration of MB molecules adsorbed on clay. For high MB concentration, MB aggregation in dimers and H-aggregates will increase (the peaks are associated to the wavelength between 570 and 600 nm), and then it may bias the result of MB adsorption based on the spectrophotometric measure of the monomers peaks. Such effect is illustrated on Figure 98 for laponite suspension.

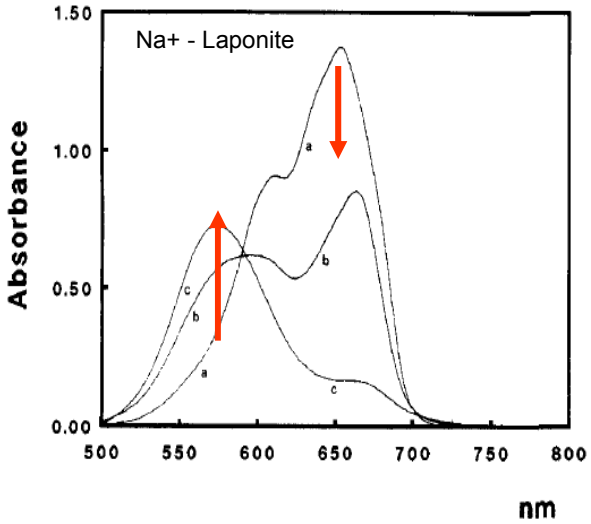

Figure 98 Absorbance of MB-Na^+-Laponite suspension after 1 day agitation in various MB concentrations that represent: (a) 1%, (b) 10% and (c) 100% of the CEC value of the sample (*Schoonheydt and Heughebaert, 1992*).

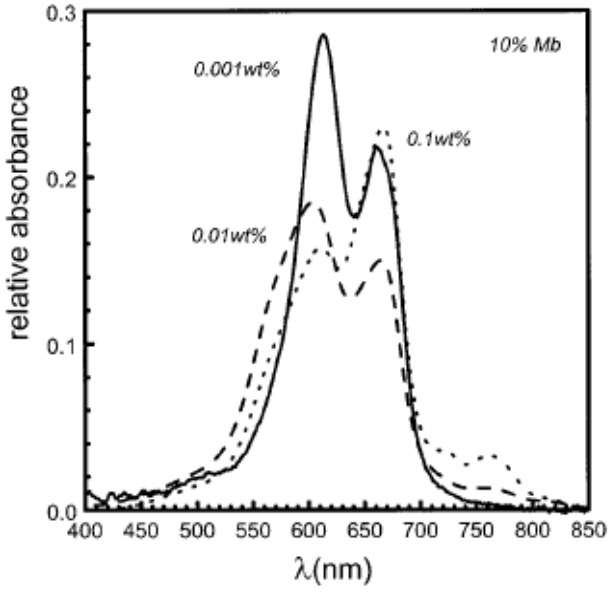

Figure 99 Absorption spectra of MB–hectorite suspensions in contact with a 10% MB solution and with various clay concentrations: 0.001 wt% (solid line), 0.01 wt% (dashed line), 0.1 wt% (dotted line) (*Jacobs, 1999 223 /id*).

The molecular configurations of MB may be changed by the variation of clay amount in MB suspension as well. At low covering of clay surface (small quantity of available MB molecules per unit surface of clay or

unit charge of clay measured by CEC), the spectra are dominated by the MB monomers. At high covering of clay (low quantity of clay for a high MB concentration), MB dimers are favored. MB and clay concentrations have to be both mentioned for each experiment in order to understand the MB aggregation level. The results in Figure 99 should be interpret in first approach as a deviation from the generally expected increased clay dispersibility at small clay concentration, resulting in a higher surface availability and thus a better spreading of adsorbed molecules. Therefore, clay aggregates size and dispersibility are impacted by the concentration of MB solution that compensate the effect of the low concentration of clay.

2.3 The effect of pH value

From the work of *Al-Ghouti (2003) on diatomite*[13], the increase of pH value decreases the surface charge of clay. It is because the hydroxyl groups present on the silica surface can gain or lose a proton, resulting in a surface charge that varies with changing pH., However, the configuration of MB molecules on such material seems not to be significantly modified by pH (Figure 100).

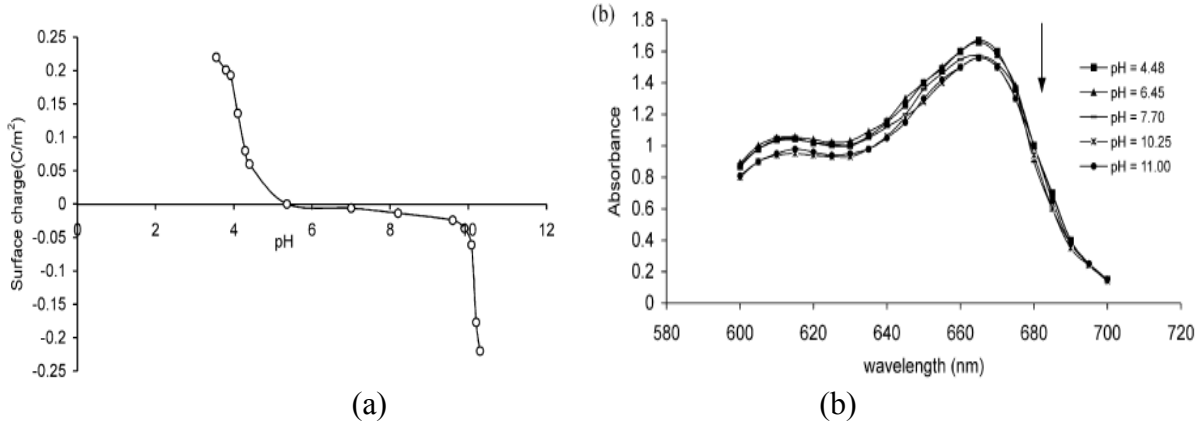

Figure 100 (a) Variation of diatomaceous earth surface charge versus pH, (b) Effect of the pH of MB solution in contact with diatomaceous earth (*Al-Ghouti, 2003*)

On the contrary, *Ghosh and Bhattacharyya (2002)* stated that a minimum methylene blue adsorption on kaolinite occurs when pH value is around 4. The increased adsorption in alkaline conditions may be related to the increase of basic sites after deprotonation of surface groups (the edge of clay platelets contribute to the variable charge while the basal surfaces contribute to the permanent charge). The pH 4 corresponds to the point of zero net proton charge (PZNPC) for kaolinite (*Schroth et Sposito, 1997*). The methylene blue adsorption at pH 4 can no longer be adsorbed by the edges of clay platelets as they are no longer charged *(Ghosh and Bhattacharyya 2002*). It's why we can see a minimum in adsorption on Figure 101. At higher or lower pH, MB molecules are still adsorbed by negatively charge basal surface.

[13] Diatomite : Diatomite is a chalk-like, soft, friable, earthy, very fine-grained, **siliceous sedimentary rock** It is very finely porous, very low in density, and essentially chemically inert in most liquids and gases. Diatomite is now used principally as a filter aid but it has many other applications, such as an absorbent for industrial spills and as pet litter, a filler in a variety of products from paints to dry chemicals, an insulation material as sawn and molded shapes as well as loose granular, a mild abrasive in polishes, and a silica additive in cement and various other compounds.(http://minerals.usgs.gov/minerals/pubs/commodity/diatomite/)

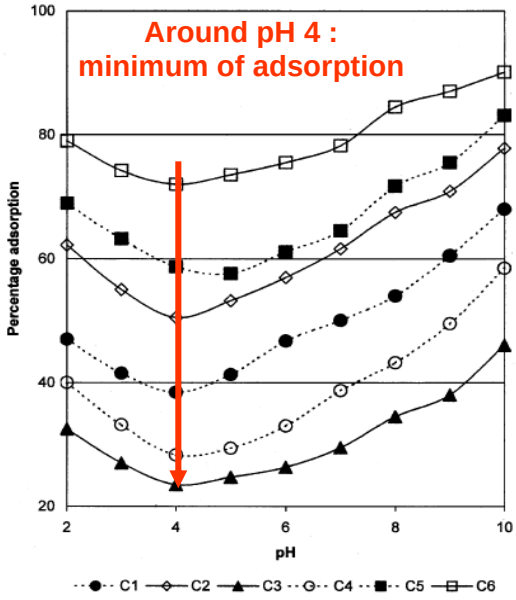

Figure 101 Variation of the methylene blue adsorption with pH. Contact time 3 h, initial methylene blue concentration 15 mg/l, kaolin dose 0.8 g/l. Ci correspond to raw, pure or treated kaolin (*Ghosh and Bhattacharyya, 2002*).

Gurses (2006) and Zhang et al. (2013) stated that the pH modifies the particle size of clay and the configuration of MB molecules, and then induces the variability of MB adsorption. In Figure 102, the higher MB absorptions are obtained under the extreme acid and basic environment, and evolve with time. In other words, the adsorption of dye from aqueous solution onto surface is highly dependent on pH of the solution that affects both surface properties and topography of the sorbent and dye structure.

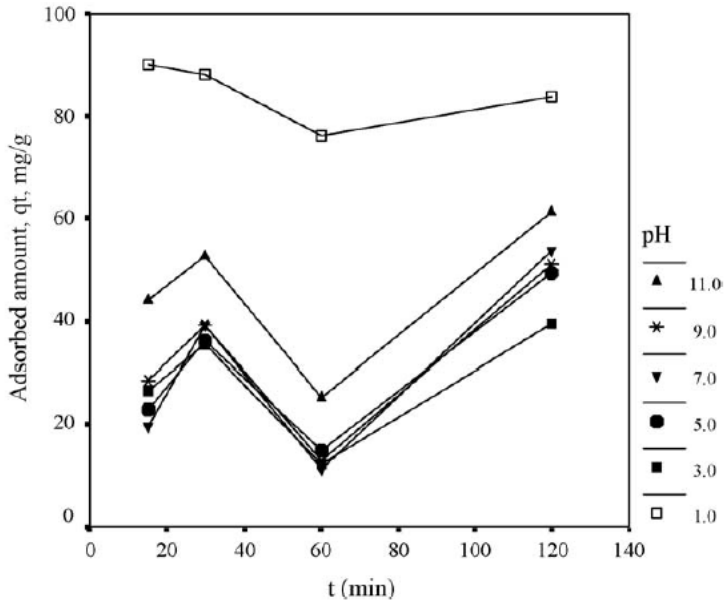

Figure 102 Effect of initial suspension pH and time evolution on the adsorption of MB onto clay (*Gurses et al. 2006*)

2.4 Effect of the operating time

Cione (1998) reported that the configuration of MB molecules in MB-clay suspension is related to the contacting time. The reorganization processes of MB molecules in MB-montmorillonite suspension starts to occur immediately after the mixing of MB solution with clay (Figure 103a), whereas the evolution of MB configuration in MB-laponite suspension is mainly due to the association-dissociation process of the clay particles with time (Figure 103b). At long terms, clay association processes are also responsible for significant spectral changes in MB-montmorillonite suspension. The contact time effect was discussed previously in chapter dealing with the charge effect (chap 1.2.1.1).

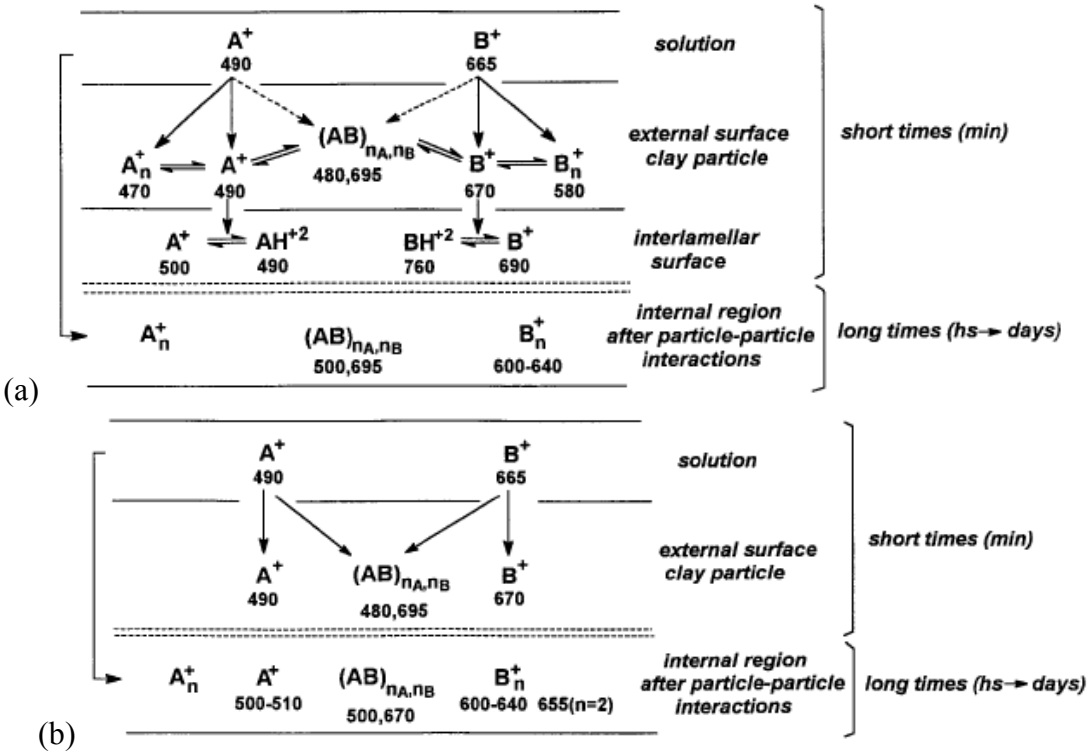

Figure 103 Processes occurring after the addition of dyes A and B to (a) montmorillonite and (b) laponite suspensions. B corresponds to Methylen Blue (A to an other dye). Broken arrows represent processes observed only when the sample is prepared according to a quick method (*Cione, 1998*)

2.5 The effect of the nature of the exchangeable cations in clay

The exchangeable cations present on clay surface play a fundamental role in the interactions between clay particles and between clay and methylene blue molecules. It plays also a role in clay bitumen interactions (especially calcium a divalent cation). The understanding of the role of each cation on MB adsorption onto clay needs to couple several cation characteristics such as valence, hydrated radius or probably hydration energy $\Delta H_h°$.

The nature of the exchangeable cations (as well as the contacting time and the clay layer charge) may significantly affect the aggregation of MB molecules. It impact on the particle size and the physical characteristics of the electric double layer in the vicinity of clay particles. The valence of inorganic cations

present in the electric double layer affects the water adsorption (swelling) and the dispersion properties of colloids as well.

The Figure 104 presents the effect of the nature of exchangeable cations present onto clay on MB molecule configurations when MB is put in contact with clay (the same cation saturation was imposed) *(Czímerová., 2004; Neumann, 2002).*

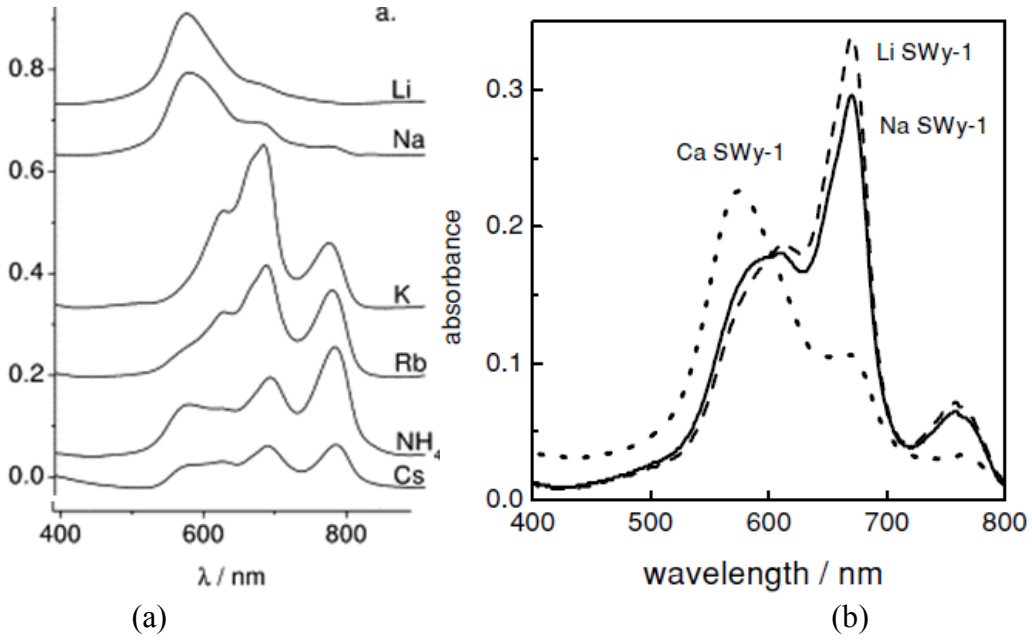

Figure 104 UV-visible wavelength of absorption peak related to methylene blue molecule in (a) the presence of montmorillonite (CEC=110 meq/100 g) saturated by alkali ions and ammonium NH_4. The spectra were measured 24 h after mixing with MB solution (*Czímerová, 2004*) and (b) the presence of montmorillonite (CEC=79 meq/100 g) saturated by various cations. The measure was made immediately after mixing with MB solution (*Neumann et al. 2002*)

First, Figure 104 shows that the cations exchange capacity of montmorillonite (given by CEC) induced by its structural layer charge is a primary parameter to consider in order to understand the various configuration of MB in clay suspension. With the high layer charge montmorillonite (Figure 104a), H-aggregate formed by MB molecules is the main configuration appearing in Li-montmorillonite suspension mixed with MB, and Na-montmorillonite is covered by both H-aggregates and monomers (*Czímerová, 2004*). Even after 24hours of contact time, H aggregates didn't disaggregate in monomers or dimers forms. At the opposite, the MB molecules on montmorillonite with lower layer charge (Figure 104b) and exchanged with the same cations (Li^+ or Na^+) are mainly configured under a low energy aggregates that's to say monomers just after MB addition in the suspension (*Neumann et al. 2002*). The presence of alkali metal cations (K^+, Rb^+, and Cs^+ with larger size – see Table 75) or NH_4^+ which are less mobile and partially fixed onto clay surface, significantly influence the MB-cation reaction. Lower mobility of these cations may lead to incomplete exchange with MB molecules when put in contact with clay suspension (*Dzene, 2015*). Furthermore, H-aggregates may decompose after 24 h in favor of lower molecular assemblies, such as monomers, and J-aggregates.

In presence of different cations onto clay, MB molecules are capable to replace all of them within the electrostatic double layer (*Li, 2011*) with a competition between the hydrated ions (Li^+, Na^+ or K^+) on clay

surface (*Xu et al. 2008*). It has been reported that this competition is related to the ions hydrated radius (*Cotton, 1980*) (Figure 105 and Table 10). The cation with the smaller hydrated radius could not easily escape from the adsorbent surface, and would occupy more active sites, leading to a stronger competitive force with positively charged adsorbate. To interpret the different cation effect on MB aggregation, hydrated radius has to be combined with ion valence too. For example, MB molecules adsorbed on Ca^{2+}-montmorillonite (Figure 104b) behave differently to montmorillonite suspension exchanged with monovalent ions such as Li^{+} or Na^{+}. High valence seems to promote the H-aggregates formation.

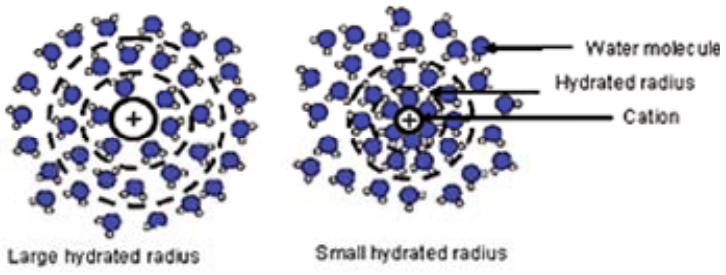

Figure 105 Hydrated radius of ions (*Tansal et al. 2006 cited by Conway, 1998*)

Table 75 Properties of ions (*Tansal et al. 2006 cited by Conway, 1998*)

Cation	Density (g/cm^3)	Radius (Å)	Crystal ionic radius (Å)	Hydrated radius of ions (Å)	Negative electron Pauling scale	Number of H_2O within the electron double layer	Hydration energy[a] $\Delta H_h°$(kJ/mol)	Number of H_2O after drying montm. at 110°C [b]
Li (+)	0,54	1,23	**0,60**	3.4	1,0	5+/-1	-515	1.54
Mg (2+)			**0.78**	**3.00/ 4.28**			**-1926**	**4.2**
Na (+)	0,97	1,57	**0,95**	1.78 / 3.58 / 2.76	0,9	5+/-1	-405	1.36
Ca (2+)			**0.99**	**2.6/4.12**		**+/-**	**-1579**	**4.4**
K (+)	0,86	2,03	**1,33**	2.01/ 3.31	0,8	4+/-2	-321	1.0
Ba (2+)			**1.43**	**5.9**			**-1309**	**1.8**
Rb (+)	1,53	2,16	**1,48**	2.28	0,8	3+/-1	-296	1.18
Cs (+)	1,87	2,35	**1,69**	3.29	0,7	< 3	-268	1.02
NH_4 (+)	--	--	**1.48**	1.04/3.31			--	--
La (3+)	--		**1.15**	4.52			--	--

[a] Enthalpy of hydration of gaseous ions *(Smith, 1977)*
See also *http://www.elementschimiques.fr/?fr/proprietes/chimiques/rayon-ionique*
[b] *(Michot and Villieras 2006)*

Moreover, not only ion valence but also ion concentration (see next paragraph on the effect of ionic force) impact on MB aggregation and on clay flocculation. Indeed, zeta potential measured on minerals in solution usually decreases (in absolute value) with increasing ionic force (or ions concentration in solution), which means that a quick coagulation (aggregation of clay platelets) can occur in this system when zeta potential becomes lose to zero *(Myers, 1999)*. It is resulting in a lower clay surface area that is accessible to MB molecules (and to aggregates formation) and thus a lower adsorption capacity of such molecule *(Zhang et al. 2013)*.

Finally, the concepts of activity and conductivity of cations in solution are also interesting characteristics to understand the interaction between MB and cations in presence of clay surface. For example, , the

conductivity of solutions for the same ionic concentration[14] decreases in the order of Cs^+, Rb^+, K^+, Na^+, Li^+. The smaller ion Li^+ should be the best charge driver with the higher conductivity, but it is not the case because it is too hydrated and moves slowly. Besides, Cs^+ has the same charge as Li^+ but cesium radius is larger than that of lithium, so the electric field is lower and ion-dipole interaction is less strong. Cesium shows the highest conductivity in the presented series.

2.6 Effect of the suspension salinity

Figure 106 illustrates the UV-visible spectra of MB-sodium SWy-1 (montmorillonite) suspensions in the presence of NaCl at various concentrations. It can be noted that the addition of NaCl in relatively high concentration induces MB aggregation (*Neumann et al. 2002*). It is well known that the addition of electrolyte increases the size of the particle aggregates in the suspension (considering the zeta potential evolution with salinity) reducing the space available for MB adsorption, leading to higher aggregation of MB molecules in H-aggregates (Figure 107) (Cione, 2000). The addition of salt may be considered as a 'treatment' that reduces the accessible surface area of clay particles

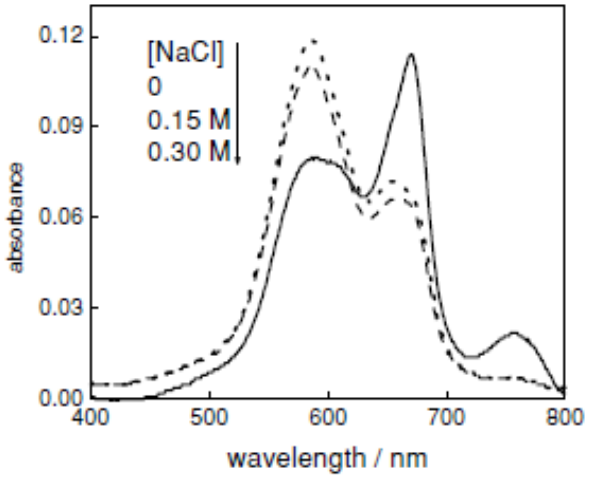

Figure 106 Absorption spectra of aqueous suspensions of MB 3.0×10^{-6} M in suspensions of sodium SWy-1 (0.11 g L^{-1}) in the absence and presence of NaCl, measured immediately after mixing (*Neumann et al. 2002*)

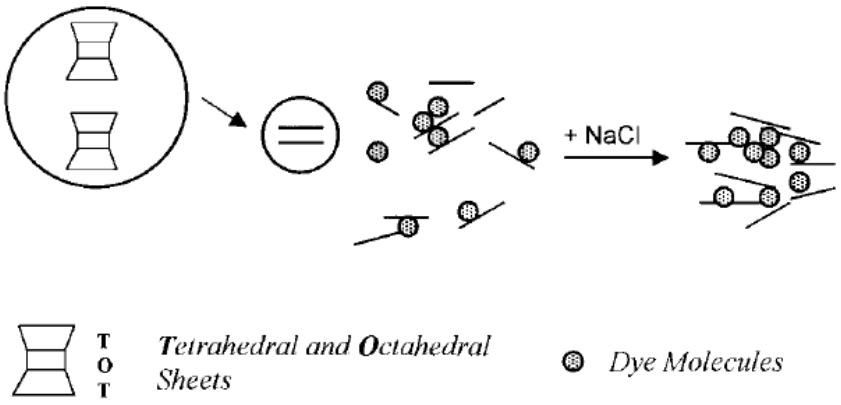

Figure 107 Processes occurring after salt addition in a clay suspension. Clay aggregation becomes dominant in the presence of salt (*Cione, 2000*)

[14] http://www.udppc.asso.fr/national/index.php/component/content/article?id=400:alcalins-presentation

Cione (2000) in Figure 108 described also the changing of MB molecular configuration after NaCl addition into MB-clay suspension. New absorption peaks appearing around 658 and 615–620 nm can be ascribed to MB cationic dye species trapped in internal regions that increase in quantity considering the clay flocculation induced by salt. The MB molecules that were initially adsorbed on the external surfaces as monomers and aggregates are relocated in internal regions during the process of clay particles association.

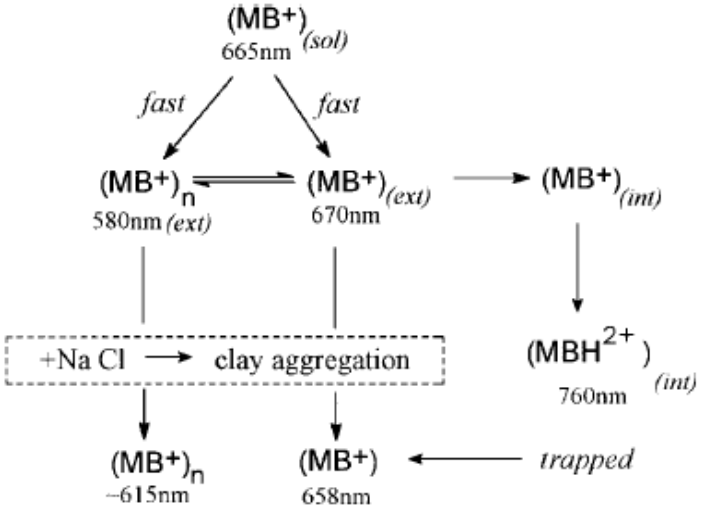

Figure 108 Idealized illustration showing the processes of approximation-association of clay particle (*Cione, 2000*)

2.7 The effect of the clay particles size

The effect of particle size on MB adsorption onto clay has been pointed out by *Neumann et al. (2002)* in Figure 109. The first tested Na-montmorillonites have particle size larger than 0.5 μm with a cation exchange capacity (CEC) equal to 144.9 meq/100 g, whereas the second one has a particle size less than 0.5 μm with a CEC value equal to 124.7 meq/100 g. As expected from the cohesion energy theory, clay with the highest layer charge leads to larger particles as proved by the high CEC. The initial configuration of MB molecules in both suspensions is mainly H-aggregates. The time evolution of the spectra shows that when particles of Na-montmorillonite are small, the rearrangement of the dye molecules is easier. Most of them end up as monomers and protonated monomers (*Kobayashi, 1996*), as evidenced by the large absorption peaks at ~670 and 760 nm, respectively.

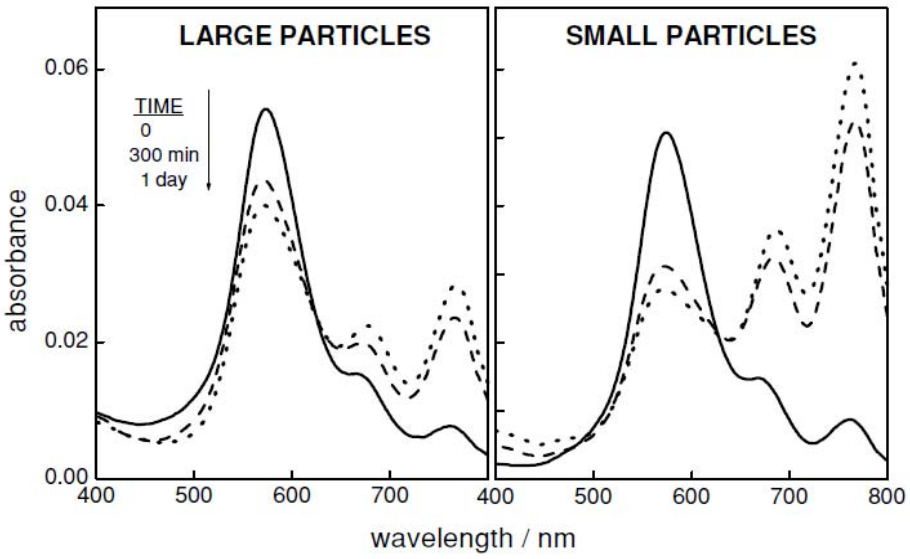

(a) (b)

Figure 109 Absorption spectra of MB in Na-montmorillonite suspensions with large (a) and small (b) particle size *(Neumann et al. 2002)*

Cione (2000) also demonstrated that the clay particle size affect the MB adsorption (Figure 110). Montmorillonite (SWy-1) and laponite which have the similar CEC value (around 72 meq/100g) were used. The particle size was big for SWy-1 (SSA = 32 m^2/g) and small from laponite (SSA = 360 m^2/g). The temporal evolution of the spectra measured on MB-clay suspensions can be explained by two different processes: (1) MB adsorption, aggregation and migration, and (2) clay particle re-arrangements (aging). Whereas the first prevails for large clay particles such as SWy-1 particles, the effects observed on small particles such as laponite ones favor the latter process.

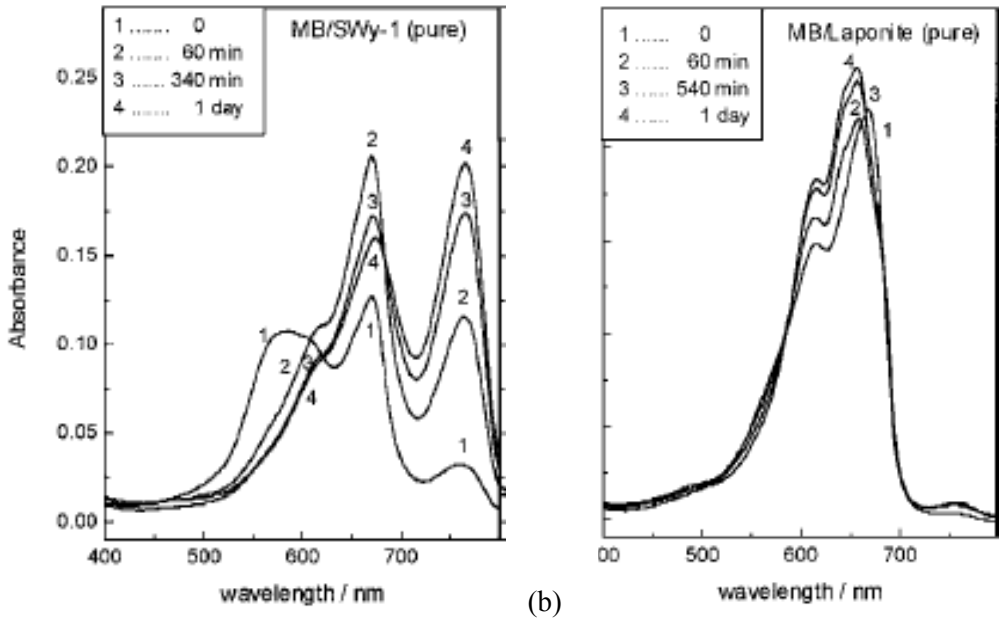

(a) (b)

Figure 110 Time dependence of the absorption spectra of MB (Conc = $4.33.10^{-6}$ M) in (a) SWy-1 montmorillonite in aqueous suspension (S/L = 0.22 g/L), and (b) laponite aqueous suspensions (S/L = 0.056 g/L) (*Cione, 2000*)

Finally, a significant side effect of the swelling properties of smectites on the dye agglomeration was proposed by *Gessner et al. (1994)* and by *Cenens and Schoonheydt (1988).* They stated that poorly-swelling clays (usually with low CEC) form large particle aggregates with small external surface area accessible for initial adsorption of cationic dye. Consequently, the dye adsorbed on such clays should be more concentrated (per unit area), which might favor the dye aggregation. However, this is not confirmed in the experiments presented here. *Bujdak (2001)* also reported that as a consequence of the formation of large clay particles (with a low layer charge), flocculation in suspension may occur. In some cases, it was observed in the form of light blue flocs or coating on the inside of the bottle.

2.8 The effect of the temperature

Regarding to the thermodynamical theory, the adsorption of MB onto clay mineral is spontaneous and exothermic due to its negative Gibbs free energy ΔG° and its enthalpy $\Delta H°$. In exothermic process, the energy released during the binding formation in new products is upper than the energy necessary to break the bounding in reactant. *Zhang et al. (2013) and Gurses (2004, 2006)* demonstrated in Figure 111 that the process of MB adsorption onto clay decrease with temperature increase which is in accordance with the Vant'Hoff law.

Vant'Hoff law : $$\ln\left(\frac{K_{T_2}}{K_{T_1}}\right) = \frac{\Delta H}{R}\left(\frac{1}{T_1} - \frac{1}{T_2}\right)$$

with the constant of reaction $K_{MB\ ads}(T) = \frac{(> CS - MB)}{(> CS)(MB)}$

and $>CS^{(-)} + MB^{+} \rightarrow >CS^{(-)} - MB^{+}$ and CS is a site on clay surface

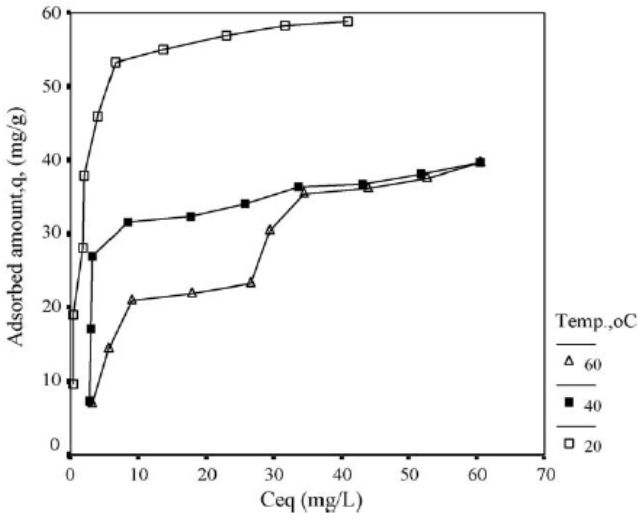

Figure 111 The variation at various temperatures of the adsorbed MB amount onto clayey material vs. equilibrium MB concentration *(Gurses et al. 2006)*

Appendix 3 Functional groups of bitumen

3.1 Saturates

Saturates usually amount for 5-15wt.% of a paving grade bitumen (*Claudy et al. 1992b;Corbett 1969*). They form a colourless or lightly coloured liquid at room temperature because of a very low glass transition temperature around −70 °C, that is typically 40 °C below the glass transition of their parent bitumen. Their hydrogen to carbon molar ratio H/C is close to 2, with only traces of hetero atoms. They comprise straight and branch-chain aliphatic hydrocarbons, together with alkyl-naphthenes and some alkyl-aromatics (Figure 112). Their number-average molecular weight is around 600 g/mol (*Lesueur 2009*) and they are mainly aliphatic: Fourier-Transform Infra-Red spectroscopy (FTIR) reveals different branching structures and some long aliphatic chains. Very few polar atoms or aromatic rings are present (*Pieri 1995*). Their solubility parameter lies between 15 and 17 MPa (*Speight 1999*) and their density at 20°C, around 0.9 g/cm3 (*Corbett 1969*).

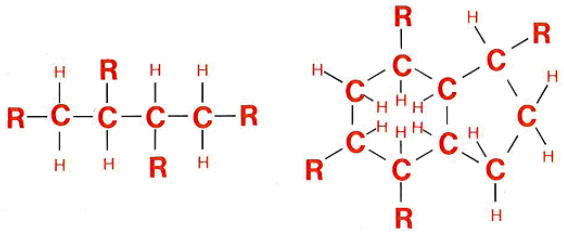

Figure 112 Saturate structure (C-Carbon; H-Hydrogen; R-Aliphatic and/or naphthenic carbon chains) (*Jones 1992*)

3.2 Aromatics

Aromatics, also called naphthene aromatics, are the most abundant constituents of a bitumen together with the resins, since they amount for 30–45 wt.% of the total bitumen (*Corbett 1969*). They form a yellow to red liquid at room temperature. They are somewhat more viscous than the saturates at the same temperature, because of a higher glass transition temperature around −20 °C, which is similar to that of the parent bitumen (*Claudy et al. 1992a 1992b*). Aromatics comprise the lowest molecular weight naphthenic aromatic compounds in the bitumen and represent the major proportion of the dispersion medium for the peptised asphaltenes (Figure 113). Their non-polar carbon skeleton is slightly aliphatic with unsaturated aromatic rings (*Pieri 1995*) and a number-average molecular weight of order 800 g/mol (*Lesueur 2009*). Hence, they have a high dissolving ability for other high molecular weight hydrocarbons (*Transportation Research Board 2003*). Their solubility parameter is between 17 and 18.5 MPa (*Speight 1999*) and their density at 20 °C close but inferior to 1 g/cm^3 (*Corbett 1969*).

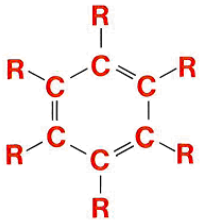

Figure 113 Aromatic structure (R- Aromatic and/or naphthenic carbon chains) (*Jones 1992*)

3.3 Resins

Resins, also called polar aromatics, consisting of high molecular weight phenols and carboxylic acids (*Wikipedia 2015*) and can be numerous (30–45 wt% from *Corbett, 1969*). If saturates and aromatics are oily liquids at room temperature, resins form a black solid at room temperature (*Corbett, 1969*) and it is not clear whether they exhibit a glass transition (*Claudy, 1992*). Koots and Speight (*1975*) showed that their composition is close to that of asphaltenes except for their lower molar mass, of circa 1100 g/mol, a somewhat higher H/C ratio between 1.38 and 1.69 and most of all a less complex aromatic structure with particle size 1-5nm (*Transportation Research Board, 2003*). Piéri (*1995*) showed that they can sometimes be more polar than asphaltenes, but again with less condensed aromatic rings. They typically contain fused aromatic rings, with a most probable structure corresponding to 2–4 fused rings. Resins are soluble in n-heptane, like asphaltenes they are largely composed of hydrogen and carbon, and contain small amount of oxygen, sulphur and nitrogen. Their solubility parameter lies between 18.5 and 20 MPa (*Speight, 1999*) and their density at 20 °C, close to 1.07 g/cm3 (*Corbett, 1969*). They play a crucial role in the stability of bitumen, since they act as a stabilizer for the asphaltenes. They are dispersing agents or peptisers for the asphaltenes and the proportion of resins to asphaltenes governs to a degree the solution (Sol) or gelatinous (Gel) type character of the bitumen (*Transportation Research Board, 2003*). Resins make up the outer protective coating of asphaltenes micelles or cluster (Figure 114). The resins are dissolved in the oil, are also surface active and polydisperse with a range of polarities and aromaticities (*Sjöblom J. 2001*).

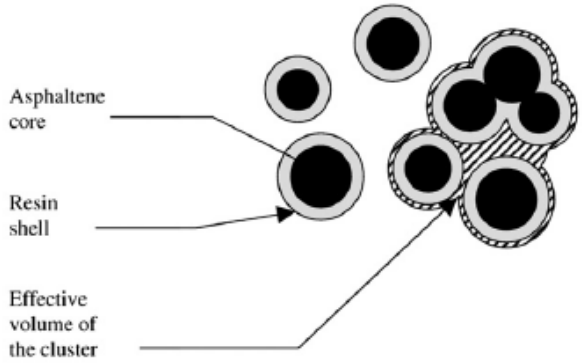

Figure 114 A simplified view of the colloidal structure of bitumen: the asphaltenes micelles are pictured as spherical to illustrate the concepts of salvation layer (resin shell) and effective volume. The oily dispersion medium is called the maltenes. (*Lesueur, 2009*)

3.4 Asphaltenes

Asphaltenes represent generally between 5 and 20 wt.% of a paving grade bitumen (*Corbett 1969;Speight 2004*) and are by far the more studied bitumen fractions because of their viscosity building role. They are also of great interest to petroleum chemists for their importance in the processing of crude oil (*Becker 1997*). They are n-heptane insoluble black or brown amorphous solids containing at room temperature (*Corbett, 1969*), in addition to carbon and hydrogen, some nitrogen, sulphur, oxygen and the traces of transition

metals from a few ppm up to a few tenth of wt.% of Ni, Va, Fe, etc.. Their elemental analysis is stable from one asphalt to the other with a H/C ratio between 0.98 and 1.56 (*Koots and Speight 1975*). Besides, they do not display any thermal transition in the normally investigated temperature range (up to 200 °C from *Claudy, 1992*). Their solubility parameter lies between 17.6 and 21.7 MPa (*Laux et al. 1997;Lian et al. 1994;Speight 1999*) and their density at 20 °C close to 1.15 g/cm^3 (*Corbett, 1969*). Asphaltenes are generally considered as highly polar and complex aromatic material of fairly high molecular weight. Different methods of determining molecular weights have led to different values ranging widely from 600 to 300,000 depending on the separation technique employed. However, the majority of test data indicates that the molecular weights of asphaltenes range from 1,000 to 10,000 (*Allsop et al. 1995a;Lesueur 2009;Speight 1999*). The covalent bonding, sigma bonds (σ bonds) and pi bonds (π bonds), mainly generates the structure of chemical compound in bitumen. In chemistry, sigma bonds are the strongest type of covalent chemical bond whereas π–π bonds are unique to aromatic molecules (*Transportation Research Board, 2003*). In comparison to other bitumen functional groups, asphaltenes contain more condensed aromatic rings and more polar groups but the presence of fused aromatic structures seems to be the fundamental feature differentiating the asphaltenes from the rest of the bitumen functional groups. Because of the many condensed aromatic rings, asphaltenes form almost planar molecules that can associate through π–π bonding to form graphite-like stacks (Figure 115, a). With these graphite-like stacks, the aliphatic structures of the molecules are found on the external part of the aggregates (Figure 115, b et c). The size of pure solid asphaltenes essentially derives from X-Ray diffraction studies. It has been indicated that 2–5 nm per one asphaltenes unit and graphite-like crystals contain an average of 5 unit sheets (*Yen et al. 1961*). When put asphaltenes in a solvent, the asphaltenes still associate and the aggregation process leads to what is generally called “micelles” (*Speight, 1999*). Micelle size depends primarily on the solvent nature, on the asphaltenes content and on temperature, as shown by their wide range of measured apparent molar masses (*Dickie and Yen 1967;Mullins and Sheu 1998;Speight 1991*). Heteroatoms among asphalt molecules develop polarity and link together by forming hydrogen bonds. Figure 115 (c) shows a hydrogen bond between two very important asphalt functional groups: a sulfoxide and a carboxylic acid. Van der Waals bonding is the weakest of the secondary bonds. They form when molecules cool or stress is removed. Van der Waals bonding is responsible for the free-flowing nature of asphalt at high temperatures versus the semisolid nature at lower temperatures (*Jones 1992*). As a point of reference, it is important to understand that covalent primary bonds within the molecule are from 10 to 100 times stronger than secondary bonds (*Transportation Research Board, 2003*).

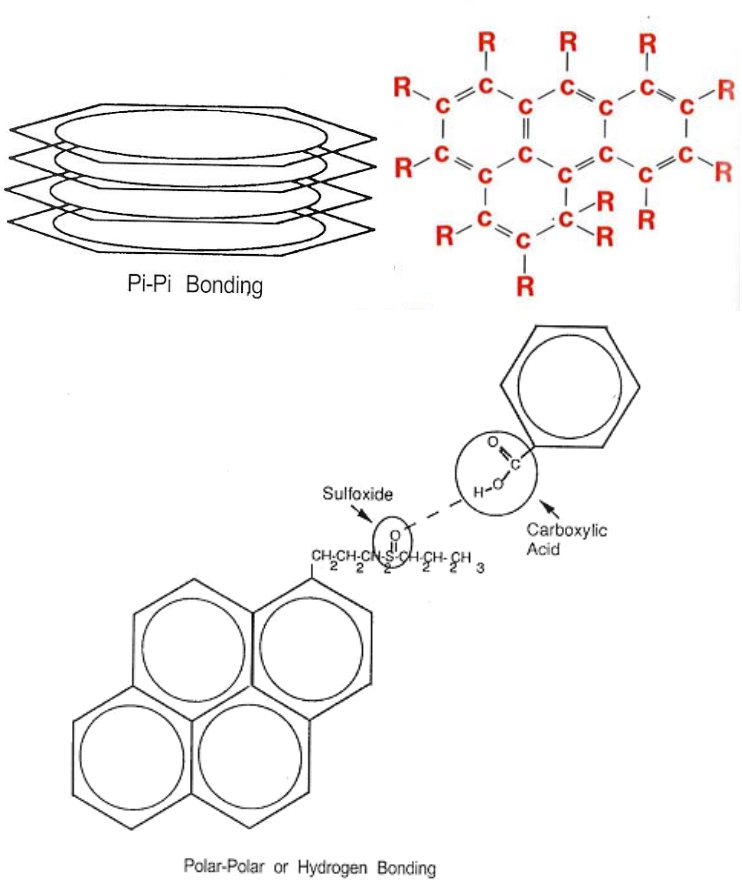

Figure 115 Asphaltenes structure (R-Aliphatic naphthenic or aromatic carbon chains) (*Allsop, 1995; Transportation Research Board, 2003; Jones, 1992*)

Appendix 4 Experiments : design of AC mixtures

4.1 Richness Modulus

Increasing bitumen content, using harder grade of bitumen and decreasing $D_{2/6mm}$ fraction of aggregate in AC mixture are suggested to improve water resistance by its physical properties.

The bitumen content is calculated from the specific surface area of the aggregates, the maximum density (MVR) value and the minimum richness modulus associated with the standard.

In the former French system, the binder content was based on the concept of "Richness Modulus", whose approach is close to the thickness of the bitumen foil and which makes the requirement independent from the grading curve of the mixture.

The richness modulus, K, is a value proportional to the conventional thickness of the hydrocarbon binder film coating the aggregate. K is independent of the density of the granular mix; it is correlated with external binder content via the following equation (*Delorme and Wendling 2007*)

$$TL_{ext} = \mathrm{K} \times \alpha \sqrt[5]{\Sigma}$$

Where

TL_{ext} is binder content, which represents the ratio of the binder mass to the dry aggregate mass, expressed as an external percentage.

Σ is the specific surface area, m^2/kg, determined by the relation:

$100\Sigma = 0.25G + 2.3S + 12s + 150f$ with:

- G the proportion of aggregate particles greater than 6.3mm
- S the proportion of aggregate particles included between 6.3 and 0.25mm
- s the proportion of aggregate particles between 0.25mm and 0.063mm
- f the proportion of aggregate particles less than 0.063mm
- α a correction coefficient relative to the density of aggregates
- $\alpha = 2.65/\rho_G$, with ρ_G being the mass density of aggregates in grams per cubic centimeter.

Therefore, the increase of richness modulus enhances the water resistance of AC mixture by thickening the asphalt film on aggregates. The hard grade of bitumen for AC mixture is used for the heavy loading pavement, and altitudes lower than 500 m. The lower diffusion coefficient from hard grade of bitumen assists its water resistance. However, to better prevent against cracking risks under severe traffic and climatic loading conditions, it would be advised to select the softest grade compatible with rutting resistance-based requirements. Last, the percentage of void in AC mixture decreases with decreasing the quantity of $D_{2/6mm}$ fraction of aggregate. Therefore, stripping is harder to initialize than the higher void of AC mixture.

4.2 Density and viscosity of materials for AC mixture

Material	Bitumen [a]	Diorite [a]	washed sand	Kao.	Illite	Montm.	Limestone [a]	Unknown A-E
Density (g/cm^3)	1.03	2.91	2.65	2.6 [b]	2.2 [b]	2.1 [b]	2.7	2.65 [b]
Viscosity (Pa*s)	0.0847	0.0767	-	-	-	-	0.0776	-
Fraction	binder	coarse	sand	clay from fines			filler from fines	fine aggregates

[a] Material database from laboratory
[b] (***Ayadi et al. 2013;Magnan 1999;Mineralogy database 2015;Morrison and Gasperikova 2015***)

Appendix 5 Particle size distribution

5.1 Particle size distribution

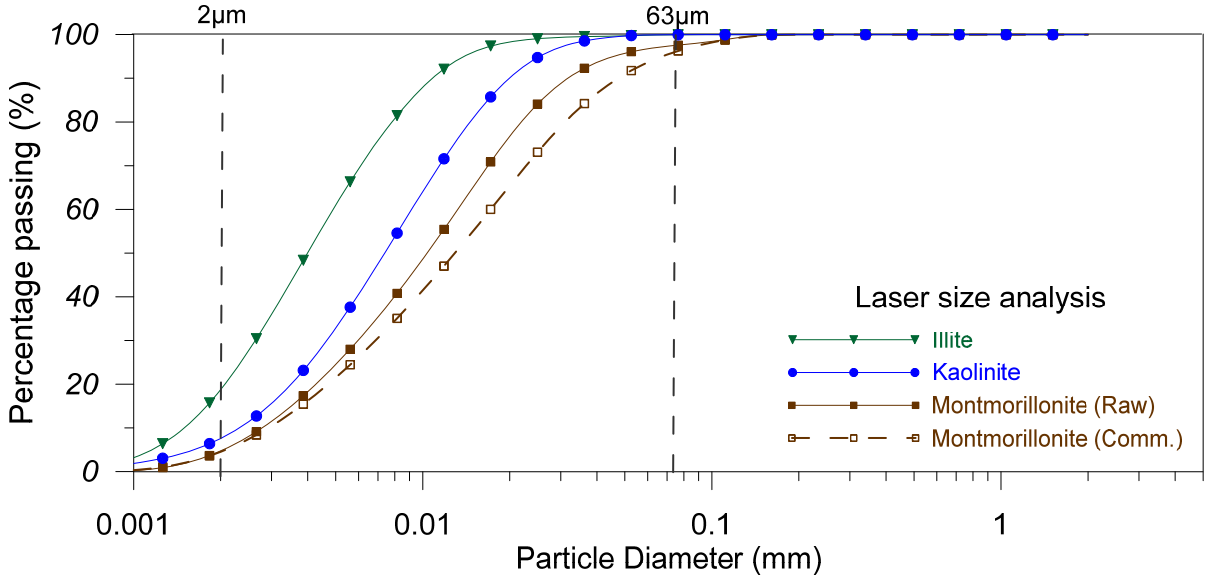

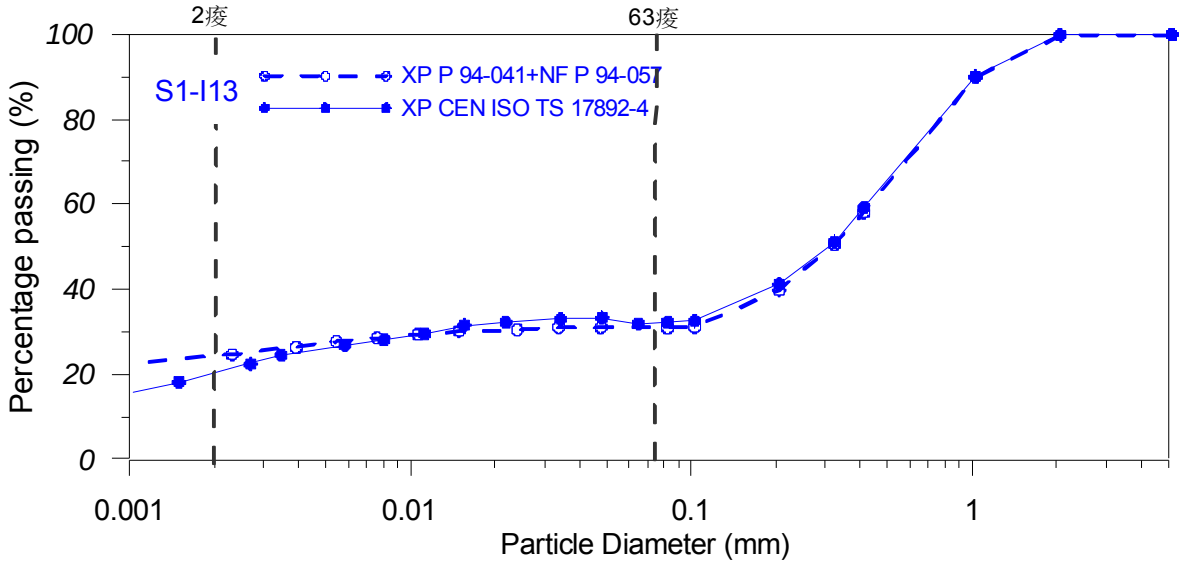

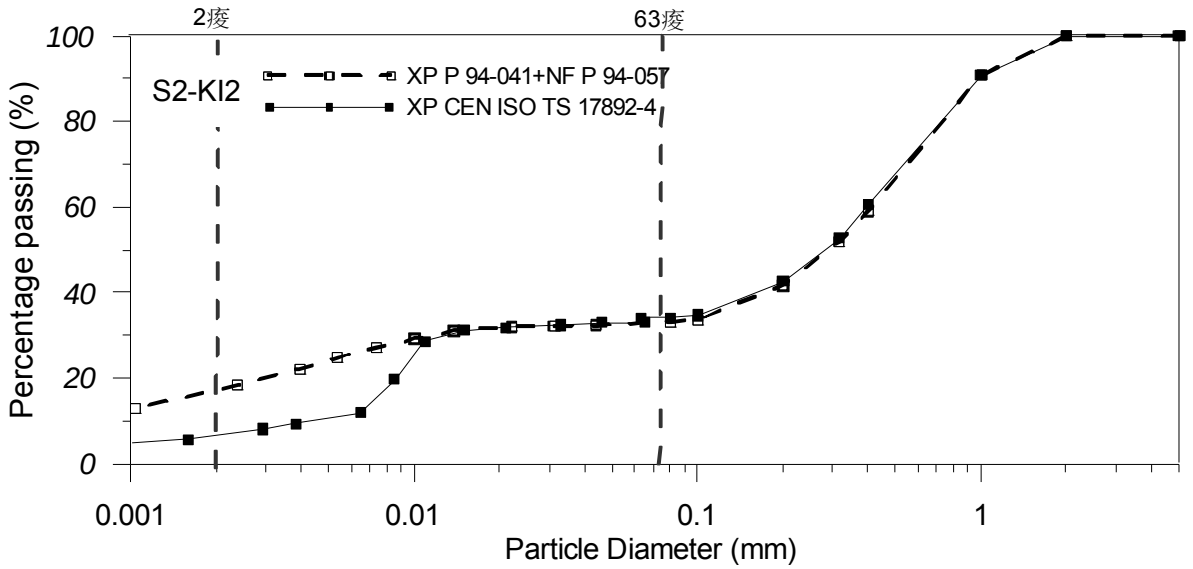
2瘘
63瘘
S2-KI2
XP P 94-041+NF P 94-057
XP CEN ISO TS 17892-4
Percentage passing (%)
100
80
60
40
20
0
0.001
0.01
0.1
1
Particle Diameter (mm)

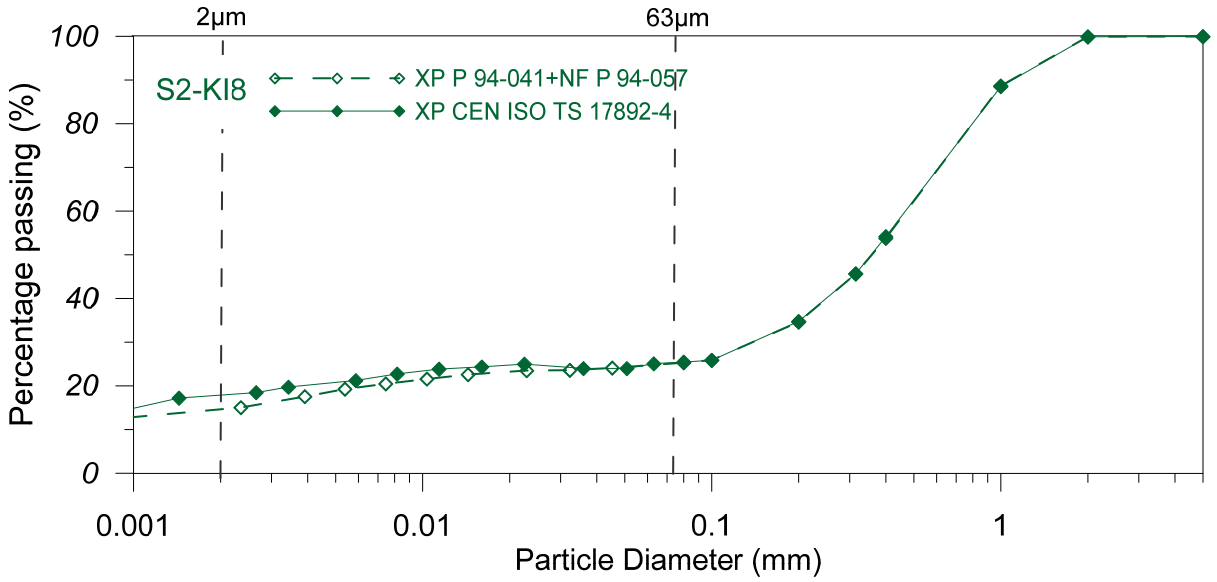
2μm
63μm
S2-KI8
XP P 94-041+NF P 94-057
XP CEN ISO TS 17892-4
Percentage passing (%)
100
80
60
40
20
0
0.001
0.01
0.1
1
Particle Diameter (mm)

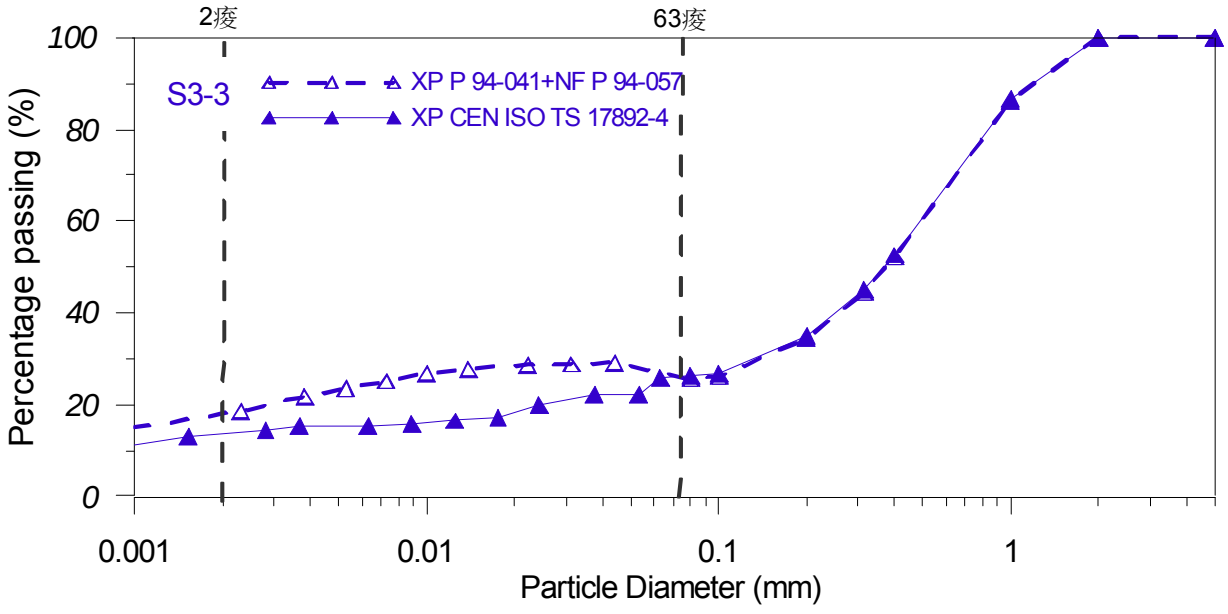
2瘘
63瘘
S3-3
XP P 94-041+NF P 94-057
XP CEN ISO TS 17892-4
Percentage passing (%)
100
80
60
40
20
0
0.001
0.01
0.1
1
Particle Diameter (mm)

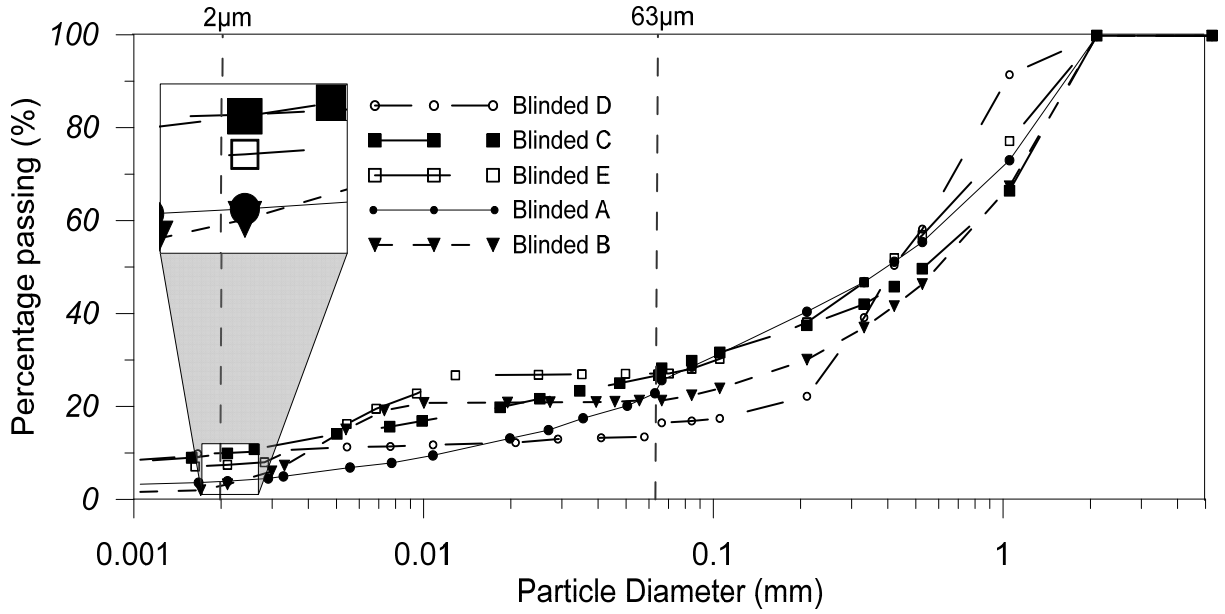
2μm
63μm
100
80
60
40
20
0
Percentage passing (%)
Blinded D
Blinded C
Blinded E
Blinded A
Blinded B
0.001
0.01
0.1
1
Particle Diameter (mm)

5.2 MB adsorption studied on MB-pHs-clays suspension by UV-photometric method

MB adsorption studied from MB-pHs-kaolinite suspension after 5 days of contact. CEC (meq/100g) = 1.3

Sample n°	pH	Init. MB covering percentage %	Abs.	MB (g/kg)	Fin. MB covering percentage % [c]
high 7	1.0	531.93	0.29	5.60	137.31
high 6	1.8	510.17	0.30	5.19	127.25
high 3	2.7	552.89	0.34	4.75	116.49
high 5	3.6	570.46	0.34	5.13	125.65
low 2	4.7	233.69	0.08	5.57	136.49
high 4	5.3	532.06	0.28	6.48	158.77
high 2 (water)	5.4	1516.53	0.75	20.71	507.58
high 8	7.0	527.13	0.26	8.27	202.77
high 9	7.5	709.81	0.42	6.51	159.48
high 10	7.9	569.49	0.31	7.02	172.19
high 11	8.8	602.09	0.29	9.64	236.32
high 12	11.0	513.43	0.12	14.56	357.02
high 13	11.1	750.98	0.15	22.74	557.47
high 14	11.9	1111.87	0.03	43.86	1075.18
low 15	12.6	0.00	0.00	0.00	0.00
		Methylene blue (UV) 2hrs			
		Init. MB covering percentage % [b]	Abs.	MB (g/kg)	Fin. MB covering percentage % [c]
		154.1	0.51	6.4	153.9

MB adsorption studied from MB-pHs-illite suspension after 5 days of contact. CEC(meq/100g) =23.3

Sample n°	pH	Init. MB covering percentage %	Abs.	MB (g/kg)	Fin. MB covering percentage % [c]
Low 1	0.9	67.02	0.00	49.96	67.02
High 7	0.9	133.99	0.75	59.13	79.33
High 6	2.0	100.84	0.68	39.40	52.86
High 3	3.2	104.31	0.73	39.31	52.73
High 5	5.3	101.78	0.63	43.77	58.71
High 4	6.9	105.93	0.57	48.51	65.08
High 8	7.0	106.92	0.61	48.26	64.75
Low 2	7.1	77.49	0.24	44.94	60.29
High 9	7.2	98.56	0.47	48.71	65.34
High 10	7.3	107.47	0.57	49.63	66.58
High 11	7.8	107.26	0.85	41.86	56.15
High 2 (water)	8.4	119.45	0.18	80.25	107.65
High 12	9.8	99.56	0.47	50.05	67.14
High 13	11.0	96.29	0.31	56.44	75.72
Low 14	12.1	92.88	0.07	65.45	87.81
Low 15	12.6	57.95	0.00	43.20	57.95
		Methylene blue (UV) 2 hrs			
		Init. MB covering percentage % [b]	Abs.	MB (g/kg)	Fin. MB covering percentage % [c]
		62.5	1.80	46.3	62.1

MB adsorption studied from MB-pHs-montmorillonite suspension after 5 days of contact. CEC(meq/100g) = 103.6

Sample n°	pH	Init. MB covering percentage %	Abs.	MB (g/kg)	Fin. MB covering percentage % [c]
14	1.9	91.85	0.15	296.90	89.60
13	2.7	78.60	0.13	253.52	76.51
12	3.4	91.56	0.14	296.13	89.36
11	4.2	77.71	0.15	249.55	75.31
10	5.3	77.51	0.20	247.15	74.58
9 (water)	6.0	78.52	0.17	251.59	75.92
8	6.7	93.08	0.17	299.82	90.48
7	7.5	80.63	0.13	260.64	78.66
6	8.8	77.72	0.09	253.12	76.39
5	9.7	84.38	-0.21	290.39	87.63
3	11.2	79.70	0.11	258.84	78.11
2	11.5	79.47	0.13	256.92	77.53
1	12.7	83.90	0.15	270.88	81.74

		Methylene blue (UV) 2 hrs Init. MB covering percentage % [b]	Abs.	MB (g/kg)	Fin. MB covering percentage % [c]
		92.3	1.05	304	91.7

5.3 Duriez results of AC mixtures related to extracted clay content in artificial fine aggregates

Mixture	Ext. clay content in $D_{0/2mm}$ fraction (%)				% clay/$D_{0/2mm}$	% clay/all-in fraction	v% (residual voids)	Duriez (i/c)	S.D.	Retaining tensile strength (%)	S.D.
	sand	kao	illite	montm							
Non-clay reference	100.00	0	0	0	0.00	9.00	9.85	1.00	0.07	100.00	7.45
S1 K2	78.56	21.44	0.00	0.00	21.44	4.37		0.94	0.03	93.67	3.24
S1 K3	70.00	30.00	0.00	0.00	30.00	6.86		0.87	0.04	86.76	4.19
Kao-reference	65.42	34.58	0.00	0.00	34.58	8.46	12.51	0.74	0.06	74.00	6.37
S1 I4	92.78	0.00	7.22	0.00	7.22	1.24		0.89	0.03	88.61	3.31
S1 I9	80.00	0.00	20.00	0.00	20.00	4.00	10.32	0.77	0.03	76.66	2.58
S1 I13	70.00	0.00	30.00	0.00	30.00	6.86	9.96	0.60	0.03	60.00	2.90
Illite-reference	63.90	0	36.096	0	36.10	9.04	9.32	0.56	0.03	56.00	2.64
S1 M2	99.48	0.00	0.00	0.52	0.52	0.08	11.08	0.90	0.05	89.71	4.91
S1 M4	98.63	0.00	0.00	1.37	1.37	0.22	11.20	0.87	0.14	86.77	14.09
S1 M12	95.23	0.00	0.00	4.77	4.77	0.80	11.56	0.75	0.05	75.17	5.40
Montm-reference	65.09	0	0	34.91	34.91	8.58	9.49	0.11	0.01	11.00	1.12
S2-KI2	67.38	26.27	6.35	0.00	32.62	7.75	11.73	0.79	0.07	79.47	7.39
S2-KI8	75.66	8.91	15.43	0.00	24.34	5.15	10.82	0.85	0.08	84.69	7.71
S2-IM6	88.21	0.00	7.47	4.31	11.79	2.14	11.81	0.70	0.09	69.66	8.71
S2-IM10	90.28	0.00	3.56	6.16	9.72	1.72	12.12	0.61	0.07	60.88	6.51
S2-KM3	69.86	27.24	0.00	2.90	30.14	6.90	11.62	0.90	0.06	90.12	5.79
S2-KM11	88.14	4.34	0.00	7.52	11.86	2.15	11.60	0.63	0.04	63.37	3.57
S3-2	69.35	28.43	1.56	0.66	30.65	7.07	11.65	0.76	0.09	76.18	9.30
S3-3	73.41	16.63	6.92	3.05	26.59	5.80	11.05	0.69	0.03	68.56	3.39
S3-5	81.60	9.61	3.22	5.57	18.40	3.61	11.27	0.65	0.04	64.68	3.87

References

AASHTO T 283. Resistance of compacted hot-mix asphalt to moisture-induced damage. 2014.

AASHTO T165. Standard method of test for effect of water on cohesion of compacted bituminous mixtures twentieth edition. 1997.

AgriInfo.in. My agriculture information bank. http://www.agriinfo.in/?page=topic&superid=4&topicid=249 . 2011.

Akbulut S., Kurt C.N., & rasan S. 2012. Surfactant modified clays' consistency limits and contact angles. *Earth sciences research*, 16, (2) 13-19

AkzoNobel 2015, *Adhesion promoters* 5.

Al-Ghouti, M.A., Khraisheh, M.A.M., Allen, S.J., & Ahmad, M.N. 2003. The removal of dyes from textile wastewater: a study of the physical characteristics and adsorption mechanisms of diatomaceous earth. *Journal of Environmental Management*, 69, 229-238

Alexander, M. 2004, "Catalytic and adsorption properties of modified clay surface," *In Clay Surfaces fundamentals and applications*, W. Fernando & G. S. Kestur, eds., *Universidade Federal do Paraná,* Curitiba, Brazil.

Allsop, R., Dussek, I., Hayton, B., Heimerikx, G., Prince, L., Rosa, J. D., Southern, M., Vonk.W., Whiteoak, D., Woolf, L., & Yin, P. 1995, "The manufacture, storage and handling of bitumen," *In The shell bitumen industrial handbook*, Chersey: Shell bitumen, pp. 39-86.

Allsop, R., Dussek, I., Hayton, B., Heimerikx, G., Prince, L., Rosa, J. D., Southern, M., Vonk.W., Whiteoak, D., Woolf, L., & Yin, P. 1995, "Specification, testing and properties of bitumen," *In The shell bitumen industrial handbook*, Chersey: Shell bitumen, pp. 63-117.

Arambula, E., Caro, S., & Masad, E. 2010. Experimental measurements and numerical simulation of water vapor diffusion through asphalt pavement material. *Journal of Materials in Civil Engineering*, 22, 588-598

Ardebrant, H. & Pugh, R.J. 1991. Surface acidity/basicity of road stone aggregates by adsorption from non-aqueous solutions. *Colloids and Surfaces*, 53, (1) 101-116

Aschenbrener, T. 1995, *Evaluation of Hamburg Wheel-Tracking Device to predict moisture damage in hot mix asphalt*, National Research Council, Washington D.C., 1492.

ASTM D1075-11. Standard test method for effect of water on compressive strength of compacted bituminous mixtures. 2011.

ASTM D1370. Standard test method for contact compatibility between asphaltic materials (Oliensis test). 12. 7-15-2012.

ASTM D3279. Standard test method for n-heptane insolubles. 2007.

ASTM D3625. Standard practice for effect of water on bituminous-coated aggregate using boiling water. 2005.

ASTM D4541. Standard test method for pull-off strength of coatings using portable adhesion testers. 2009.

ASTM D7503-10. Standard test method for measuring the exchange complex and cation exchange capacity of inorganic fine-grained soils. 7-1-2010.

Ayadi, A.J., Soro, J., Kamoun, A., & Baklouti, S. 2013. Study of clay's mineralogy effect on rheological behavior of ceramic suspensions using an experimental design. *International Journal of Research and Reviews*

in Applied Sciences, 14, (2) 374-384 available from: www.arpapress.com/Volumes/Vol14Issue2/IJRRAS_14_2_17.pdf

Ayari F., Srasra E., Trabelsi-Ayadi M. Retention of organic molecule "quinalizarin" by bentonitic clay saturated with different cations, *Desalination*, 206 (2007), pp. 499–506

Bagampadde, U., Isacsson, U., & Kiggundu, B.M. 2004. Classical and contemporary aspects of stripping in bituminous mixture. *Road material and pavement design*, 5, 7-43

Bagampadde, U. & Isacsson, U. 2005. Influence of aggregate chemical and mineralogical composition on stripping in bituminous mixtures. *International journal of pavement engineering*, 6, 229-239

Bagampadde, U., Isacsson, U., & Kiggundu, B.M. 2006. Impact of bitumen and aggregate composition on stripping in bituminous mixtures. *Materials and Structures*, 39, 303-315

Bahia, H. & Seemab, A. 1999, *Evaluation and correlation of lab and field tensile strength ratio (TSR) procedures and values in assessing the stripping potential of asphalt mixes*, University of Wisconsin, Madison, WIISPR-10-99.

Bailey, S.W. 1980. Summary of recommendations of AIPEA nomenclature committee on clay minerals. *American Mineralogist*, 65, 1-7 available from: http://www.minsocam.org/msa/collectors_corner/arc/nomenclaturecl1.htm

Basu, S., Nandakumar K., & Masliyah J.H. 2000. A study on daughter droplets formation in bitumen glass water contact line displacement due to instability. *Fuel*, 79, 837-841 available from: www.elsevier.com/locate/fuel

Basu, S., Nandakumar, K., & Masliyah, J.H. 1996. A Study of Oil Displacement on Model Surfaces. *Journal of Colloid and Interface Science*, 182, (1) 82-94 available from: http://www.sciencedirect.com/science/article/pii/S0021979796904397

Basu, S., Nandakumar, K., & Masliyah, J.H. 1998. Effect of NaCl and MIBC kerosene on bitumen displacement by water on a glass surface. *Colloids and Surfaces A: Physicochcmical and Engineering Aspects*, 136, 71-80

Basu, S., Nandakumar, K., Lawrence, S., & Masliyah, J. 2004. Effect of calcium ion and montmorillonite clay on bitumen displacement by water on a glass surface. *Fuel*, 83, (1) 17-22 available from: http://www.sciencedirect.com/science/article/pii/S0016236103002229

Becker, J.R. 1997. Crude Oil -Waxes*, Emulsions and Asphaltenes* PennWell, Tulsa.

Bell, C. 1989, *Summary report on aging of asphalt-aggregate systems*, National Research Council, Washington D.C., A-305.

Bentahar, B. La nocivité des fines argileuses sur la tenue a l'eau des enrobés tièdes. Centre d'Etude Technique de l'Equipement (CETE) Aix en Provence. 9-9-2010.

Bergaya, F. & Lagaly, G. 2006, "General introduction: clay, clay minerals ans clay science," *In Hand book of clay science*, Bergaya F., Theng B.K.G., & Agaly G., eds., Elsevier, pp. 1-18.

Bergman, K. & , O.C.T. 1963. A spectroscopic study of methylene blue monomer, dimer and complexes with montmorillonite. *The Journal of Physical Chemistry*, 67, (2169) 2177

Bhattacharyya, K.G. & Gupta, S.S. 2008. Adsorption of a few heavy metals on natural and modified kaolinite and montmorillonite: A review. *Advances in Colloid and Interface Science*, 140, (2) 114-131

Birgisson, B., Roque, R., Tia, M., & Eyad, A. 2005, *Development and evaluation of test methods to evaluate water damage* UF #4910-4504-722-12.

Birgisson, B., Roque, R., & Page, G. 2003. Evaluation of water damage using hot mix asphalt fracture mechanics. *Association of Asphalt Paving Technologists*, 72, 516-562

Biscaye, P.E. 1964. Mineralogy and sedimentation of recent deep-sea clay in the Atlantic Ocean and adjacent seas and oceans. *Deep Sea Research and Oceanographic Abstracts*, 13, (5) 803-832

Bish, D.L. & Howard, S.A. 1988. Quantitative phase analysis using the Rietveld method. *Journal of Applied Crystallography*, 21, 86-91

Bish, D.L. & Post, J.E. 1993. Quantitative mineralogical analysis using the Rietvetd full-pattern fitting method. *American Mineralogist*, 78, 932-940

Blazek, J., Sebor, G., Maxa, D., Ajib, M., & Paniagua, H. 2000. Effect of hydrated lime addition on properties of asphalt. *Journal of Petroleum and Coal*, 42, (1) 41-45

Bodenheimer, W. & Heller, L. 1968. Sorption of methylene blue by montmorillonite saturated with different cations. *Israel Journal of Chemistry*, 6,

Bouchet, A., Meunier, A., & Sardini, P. 2000. *Minéraux argileux : structure cristalline, identification par diffraction des rayons X*, EP ed.

Bowen, N.L. 1922. The reaction principle in petrogenesis. *Journal of Geology* (3)

Bradley, W.F. 1945. Molecular associations between montmorillonite and some polyfunctional organic liquids. *Journal of the American Chemical Society*, 67, (6) 975-981

Bradley, W.F. & Grim, R.E. 1951. High temperature thermal effects of clay and related materials. *American Mineralogist*, 36, (3/4) 182-201

Brindley, G. W. 1980, "Quantitative X-ray mineral analysis of clays.," *In Crystal structures of clay minerals and their X-ray identification.*, Brindley,G.W., Brown,G. ed. pp. 411-438.

Brindley, G.W. & Brown, G. 1980. *Crystal structures of clay minerals and their X-Ray identification*.

Brindley, G.W. & Hoffman, R.W. 1962. Orientation and packing of aliphatic chain molecules on montmorillonite. *Clays and Clay Minerals*, 11, 546-556

Brown, E. C. & Kuntze, R. A. 1972, *A study of stripping in asphalt pavements*, Departmenet of Transportation and Communications, Ontario, RR117.

Brown, G. & Brindley, G. W. 1984, "X-ray diffraction procedures for clay mineral identification," *In Crystal structures of clay minerals and their X-Ray identification*, pp. 305-256.

Buckman, H.O. & Brady, N.C. 1969. *The natural and properties of soils*, 7th ed. London, Macmillan.

Bujdak, J. & Komadel, P. 1997. Interaction of methylene blue with reduced charge montmorillonite. *Journal of Physical Chemistry B*, 101, (44) 9065-9068

Bujdak, J., Janek, M., Madejova, J., & Komadel, P. 1998. Influence of the layer charge density of smectites on the interaction with methylene blue. *J Chem Soc*, 94, 3487-3492

Bujdak, J., Janek, M., Madejova, J., & Komadel, P. 2001. Methylene blue interactions with reduced-charge smectites. *Clays and Clay Minerals*, 49, (3) 244-254

Bujdak, J., lyi, N., & Fujita, T. 2002. The aggregation of methylene blue in montmorillonite dispersions. *Clay Minerals*, 37, 121-133

Bujdak, J., Iyi, N., Kaneko, Y., & Sasai, R. 2003. Molecular orientation of methylene blue cations adsorbed on clay surfaces. *Clay Minerals*, 38, 561-572

Bujdak, J. 2006. Effect of the layer charge of clay minerals on optical properties of organic dyes. A review. *Applied Clay Science*, 34, 58-73

Bukka, K., Miller, J.D., Hanson, F.V., Misra, M., & Oblad, A.G. 1994. The influence of carboxylic acid content on bitumen viscosity. *Fuel*, 73, (2) 257-268

Campanac, R. 1981. La nocivite des fines argileuses au regard des performances d'un enrobe a chaud. *bulletin de liaison des ponts et chaussées* (111) 53-60

Caro, S., Masad, E., Bhasin, A., & Little, D.N. 2008. Moisture susceptibility of asphalt mixtures, Part 1: mechanisms. *International journal of pavement engineering*, 9, 81-98

Caro, S., Beltrán, D.P., Alvarez, A.E., & Estakhri, C. 2012. Analysis of moisture damage susceptibility of warm mix asphalt (WMA) mixtures based on Dynamic Mechanical Analyzer (DMA) testing and a fracture mechanics model. *Construction and Building Materials*, 35, 460-467

Carter, D. L., Mortland, M. M., & Kemper, W. D. 1986, "Specific surface," *In Methods of soil analysis*, American Society of Agronomy ed. pp. 413-423.

Carter, R.C. & Wilde, P. 1972. Cation exchange capacity of suspended material from coastal sea water of central California. *marine geology*

Cenens, J. & Schoonheydt, R.A. 1988. Visible spectroscopy of methylene blue on hectorite, Laponite B and Barasym in aqueous suspensions. *Clays and Clay Minerals*, 36, 214-224

Chassin, P., Jouany, C., & Quiquampoix, H. 1986. Masurement of the surface free energy of calcium-montmorillonite. *Clay Minerals*, 21, 899-907 available from: http://www.minersoc.org/pages/Archive-CM/Volume_21/21-5-899.pdf

Chefetz, B., Eldad, S., & Polubesova, T. 2011. Interactions of aromatic acids with montmorillonite: Ca2+- and Fe3+-saturated clays versus Fe3+-Ca2+ clay system. *Geoderma*, 160, 608-613 available from: http://www.sciencedirect.com/science/article/pii/S0016706110003630

Cheng, D. X., Little, D. N., Lytton, R. L., & Holste, J. C. 2002 Use of surface free energy properties of the asphalt-aggregate system to predict damage potential.

Cheng, D.X., Little, D.N., Lytton, R.L., & Holste, J.C. 2003. Moisture damage evaluation of asphalt mixtures by considering both moisture diffusion and repeated-load conditions. *Transportation Research Record*

Chorom, M. & Rengasamy, P. 1995. Dispersion and zeta potential of pure clays as related to yet particle charge under varying pH, electrolyte concentratyion and cation type. *European Journal of Soil Science*, 46, 657-665

Christidis, G.E. & Eberl, D.D. 2003. Determination of layer-charge characteristics of smectites. *Clays and Clay Minerals*, 51, (6) 644-655

Chung, F.H. 1974. Quantitative interpretation of X-ray diffraction patterns of mixtures. II. Adiabatic principle of X-ray diffraction analysis of mixtures. *Journal of Applied Crystallography*, 7, 526-531

Chung, F.H. 1974. Quantitative interpretation of X-ray diffraction patterns of mixtures. I. Matrix flushing method for quantitative multicomponent analysis. *Journal of Applied Crystallography*, 7, 519-525

Cione, A.P.P., Neumann, M.G., & Gessner, F. 1998. Time-dependent spectrophotometric study of the interaction of basic dyes with clays: III. Mixed dye aggregates on SWy-1 and laponite. *Journal of Colloid and Interface Science*, 198, (1) 106-112

Cione, A.P.P., Schmitt, C.C., Neumann, M.G., & Gessner, F. 2000. The effect of added salt on the aggregation of clay particles. *Journal of Colloid and Interface Science*, 226, 205-209

Cipriano, B.H., Raghavan, S.R., & McGuiggan, P.M. 2005. Surface tension and contact angle measurements of a hexadecylimidazolium surfactant adsorbed on a clay Surface. *Colloids and Surfaces A: Physicochemical and Engineering Aspects*, 262, 8-13

Claudy, P., Letoffe, J.M., King, G.N., & Planche, J.P. 1992. Characterization of asphalts cements by thermomicroscopy and differential scanning calorimetry: Correlation to classic physical properties. *Fuel*, 10, (4) 735-765

Claudy, P., Letoffe, J.M., King, G.N., & Planche, J.P. 1992. Caractérisation des bitumes routiers par analyse calorimétrique différentielle (ACD). Analyse thermo-optique (ATO). Corrélation entre propriétés physiques et résultats ACD. *Bull Liaision Lab Ponts et Chaussees*, 177, 45-51

Clement, C. 1988. *Etude de coulis hydrauliques pour la rétention de cations polluants : Pb, Cd, Hg, Sr, Cs.* Ecole Nationale Supérieure des Mines de Paris.

Conway, B.E. & Ayranci, E. 1998. Effective ionic radii and hydration volumes for evaluation of solution properties and ionic adsorption. *Journal of Solution Chemistry*, 28, (3) 163-192

Corbett, L.W. 1969. Composition of asphalt based on generic fractionation, using solvent deasphaltening, elution-adsorption chromatography and densimetric characterization. *Analytical Chemistry*, 41, (4) 576-579

Cotton, F. & Wilkinson, G. 1980. *Advanced Inorganic Chemistry*, 4 ed. New York.

Curtis, C. W. Investigation of asphalt-aggregate interactions in asphalt pavements. American Chemical Society(Feul) 37, 1292-1297. 1992.

Curtis, C. W., Ensley, K., & Epps, J. 1993, *Fundamental Properties of Asphah-Aggregate Interactions Including Adhesion and Adsorption*, SHRP-A-341,National Research Council,Washington,DC.

Czímerová, A., Jankovic, L., & Bujdák, J. 2004. Effect of the exchangeable cations on the spectral properties of methylene blue in clay dispersions. *Journal of Colloid and Interface Science*, 274, 126-132

Czímerová A., Bujdak, J., & Dohrmann, R. 2006. Traditional and novel methods for estimating the layer charge of smectites. *Applied Clay Science*, 34, (1-4) 2-13

del Monte, E. & Levy, D. 1999. Identification of oblique and coplanar inclined fluorescent J-dimers in rhodamine 110 doped sol-gel-glasses. *Journal of Physical Chemistry*, 103, 8080-8086

Delorme, J. L. & Wendling, L. 2007, *LPC Bituminous Mixtures Design Guide, The RST Working Group "Design of bituminous mixtures "*.

Department of Scientific and Industrial Reaserch 1962. *Bituminous Materials in Road Construction* London, Her Majesty's Stationery Office.

Dharaiya, D. & Jana, S.C. 2005. Thermal decomposition of alkyl ammonium ions and its effects on surface polarity of organically treated nanoclay. *Polymer*, 46, (23) 10139-10147 available from: http://www.sciencedirect.com/science/article/pii/S0032386105011596

Diamond, S. & Kinter, E.B. 1961. Characterization of montmorillonite saturated with short-Chain amine cations: 1. interpretation of basal spacing measurements. *Clays and Clay Minerals*, 10, 167-173

Dickie, J.P. & Yen, T.F. 1967. Macrostructure of the asphaltic fractions by various instrumental methods. *Analytical Chemistry*, 39, (1847) 1852

Duc, M. 2002. *Contribution à l'étude des mécanismes de sorption aux interfaces solide-liquide : application aux cas des apatites et des oxy-hydroxydes.* Châtenay-Malabry, Ecole centrale de Paris.

Dupre, A.M. & Dupre, P. 1869. *Theorie mechanique de la chaleur* Gauthier-Villars.

Dupriet, S. Fines argileuses/partie route. Technical seminar from UNPG . 11-18-2010.

Duriez, M. & Grelot, L. 1950. *Traité de matériaux de construction* Paris.

Dutrow, B. & Clark, C. M. X-ray powder diffraction (XRD). 2015.

Dyal, R.S. & Hendricks, S.B. 1950. Total surface of clays in polar liquids as a characteristic index. *J.Soil Sci.*, 59, 421-432

Dzene, L., Tertre, E., Hubert, F., & Ferrage, E. 2015. Nature of the sites involved in the process of cesium desorption from vermiculite. *Journal of Colloid and Interface Science*, 455, 254-260

Eberl, D. D. 2003, *User's guide to RockJock- a program for determining quantitative mineralogy from powder X-Ray diffraction data* 03-78.

Fieldes, M. & Swindale, L.D. 1954. Chemical weathering of silicates in soil formation. *Journal of the Science and Technology of New Zealand*, 56, 140-154

Fotland, P. & Anfindsen, H. 1996. Electrical conductivity of asphaltenes in organic solvents. *Fuel Science and Technology International*, 14, 101-116

Fotland, P. & Anfindsen, H. 1998, "Conductivity of asphaltenes," *In Structures and Dynamics of Asphaltenes*, O. C. Mullins & E. Y. Sheu, eds., New-York: Plenum Press, pp. 247-266.

Fowkes, F.M. 1964. Dispersion force contributions to surface and interfacial tensions, contact angles, and heats of immersion. *Advances in Chemistry Series*, 43, 99-111

Fripiat, J.J., , S.A., & Leonard, D. 1962. Etude de l'adsorption des amines par les montmorillonites III. La nature de la liaison amine montmorillonite. *Bulletin de la Société Chimique de France*, 29, 635-644

Frouin, L. 1989, *Étude expérimentale des interactions surfaces minérales - bitume: cas particulier des argiles*, Laboratoire Central des Ponts et Chaussées Paris, Paris, 154.

Gaestel, C., Smadja, R., & Lamminan, K. A. 1971 Contribution a la Connaissance des proprietes des bitumen routiers, p. 466.

Ghosh, D. & Bhattacharyya, K.G. 2002. Adsorption of methylene blue on kaolinite. *Applied Clay Science*, 20, 295-300

Glaeser, R. & Mering, J. 1967. Effet du chauffage sur les montmorillonites satur6es de cations de petit rayon. *Comptes Rendus Hebdomadaires Des Seances De L'academine Des Sciences*, 265, 833-835

Goldman, L. J. & Greenfield, L. I. Clay liners for waste management facilities: design, construction and evaluation. Australian Groundwater ResearchResource for Students and Scientists. Research Triangle Institute Research Triangle Park, North Carolina . 1990.

Graf, P.E. 1986. Factors affecting moisture susceptibility of asphalt concrete mixes. *Association of Asphalt Paving Technologists*, 55, 175-213

Greene-Kelly, R. 1953. The identification of montmorillonoids in clays. *J.Soil Sci.*, 4, (2) 233-237

Greene-Kelly, R. 1955. Sorption of aromatic organic compounds by montmorillonite. I. Orientation studies. *Transactions of the Faraday Society*, 54, 412-424

Greenland, D.J., Lady, R.H., & uirk, J.P. 1962. Adsorption of glycine and its di-, tri-, and tetra-peptides by montmorillonite. *Transactions of the Faraday Society*, 58, 829-841

Grim, R.E., Allaway, W.H., & Cuthbert, F.L. 1947. Reaction of different clay minerals with some organic cations. *American Ceramic Society*, 30, (5) 137-145

Gurses, A., Karaca, S., Dogar, C., Bayrak, R., Acikildiz, M., & Yalcin, M. 2004. Determination of adsorptive properties of claywater system, methylene blue sorption. *Journal of Colloid and Interface Science*, 269, 310-314

Gurses, A., Dogar, C., Acikildiz, M., Bayrak, R., & Karaca, S. 2006. The adsorption kinetics of the cationic dye, methylene blue, onto clay. *Journal of Hazardous Materials*, B131, 217-228

Havlin, J.L., Beaton, J.D., Tisdale, S.L., & Nelson, W.L. 2010. *Soil fertility and fertilizers*, 7 ed. New Delhi, *Learning PVT Ltd*.

Hähner, G., Marti, A., Spencer, N.D., & Caseri, W.R. 1996. Orientation and electronic structure of methylene blue on mica: a near edge Xray absorption structure spectroscopic study. *The Journal of Physical Chemistry*, 104, 7749-7757

Hefer, A. & Ittle, D. 2005, *Adhesion in bitumen-aggregate systems and quantification of the effects of water on the adhesive bond* ICAR/505-1.

Hicks, R. G. 1991, *Moisture damage in asphalt concrete*, Transportation Research Board, Washington,D.C., 175.

Hillier, S. 2000. Accurate quantitative analysis of clay and other minerals in sandstones by XRD: comparison of a Rietveld and a reference intensity ratio (RIR) method and the importance of sample preparation. *Clay Minerals*, 35, 291-302

Hoffman, R.W. & Brindley, G.W. 1960. Adsorption of non-ionic aliphatic molecules from aqueous solutions on montmorillonite. Clay-organic studies--II. *Geochimica et Cosmochimica Acta*, 20, (1) 15-29

Hofmann, U. & Klemen, R. 1950. Verlust der Austauschffghigkeit yon Litbiuminonen an Bentonit durch Erhitzung. *Zeitschrift fiir anorganische und allgemeine Chemie*, 262, 95-99

Holzapffel, T. 1985. Les minéraux argileux - Préparation, analyse diffractométrique et détermination. *Société Géologique du Nord*, 12, 163

Howson, J., Masad, E., Bhasin, A., lIttle, D., & Lytton, R. 2010. Comprehensive analysis of surface free energy of asphalts and aggregates and the effects of changes in pH. *Construction and Building Materials*, 25, 2554-2564

Huang, S.C., Robertson, R.E., Branthaver, J.F., & Petersen, J.C. 2005. Impact of lime modification of asphalt and freeze-thaw cycling on the asphalt-aggregate interaction and moisture resistance to moisture damage. Journal of Materials in Civil Engineering, 17, (6) 711-718

Hubbard, P. 1938. *Adhesion of asphalt to aggregate in the presence of water* Washington D.C., Highway Research Board.

Huet, M. 1989, *Incidence de la variation de la valeur de bleu sur certaines caractéristiques des fines et des enrobes*,Bull des laboratoire des Ponts et Chaussées, 14.

Hughes, R.I., Lamb, D.R., & Pordes, O. 1960. Adhesion in bitumen macadam. *Journal of Applied Chemistry*, 10, 433-443

Hussain, S.A., Demirci, S., & Ozbayoglu, G. 1996. Zeta Potential Measurements on Three Clays from Turkey and Effects of Clays on Coal Flotation. *Journal of Colloid and Interface Science*, 184, 535-541

Isacsson, U. & Zeng, H. 1998. Cracking of asphalt at low temperature as related to bitumen rheology. *Journal of Materials Science*, 33, 2165-2170

Ishai, I. & Craus, J. 1977. Effect of the filler on aggregate-bitumen adhesion properties in bituminous mixtures. *Association of Asphalt Paving Technologists Proc* 228-258

Jada, A., Florentin, C., & Mariotti, S. 2004. Study of the electrical properties of cationic bitumen emulsions by microelectrophoresis. *Advances in Colloid and Interface Science*, 108ΓÇô109, (0) 127-132 available from: http://www.sciencedirect.com/science/article/pii/S0001868603001441

Jamieson, I.L., Moulthrop, J.S., & Jones, D.R. 1995. *SHRP results on binder- aggregate adhesion and resistance to stripping*.

Janczuk, B., Chibowski, E., Hajnos, M., & Bialopiotrowicz, T. 1989. Influence of exchangeable cations on the surface free energy of kaolinite as determined from contact Angles. *Clays and Clay Minerals*, 37, 269-272

Jelavic, S. 2012. *Quantitative mineralogy of clay-bearing samples with X-ray powder diffraction and the Rietveld method.* Master International Master in Advanced Clay Science; Institut des Sciences de la Terre, Université Joseph Fourier.

Jeon, Y. W. & Curtis, W. C. 1990, *A literature review of the adsorption of asphalt functionalities on aggregate surfaces*, National Research Council. Washington, D.C, SHRP-A/IR-90-014.

Jermouni, S. 2015. *Etude sur la nocivité des argiles dans les sables utilisés dans les couches de roulement.* Internship report Technicien Supérieur Physique Chimie - AFPA.

Johansson, L. S., Branthaver, J. F., & Robertson, R. E. A study of rheological properties of lime treated paving asphalts aged at 60 °C in a pressure aging vessel. Fuel Science and Technology International 13[10], 1317-1343. 1995.

Jones, D. R. 1992, An asphalt primer: understand how the origin and composition of paving-grade asphalt cements affect their performance, Strategic Highway Research Program, National Research Council, Washington, D.C., 4.

Jouany, C. 1991. Surface free energy components of clay synthetic humic acid complexes from contact angle measurements. *Clay Minerals*, 39, (1) 43-49 available from: http://geoscience.net/research/002/236/surface-free-energy-components-clay-synthetic-humic-acid-complexes-contact-angle-measurements.php

Jouany, C. & Chassin, P. 1987. Determination of the surface energy of clay organic complexes by contact angle measurements. *Colloids and Surfaces*, 27, (4) 289-303 available from: http://www.sciencedirect.com/science/article/pii/016666228780152X

Kandhal, P. S., Lynn, C. Y., & Parker, F. 1998, *Tests for plastic fines in aggregates related to stripping in asphalt paving mixtures*, National Center for Asphalt Technology, NCAT Report No. 98-3.

Kandhal, P.S. & Rickarda, I.J. 2001. Premature failure of asphalt overlays from stripping: case histories. *Association of Asphalt Paving Technologists*, 70, 347-406

Kanitpong, K. & Bahia, H.U. 2003. Role of adhesion and thin film tackiness of asphalt binders in moisture damage of HMA. *J Assoc Asphalt Pav Technol (AAPT)*, 72, 611-642

Kennedy, T. W., Robert, F. L., Lee, K. W., & Anagnos, J. N. 1982, *Texas Freeze-Thaw Pedestal Test for evaluating moisture susceptibility for asphalt mixtures*, Center for Transportation Research, Austin, TX, 253-3.

Kennedy, T.W., Robert, F.L., & Lee, K.W. 1984. Evaluating moisture susceptibility of asphalt mixtures using the texas boiling test. *Transportation Research Record*, 968, 45-54

Kiggundu, B. M. & Robberts, F. L. 1988, *Stripping in HMA mixtures state-of-the art and critical review of test methods*, National Center for Asphalt Technology, Auburn University, Alabama; 88-2.

Kleeberg, R., Monecke, T., & Hillier, S. 2008. Preferred orientation of mineral grains in sample mounts for quantitative XRD measurements: How random are powder samples? *Clays and Clay Minerals*, 56, 404-415

Kobayashi, T. 1996, "J-Aggregates," *In World Scientific*, Singapore ed.

Koots, J.A. & Speight, J.G. 1975. Relation of petroleum resins to asphaltenes. *Fuel*, 54, 179-184

Laribi, S., Audiguier, M., & Cojean, R. 2008. Assessing shrink/swell properties of two argillaceous soils from the Paris Basin: a comparison of cation exchange determination methods. *Bulletin of Engineering Geology and the Environment*, 67, 415-424

Laruaz, R., Jeanneau, E., & Vera, R. Extraction des fractions argileuses contenues dans un échantillon brut en vue de leur analyse par diffraction des rayons x sur poudres. 2013. Centre de diffractométrie Henri Longchambon, Université Claude Bernard – Lyon1

Laux, H., Rahimian, I., & Butz, T. 1997. Thermodynamics and mechanic of stabilization and precipitation of petroleum colloids. *Fuel Processing Technology*, 53, 69-79

Le Guen, L., Huchet, F., & Tamagny, P. Drying and heating modelling of granular flow Application to the mix-asphalt processes. 2013.

Le Roux, A. & Unikowski, Z. 1980. Mise en évidence de l'influence des fines argileuses dans les granulats à béton. *Bull Liaison Lab Ponts Chauss,* (110) 101-108

Lesueur, D., Petit, J., & Ritter, H.J. 2013. The mechanisms of hydrated lime modification of asphalt mixtures a state-of the art review. *Road material and pavement design*, 14, (1) 1-16

Lesueur, D. 2009. The colloidal structure of bitumen: Consequences on the rheology and on the mechanisms of bitumen modification. *Advances in Colloid and Interface Science*, 145, 42-82 available from: http://www.sciencedirect.com/science/article/pii/S0001868608001413

Li, Z., Chang, P.H., Jiang, W.T., Jean, J.S., & Hong, H. 2011. Mechanism of methylene blue removal from water by swelling clays. *Chemical Engineering Journal*, 168, (1193) 1200

Lian, H., Lin, J.R., & Yen, T.F. 1994. Peptization studies of asphaltene and solubility parameter spectra. *Fuel*, 73, 423-428

Little, D.N. 1995. *Handbook for stabilization of pavement subgrades and base courses with lime* Dubuque, I.A., Kendall Hunt Publishing Company.

Liu, J., Xu, Z., & MasliyahN, A. 2004. Role of fine clays in bitumen extraction from oil sands. *AIChE Journal*, 50, (8) 1917-1927

Liu, J., Xu, H., & Masliyah, J. 2005. Interaction forces in bitumen extraction from oil sands. *Journal of Colloid and Interface Science*, 287, (2) 507-520 available from: http://www.sciencedirect.com/science/article/pii/S0021979705001827

Liu L. P, Zhang L. Adsorption of dyes from aqueous solutions or suspensions with clay nano-adsorbents, *Separation and Purification Technology*, 58, 1, 2007, pp 32–39

Lottman, R. P. 1978, *Predicting moisture-induced damage to asphaltic concrete*, Transportation Research Record, Washington, D.C., 192.

López-Durán, J.D.G., Khaldoun, A., Kerkeb, M.L., Ramos-Tejada, M.M., & González-Caballero, F. 2003. Wettability of montmorillonite clays in humic acid solutions. *Clays and Clay Minerals*, 51, 65-74

Maes, A. & Cremers, A. 1979, "Cation exchange in clay minerals: some recent developments," *In Soil chemistry B, Physical-chemical models*, Bolt G.H., ed., Developments in Soil Science, pp. 205-232.

Magnan, J. P. 1999, "Les materiaux naturals:sols et roches," *In Mécanique des sols et des roches*, p. 1.1-1.146.

Margulies, L., Rozen, H., & Nit, S. 1988. Model for competitive adsorption of organic cations on clay. *Clays and Clay Minerals*, 36, 270-276

Masad, E., Zollinger, C., Bulut, R., Little, D.N., & Lytton, R. 2006. Characterization of HMA moisture damage using surface energy and fracture properties (with discussion). *Journal of the Association of Asphalt Paving Technologists*, 75, 713-754

Masliyah, J. Extraction of Oilsands Bitumen. 2003. Intensive Short Course, University of Alberta, Edmonton, AB.

Masson, J.-F. & Collins, P. 2008, *FTIR study of the reaction of polyphospheric acid and model bitumen sulfur compounds* NRCC-50828.

Maurice, P.A. 2009. *Environmental surfaces and interfaces from the nanoscale to the global scale*, 1 ed. John Wiley & Sons, Inc., USA.

McManus, D.A. 1991. Suggestions for authors whose manuscripts include quantitative clay mineral analysis by X-ray diffraction. *marine geology*, 98, 1-5

Mehrara, A. & Khodaii, A. 2013. A review of state of the art on stripping phenomenon in asphalt concrete. *Construction and Building Materials*, 38, (0) 423-442 available from: http://www.sciencedirect.com/science/article/pii/S0950061812006289

Michot, L. J. & Villieras, F. 2006, "Surface area and porosity," *In Handbook of clay science*, pp. 965-978.

Miller, R.W. & Donahue, R.L. 1977. *Soils: an introduction to soils and plant growth*, 4 ed. Inglewood Cliffs, New Jersey, Prentice- Hall.

Mineralogy database. Mineralogy database. 2015.

Mo, L., Huurman, M., Wu, S., & Molenaar, A.A.A. 2009. Raveling investigation of porous asphalt concrete based on fatigue characteristics of bitumen-stone adhesion and mortar. *Materials and Design*, 30, 170-179

Mohammad, L.N., Saadeh, S., Kabir, M., & Othman, A. 2008. Mechanistic properties of hot-mix asphalt mixtures containing hydrated lime. *Transportation Research Record*, 2051, 49-63

Moore D.M. & Reynolds R.C. 1997. *X-ray diffraction and the identification and analysis of clay minerals*, Oxford, New York ed.

Moore, D. M. & Reynolds, R. C. Jr. 1989, "*X-ray diffraction and the identification and analysis of clay minerals*," Oxford ed. p. 332.

Morrison, F. & Gasperikova, E. Density of minerals, soils and rocks. The Berkeley course in applied geophysics. 2015.

Mullins, O. & Sheu, E.Y. 1998. *Structures and Dynamics of Asphaltenes* New-York, Plenum Press.

Myers, D. 1999. *Surfaces, Interfaces, and Colloids: Principles and Applications*, 2 ed. New York 244.

National lime association 2003, *How to Add Hydrated Lime to Asphalt An Overview of Current Methods*.

Nelson, S. A. Weathering & clay minerals. EENS 2110, Tulane University, 11-18-2014.

Nesse, W. D. 2000, "Introduction to mineralogy," 1 ed. USA: Oxford University Press.

Neumann, A. W. & Good, R. J. 1979, "Techniques of measuring contact angles," *In Surface and Colloid Science*, R. J. Good & R. R. Stromberg, eds., New York: pp. 31-91.

Neumann, M.G., Gessner, F., Schmitt, C.C., & Sartori, R. 2002. Influence of the layer charge and clay particle size on the interactions between the cationic dye methylene blue and clays in an aqueous suspension. *Journal of Colloid and Interface Science*, 255, 254-259

NF EN 12697-12. Bituminous mixtures, Test methods for hot mix asphalt, Part 12: Determination of the water sensitivity of bituminous specimens. 2008.

NF EN 12697-22. Bituminous mixtures - Test methods for hot mix asphalt - Part 22 : wheel tracking. Expert Systems with Applications . 2010.

NF EN 12697-35+A1. Bituminous mixtures, Test methods for hot mix asphalt, Part 35: Laboratory mixing. 2007.

NF EN 13043. Aggregates for bituminous mixtures and surface treatments for roads, airfields and other trafficked areas. 2003.

NF EN 13108-1. Material specification Part1: Asphalt concrete. 2006.

NF EN 933-8. Tests for geometrical properties of aggregates - Part 8 : assessment of fines - Sand equivalent test. 2015.

NF EN 933-9. Tests for geometrical properties of aggregates, Part 9: Assessment of fine-Methylene blue test. 2009.

NF EN ISO 23470. Détermination de la capacité d'échange cationique CEC. 2011.

NF P 98-251-1. Test relating to pavements- Static test on bituminous mixtures-Part 1: DURIEZ test on hot mix. 2002.

NF P94-048. Détermination de la teneur en carbonate dissous à froid: dosage de la calcite. 2003.

NF P94-057. Sols : reconnaissance et essais - Analyse granulométrique des sols - Méthode par sédimentation. 1996.

NF P98-150-1. Bituminous asphalts - Laying of pavement bases, binder and wearing courses - Part 1 : hot-mix asphalts - Constituents, formulation, fabrication, transport, laying and site inspection. 2008.

NF X31-130. Qualité des sols - Méthodes chimiques - Détermination de la capacité d'échange cationique (CEC) et des cations extractibles. 1999.

Ono, S.S., Yao, H., Matsuoka, O., Kawabata, R., Kitamura, N., & Yamamoto, S. 1999. Anisotropic growth of J aggregates of pseudoisocyanine dye at a mica/solution interface revealed by AFM and polarization absorption measurements. *The Journal of Physical Chemistry*, B103, 6909-6921

Ottner, F., Gier, S., Kuderna, M., & Schwaighofer, B. 2000. Results of an inter-laboratory comparison of methods for quantitative clay analysis. *Applied Clay Science*, 17, 223-243

Owens, D. & Wendt, R. 1969. Estimation of the Surface Free Energy of Polymers. *Journal of Applied Polymer Science*, 13, 1741-1747

Pentrák, M., Czímerová, A., Madejová, J., & Komadel, P. 2012. Changes in layer charge of clay minerals upon acid treatment as obtained from their interactions with methylene blue. *Applied Clay Science*, 55, 100-107

Petersen, C.J., Planche, H., Ensley, E.K., Miyake, G., & Venable, R.L. 1982. Chemistry of asphalt-aggregate interaction: Relationship with moisture damage prediction test. *Transportation Research Record* (843) 95-104

Petersen, J.C. & Planche, H. 1998. Model studies and interpretive reviewof the competitive adsorption and water displacement of petroleum asphalt chemical functionalities on mineral aggregate surfaces. *Petroleum Science and Technology*, 16, 89-131

Pfeiffer, J.P. & van Doormaal, P.M. 1936. Classifying asphalts by means of penetration index. *Journal of Petroleum Technology*, 22, 414

Pfeiffer, J.P. & Saal, R.N. 1940. Asphaltic bitumen as colloid system. *Journal of Physical Chemistry*, 44, 139

Pham, T.H. & Brindley, G.W. 1973. The natural of garnierites-III. Thermal transformations. *Clays and Clay Minerals*, 21, 51-57

Pham, T.L. 2008. *Erosion et dispearsion des sols agrileux par un fluide.* L'Ecole Nationale des Ponts et Chaussees.

Pieri, N. 1995. *Etude du Vieillissement Simulé et In-Situ des Bitumes Routiers par IRTF et Fluorescence UV en Excitation-Emission Synchrones.* PhD University Aix-Marseille St-Joseph, France.

Plancher, H., Dorrence, S.M., & Petersen, C.J. 1977. Identification of chemical types in asphalts strongly adsorbed at the asphalt-aggregate interface and their relative displacement by water. *Association of Asphalt Paving Technologists*, 46, 151

Raven, M. D. & Self, P. G. Accuracy in quantitative phase analysis of complex mineral assemblages-A decade of Reynolds Cup round robins. 4-24-2013.

Read, J. & Whiteoak, D. 2003. *The shell bitumen handbook*, 5 ed. London, Thomas Telford Publishing.

Reed, M. G. Retention of crude oil bass by clay-containing sandstone. Clays and Clay Minerals 16, 173-178. 1968.

Richardson, C. 1910. *The modern asphalt pavement*, 2 ed. New York, Wiley.

Rietveld, H.M. 1969. A profile refinement method for nuclear and magnetic structure. *Journal of Applied Crystallography*, 2, 65-71

Robertson, R.E. 2000. *Chemical properties of asphalts and their effects on pavement performance* Washington, D.C., Transportation Board.

Rogers, K., Takacs, E., & Thompson, M. R. Contact angle measurement of select compatibilizers for polymer-silicate layer nanocomposites. Polymer testing 24[4], 423-427. 2005.

Schellenberg, K. & Eulitz, H.J. 1999. Verbesserung von Asphalteigenschaften durch Einsatz von Kalkhydrat. *Bitumen*, 1, 2-8

Schoonheydt, R.A. & Heughebaert, L. 1992. Clay adsorbed dyes: methylene blue on laponite. *Clay Minerals*, 27, 91-100

Schroeder, P. 16 - Lecture notes for Clay Mineralogy. Clay Mineralogy at the University of Georgia . 2015. UGA Clay Science.

Schroth, B.K. & Sposito, G. 1997. Surface charge properties of kaolinite. *Clays and Clay Minerals*, 45, (1) 85-91

Schultz L.G. 1964, *Quantitative interpretation of mineralogical composition from X-ray and chemical data for the Pierre Shale* 391C.

Scott, J.A.N. 1978. Adhesion and disbonding mechanisms of asphalt used in highway construction and maintenance. *Association of Asphalt Paving Technologists Proc*, 47, 19-48

Serratosa, J.M. 1960. Dehydration studies by infrared spectroscopy. *American Mineralogist*, 45, 1101-1104

Shang, J., Flury, M., Harsh, J.B., & Zollars, R.L. 2008. Comparison of different methods to measure contact angles of soil colloids. *Journal of Colloid and Interface Science*, 328, 299-307 available from: http://www.deepdyve.com/lp/elsevier/comparison-of-different-methods-to-measure-contact-angles-of-soil-d9zsyoHqf1

Shang, J., Flury, M., Harsh, J.B., & Zollars, R.L. 2010. Contact angles of aluminosilicate clays as affected by relative humidity and exchangable cations. *Colloids and Surfaces A: Physicochemical and Engineering Aspects*, 353, 1-9

shell bitumen 1995. *The shell bitumen industrial handbook* Chersey, Shell bitumen.

Sieskind, O. & Wey, R. 1958. Influence du pH sur l'adsorption d'amines aliphatiques normales par la montmorillonit-H. *Comptes Rendus Hebdomadaires Des Seances De L'academine Des Sciences*, 247, 74-76

Simmons, G.W. & Beard, B.C. 1987. Characterization of acid-base Properties of the hydrated oxides on iron and titanium metal surface. *Journal of Physical Chemistry*, 91, (5) 1143-1148

Smith, D.W. 1977. Ionic hydration enthalpies. *Journal of Chemical Education*, 54, (9) 540

Snyder, R. L. & Bish, D. L. 1989, "Quantitative analysis. In: editors," *In Modern powder diffraction*, Washington, DC: Rev Mineral 20. Mineral Soc Am ed. P. J. BishDL, ed., pp. 101-142.

Somé, S.C. 2012. *Comportement thermomécanique des enrobés tièdes et de l'interface bitume-granulat.*

Soukup, D. A., Buck, B. J., & Harris, W. 2008, "Preparing soils for mineralogical analyses," *In Methods of soil analysis*, vol. 5 Drees L.R. & Ulery A.L., eds., pp. 13-31.

Speight, J. G. 1991 Molecular models for petroleum asphaltenes and implication for asphalt science and technology, Roma: pp. 154-207.

Speight, J.G. 1999. *The chemistry and technology of petroleum*, 3 ed. New-York.

Speight, J.G. 2004. Petroleum asphaltenes. Part 1. Asphaltenes, resins and the structure of petroleum. *Oil Gas Sci Technology*, 59, 467-477

Sposito, G. 1984. *The surface chemistry of soils*, 1 ed. Oxford University Press.

Srodon, J., Drits, V.A., McCarty, D.K., Hsieh, J.C.C., & Eberl, D.D. 2001. Quantitative X-ray diffraction analysis of clay-bearing rocks from random preparations. *Clays and Clay Minerals*, 49, (6) 514-528

Talibudeen, O. 1954. Complex formation between montmorillonoid clays and amino-acids and proteins. *Transactions of the Faraday Society*, 51, 582-590

Tansel, B., Sagerb, J., Rectorc, T., Garlandc, J., Strayerc, R.F., Levinec, L., Robertsc, M., Hummerickc, M., & Bauerc, J. 2006. Significance of hydrated radius and hydration shells on ionic permeability during nanofiltration in dead end and cross flow modes. *Seperation and Purification Technology*, 51, 40-47

Tarrer, A.R. 1996. *Use of Hydrated Lime to Reduce Hardening and Striping in Asphalt Mixes.* email to Auburn University.

Tarrer, A. R. 1986, *Stripping of asphalt concrete - chemical testing*, Alabama high way Research, Auburn University, 2.

Tarrer, A. R. & Wagh, V. 1991, *The effect of the physical and chemical characteristics of the aggregate on bonding*, Strategic Highway Research Program, National Research Council, SHRP-A/UWP-91-510.

Taylor, D. W. 1969, "Normal stress between soil particles," *In Soil Mechanics*, p. 55.

Taylor, S.E. 1998. The electrodeposition of asphaltenes and implications for asphaltene structure and stability in crude and residual oils. *Fuel*, 77, 821-828

Terrel, R. L. & Shute, J. W. 1989, *Summary Report on Water Sensitivity*, National Research Council, Washington D.C., SHRP-A/IR-89-003.

The clay mineral society. Reynolds cup. 11-6-2013.

Thomas, F., Michot, L.J., Vantelon, D., Montarges, E., Prelot, B., Cruchaudet, M., & Delon, J.F. 1999. Layer charge and electrophoretic mobility of smectites. *Colloids and Surfaces A: Physicochemical and Engineering Aspects*, 159, 351-358

Thomas, K. 2002, *Quarterly Technical Report*, Western Research Institute, Laramie, Wyo, DTFH61-99C-00022.

Transportation Research Board 2003. *Moisture Sensitivity of Asphalt Pavements-a national seminar*, TRB Committee on Bituminous-Aggregate Combinations to Meet Surface Requirements ed. Transportation Research Board.

Traxler, R.N. 1961. Relation between asphalt composition and hardening by volatilization and oxidation. *Association of Asphalt Paving Technologists Proc*, 30, 359-372

Umemura, Y. 2003. Preparation of methylene blue-clay hybrid films by a modified Langmuir-Blodgett method and molecular orientation of methylene blue in the film. *Nendo Kagaku*, 42, 218-222

van Oss, C. J., Chaudhury, M. K., & Good, R. J. Monopolar surfaces. Advances in Colloid and Interface Science 28, 35-64. 1987.

van Oss, C.J. & Dekker, M. 1994. *Interfacial forces in aqueous media*.

Vane, L.M. & Zang, G.M. 1997. Effect of aqueous phase properties on clay particle zeta potential and electro-osmotic permeability: Implications for electro-kinetic soil remediation processes. *Journal of Hazardous Materials*, 55, 1-22

Vansant, E.E. & Uytterhoeven, J.B. 1972. Thermodynamics of the exchange of n-alkylammonium ions on Na-montmorillonite. *Clays and Clay Minerals*, 20, 47-54

Vecchione, A.C. 2014. *Clay quantification and application to the study of the lime-treated clay-rich sands.* Master International Master in Advanced Clay Science; IFSTTAR.

Velde, B. & Meunier, A. 2008, "Clay mineral formation in weatered rocks: water-rock interaction," *In The Origin of Clay Minerals in Soils and Weathered Rocks*, springer, pp. 163-167.

Wikipedia. Asphalt. http://en.wikipedia.org/wiki/Asphalt . 3-21-2015.

WRI 2003, *Fundamental Properties of Asphalts and Modified Asphalts, Volume 1: Interpretive report*, Western Research Institue, Wyoming, DTFH61-99C-0022.

Wright, J. R. 1965, "Weathering: theoretical and practical aspects of asphalt durability," *In Bituminous Materials: Asphalts, Tars and Pitches*, A. J. Hoiberg, ed., New York: Interscience, pp. 249-306.

Wu, S. 1973. Polar and nonpolar interactions in adhesion. *Journal of Adhesion and Adhesives* (5) 39-55

XP CEN ISO TS 17892-4. Geotechnical investigation and testing - Laboratory testing of soil - Part 4: Determination of particle size distribution. 2005.

Xu, D., Tan, X.L., Chen, C.L., & Wang, X.K. 2008. Adsorption of Pb(II) from aqueous solution to MX-80 bentonite: effect of pH, ionic strength, foreign ions and temperature . *Applied Clay Science*, 41, 37-46

Yen, T.F., Erdman, J.G., & Pollack, S.S. 1961. Investigation of the structure of petroleum asphaltenes by X-ray diffraction. *Analytical Chemistry*, 33, 1587-1594

Yenera, N., Bicer, C., Onal, M., & Sarikaya, Y. 2012. Simultaneous determination of cation exchange capacity and surface area of acid activated bentonite powders by methylene blue sorption . *Applied Surface Science*, 258, 2534-2539

Yoon, H. H. & Tarrer, A. R. 1988, "Effect of Aggregate Properties on Stripping," *In Transportation Research Board 1171*, TRB, ed., Washington, D.C.: National Research Council, pp. 37-43.

Yoon, H.J. 1987. *Interface Phenomenon and Surfactants in Asphalt Paving Materials.* Auburn University.

Young, T. 1805. An essay on the cohesion of fluids. *Philosophical Transactions of the Royal Society*, 95, 65-87

Yu, S. & Dekker, M. Harmonic mean, derived from interfacial tension data. Polymer Interface and Adhesion , 151. 1982.

Yukselen, Y. & Kaya, A. 2008. Suitability of the methylene blue test for surface area, cation exchange capacity and swell potential determination of clayey soils. *Engineering Geology*, 102, (1-2) 38-45 available from: http://www.sciencedirect.com/science/article/pii/S0013795208001622

Zahouani, H., Vargiolu, R., Do, M.T. Characterization of microtexture related to wet road/tire friction, in: proceedings of the 4th International Symposium on Pavement Surface Characteristics, Nantes, France, 22–24 May, 2000.

Zhang, J., Cai, D., Zhang, D., Cai, C., Zhang, C., Qiu, G., Zheng, K., & Wu, Z. 2013. Adsorption of methylene blue from aqueous solution onto multiporous palygorskite modified by ion beam bombardment Effect of contact time, temperature, pH and ionic strength. *Applied Clay Science*, 83-84, 137-143

Abstract

The need to save natural aggregate resources in a sustainable development approach led to consider quarry sands of bad quality. The presence of clays in the fine fraction of these sands has been known for long to increase the water sensitivity of hot-mixed asphalt (HMA), with the risk of mitigating the lifetime of asphalt concrete pavements. In order to detect the presence of clay fines and quantify their harmfulness, methylene blue (MB) tests are routinely performed on sands used for HMA mix design. As the relation between the MB value of a fine aggregate and the Duriez value assessing the water sensitivity of a HMA mixture is questionable, MB tests may by mistake disqualify some sands. The present research investigates the clay mineralogy of various sands to better predict the water sensitivity of a HMA mixture. Water sensitivity seems to be caused by cohesive failure in kaolinite-HMA mixtures, whereas swelling properties of clays are responsible for the stripping of HMA incorporating illite or montmorillonite. As a consequence, HMA mixtures comprising kaolinite have a higher water resistance than HMA mixtures comprising illite or montmorillonite. Furthermore, the high valence of compensating cations onto clay surface coupled to small cation radius (eg. Ca^{2+} and La^{3+}) may improve the water resistance of illite- and montmorillonite- HMA mixtures. Upon observing the correlations between Duriez test, MB value or CEC value and clay mineralogy, a new methodology for sand qualification was suggested and validated successfully on several natural fine aggregates. This methodology is comprised of four steps: when the conventional MBdrop test (step 1) used to qualify fine aggregates in France is in excess of MB2 threshold, cation exchange capacity (CEC or MB_{CEC}) (step 2) measurements are performed which generally extend the range for fine aggregates qualification. Would the fine aggregate remain non-qualified, clay mineralogy is identified and quantified using XRD powder pattern and Reitveld method, as far as possible validated by a complementary method using chemical analysis. The clay mineralogy is then used to calculate the Duriez value that has to be compared to the 0.8 threshold (step 3) whereas the experimental Duriez test (step 4) is performed when the conclusions from step 3 are unclear.

Key words: clay, mineralogy, asphalt concrete pavement, hot mix asphalt, stripping, methylene blue value, qualification, Duriez test, surface energy.

Résumé

La nécessité d'économiser les ressources naturelles en granulats dans une logique de développement durable conduit à s'intéresser à certains sables stériles de carrière. La présence d'argiles dans la fraction fine de ces sables est connue pour accroître la sensibilité à l'eau des enrobés hydrocarbonés à chaud (EHC), avec le risque de raccourcir la durée de vie des chaussées. Afin de détecter la présence de telles fines et de quantifier leur nocivité, des essais de bleu de méthylène (MB) sont usuellement réalisés sur les sables entrant dans la confection des EHC. Cependant, la relation entre la valeur MB d'un sable et la valeur de Duriez caractérisant la sensibilité à l'eau d'un EHC n'étant pas explicite, cette pratique est susceptible de disqualifier à tort certains sables. La présente recherche examine la minéralogie des argiles de différents sables afin de mieux prédire la sensibilité à l'eau d'un EHC. Celle-ci semble se traduire par une rupture cohésive de la phase liant à l'interface eau-bitume-argile dans un EHC contenant de la kaolinite, alors que les propriétés de gonflement des argiles de type illite et montmorillonite sont responsables du désenrobage dans les EHC correspondants. Par conséquent, un EHC contenant de la kaolinite est moins sensible à l'eau qu'un EHC contenant de la montmorillonite ou de l'illite. De surcroît, la valence élevée des cations compensateurs à la surface de l'argile ainsi que leurs petits rayons (par exemple Ca^{2+} et La^{3+}) peuvent améliorer la résistance à l'eau d'un EHC contenant de l'illite ou de la montmorillonite. A partir de l'observation des corrélations entre l'essai Duriez, la valeur de bleu ou la capacité d'échange cationique et la minéralogie de leurs argiles, une nouvelle méthodologie de qualification des sables pour EHC est proposée et a été validée avec succès sur quelques sables naturels. Quatre étapes composent cette méthodologie: lorsque la valeur de bleu MBdrop classique (étape 1) utilisée pour qualifier des sables en France est supérieure au seuil MB2 habituel, la mesure de la capacité d'échange cationique (CEC ou MB_{CEC}) (étape 2) permet d'élargir la gamme des sables qualifiables. Faute de qualification, les argiles sont ensuite identifiées et quantifiées en soumettant le sable à une analyse par diffraction de rayons X sur poudre avec exploitation du diffractogramme par la méthode Reitveld, si possible suivie d'une validation par une méthode 'complémentaire' utilisant l'analyse chimique. La minéralogie de l'argile est alors utilisée pour estimer la valeur de Duriez qui doit être comparée au seuil de 0,8 (étape 3), tandis que la mesure de la valeur de Duriez (étape 4) est réalisée lorsque les conclusions de l'étape 3 ne sont pas claires.

Mots-clés: argile, minéralogie, mélanges bitumineux pour couche de chaussées, bitume à chaud, désenrobage, bleu de méthylène, qualification, test Duriez, énergie de surface.